

Antonella Bianca Francavilla **ROBUSTNESS AND SEISMIC BEHAVIOUR OF STRUCTURES EQUIPPED WITH TRADITIONAL AND INNOVATIVE BEAM-TO-COLUMN CONNECTIONS**



PhD course  
In Civil Engineering, Building Engineering – Architecture, Environmental  
and Territorial Engineering  
University of Salerno



PhD course  
In Engineering Sciences and Technology  
University of Liège

Antonella Bianca Francavilla

***Robustness and seismic behaviour of structures  
equipped with traditional and innovative  
beam-to-column connections***

XV Cycle - new series (a.a. 2014 - 2016)



**DEPARTMENT OF CIVIL  
ENGINEERING**

***PhD course in Civil  
Engineering, Building  
Engineering – Architecture,  
Environmental and  
Territorial Engineering***

**XV CYCLE - N.S. (2014-2016)**

*University of Salerno*

**DEPARTMENT ArGEnCo**

***PhD course in Engineering  
Sciences and Technology***

*University of Liège*

**ROBUSTNESS AND SEISMIC BEHAVIOUR OF  
STRUCTURES EQUIPPED WITH TRADITIONAL AND  
INNOVATIVE BEAM-TO-COLUMN CONNECTIONS**

*Antonella Bianca Francavilla*

**Thesis supervisor**

*Prof. Gianvittorio Rizzano*

**Thesis supervisor**

*Prof. Jean-Pierre Jaspart*

**President of the Doctoral  
College**

*Prof. Ciro Faella*

**President of the Doctoral  
College**

*Prof. Frederic Nguyen*



**DIPARTIMENTO DI  
INGEGNERIA CIVILE**

***Dottorato di Ricerca in  
Ingegneria Civile, Edile-  
Architettura, Ambientale e  
del Territorio***

***XV CYCLE - N.S. (2014-2016)***

*Università degli Studi di Salerno*

**DIPARTIMENTO ArGENCo**

***Dottorato di Ricerca in  
Ingegneria, Scienze e  
Tecnologia***

*Università di Liège*

**ROBUSTNESS AND SEISMIC BEHAVIOUR OF  
STRUCTURES EQUIPPED WITH TRADITIONAL AND  
INNOVATIVE BEAM-TO-COLUMN CONNECTIONS**

*Antonella Bianca Francavilla*

**Tutor**

*Prof. Gianvittorio Rizzano*

**Tutor**

*Prof. Jean-Pierre Jaspart*

**Coordinatore del dottorato**

*Prof. Ciro Faella*

**Coordinatore del dottorato**

*Prof. Frederic Nguyen*

# Ringraziamenti

Giunta al termine di questo percorso, sentito e doveroso è ringraziare chi in questi ultimi tre anni mi ha accompagnata.

Mi preme ringraziare il Prof. Gianvittorio Rizzano ed il Prof. Vincenzo Piluso per la grande opportunità che mi hanno dato: collaborare con loro che sono per me esempio di enorme bravura e sconfinata conoscenza. Nei trascorsi anni di dottorato, ogni momento di confronto è stato per me un enorme arricchimento. Ringrazio il Prof. Jean Pierre Jaspart ed il Prof. Jean François Demonceau per aver condiviso con estrema gentilezza e dedizione le loro conoscenze, per aver aperto la mia mente a nuovi modi di trattare tematiche complesse.

Senza il supporto e la guida sapiente di tutti loro, questa tesi non esisterebbe.

Un ringraziamento sincero e profondo va a Massimo Latour per la pazienza infinita con cui ha seguito il mio lavoro. Mai mi ha negato il suo aiuto ed il suo supporto, per me sempre preziosi.

Ringrazio sentitamente Corrado Chisari e Giovanni Ferrante Cavallaro per la loro collaborazione nello svolgere attività di ricerca e per aver quindi contribuito all'ottenimento dei risultati presentati.

Ringrazio di cuore Roberta, meravigliosa compagna di avventura, con la quale ho condiviso tanto, tutto. La ringrazio perché ha reso vera e profonda la nostra amicizia.

Davvero di cuore ringrazio chi con me ha condiviso quotidianamente gli spazi, le ansie, le preoccupazioni, la *“pausa caffè”* e le partite al calcio balilla durante il pranzo. Per questo ringrazio Agostina, Marco, Elide, Francesco, Jamil ed Alessandro. Ed ancora Massimo, Roberta, Corrado e Giovanni.

Inoltre, mi rende felice ringraziare Bartolomeo col quale ho condiviso prima gli anni dedicati al conseguimento della laurea e poi questo percorso di dottorato, sebbene i mille impegni abbiano reso poco frequenti le nostre chiacchierate. In particolar modo, ringrazio Lui e Marina per aver reso un'esperienza piacevolissima il mio soggiorno a Liège. Senza loro avrebbe avuto un sapore diverso.

Ancora e sempre ringrazio i miei genitori e mio fratello per il loro credere in me e nelle mie capacità, pur non facendo parte di questo mio mondo fatto di libri, numeri e computer.

Ringrazio Ivano, mia metà, presenza costante ed indispensabile, al quale devo tutto quanto fatto finora. Gli sono grata per l'amorevole supporto e l'inesauribile pazienza che quotidianamente dimostra.

# Contents

<b>List of figures</b> .....	v
------------------------------	---

<b>List of tables</b> .....	xiii
-----------------------------	------

## **1. Introduction**

Seismic behaviour of Moment-Resisting Frames	
1.1 (MRFs).....	17
1.1.1 Configuration of moment-resisting frames .....	19
1.1.2 Type of connectors used in MRFs .....	20
1.2 Influence of the joints and their classification .....	22
1.3 Frame classification .....	27
1.4 Design strategies of earthquake-resistant structures .....	32
1.5 Objectives of the Thesis .....	36
1.6 References .....	39

## **2. Full strength bolted beam-to-column connections and design criteria**

2.1	Component method: general aspects .....	41
2.2	Problem of the distribution of the plasticity between joint and beam .....	46
2.3	Full strength joints .....	51
2.3.1	Design procedure .....	54
2.3.2	Validation of the procedure with FEM simulations ....	60
2.4	Application of the design procedure to the “dog bone” joint typology .....	78
2.5	References .....	83

## **3. Innovative Partial strength beam-to-column connections and design criteria**

3.1	Innovative joints typologies .....	87
3.2	Friction joints .....	90
3.2.1	Friction materials: experimental tests .....	93
3.2.1.1	Experimental Layout .....	95
3.2.1.2	Result of the tests – 1 <sup>st</sup> phase .....	100
3.2.1.3	Result of the tests – 2 <sup>nd</sup> phase .....	118
3.2.2	Design procedure .....	146
3.3	References .....	162

## **4. Cyclic behaviour of external beam-to-column joints with friction pads: experimental tests**

4.1	Introduction .....	167
4.2	Description of the test setup .....	168
4.3	Description of the specimens .....	179

4.3.1	Design of the specimen FREEDAM-CYC 01 .....	179
4.3.2	Design of the specimen FREEDAM-CYC 02 .....	194
4.4	Results of the experimental tests .....	210
4.4.1	Test FREEDAM-CYC 01 .....	210
4.4.2	Test FREEDAM-CYC 02 .....	218
4.4.3	Test FREEDAM-CYC 03 .....	225
4.4.4	Test FREEDAM-CYC 04 .....	232
4.5	Comparison among the tests .....	238
4.6	References .....	241

## **5. Influence of the beam-to-column joints on the seismic behaviour of steel MRFs**

5.1	Introduction .....	243
5.2	Seismic design of the frame by TPMC .....	246
5.3	Cyclic modelling and calibration of the parameters: implementation of genetic algorithm .....	264
5.3	Individuation of the earthquake record .....	273
5.4	Seismic response of steel MRFs .....	275
5.5	References .....	281

## **6. Influence of the beam-to-column joints on the structural robustness**

6.1	Introduction .....	283
6.2	Robustness of the structures: general aspect .....	284
6.3	Modelling of the connections in order to evaluate the structural robustness .....	286
6.3.1	Extension of the component approach to joint subjected to axial and bending loads .....	289



6.4	Analyses of frames under exceptional loads .....	339
6.5	Results of the Pushdown analyses .....	342
6.5	References .....	352
<b>Conclusions</b> .....		355
<b>Annex A</b> .....		361
<b>Annex B</b> .....		377

# List of figures

<b>Fig. 1.1</b> -	Structural typologies of moment resistant frames .....	17
<b>Fig. 1.2</b> -	Spatial distribution: a) space frames; b) perimeter frames; c) MRFs in only a few rigid bays – Source: Astaneh-Asl [1] .	19
<b>Fig. 1.3</b> -	Type of connectors used: a) rivets; b) bolts; c) welds .....	21
<b>Fig. 1.4</b> -	Beam-to-column joints classification according to their rotational stiffness: a) pinned; b) rigid; c) semirigid .....	23
<b>Fig. 1.5</b> -	Beam-to-column joints classification according to their flexural resistance .....	24
<b>Fig. 1.6</b> -	Classification of the MRFs on the base of the so-called “5% criterion” .....	29
<b>Fig. 2.1</b> -	Components identification .....	43
<b>Fig. 2.2</b> -	Modelling of the of bolted end plate connections .....	43
<b>Fig. 2.3</b> -	Beam-joint system .....	46
<b>Fig. 2.4</b> -	Plastic rotation supply of the beam-joint system .....	48
<b>Fig. 2.5</b> -	Reference structural scheme considering seismic actions from left to right .....	55
<b>Fig. 2.6</b> -	Simplified model for the design of the tension zone .....	58
<b>Fig. 2.7</b> -	Building plan layout of study cases .....	60
<b>Fig. 2.8</b> -	Analysed structural scheme .....	62
<b>Fig. 2.9</b> -	Components of the finite element model .....	64

<b>Fig. 2.10</b> -	Material constitutive laws: a) plates and profiles; b) bolts; c) welds .....	65
<b>Fig. 2.11</b> -	Definition of the contacts: a) end-plate/column flange; b) bolt head/end-plate; c) end-plate/beam end .....	66
<b>Fig. 2.12</b> -	a) Coupling internal constrains; b) application of external pressure .....	67
<b>Fig. 2.13</b> -	ABAQUS Model .....	68
<b>Fig. 2.14</b> -	Buckling modes of beam-to-column joints .....	69
<b>Fig. 2.15</b> -	Ultimate behaviour of the analysed joints ( Von Mises stresses) .....	70
<b>Fig. 2.16</b> -	Moment-rotation curves (case A) .....	71
<b>Fig. 2.17</b> -	Moment-rotation curves (case B) .....	72
<b>Fig. 2.18</b> -	Moment-rotation curves (case C) .....	73
<b>Fig. 2.19</b> -	Dog bone joint typology: a) Rendering; b) main parameters	79
<b>Fig. 2.20</b> -	Simplified model for the design of the tension zone .....	80
<b>Fig. 3.1</b> -	FREEDAM connection .....	90
<b>Fig. 3.2</b> -	a) Typical layout of a specimen; b) specimen in the machine .....	96
<b>Fig. 3.3</b> -	Tightening sequence .....	99
<b>Fig. 3.4</b> -	Typical Torque vs Pre-load diagram .....	100
<b>Fig. 3.5</b> -	Hysteretic behaviour of hard materials: 3M friction shims .	102
<b>Fig. 3.6</b> -	Hysteretic behaviour of hard materials: Carbide M6 .....	103
<b>Fig. 3.7</b> -	Hysteretic behaviour of hard materials: Carbide M7 .....	104
<b>Fig. 3.8</b> -	Damage of the interfaces: a) M6; b) 3M friction shims .....	105
<b>Fig. 3.9</b> -	Typical diagrams of the bolt forces .....	106
<b>Fig. 3.10</b> -	Actual“ friction coefficient vs cumulative travel: M6	107
<b>Fig. 3.11</b> -	Hysteretic behaviour of soft materials: M2 .....	108
<b>Fig. 3.12</b> -	Hysteretic behaviour of soft materials: M3 .....	109
<b>Fig. 3.13</b> -	Hysteretic behaviour of soft materials: M1 .....	109
<b>Fig. 3.14</b> -	Hysteretic behaviour of soft materials: M4 .....	110
<b>Fig. 3.15</b> -	Actual friction coefficient – M4 .....	111
<b>Fig. 3.16</b> -	Bolt forces – M4 .....	112
<b>Fig. 3.17</b> -	Damage of the interfaces: a) M1; b) M4 .....	112
<b>Fig. 3.18</b> -	Comparisons: “Actual” friction coefficient vs cumulated displacement .....	113

<b>Fig. 3.19</b> -	Comparisons: “Effective” friction coefficient vs cumulated displacement .....	114
<b>Fig. 3.20</b> -	Energy dissipation capacity .....	116
<b>Fig. 3.21</b> -	Energy degradation .....	117
<b>Fig. 3.22</b> -	Influence of the bolts’ preload over the force-displacement hysteretic response (M1) .....	119
<b>Fig. 3.23</b> -	Influence of the bolts’ preload over the force-displacement hysteretic response (M4) .....	121
<b>Fig. 3.24</b> -	Influence of the bolts’ preload over the force-displacement hysteretic response (M6) .....	123
<b>Fig. 3.25</b> -	Influence of the bolts’ pre-load over the actual friction coefficient .....	125
<b>Fig. 3.26</b> -	Bolts’ preloading and effective damping for material M6 ....	127
<b>Fig. 3.27</b> -	Bolts’ preloading and effective damping for material M1 ....	128
<b>Fig. 3.28</b> -	Bolts’ preloading and effective damping for material M4 ....	129
<b>Fig. 3.29</b> -	Effect of disc springs .....	130
<b>Fig. 3.30</b> -	Influence of the disc spring configuration over the hysteretic response (M1) .....	131
<b>Fig. 3.31</b> -	Influence of the disc spring configuration over the hysteretic response (M4) .....	133
<b>Fig. 3.32</b> -	Influence of the disc spring configuration over the hysteretic response (M6) .....	135
<b>Fig. 3.33</b> -	Bolts’ preloading and effective damping for material M1 ....	137
<b>Fig. 3.34</b> -	Bolts’ preloading and effective damping for material M4 ....	138
<b>Fig. 3.35</b> -	Bolts’ preloading and effective damping for material M6 ....	139
<b>Fig. 3.36</b> -	Influence of the disc spring configuration over the preload and effective friction coefficient .....	144
<b>Fig. 3.37</b> -	Design values of the friction coefficient (static or dynamic) for the three materials .....	148
<b>Fig. 3.38</b> -	FREEDAM joint configurations: a) horizontal friction device; b) vertical friction device .....	152
<b>Fig. 3.39</b> -	Lever arm of friction joints: a) configuration n.1; b) configuration n.2 .....	156
<b>Fig. 3.40</b> -	Distance between the axis of the beam plastic hinge and the column flange: a) configuration n.1; b) configuration n.2 .....	158

<b>Fig. 4.1</b> -	Typologies of joints: a) FREEDAM-CYC01/03; b) FREEDAM-CYC02/04 .....	168
<b>Fig. 4.2</b> -	Constraining devices used in the experimental campaign ..	169
<b>Fig. 4.3</b> -	MTS hydraulic actuator .....	170
<b>Fig. 4.4</b> -	Displacement transducer LVDT .....	171
<b>Fig. 4.5</b> -	Structural scheme: a) action in a frame due to the seismic loads; b) reproduced scheme in the laboratory .....	172
<b>Fig. 4.6</b> -	AISC loading history for beam-to-column joints .....	172
<b>Fig. 4.7</b> -	Position of the LVDTs: a) FREEDAM-CYC01; b) FREEDAM-CYC02; c) FREEDAM-CYC03; d) FREEDAM-CYC04 .....	176
<b>Fig. 4.8</b> -	Experimental layout .....	178
<b>Fig. 4.9</b> -	FREEDAM-CYC01 joint configuration .....	180
<b>Fig. 4.10</b> -	Geometry of the specimen FREEDAM-CYC01 .....	193
<b>Fig. 4.11</b> -	FREEDAM-CYC02 joint configuration .....	194
<b>Fig. 4.12</b> -	Rigid deformation of the FREEDAM-CYC02 joint .....	198
<b>Fig. 4.13</b> -	Geometry of the specimen FREEDAM-CYC02 .....	209
<b>Fig. 4.14</b> -	FREEDAM-CYC01 specimen .....	210
<b>Fig. 4.15</b> -	Hysteretic curve of the specimen FREEDAM-CYC01 .....	211
<b>Fig. 4.16</b> -	Moment-rotation curve of the specimen FREEDAM-CYC01	211
<b>Fig. 4.17</b> -	Position of the instruments – FREEDAM-CYC01 .....	212
<b>Fig. 4.18</b> -	Preload force in the bolts of the friction damper .....	213
<b>Fig. 4.19</b> -	Slip force vs displacement curve of the friction damper .....	214
<b>Fig. 4.20</b> -	Compression force vs displacement curve (T-stub web- beam flange) .....	215
<b>Fig. 4.21</b> -	Force vs displacement curve (T-stub flange) .....	215
<b>Fig. 4.22</b> -	Force vs displacement curve: a) L-stub flange/column flange; b) T-stub flange/column flange .....	216
<b>Fig. 4.23</b> -	Force vs displacement curve (haunch) .....	217
<b>Fig. 4.24</b> -	FREEDAM-CYC01 specimen in the deformed configuration	217
<b>Fig. 4.25</b> -	FREEDAM-CYC02 specimen .....	218
<b>Fig. 4.26</b> -	Hysteretic curve of the specimen FREEDAM-CYC02 .....	219
<b>Fig. 4.27</b> -	Moment-rotation curve of the specimen FREEDAM-CYC02	219
<b>Fig. 4.28</b> -	Position of the instruments – FREEDAM-CYC02 .....	220
<b>Fig. 4.29</b> -	Preload force in the bolts of the friction damper .....	221

<b>Fig. 4.30</b> -	Slip force vs displacement curve of the friction damper .....	221
<b>Fig. 4.31</b> -	Compression force vs displacement curve (T-stub web-beam flange) .....	222
<b>Fig. 4.32</b> -	Force vs displacement curve (L-stub flange) .....	223
<b>Fig. 4.33</b> -	Force vs displacement curve (haunch) .....	223
<b>Fig. 4.34</b> -	Force vs displacement curve: a) L-stub flange/column flange; b) T-stub flange/column flange .....	224
<b>Fig. 4.35</b> -	FREEDAM-CYC02 specimen in the deformed configuration	225
<b>Fig. 4.36</b> -	FREEDAM-CYC03 specimen .....	225
<b>Fig. 4.37</b> -	Hysteretic curve of the specimen FREEDAM-CYC03 .....	226
<b>Fig. 4.38</b> -	Position of the instruments – FREEDAM-CYC03 .....	227
<b>Fig. 4.39</b> -	Preload force in the bolts of the friction damper .....	228
<b>Fig. 4.40</b> -	Slip force vs displacement curve of the friction damper .....	228
<b>Fig. 4.41</b> -	Compression force vs displacement curve (T-stub web-beam flange) .....	229
<b>Fig. 4.42</b> -	Force vs displacement curve (L-stub flange) .....	229
<b>Fig. 4.43</b> -	Force vs displacement curve: a) L-stub flange/column flange; b) T-stub flange/column flange .....	230
<b>Fig. 4.44</b> -	Force vs displacement curve (haunch) .....	231
<b>Fig. 4.45</b> -	FREEDAM-CYC03 specimen in the deformed configuration	231
<b>Fig. 4.46</b> -	FREEDAM-CYC04 specimen .....	232
<b>Fig. 4.47</b> -	Hysteretic curve of the specimen FREEDAM-CYC04 .....	233
<b>Fig. 4.48</b> -	Position of the instruments – FREEDAM-CYC04 .....	234
<b>Fig. 4.49</b> -	Slip force vs displacement curve of the friction damper .....	234
<b>Fig. 4.50</b> -	Preload force in the bolts of the friction damper .....	235
<b>Fig. 4.51</b> -	Compression force vs displacement curve (T-stub web-beam flange) .....	235
<b>Fig. 4.52</b> -	Force vs displacement curve: a) L-stub flange/column flange; b) T-stub flange/column flange .....	236
<b>Fig. 4.53</b> -	Force vs displacement curve (L-stub flange) .....	237
<b>Fig. 4.54</b> -	FREEDAM-CYC04 specimen in the deformed configuration	237
<b>Fig. 5.1</b> -	Typologies of joints: a) EEP-DB-CYC03; b) TS-CYC04 .....	244
<b>Fig. 5.2</b> -	Hysteretic curve: a) EEP-DB-CYC03; b) TS-CYC04 .....	245
<b>Fig. 5.3</b> -	Collapse mechanism typologies for MRFs .....	248
<b>Fig. 5.4</b> -	Design requirement concerning mechanism equilibrium curves .....	255

<b>Fig. 5.5</b> -	Analysed frame .....	261
<b>Fig. 5.6</b> -	EEP-DB-CYC03 joint: a) Hysteretic curve; b) energy dissipation .....	269
<b>Fig. 5.7</b> -	TS-CYC04 joint: a) hysteretic curve; b) energy dissipation .	270
<b>Fig. 5.8</b> -	FREEDAM-CYC01 joint: a) hysteretic curve; b) energy dissipation .....	271
<b>Fig. 5.9</b> -	Analysed structure modelled in SeismoStruct v.2016 computer program .....	273
<b>Fig. 5.10</b> -	Spectrum .....	274
<b>Fig. 5.11</b> -	Results of IDA in terms of maximum spring rotation versus spectral acceleration: a) EEP-DB-CYC03; b) TS- CYC04; c) FREEDAM-CYC01 .....	277
<b>Fig. 5.12</b> -	Results of IDA in terms of maximum interstorey drift versus spectral acceleration: a) EEP-DB-CYC03; b) TS- CYC04; c) FREEDAM-CYC01 .....	278
<b>Fig. 6.1</b> -	Notation for the geometrical properties: a) EEP-DB-CYC03; b) TS-CYC04; c) FREEDAM-CYC01 .....	286
<b>Fig. 6.2</b> -	Moment - rotation curves for the IPE 270 profile .....	290
<b>Fig. 6.3</b> -	Moment - rotation curves for the reduced beam section .....	291
<b>Fig. 6.4</b> -	Mechanical model for the bolted connections: a) refined model; b) simplified model .....	296
<b>Fig. 6.5</b> -	EEP-DB-CYC 03: Mechanical model .....	297
<b>Fig. 6.6</b> -	EEP-DB-CYC 03: Force – displacement curve (HE300B – IPE 270) .....	299
<b>Fig. 6.7</b> -	EEP-DB-CYC 03: Force – displacement curve (HE280B – IPE 270) .....	301
<b>Fig. 6.8</b> -	EEP-DB-CYC 03: Force – displacement curve (HE260B – IPE 270) .....	303
<b>Fig. 6.9</b> -	EEP-DB-CYC 03: Force – displacement curve (HE220B – IPE 270) .....	305
<b>Fig. 6.10</b> -	TS-CYC 04: Mechanical model .....	306
<b>Fig. 6.11</b> -	TS-CYC 04: Force – displacement curve (HE300B – IPE 270) .....	309
<b>Fig. 6.12</b> -	TS-CYC 04: Force – displacement curve (HE280B – IPE 270) .....	310
<b>Fig. 6.13</b> -	TS-CYC 04: Force – displacement curve (HE260B – IPE 270) .....	313

<b>Fig. 6.14</b> -	TS-CYC 04: Force – displacement curve (HE220B – IPE 270) .....	315
<b>Fig. 6.15</b> -	Mechanical model of FREEDAM-CYC 01 joint: a) hogging moment; b) sagging moment .....	317
<b>Fig. 6.16</b> -	FREEDAM-CYC 01: Force – displacement curve (HE300B – IPE 270); a) spring modelling the upper part; b) spring modelling the lower part .....	323
<b>Fig. 6.17</b> -	FREEDAM-CYC 01: Force – displacement curve (HE280B – IPE 270); a) spring modelling the upper part; b) spring modelling the lower part .....	328
<b>Fig. 6.18</b> -	FREEDAM-CYC 01: Force – displacement curve (HE260B – IPE 270); a) spring modelling the upper part; b) spring modelling the lower part .....	333
<b>Fig. 6.19</b> -	FREEDAM-CYC 01: Force – displacement curve (HE220B – IPE 270); a) spring modelling the upper part; b) spring modelling the lower part .....	338
<b>Fig. 6.20</b> -	Analysed structural scheme: initial conditions .....	340
<b>Fig. 6.21</b> -	Analysed MRF: SAP2000 model .....	341
<b>Fig. 6.22</b> -	Bolted joint' structural scheme: a) dogbone connection; b) T-stub connections; c) FREEDAM connections .....	342
<b>Fig. 6.23</b> -	Analysed structural scheme: pushdown configuration .....	343
<b>Fig. 6.24</b> -	Pushdown curve .....	344
<b>Fig. 6.25</b> -	Nonlinear structural response .....	345
<b>Fig. 6.26</b> -	Analysed beam-to-column connections of the directly affected structure .....	346
<b>Fig. 6.27</b> -	Achievement of the ultimate conditions: a) EEP-DB-CYC 03; b) TS-CYC 04; c) FREEDAM-CYC 01 .....	347
<b>Fig. 6.28</b> -	Analysed structural scheme equipped with EEP-DB-CYC 03 in the damaged configuration .....	348
<b>Fig. 6.29</b> -	Pushdown curves .....	349
<b>Fig. A.1</b> -	Determination of the effective length for a single bolt row on the basis of the possible collapse mechanisms .....	367
<b>Fig. A.2</b> -	Geometrical properties of column flange .....	373
<b>Fig. A.3</b> -	Abacus .....	374
<b>Fig. B.1</b> -	T-stub model: a) Geometrical discretization of the T-stub; b) Non-linear mechanical model .....	377



<b>Fig. B.2</b> -	Stress-strain laws of the materials composing the T-stub: a) Flange plate; b) Bolts .....	382
<b>Fig. B.3</b> -	Classical definition of the failure modes .....	385
<b>Fig. B.4</b> -	Example of non-dimensional moment-curvature diagram ..	388
<b>Fig. B.5</b> -	Assumed kinematic collapse mechanism .....	389
<b>Fig. B.6</b> -	Cantilever scheme for evaluating the plastic rotations .....	390
<b>Fig. B.7</b> -	Typical moment-rotation behaviour of the plastic hinge .....	392
<b>Fig. B.8</b> -	Deformed shape of the flange .....	396
<b>Fig. B.9</b> -	Flow-chart for solving the system of equation (B.21) .....	398

# List of tables

<b>Table 1.1</b> -	Joint classification .....	26
<b>Table 1.2</b> -	Classification of structures with reference to their ductility supply .....	30
<b>Table 1.3</b> -	Connection required ductility .....	32
<b>Table 2.1</b> -	Definition of the lever arm .....	45
<b>Table 2.2</b> -	Mechanical properties of the material .....	54
<b>Table 2.3</b> -	Input data of study cases .....	61
<b>Table 2.4</b> -	Design solutions for analysed study cases .....	62
<b>Table 2.5</b> -	Damage to joint components expressed as PEEQ and NPEEQ (NPEEQ=PEEQ/ $\epsilon_y$ ) – study case A .....	75
<b>Table 2.6</b> -	Damage to joint components expressed as PEEQ and NPEEQ (NPEEQ=PEEQ/ $\epsilon_y$ ) – study case B .....	76
<b>Table 2.7</b> -	Damage to joint components expressed as PEEQ and NPEEQ (NPEEQ=PEEQ/ $\epsilon_y$ ) – study case C .....	76
<b>Table 3.1</b> -	Summary of the tests – 1st phase .....	118
<b>Table 3.2</b> -	Summary of the tests – 2nd phase (The round brackets represent the disc springs configuration, n° of parallel or series) .....	141
<b>Table 3.3</b> -	Static friction coefficients for every tests .....	147
<b>Table 3.4</b> -	Design values of the friction coefficients .....	149

<b>Table 3.5</b> -	Coefficient of variation for the preload force .....	150
<b>Table 3.6</b> -	Values of the overstrength factor $\gamma_{ov}$ .....	151
<b>Table 4.1</b> -	Loading displacement history .....	173
<b>Table 4.2</b> -	Comparison between experimental and design values of friction moments .....	238
<b>Table 5.1</b> -	Notation .....	249
<b>Table 5.2</b> -	Parameters used for the definition of the Rayleigh damping.....	264
<b>Table 5.3</b> -	Parameters of the smooth model .....	272
<b>Table 5.4</b> -	Basic data of the selected ground motions .....	275
<b>Table 5.5</b> -	Spectral acceleration up to achievement of the ultimate conditions .....	279
<b>Table 6.1</b> -	Measured geometrical properties of the joints .....	285
<b>Table 6.2</b> -	Endplate mechanical properties .....	286
<b>Table 6.3</b> -	Column and beam mechanical properties .....	286
<b>Table 6.4</b> -	Resistance of the rigid-plastic components .....	290
<b>Table 6.5</b> -	Resistance of the elastic-plastic components .....	291
<b>Table 6.6</b> -	EEP-DB-CYC 03: Stiffness coefficients (HE300B – IPE 270) .....	296
<b>Table 6.7</b> -	EEP-DB-CYC 03: Resistance parameters (HE300B – IPE 270) .....	297
<b>Table 6.8</b> -	EEP-DB-CYC 03: Stiffness coefficients (HE280B – IPE 270) .....	298
<b>Table 6.9</b> -	EEP-DB-CYC 03: Resistance parameters (HE280B – IPE 270) .....	298
<b>Table 6.10</b> -	EEP-DB-CYC 03: Stiffness coefficients (HE260B – IPE 270) .....	300
<b>Table 6.11</b> -	EEP-DB-CYC 03: Resistance parameters (HE260B – IPE 270) .....	300
<b>Table 6.12</b> -	EEP-DB-CYC 03: Stiffness coefficients (HE220B – IPE 270) .....	302
<b>Table 6.13</b> -	EEP-DB-CYC 03: Resistance parameters (HE220B – IPE 270) .....	303
<b>Table 6.14</b> -	TS-CYC 04: Stiffness coefficients (HE300B – IPE 270) .....	306
<b>Table 6.15</b> -	TS-CYC 04: Resistance parameters (HE300B – IPE 270) ..	307
<b>Table 6.16</b> -	TS-CYC 04: Stiffness coefficients (HE280B – IPE 270) .....	308
<b>Table 6.17</b> -	TS-CYC 04: Resistance parameters (HE280B – IPE 270) ..	309

<b>Table 6.18</b>	- TS-CYC 04: Stiffness coefficients (HE260B – IPE 270) .....	310
<b>Table 6.19</b>	- TS-CYC 04: Resistance parameters (HE260B – IPE 270) ..	311
<b>Table 6.20</b>	- TS-CYC 04: Stiffness coefficients (HE220B – IPE 270) .....	312
<b>Table 6.21</b>	- TS-CYC 04: Resistance parameters (HE220B – IPE 270) ..	313
<b>Table 6.22</b>	- FREEDAM-CYC 01: Stiffness coefficients (HE300B – IPE 270) – <i>UPPER SPRING</i> .....	317
<b>Table 6.23</b>	- FREEDAM-CYC 01: Resistance parameters (HE300B – IPE 270) – <i>UPPER SPRING</i> .....	318
<b>Table 6.24</b>	- FREEDAM-CYC 01: Stiffness coefficients (HE300B – IPE 270) – <i>LOWER SPRING</i> .....	319
<b>Table 6.25</b>	- FREEDAM-CYC 01: Resistance parameters (HE300B – IPE 270) – <i>LOWER SPRING</i> .....	320
<b>Table 6.26</b>	- FREEDAM-CYC 01: Stiffness coefficients (HE280B – IPE 270) – <i>UPPER SPRING</i> .....	322
<b>Table 6.27</b>	- FREEDAM-CYC 01: Resistance parameters (HE280B – IPE 270) – <i>UPPER SPRING</i> .....	323
<b>Table 6.28</b>	- FREEDAM-CYC 01: Stiffness coefficients (HE280B – IPE 270) – <i>LOWER SPRING</i> .....	324
<b>Table 6.29</b>	- FREEDAM-CYC 01: Resistance parameters (HE280B – IPE 270) – <i>LOWER SPRING</i> .....	325
<b>Table 6.30</b>	- FREEDAM-CYC 01: Stiffness coefficients (HE260B – IPE 270) – <i>UPPER SPRING</i> .....	327
<b>Table 6.31</b>	- FREEDAM-CYC 01: Resistance parameters (HE260B – IPE 270) – <i>UPPER SPRING</i> .....	328
<b>Table 6.32</b>	- FREEDAM-CYC 01: Stiffness coefficients (HE260B – IPE 270) – <i>LOWER SPRING</i> .....	329
<b>Table 6.33</b>	- FREEDAM-CYC 01: Resistance parameters (HE260B – IPE 270) – <i>LOWER SPRING</i> .....	330
<b>Table 6.34</b>	- FREEDAM-CYC 01: Stiffness coefficients (HE220B – IPE 270) – <i>UPPER SPRING</i> .....	332
<b>Table 6.35</b>	- FREEDAM-CYC 01: Resistance parameters (HE220B – IPE 270) – <i>UPPER SPRING</i> .....	333
<b>Table 6.36</b>	- FREEDAM-CYC 01: Stiffness coefficients (HE220B – IPE 270) – <i>LOWER SPRING</i> .....	334
<b>Table 6.37</b>	- FREEDAM-CYC 01: Resistance parameters (HE220B – IPE 270) – <i>LOWER SPRING</i> .....	335
<b>Table 6.38</b>	- Main results of pushdown analysis .....	348



# **Chapter 1**

**Introduction**



## 1.1. Seismic behaviour of Moment-Resisting Frames (MRFs)

Moment Resistant Frames are structures in which the horizontal forces are mainly resisted by members acting in an essentially flexural manner. Their main source of stiffness and lateral strength is given by the flexural resistance of members and connections, and the seismic energy dissipation capacity and ductility is provided by the formation of a high number of dissipative zones which can be located in beams, columns or joints depending on the applied design philosophy (Fig.1.1).

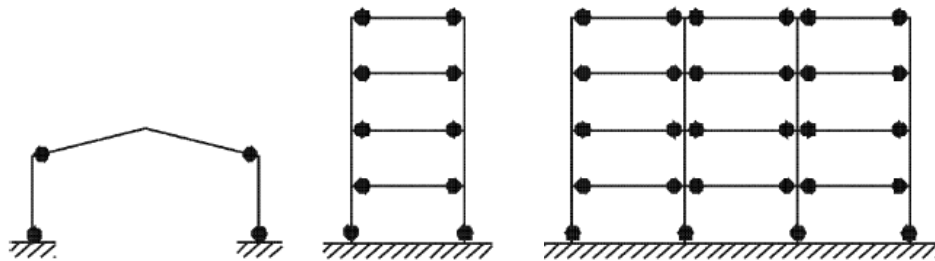


**Fig. 1.1** – Structural typologies of moment resistant frames

Classically, framed structures are designed to possess strong columns, weak beams and full strength rigid connections, so that the earthquake input energy is dissipated through the plastic engagement of the end of beams and of the end of columns of the first storey. However, an alternative design approach consists in the dissipation of the seismic input energy by means of the plastic engagement of dissipative joint components.



MRFs can provide large open spaces without the obstruction usually caused by braces or shear walls. In addition, because of their flexibility and relatively long period of vibration, MRFs usually attract smaller seismic forces than the comparable braced or shear wall systems.

Notwithstanding the undoubted advantages which are possible to obtain by using Moment Resisting Frames, this structural typology possesses some weak points. First of all, the low lateral stiffness can significantly affect the response of the structure both at the ULS and at the SLS. In fact, the susceptibility to second order effects and the fulfilment of the serviceability limit states in terms of maximum lateral drifts, can become governing parameters of the design process, leading to member size greater than the minimum needed for the satisfaction of the strength requirements.

However, since the early days of riveting, steel MRFs have been very popular in building construction. Many structures including the monumental high-rises of the late 19<sup>th</sup> and early 20<sup>th</sup> centuries have been built using riveted steel MRFs. Since the 1960's, with the advent of high strength bolting as well as welding technologies, bolted steel moment-resisting frames (BMRFs) and welded steel moment-resisting frames (WMRFs) have been one of the main structural systems used in office and residential buildings.

According to Astaneh-Asl [1], a classification of MRFs can be made on the basis of the spatial configuration, the type of connectors used, the ductility of connections and the relative rotational stiffness, relative flexural resistance and relative rotation supply of the connections and the members.

### 1.1.1. Configuration of moment-resisting frames

According to the spatial distribution, MRFs can be classified as: space frames, perimeter frames and MRFs in only a few rigid bays.

A typical space MRF is shown in Fig. 1.2a where a three-directional structural system composed of columns, girders and connections resist the applied load primarily by the flexural stiffness, strength and ductility of its members and connections, with or without the aid of the horizontal diaphragms or floor bracing systems.

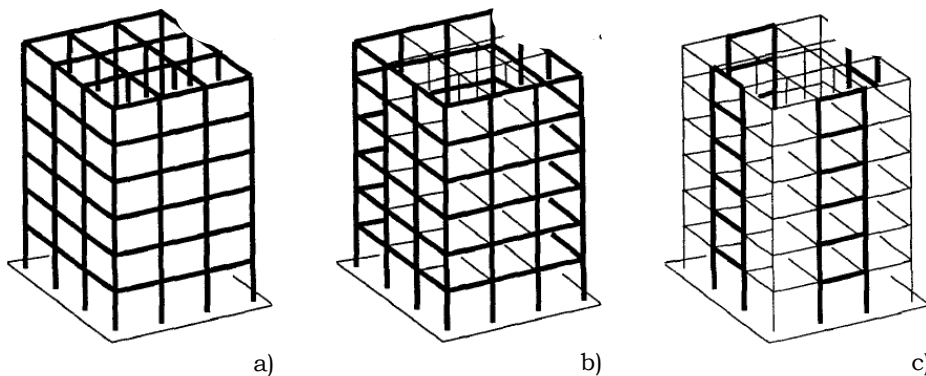


**Fig. 1.2** – Spatial distribution: a) space frames; b) perimeter frames; c) MRFs in only a few rigid bays – Source: Astaneh-Asl [1]

In a perimeter MRF system, as shown in Fig. 1.2b, only the exterior frames are moment-resisting frames providing a moment-resisting frame box to resist the lateral load of the entire building. The interior columns and girders that are not part of the perimeter moment-resisting frame are all connected by shear (simple) connections to carry only their tributary gravity loads.

It is often assumed that gravity columns do not participate in resisting the lateral loads. However, during an earthquake, the gravity columns,

girders and their connections that were assumed not to participate in lateral-load resisting will, in fact, do so to some extent. In addition, the floor diaphragms and some non-structural elements also provide unknown amounts of stiffness, strength and damping. By using steel perimeter MRFs instead of space MRFs, the number of rigid moment connections is reduced, in many cases, to less than one half of the number of connections in the comparable space frame. As a result, significant cost saving is achieved. However, in doing so the redundancy of the lateral-load resisting system is also reduced.

Another type of steel MRF system that has been used frequently is frame with only a few moment-resisting bays as shown in Fig. 1.2c. In this system only a few bays of the entire planar frame have rigid connections while all other connections are shear connections. The columns that are not part of the moment-resisting frame, are leaner (gravity) columns and are not considered in design to participate in resisting lateral load.

### **1.1.2. Type of connectors used in MRFs**

Steel MRFs can be categorized on how flanges of a girder are connected to the columns. The categories are:

- Riveted;
- Field - Bolted;
- Field - Welded.

In ordinary practice, before the 20's, steel structures were built exclusively assembling girders and columns by means of riveted joints (Fig. 1.3a). The rivet is a mechanical fastener that consists, before the

installation, of a shaft with a head only on one end. Typically, rivets are positioned in pre-drilled holes and the termination of the shaft without the head is mechanically deformed to about 1.5 times the original diameter. As a consequence, a connection which can sustain both shear and tension loads is obtained.

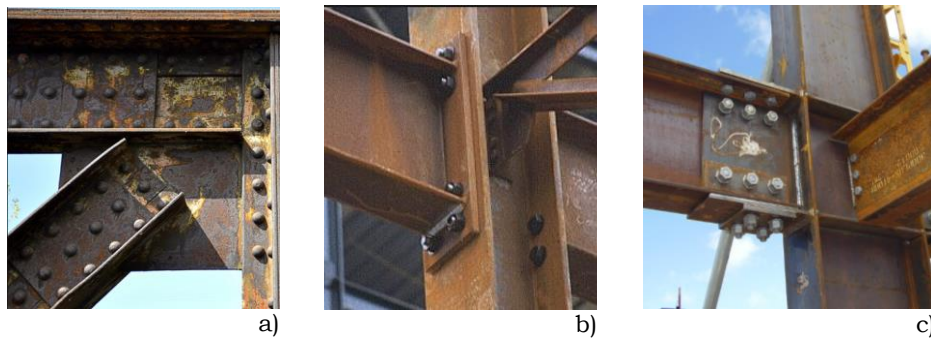


**Fig. 1.3** – Type of connectors used: a) rivets; b) bolts; c) welds

Between the 1920s and 1950s the introduction of High Strength Bolts represented a significant innovation (Fig.1.3b). High strength bolts allowed to fasten plates through high contact pressures, leading to the development of the so called slip resistant joints. In this type of connections the force transfer is achieved by means of the friction exploited between two clamped surfaces. The adoption of High Strength bolts allowed significant time-savings associated with the ease of installation due to threads and washers.

At the same time, during the 20's, the use of welding was becoming popular (Fig. 1.3c) in the mechanical industry due to the introduction of advanced techniques, such as the automatic welding, in which the weld was made by means of the continuous fusion of an electrode wire, or the shielded metal arc welding. Up to the 50's, welds have been applied

only in the fabrication process of electric motors or mechanical equipment. Starting from the 60's, with the refinement of the welding procedures and the reduction of the cost of the welding process, such a technique has also been applied to steel structures, allowing to join girders and columns only by the melting of the two parts and by adding a filler material. Firstly, welds have been used to absorb exclusively shear actions, connecting only the web of beams to the columns, but successively welded details have also been applied to connect flanges, allowing to easily obtain "fully-restrained joints" and, as a consequence to reduce moments and deflections of girders as well as to enhance the lateral stiffness of frames.

Notwithstanding the significant advantages provided by the adoption of welded connections, in last years, after the earthquakes of Northridge and Kobe, the adoption of welded details in MRFs has been subject of discussions and strongly reconsidered. In fact, in both the seismic events, several Perimeter and Space Moment Resisting Steel Frames experienced damages due to the unexpected failure of welded connections. Different reasons have been individuated to explain the unsatisfactory behaviour of Northridge and Kobe welded joints, above all the welding techniques of that time have been harshly criticized.

## **1.2. Influence of the joints and their classification**

Structural response of MRFs strongly depends on the behaviour of its connections. In fact, stiffness and strength of joints deeply affect dynamic properties of frames and their post-elastic behaviour. Furthermore, also the internal actions arising in the structure, both due

to Serviceability and Ultimate loads, depend on the elastic and post-elastic stiffness of the connecting elements. There are several systems to obtain connections. In fact, by varying the structural detail of the connection, different non-linear behaviour ranging from the quasi-perfectly rigid (full welded, extended end plates) to flexible (double web angle) can be observed. As well known, before the introduction of the concept of semirigidity [2,3], steel frame design was accomplished by properly considering a limit assumption regarding the joint behaviour.

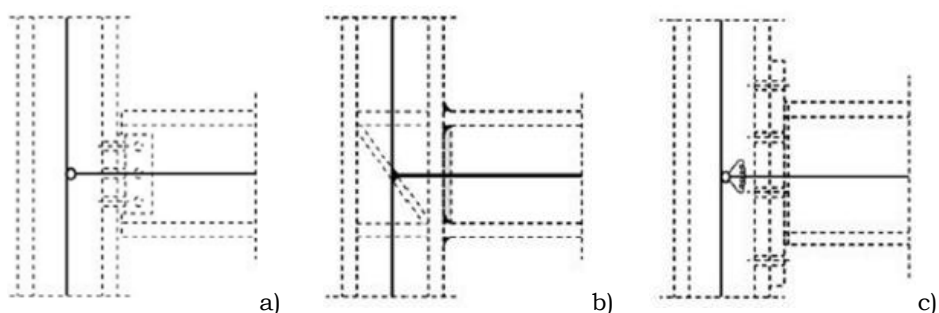


**Fig. 1.4** – Beam-to-column joints classification according to their rotational stiffness: a) pinned; b) rigid; c) semirigid

Depending on the beam-to-column joint typology, it can be either assumed that all the ends of the members converging in the joint are subjected to the same rotation and the same displacements or assumed that the joints are able to permit free rotations. The first case leads to continuous frames, while the second one to pinned frames. In fact, in case of elastic design, the classification system requires only the **rotational stiffness** criterion leading to three categories:

- **Nominally pinned** connections are assumed to transfer the shear and eventually the axial forces from the beam to the column. In

addition, they are able to rotate without developing significant moment that could negatively influence the column resistance capacity (Fig. 1.4a);

- **Rigid** connections transmit all the end reactions and their deformation is so small that their influence on the overall moment distribution can be neglected (Fig. 1.4b);
- **Semirigid** connections are designed in order to provide an interaction between members based on the design of moment-rotation curve of the joint (Fig. 1.4c).

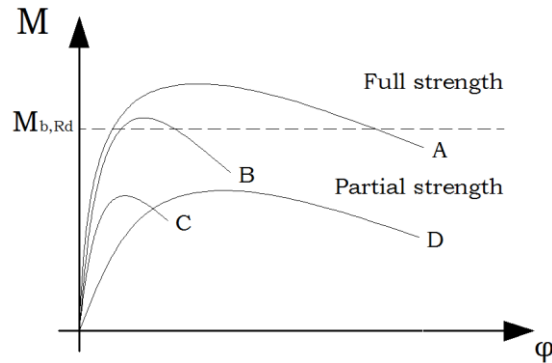


**Fig. 1.5** – Beam-to-column joints classification according to their flexural resistance

In case of rigid-plastic design, the classification criterion based on joint **flexural resistance** is of concern. According to Eurocode 3 [2], connections can be classified in two categories (Fig. 1.5):

- **Full strength** connections have a design resistance at least equal to that of the connected member so that a plastic hinge will not develop in the connection but in the adjacent member (Fig. 1.5 – Case A).

$$M_{b,pl,Rd} \geq M_{j,Rd}$$

In that case, the plastic rotation supply depends on the width-to-thickness ratios of the plates element constituting the beam section. However, the overstrength of the connection, due to the strain-hardening of the material, could not be sufficient to prevent the yielding of the connection (Fig. 1.5 – Case B). In that case, only a part of the rotation capacity of the beam can be exploited and, as a consequence, the plastic rotation supply of the connection becomes of primary importance;

- **Partial strength** connections have a lesser design resistance of the connected member:

$$0.25M_{b,pl,Rd} < M_{j,Rd} < M_{b,pl,Rd}$$

In the connection, a plastic hinge will develop and, in such case, sufficient rotation capacity is required (Fig. 1.5 – Case D). That means that in case C the rotation capacity of the connection could be exceeded under design loads;

- **Nominally pinned** connections have a design resistance much lower than that of the connected member:

$$M_{j,Rd} < 0.25M_{b,pl,Rd}$$

Finally, the third classification criterion, on the base of the plastic **rotation supply**, identifies two categories:

- **Full ductility** connections are able to develop a plastic rotation supply equal or greater than that of the connected member;



- **Partial ductility** connections are characterized by the capability of develop a plastic rotation supply less than that of the connected member.

In conclusion, when elastic-plastic analyses are performed, internal actions and deflections are only influenced by connections rotational stiffness and, as a consequence, the joints have to be classified as pinned, semi-rigid or rigid; when an elastic-plastic analysis is considered both initial stiffness and flexural resistance have to be accounted for and a classification according to both parameters is needed; if a rigid-plastic analysis is lead, the only parameter which plays a role on the overall response is the connection bending resistance and, as a result, joints can be classified as full-strength, partial strength or pinned (Table 1.1).

**Table 1.1** – Joint classification

<b>Method of global analysis</b>		<b>Classification of the joint</b>		
elastic	nominally pinned	rigid	semi-rigid	Semi-rigid and partial-strength
elastic - plastic	nominally pinned	rigid and full-strength	rigid and partial-strength	Semi-rigid and full-strength
rigid - plastic	nominally pinned	full-strength	partial-strength	
<b>Type of joint model</b>	<b>Simple</b>	<b>Continuous</b>	<b>Semi-continuous</b>	

---

*Robustness and seismic behaviour of structures equipped with traditional and innovative beam-to-column connections*

### 1.3. Frames classification

Classification of joints and frames are strictly related. As discussed earlier, the overall structural response of MRFs is strongly influenced by joints strength, stiffness and rotational capacity. In fact, the distribution of the internal actions, the structural ductility, the susceptibility to second order effects and the location of the plastic zones are all parameters which are influenced by the existing relationship between the bending moment and the joint rotation.

Last version of Eurocode 3 [2] classifies MRFs according to the following two characteristics: the susceptibility to second order effects and the presence of a bracing system.

On the base of the first feature MRFs are divided in sway and non-sway. A frame is defined non-sway if its lateral displacements are small enough to retain that the internal actions due to the deformability of the frame are negligible. Conversely, a frame is called sway if the deformed geometry leads to a substantial increase of the internal actions or modify significantly the structural behavior.

According to [4] a frame can be considered to be non-sway if the following relationship are satisfied:

- $\alpha_{cr} = \frac{F_{cr}}{F_{Ed}} > 10$  for elastic analysis
- $\alpha_{cr} = \frac{F_{cr}}{F_{Ed}} > 15$  for plastic analysis

where  $\alpha_{cr}$  is the factor by which the design loading would have to be increased to cause elastic instability in a global mode,  $F_{cr}$  is the elastic critical buckling load for global instability mode based on initial elastic

stiffness and  $F_{Ed}$  is the design loading on the structure. In all the other cases frames have to be classified as sway. Moreover, frames are divided in braced or unbraced. In the first case MRFs are stiffened by specific elements which reduce the lateral displacement of at least the 80%, in the second case frames are defined unbraced.

A further classification of MRFs, depending on the joints characteristics, is provided by [2], where frames are categorized in:

- **Simple:** joints do not transmit bending moment to the column;
- **Continuous:** the behaviour of the joint may be assumed rigid;
- **Semi-continuous:** the behaviour of the joint has to be taken into account by adopting proper models.

In the first case, joints are able to transfer to the columns only shear and beams are free to rotate, as a consequence the obtained structural system is pendular and joints can be faithfully modelled by means of hinges. In the second case, joints behaviour is rigid and their resistance is greater than the flexural strength of the connected beam, so that connections can be structurally represented by means of clamps. In the case of semi-continuous frames, joints are intermediate between the extreme situation of pinned and rigid-full strength, so that their structural behaviour has to be properly accounted for by means of accurate models representing the actual moment-rotation curve.

Aiming to individuate quantitatively the boundaries between rigid, semi-rigid and pinned behaviour, Eurocode 3 Part 1-8 introduces the following two parameters:

$$S_b = \frac{EI_b}{L_b} \quad \text{and} \quad S_c = \frac{EI_c}{L_c}$$

where  $S_b$  is the bending stiffness of the beam,  $S_c$  is the bending stiffness of the column,  $E$  is the steel elastic modulus,  $I_b$  and  $I_c$  are the beam and column inertia modulus,  $L_b$  and  $L_c$  are the beam and column lengths. Eurocode boundaries are determined by defining “rigid” a joint whose stiffness do not reduce by more than the 5% the Euler buckling load of the structure with full rigid attachments.

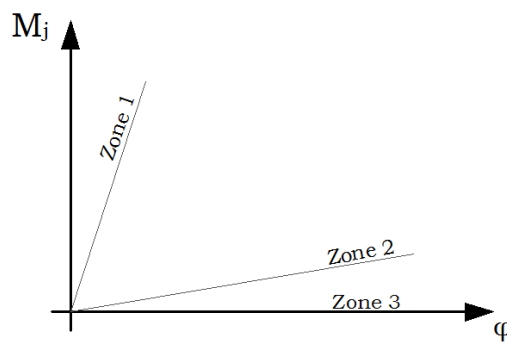


**Fig. 1.6** – Classification of the MRFs on the base of the so-called “5% criterion”

On the base of the so-called “5% criterion”, the following classifications derive (Fig.1.6):

- **Zone 1: rigid**, if  $S_{j,ini} > k_b \frac{EI_b}{L_b}$  where  $k_b = 8$  for frames where the bracing system reduced the horizontal displacement by at least 80% and  $k_b = 25$  for the other frames, provided that in every storey  $k_b/k_c \geq 0.1$  (for frames where  $k_b/k_c < 0.1$  the joints should be classified as semi-rigid);
- **Zone 2: semi-rigid**, all the joints in zone 2 should be classified as semi-rigid. Joints in zone 1 or 3 may optionally also be treated as semi-rigid;
- **Zone 3: nominally pinned**, if  $S_{j,ini} > 0.5 \frac{EI_b}{L_b}$ .

$k_b$  is the mean value of  $I_b/L_b$  for all the beams at the top of that storey and  $k_c$  is the mean value of  $I_c/L_c$  for all the columns in that storey.

Finally, a classification of the structures with reference to their ductility supply is proposed by both European and U.S. codes. In case of MRFs, global ductility assumes the meaning of ratio between the ultimate top sway displacement, accounting for second order effects, and the top sway displacement evaluated in correspondence of the elastic limit. Moreover, the definition of local ductility of MRFs is concerned with the rotational capacity of the plastic hinges, i.e. of beam ends and/or of joints [5]. As a result of the importance in current approach of the ductility supply, international codes provide a classification of structures with reference to their capacity of resisting deformations in plastic field. In Eurocode 8 [6] and AISC 2010 [7], MRFs can be designed to be less or more ductile, according to the three following categories:

**Table 1.2** - Classification of structures with reference to their ductility supply

<b>EUROCODE 8</b>	<b>AISC 2010</b>
Ductility Class LOW (DCL)	Ordinary Moment Frame (OMF)
Ductility Class MEDIUM (DCM)	Intermediate Moment Frame (IMF)
Ductility Class HIGH (DCH)	Special Moment Frame (SMF)

In both European and U.S. codes, provided that some requirements on strength and ductility supply are satisfied, yielding is allowed to occur either in beam, panel zone or connections. The formation of plastic hinges in columns is prohibited, made exception for base plates, column ends at the top of multistorey frames, and in case of single storey MRFs. Eurocode 8 favours a design of MRFs which provides the

---

*Robustness and seismic behaviour of structures equipped with traditional and innovative beam-to-column connections*

development of plastic hinges at beam ends rather than in other zones. Dissipation in beam-to joints is allowed but strongly limited in everyday practice. In fact, when the weak connection-strong column-strong beam design philosophy is adopted, the ductility supply and strength of connections have to be certified by experimental evidence, providing cyclic tests of joints. AISC 2010 also favours design of MRFs which provide the formation of plastic hinges at beam ends, but still offers the possibility to dissipate an amount of seismic input energy by the inelasticity of joints. In particular, AISC 2010 requires that both in case of full-strength and partial strength joints a “conformance demonstration” of the cyclic behaviour of beam-to-column connections adopted in the Seismic Load Resisting System (SLRS) is provided by the designer. As a result, connections have to be prequalified in order to satisfy code requirements in terms of plastic rotation supply and flexural/shear strength, compatibly with the ductility class of the designed MRF. Therefore, designers have two alternatives: the adoption of prequalified joints or the qualification of specific details. In the former case, joints whose cyclic characteristic have already been qualified, such as the prequalified connections contained in document FEMA 358 [8], are used. In the latter case, joint dissipative characteristics have to be demonstrated to be adequate by means of the qualification procedures contained in AISC 2010. In particular, in AISC 2010 and Eurocode 8, connections are required to sustain an interstorey drift angle of 0.04 rad and of 35 mrad respectively.

In case of DCL/OMF, MRFs are expected to exhibit a low dissipative behaviour and connections are not required to possess specific plastic rotation supply (Table 1.3). In case of DCM/IMF the behaviour is expected to be intermediate between high and low dissipative and,

according to Eurocode 8 and AISC 2005, connections are required to sustain rotations of 0.025 and 0.020 rad.

**Table 1.3** – Connection required ductility

<b>EUROCODE 8</b>		<b>AISC 2010</b>	
<b>Ductility Class</b>	<b>Rotational Capacity [mrad]</b>	<b>Ductility Class</b>	<b>Rotational Capacity [mrad]</b>
Ductility Class LOW (DCL)	35	Ordinary Moment Frame (OMF)	40
Ductility Class MEDIUM (DCM)	25	Intermediate Moment Frame (IMF)	20
Ductility Class HIGH (DCH)	-	Special Moment Frame (SMF)	-

#### **1.4. Design strategies of earthquake-resistant MRFs**

In the seismic design of steel frames, the dissipation of the seismic input energy is provided by the plastic engagement of some zones of structural members, the so-called “dissipative zones” which have to be properly detailed in order to assure wide and stable hysteresis loops. In addition, as it is well known, it is important to promote the plastic engagement of the greatest number of dissipative zones, so that both European and American seismic codes suggest the use of the member hierarchy criterion aiming to prevent the premature plastic engagement of the columns which can lead to a non-dissipative collapse mechanism, such as storey mechanism.

---

*Robustness and seismic behaviour of structures equipped with traditional and innovative beam-to-column connections*

Once avoided the yielding of columns, a global dissipative collapse mechanism could be ensured by the formation of plastic hinges at the ends of the beams or in the connections, provided that the elements involved in plastic range have an adequate energy dissipation capacity. Within this framework the beam-to-column joints can be designed either as Full Strength (FS) or Partial Strength (PS). In Europe, the first design approach was strictly followed by the previous code versions of both Eurocode 8 [6] and ECCS-CECM-EKS [8] imposing that the joint components have to possess a sufficient degree of over strength. FS joints are generally characterized by the use of welded connections, continuity plates and eventually web plates in column panel zone. As previously said, after Kobe and Northridge seismic events, the inadequacy of the classical welded connections was recognised and the scientific community worked on two different directions. On one hand many studies were aimed to improve the plastic rotation supply of fully welded connection by strengthening the critical area subjected to fracture or by guarantying the concentration of the energy dissipation in the beam by reducing the bending resistant area of beams by properly cutting the flanges in a zone close to beam-to-column connection, commonly called RBS (Reduced Beam Section) [9-15]. On the other hand a great attention was devoted to bolted connections aimed to set adequate design rules starting from an accurate knowledge of their monotonic and cyclic behaviour up to collapse.

In addition, one of the causes of the significant and premature joint damage during the seismic events of Northridge and Kobe was recognised in the use of design criteria not able to assure a degree of over strength sufficient to allow the full development of the beam plastic rotation capacity. For this reason, in USA the FEMA/SAC test programs



were developed providing design guidelines to be followed for beam-to-column connections in order to guarantee the minimum joint plastic rotation capacity required for Ordinary, Intermediate and Special Moment-Resisting frames [16] while in Europe, the last version of Eurocode 8 [6] states the degree of Joint over strength required to assure the beam end yielding. Nevertheless, even though the classical design approach of FS joints is potentially the best solution because it is based on the good plastic behaviour of beam profiles, the rules for evaluating the joint over strength able to cover both the joint strain hardening and the material random variability require, still today, a discussion and analysis and design methods for FS bolted connections able to ensure the full exploitation of the beam plastic resources are not yet satisfactory. Within this framework, an alternative design approach consists in the dissipation of the seismic input energy by means of the plastic engagement of dissipative joint components.

It is important to underline that the last version of Eurocode 8 [6], has explicitly opened the door to the use of PS joints underlining the possible location of the dissipative zones at the beam ends or in the connections of the beams to the columns, but not in the columns. In addition, it can be recognized that PS joints can lead also to structural solutions convenient from an economical point of view. In fact, as already underlined, the seismic design of steel frames requires the respect of the hierarchy criterion or the use of alternative design procedures, like that suggested by Piluso et al. [17], able to assure the development of a global failure mode. These design criteria, in the case of buildings with a low number of floors and long spans, often lead to columns whose size is greater than that strictly necessary for satisfying strength and deformability checks. The introduction of partial strength

joints allows to avoid the plastic engagement of columns without their over sizing and, as a consequence, with a reduction of the structural cost [18]. The seismic behaviour of semirigid steel frames with PS joints has been already examined by many authors and some proposals for the behaviour factor of semirigid PS frames have been outlined [19,20,14]. Despite of the above research efforts, even though it was recognized that semi-rigid PS connections can lead to dissipation and ductility capacity compatible with the seismic demand, provided that they are properly designed by means of an appropriate choice of the joint component where the dissipation has to occur, detailed design procedures for the seismic design of semirigid PS frames able to guide the designer up to the complete detailing of beam-to-column joints still deserves additional investigations. Finally, in recent years, a growing interest of the scientific community has been addressed to structural systems able to perform adequately during the seismic events and, at same time, free from damage or easy to replace after the earthquake. These goals can be reached equipping the structure with supplemental damping devices able to dissipate a part of the seismic input energy reducing the seismic demand on the structural elements. Many works have been carried out in recent studies on this topic, leading to relevant results and to the development of a large number of high dissipation capacity dampers, either of friction or of yielding type [21-23].

## 1.5. Objectives of the Thesis

Starting from the above considerations, in this work, the possibility of using steel frames with innovative bolted connections has been analysed with the aim of providing the structure of supplemental damping devices by means of properly detailed beam-to-column joints. In particular, in order to overcome the drawbacks of the traditional and passive control design strategies, the aim of the work is the development of a new design strategy whose goal is the design of connections able to withstand frequent and occasional seismic events but also destructive earthquakes such as those corresponding to rare and very rare events without any damage. In addition, with reference to structural robustness, has been underlined that, because of the specific behaviour of beam-to-column connections equipped with friction pads, significant benefits are in the catenary action resulting, as example, in case of a column loss due to blast loading or impact loading. The development of this design strategy is also the subject of the FREEDAM project, which is an RFCS project, granted by the European Community.

In the first part of the thesis, the attention is focused on the design procedures of full-strength and partial-strength beam-to-column connections. In particular, in the second chapter general concepts concerning the component method, as introduced by last version of Eurocode 3, are given and a design procedure of the full-strength full-ductility joints has been proposed and validated through the comparison with the results obtained by means FEM analyses performed in ABAQUS 6.13 software. Chapter 3 provides the results of an experimental programme consisting of 63 specimens, developed at

the STRENGTH laboratory (STRuctural ENgineering Testing Hall) of the University of Salerno, devoted to know with a sufficient level of accuracy the value of the bolts' preloading and the value of the static and dynamic friction coefficients of the friction material employed in FREEDAM connections. A design procedure of the friction beam-to-column connections has been proposed and followed in the designing of the two specimens typologies tested at the STRENGTH laboratory. Chapter 4 deals with the experimental investigation of the behaviour of the FREEDAM joints. Therefore the results obtained by cyclic tests is presented and it is pointed out how the typology of the hysteresis loops is mainly governed by the weakest joint component.

In the second part of the thesis the seismic response and the structural robustness of the frame where the friction connections have been adopted, have been analysed and compared to the performance of the same MRF equipped with a traditional double split tee connection (partial strength joints) and with the dogbone connection (full strength joints) whose cyclic response have been experimentally analysed in the past years at the University of Salerno. In particular, aiming to evaluate the seismic response of the structures by varying the beam-to-column joint detail, in chapter 5 an accurate modelling of the structure and, in particular, of the beam-to-column connections is reported; considering eight ground motion records, the Inelastic Dynamic Analyses (IDA) have been performed by means SeismoStruct v.2016 software and the results have been presented. Finally, in order to evaluate the robustness of the earthquake resistant moment resistant frame analysed in chapter 5 under seismic load, the pushdown analyses of the structures by varying the beam-to-column connections have been performed in SAP 2000 computer program. To this scope, the beam-to-column joints described

in the previous chapters preliminarily the component method for predicting the whole moment-rotation curve of the joint has been modified in order to account for the development of axial forces and to introduce the ultimate deformation of the single joint components.

## 1.6. References

- [1] A. Astaneh-Asl: “*Seismic Design of Bolted Steel Moment-Resisting Frames*”. July, 1995.
- [2] CEN: “*Eurocode 3: Design of Steel Structures – Part 1-8: Design of Joints*”, EN 1993-1-8, 2005.
- [3] C. Faella, V. Piluso and G. Rizzano: “*Structural Steel Semirigid Connections*”, CRC Press, Boca Raton, Ann Arbor, London, Tokyo. ISBN 0-8493-7433-2, 1999.
- [4] CEN: “*Eurocode 3: Design of Steel Structures – Part 1-1: General rules and rules for buildings*”, EN 1993-1-1, 2005.
- [5] V. Giuncu and F. Mazzolani: “*Seismic Resistant Steel Structures*”. New York: CISM Courses and Lectures No 420, 2000.
- [6] CEN, EN 1998-1-1: “*Eurocode 8: Design of structures for earthquake resistance - Part 1: General rules, seismic actions and rules for buildings*”, European committee for standardization, 2005.
- [7] American Institute of Steel Construction, ANSI/AISC 341-10, AISC, 2010.
- [8] FEMA-358: “*Prequalified Connections for Special and Intermediate Steel Moment Frames for Seismic Applications*”, AMERICAN INSTITUTE OF STEEL CONSTRUCTION, 2010, incl. Supplement No. 1.
- [9] ECCS-CECM-EKS: “*European Recommendation for Steel Structures in Seismic Zones, Technical Working Group 1.3: Seismic Design*”, n. 54, 1988.
- [10] K.S. Moore, J.O. Malley and M.D. Engelhardt: “*Design of reduced Beam Section (RBS) Moment Frame Connections*”, AISC Structural Steel Educational Council, Moraga, CA., 1999.
- [11] C.J. Carter and N. Iwankiw: “*Improved Ductility in Seismic Steel Moment Frames with Dogbone Connections*”, Journal of Constructional Steel Research, Vol. 46, No. 1-3, Paper No. 253.
- [12] C. Joh and W.F. Chen: “*Fracture Strength of Welded Flange-Bolted Web Connections*”, Journal of Structural Engineering, ASCE, Vol. 125, No. 5, pp. 565-571, 1999.

- [13] S.J. Chen, J.M. Chu and Z.L. Chou: “*Dynamic Behaviour of Steel Frames with Beam Flanges Shaved Around Connection*”, Journal of Constructional Steel Research, Vol. 42, No. 1, pp. 49-70, 1997.
- [14] R. Richard, J.E. Partridge, J. Allen and S. Radau: “*Finite Element Analysis and Tests of Beam-to-Column Connections*”, Modern Steel Construction, AISC, Vol. 35, No. 10, pp. 44-47, 1995.
- [15] D. Grecea, F. Dinu and D. Dubina: “*Performance criteria for MR steel frames in seismic zones*”, Journal of Constructional Steel Research, Vol. 60, pp. 739-749, 2004.
- [16] FEMA 351. “*Recommended Seismic Evaluation and Upgrade Criteria for Existing Welded Steel Moment-Frame Buildings*”, Federal Emergency Management Agency, Washington, 2000.
- [17] SAC: “*Recommended Design Criteria for New Steel Moment Resisting Frames Buildings*”, California, 2000.
- [18] R. Montuori, E. Nistri and V. Piluso: “*Advances on the theory of Plastic Mechanism Control: Close Form solution for MR Frames*”, Earthquake Engineering & Structural Engineering, vol. 4, pp. 1035-1054, 2014.
- [19] C. Faella, R. Montuori, V. Piluso and G. Rizzano: “*Failure Mode Control: Economy of Semi-Rigid Frames*”, Proc. of the XI European Conference on Earthquake Engineering, Paris, 6-13 September, 1998.
- [20] J.M. Aribert and D. Grecea: “*Numerical investigation of the q-factor for steel frames with semi-rigid and partial-strength joints*”, Proc. of the Third International Conference STESSA 2000, Montreal, August 21-24, 2000.
- [21] A. Astaneh-Asl and N. Nader: “*Proposed code provision for seismic design of steel semi-rigid and rigid frames*”, Proc. of the 5th U.S. National Conference of Earthquake Engineering, EERI, Chicago, 1994.
- [22] ID Aiken, PW Clark and J.M. Kelly: “*Design and Ultimate-Level Earthquake Tests of a 1/2.5 Scale Base-Isolated Reinforced-Concrete Building*”. Proceedings of ATC-17-1 Seminar on seismic Isolation, Passive Energy Dissipation and Active Control. San Francisco. California, 1993.
- [23] M.C. Constantinou, T.T Soong and G.F. Dargush: “*Passive Energy Dissipation Systems for Structural Design and Retrofit*”. Multidisciplinary Center for Earthquake Engineering Research, University at Buffalo, State of New York, 1998.

# **Chapter 2**

**Full strength beam-to-column  
connections and design criteria**





## 2.1. Component method: general aspects

Within the analysis of steel structures, the modelling of the ultimate behaviour of beam-to-column joints is one of the most studied topic. The application of the semirigidity concept has required the development of a general methodology working out in detail the prevision of the rotational stiffness and the flexural resistance of joints. This resulted in a strong effort, in Europe more than in United States, which has led to the complete definition and codification of the component method [1-4]. Such a method is essentially based on mechanical models constituted by the assembling of spring elements modelling the joint components. The non-linearity of the joint moment-rotation response is obtained starting from the inelastic constitutive laws adopted for the components. The method is suitable for the modelling of any kind of joint provided that the components are properly identified and their constitutive law is deservedly modelled. After that, it is possible to assemble the components for evaluating the moment-rotation curve of the whole joint so that it results to be characterized in terms of resistance, stiffness and rotational capacity. In this framework [1], the application of the method to structural connections is still limited to a range of cases. In fact, only connections between I or H sections profile are available. In particular, the beam-to-column connections typologies dealt with are:

- fully welded connections;
- end plate connections;
- top and seat angle connections.
- Top and seat angle with single/double web angle connections.

Eurocode 3 [1] provides the rules for calculating the plastic resistance and the initial stiffness for each joint component considered:

- column web panel in shear;
- column web in transverse tension;
- column web in transverse compression;
- column flange in bending;
- end plate in bending;
- flange cleat in bending;
- beam flange and web in compression;
- beam web in tension;
- bolts in shear;
- bolts in tension;
- plates in bearing;
- welds;
- hunched beam.

As an example, in case of bolted end plate connection, the component considered have been reported in Fig.2.1. First of all it is possible to realize that some components are either source of rotational stiffness and flexural resistance, namely the column web panel in shear (*cws*), the column flange in bending (*cfb*), column web in tension (*cwt*), end plate in bending (*epb*), beam web in tension (*bwt*) and bolts in tension (*bt*), and can be modelled by means of simple rigid-plastic model. Conversely, beam flange and web in compression (*bfc*) and column web in tension (*cwt*) have to be considered in the evaluation of of the joint flexural resistance only.

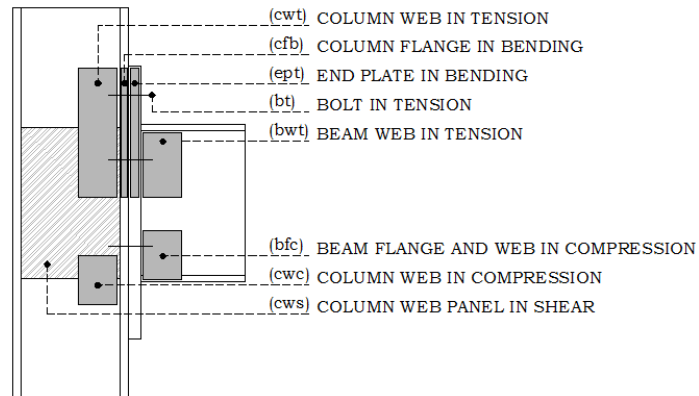


**Fig. 2.1** – Components identification

With reference to the mechanical model reported in Fig. 2.2, assuming pure bending and centre of compression located in correspondence of the axis of the compressed beam flange, the joint resistance is governed by the resistance of the weakest component:

$$F_{Rd} = \min\{F_{cwc,Rd}; F_{cwt,Rd}; F_{cws,Rd}; F_{cfb,Rd}; F_{epb,Rd}; F_{bt,Rd}; F_{bfc,Rd}\} \quad (2.1)$$

where  $F_{Rd}$  is the component minimum resistance.

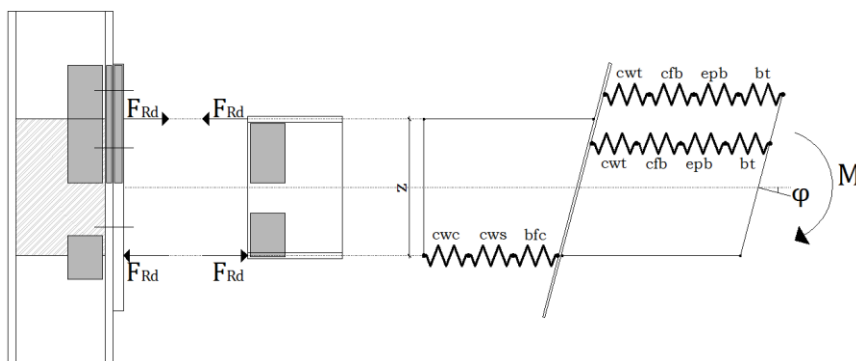


**Fig. 2.2** – Modelling of the of bolted end plate connections

The height of the lever arm, as shown in Table 2.1, depends on the joint typology.

As a consequence, the joint flexural resistance can be determined as follows:

$$M_{j,Rd} = F_{Rd} \cdot z \quad (2.2)$$

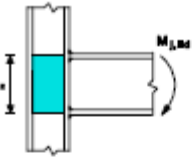
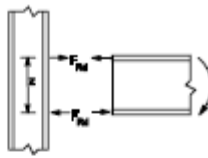
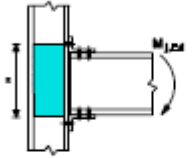
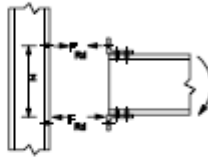
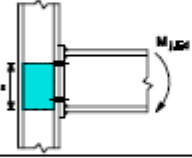
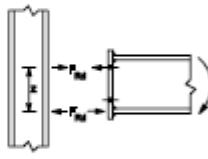
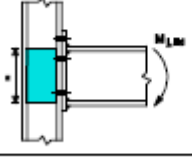
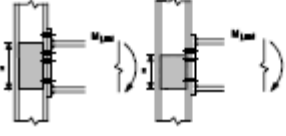
where  $M_{j,Rd}$  is the joint flexural resistance and  $z$  is the lever arm. In a similar way, stiffness can be determined starting from the flexibilities of the basic components, obtaining:

$$S_{j,in} = \frac{E \cdot z^2}{\sum_i \frac{1}{k_i}} \quad (2.3)$$

where  $S_{j,in}$  is the elastic stiffness,  $E$  is the steel Young modulus and  $k_i$  is the stiffness of the  $i$ -th basic component contributing to the bending stiffness.

In conclusion, even though some authors have already investigated some aspects related to the prediction of the plastic deformation capacity [5-8] and of the cyclic behaviour of connections [9-13] past experimental and theoretical researches have often focused their attention mainly on the prediction of the stiffness and resistance of joint components. Therefore, the prediction of the plastic deformation capacity of connections is still an open research field whose primary aim is devoted to the prediction of the plastic rotation capacity of partial strength connections.

**Table 2.1** – Definition of the lever arm

Type of connection	Centre of compression	Lever arm	Force distributions
a) Welded connection 	In line with the mid-thickness of the compression flange	$z = h - t_{fb}$ $h$ is the depth of the connected beam $t_{fb}$ is the thickness of the beam flange	
b) Bolted connection with angle flange cleats 	In line with the mid-thickness of the leg of the angle cleat on the compression flange	Distance from the centre of compression to the bolt-row in tension	
c) Bolted end-plate connection with only one bolt-row active in tension 	In line with the mid-thickness of the compression flange	Distance from the centre of compression to the bolt-row in tension	
d) Bolted extended end-plate connection with only two bolt-rows active in tension 	In line with the mid-thickness of the compression flange	Conservatively $z$ may be taken as the distance from the centre of compression to a point midway between these two bolt-rows	
e) Other bolted end-plate connections with two or more bolt-rows in tension 	In line with the mid-thickness of the compression flange	An approximate value may be obtained by taking the distance from the centre of compression to a point midway between the farthest two bolt-rows in tension	A more accurate value may be determined by taking the lever arm $z$ as equal to $z_{eq}$ obtained using the method given in 6.3.3.1.

## 2.2. Problem of the distribution of the plasticity between joint and beam

The classification of beam-to-column joints as full-strength or as partial-strength is too simplistic, because it is rigorous only in the pure theoretical case in which both the joint that the connected member exhibit a perfectly plastic behaviour. As soon as the distinction between the joint and the connection is made (Fig.2.3), allowing the definition of the joint as the combination in series of the connection and the panel zone of the column web, also the concept of **beam-joint system** becomes noticeable, being constituted by the combination in series of the beam-to-column joint and the beam end.

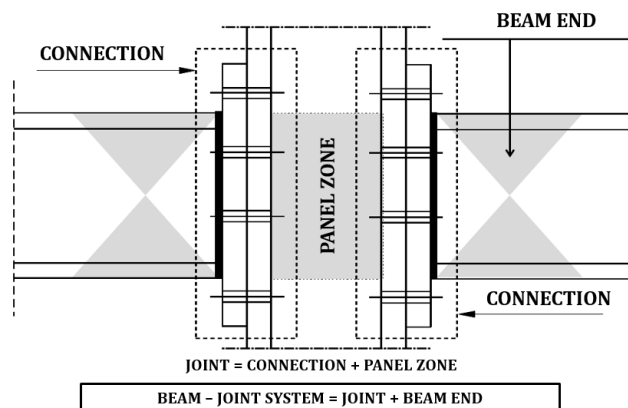


**Fig. 2.3** - Beam-joint system

This concept is of primary importance under the point of view of yielding location and, therefore, for seismic design purposes. This statement can be easily explained considering a tri-linear modelling of the moment-rotation curve of both the beam-to-column joint and the beam end (Fig.2.4). In fact, generally the plastic rotation supply  $\theta_{pu}$  of

the beam-joint system can be regarded as the sum of two contributions: the plastic rotation of the beam-to-column joint  $\varphi_p$  and the plastic rotation provided by the beam end  $\vartheta_p$ . Therefore, an accurate evaluation of the moment-rotation curve of the beam-to-column joint is required, because the plastic rotation provided by the beam end is strictly dependent on the flexural resistance that the beam-to-column joint is able to develop [4].

Concerning beam-to-column joint,  $M_{j,y}$  is the value of the bending moment leading to first yielding,  $M_{j,p}$  is the conventional plastic moment defining the knee of the moment-rotation curve according to Eurocode 3,  $M_{j,u}$  is the theoretical ultimate flexural resistance of the beam-to-column joint. Regarding the beam,  $sM_{pb}$  is the bending moment corresponding to the occurrence of local buckling of the beam compressed flange. The parameter  $s$  is the non-dimensional buckling stress depending on the width-to-thickness ratios of the plate elements constituting the beam section and on the longitudinal stress gradient. Starting from the analysis of the experimental data [14,15], by means of a multiple regression analysis, Mazzolani and Piluso [5] defined the following empirical relationship:

$$s = \frac{1}{0.546 + 1.633\lambda_f^2 + 0.062\lambda_w^2 - 0.602\frac{b_f}{L_e} + 0.001471\frac{E}{E_h} + 0.007766\frac{\varepsilon_h}{\varepsilon_y}} \leq \frac{f_u}{f_y} \quad (2.4)$$

where  $\lambda_f$  and  $\lambda_w$  are, respectively, the normalized slenderness parameters of the flange and of the web equal to:



$$\bar{\lambda}_f = \frac{b_f}{2 t_f} \sqrt{\frac{f_{ym.f}}{E}} \quad \text{and} \quad \bar{\lambda}_w = \frac{d_w}{2 t_w} \sqrt{\frac{f_{ym.w}}{E}} \quad (2.5)$$

where  $b_f$  is the flange width,  $t_f$  is the flange thickness,  $d_w$  is the compressed part of the beam web,  $t_w$  is the web thickness,  $L_e$  is the shear length of the beam,  $E$  is the Young modulus,  $E_h$  is the hardening modulus,  $\varepsilon_y$  is the strain corresponding to yielding and  $\varepsilon_h$  is the strain corresponding to the end of the yield plateau.

Four significant cases can arise [4] (Fig.2.4):

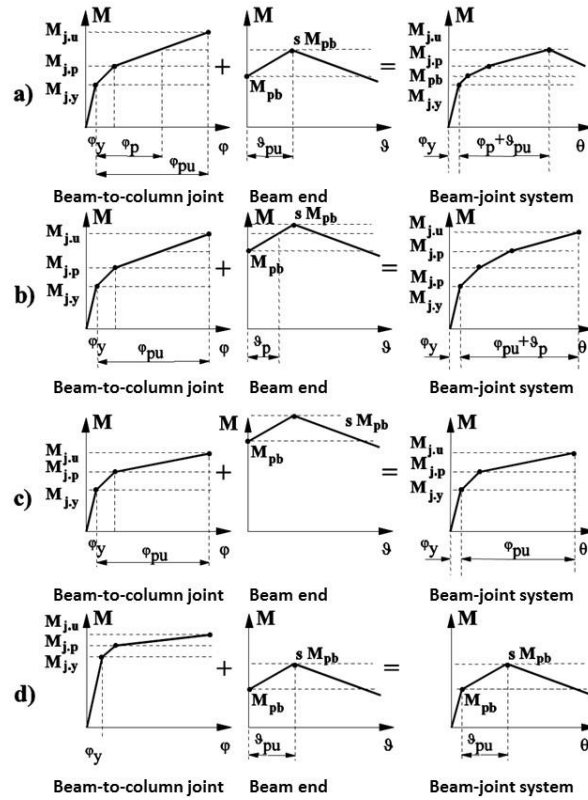


**Fig. 2.4** - Plastic rotation supply of the beam-joint system

$$\text{a) } M_{j,u} \geq s M_{pb}$$

In this case the ultimate resistance of the beam-to-column joint allows the complete exploitation of the beam plastic reserves, so that:

$$\vartheta_p = \vartheta_{pu} \quad \text{and} \quad \varphi_p \leq \varphi_{pu} \quad (2.6)$$

where  $\vartheta_{pu}$  is the ultimate plastic rotation of the beam and  $\varphi_{pu}$  is the theoretical value of the ultimate plastic rotation of the beam-to-column joint.

Therefore, the plastic rotation supply of the beam-joint system is given by the sum of the beam plastic rotation supply and a part, for  $M_{j,u} > s M_{pb}$ , or the total value, for  $M_{j,u} = s M_{pb}$ , of the plastic rotation supply of the beam-to-column joint. As the plastic rotation supply of the beam-joint system is greater than the plastic rotation capacity of the connected beam, the beam-to-column joints can be defined as full-strength full-ductility.

$$\text{b) } M_{pb} \leq M_{j,u} < s M_{pb}$$

In this case, even though the beam end can be engaged in plastic range, the ultimate resistance of the beam-to-column joint is not sufficient to completely exploit the beam plastic reserves, so that:

$$\vartheta_p < \vartheta_{pu} \quad \text{and} \quad \varphi_p = \varphi_{pu} \quad (2.7)$$

Therefore, the plastic rotation supply of the beam-joint system is given by the sum of the plastic rotation supply of the joint and of a part of that of the connected beam. The beam-to-column joint can be defined as full-strength (because  $M_{j,u} > M_{pb}$ ), but cannot be defined “a priori” as

full-ductility, because the plastic rotation capacity of the beam-joint system is strictly dependent on the contribution ( $\varphi_{pu}$ ) due to the beam-to-column joint.

$$c) \quad M_{j,u} \leq M_{pb}$$

In this case, the ultimate resistance of the beam-to-column joint is not sufficient to engage the beam in plastic range, so that:

$$\vartheta_p = 0 \quad \text{and} \quad \varphi_p = \varphi_{pu} \quad (2.8)$$

Therefore, the ultimate plastic rotation of the beam-joint system is coincident with the plastic rotation of the beam-to-column joint. The beam-to-column joint can be defined as partial-strength. Nothing can be said, a priori, about on the degree of restoration of rotation capacity, because the plastic rotation capacity of the beam-joint system is strictly dependent on  $\varphi_{pu}$ .

$$d) \quad M_{j,y} > sM_{pb}$$

In this case, the elastic flexural resistance is sufficient to completely exploit the plastic reserves of the beam, so that:

$$\vartheta_p = \vartheta_{pu} \quad \text{and} \quad \varphi_p = 0 \quad (2.9)$$

Consequently, the plastic rotation of the beam-joint system is equal to the plastic rotation of the beam end. The beam-to-column joint can be referred as full-strength full-ductility. The difference with respect to case a) is that the beam-to-column joint remains in elastic range ( $\varphi_p = 0$ ).

Regarding the evaluation of the plastic rotation of the beam end, simple relations are available in literature [6-9]. In addition, the plastic rotation of the beam-to-column joints can be determined starting to the knowledge of the plastic deformation of each component, through an advanced modelling of their force-displacement law (up to the ultimate displacement). In fact, the plastic displacement occurring at the tensile flange level is equal to the sum of the ultimate displacement of the weakest component and of the contributions of the other components. The resulting plastic rotation is given by the ratio of that such plastic displacement and the level arm [4].

### 2.3. Full strength joints

The seismic design of beam-to-column joints is traditionally aimed to assure that yielding occurs at the beam ends of the connected beam where the dissipation of the earthquake input energy is expected relying on wide and stable hysteresis loops. To this aim, Eurocode 8 [10] requires that the degree of overstrength required is guaranteed in case of full penetration butt welds or satisfying, in case of other joint typologies, the following relationship:

$$M_{j,Rd} > 1.1 \cdot \gamma_{ov} \cdot M_{b,Rd} \quad (2.10)$$

where  $M_{j,Rd}$  represents the joint design resistance,  $M_{b,Rd}$  the plastic moment of the connected beam and  $\gamma_{ov}$  is an overstrength factor accounting for the random variability of the steel yield strength, while the coefficient 1.1 covers the effects of material strain hardening. Eurocode 8 recommends the use of  $\gamma_{ov} = 1.25$ ; conversely, the Italian

code [23] suggests a joint overstrength coefficient depending on the steel grade ( $\gamma_{ov} = 1.20$  for S235,  $\gamma_{ov} = 1.15$  for S275 and  $\gamma_{ov} = 1.10$  for S355).

One of the causes of significant and premature joint damage during the seismic events of Northridge and Kobe can be recognised in the use of design criteria not able to assure a sufficient degree of overstrength to allow the full development of the beam plastic rotation capacity. In fact, regarding the overstrength which the beam is able to exhibit, due to strain hardening, it depends on the width-to-thickness ratios of flanges and web. As a consequence, the joint overstrength needed to assure the full-strength requirement is strictly related to the behavioural class of the beam section (i.e. ductile, compact, semi-compact and slender). It means that, decreasing the width-to-thickness ratios of flanges and web, the plastic deformation capacity of the beam increases, but this beneficial effect could be vanished if the beam-to-column joint does not possess the overstrength required by the simultaneous increase of the beam ultimate resistance. In addition, also the influence of random material variability both on the beam flexural resistance and the beam-to-column joint moment resistance has to be properly accounted for.

Only a few studies concerning the influence of random material variability on the behaviour of steel connections are available [12-15]. In particular, it has been proposed [12] to formulate the design requirement for full-strength and full-ductility joints by means of a probabilistic approach calibrated on the basis of the results coming from Monte Carlo simulations [16], including both the random material variability of the plate elements and that of bolt properties [17].

A simplified approach to account for the influence of random material variability is herein proposed by assuming an overstrength factor

$\gamma_{ov,rm}$  equal to the ratio between the average value of the yield strength of beam flanges  $f_{ym,bf}$  and the nominal yield strength  $f_{y,b}$ . Conversely, the amount of overstrength due to the development of strain-hardening up to the occurrence of local buckling is taken into account directly considering the width-to-thickness ratios of beam flanges and web. Therefore, the ultimate beam flexural resistance at the plastic hinge location is evaluated as [18]:

$$M_{b,u} = \gamma_{ov,rm} \cdot \gamma_{ov,sh} \cdot \gamma_{M0} \cdot M_{b,p} \quad (2.11)$$

where:

$$M_{b,p} = \frac{Z_b \cdot f_{y,b}}{\gamma_{M0}} \quad (2.12)$$

being  $Z_b$  the plastic modulus of the beam section and  $\gamma_{M0}$  the partial safety factor.

The average yield strength of beam flanges is evaluated accounting for the influence of the flange thickness  $t_{bf}$ , so that:

$$\gamma_{ov,rm} = \frac{f_{ym,bf}}{f_{y,b}} = \frac{f_0 - \beta t_{bf}}{f_{y,b}} \quad (2.13)$$

where the parameters  $f_0$  and  $\beta$  depend on the steel grade (Table 2.2).

**Table 2.2** - Mechanical properties of the material

<b>Steel classes</b>	<b><math>f_0</math></b>	<b><math>\beta</math></b>
	<b>[MPa]</b>	<b>[MPa/mm]</b>
<b>S 235</b>	313.4	2.254
<b>S 275</b>	323.3	0.910
<b>S 355</b>	444.2	2.987

The coefficient  $\gamma_{ov,sh}$  accounting for the influence of strain hardening is given by  $\gamma_{ov,sh} = s$  [5], where  $s$  is the parameter given by Eq. (2.4).

#### **2.4.1. Design procedure**

Starting from the average ultimate resistance of the beam provided by Eq. (2.8), a design procedure aiming to the development of full-strength full-ductility joints is proposed and discussed with reference to extended end-plate joints with four bolts in tension. The end-plate is unstiffened. The design goal is accomplished by properly applying the basic principles of "capacity design" at component level, considering all the joint components defined by Eurocode 3 within the framework of the "component method".

In particular, the proposed procedure starts from the identification of the maximum internal actions which the fully yielded and strain-hardened beam is able to transmit to the joint. The reference structural scheme is depicted in Fig. 2.5.

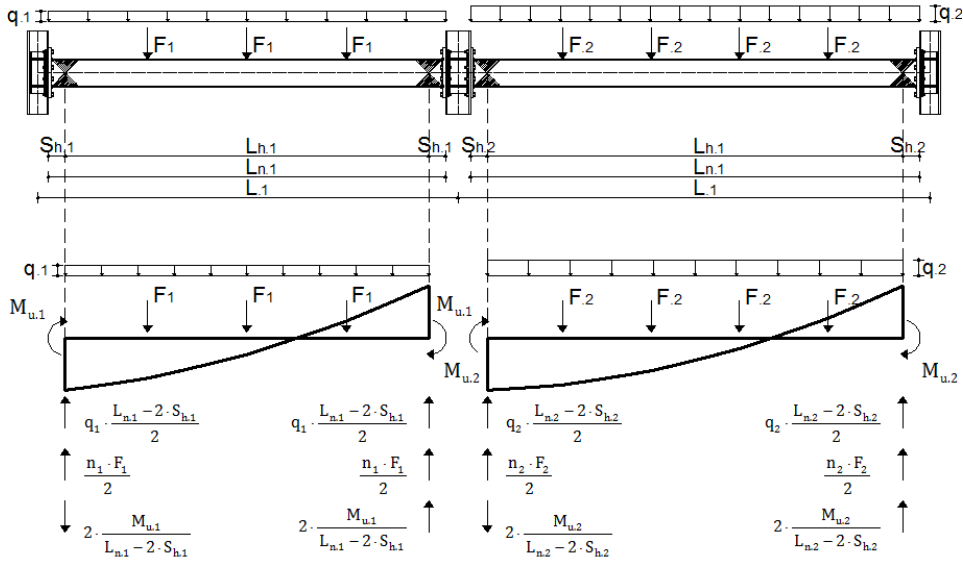


**Fig. 2.5** - Reference structural scheme considering seismic actions from left to right

By denoting with  $i$  the left end joint and with  $j$  the right end joint for each beam and considering seismic actions from left to right, the shear action occurring at the plastic hinge locations are given by:

$$\begin{aligned}
 V_{bu,i}^{(1)} &= \frac{q_1 L_{h1}}{2} + \frac{n_{F1} F_1}{2} - \frac{2 M_{bu,1}}{L_{h1}} & V_{bu,j}^{(1)} &= \frac{q_1 L_{h1}}{2} + \frac{n_{F1} F_1}{2} + \frac{2 M_{bu,1}}{L_{h1}} \\
 V_{bu,i}^{(2)} &= \frac{q_2 L_{h2}}{2} + \frac{n_{F2} F_2}{2} - \frac{2 M_{bu,2}}{L_{h2}} & V_{bu,j}^{(2)} &= \frac{q_2 L_{h2}}{2} + \frac{n_{F2} F_2}{2} + \frac{2 M_{bu,2}}{L_{h2}}
 \end{aligned}
 \tag{2.14}$$

where the vertical loads are those occurring in the seismic load combination ( $G_k + \psi_2 Q_k$ ) according to Eurocode 8,  $L_h$  is the distance between the two plastic hinges,  $F$  are the concentrated forces due to the secondary beams and  $n_F$  is the number of these forces. The parameter



$s_h$ , i.e. the distance between the plastic hinge and the column flange, is taken equal to the beam height.

On the basis of the maximum moment which the beams are able to transmit given by Eq. (2.11), the bending moment  $M_{cf}$  and shear action  $V_{cf}$  at the column flange can be evaluated as follows:

- in the case of external joint  $i$  of beam 1:

$$M_{cf,i}^{(1)} = M_{bu,1} - V_{bu,i}^{(1)} \cdot s_{h1} - \frac{q_1 s_{h1}^2}{2} \quad V_{cf,i}^{(1)} = V_{bu,i}^{(1)} + q_1 s_{h1} \quad (2.15)$$

- in the case of internal joint  $j$  of beam 1:

$$M_{cf,j}^{(1)} = M_{bu,1} + V_{bu,i}^{(1)} \cdot s_{h1} + \frac{q_1 s_{h1}^2}{2} \quad V_{cf,j}^{(1)} = V_{bu,i}^{(1)} + q_1 s_{h1} \quad (2.16)$$

- in the case of internal joint  $i$  of beam 2:

$$M_{cf,i}^{(2)} = M_{bu,2} - V_{bu,i}^{(2)} \cdot s_{h2} - \frac{q_2 s_{h2}^2}{2} \quad V_{cf,i}^{(2)} = V_{bu,i}^{(2)} + q_2 s_{h2} \quad (2.17)$$

- in the case of external joint  $j$  of beam 2:

$$M_{cf,j}^{(2)} = M_{bu,2} + V_{bu,i}^{(2)} \cdot s_{h2} + \frac{q_2 s_{h2}^2}{2} \quad V_{cf,j}^{(2)} = V_{bu,i}^{(2)} + q_2 s_{h2} \quad (2.18)$$

Obviously, the analysis is repeated for the case of seismic actions from left to right and the most severe internal actions are considered.

Regarding the design of column web panel stiffeners, they have to be designed considering the maximum shear action occurring when the beams are in the ultimate conditions.

- In the case of panel zone of external joint i of first bay:

$$V_{wp.Ed} = \frac{M_{cf.i}^{(1)}}{d_{b1} - t_{bf,1}} - \frac{V_{c1} + V_{c2}}{2} \quad (2.19)$$

- In the case of panel zone of internal joint:

$$V_{wp.Ed} = \frac{M_{cf,j}^{(1)}}{d_{b1} - t_{bf,1}} + \frac{M_{cf,i}^{(2)}}{d_{b2} - t_{bf,2}} - \frac{V_{c1} + V_{c2}}{2} \quad (2.20)$$

- For the external panel zone j of the beam 2:

$$V_{wp.Ed} = \frac{M_{cf,j}^{(2)}}{d_{b2} - t_{bf,2}} - \frac{V_{c1} + V_{c2}}{2} \quad (2.21)$$

In the case of extended end plate connections with four bolts in tension, according to Eurocode 3, a simplified model can be adopted to design the tension zone by means on an equivalent T-stub whose lever arm is equal to  $d_b - t_{bf}$  (Fig.2.6).

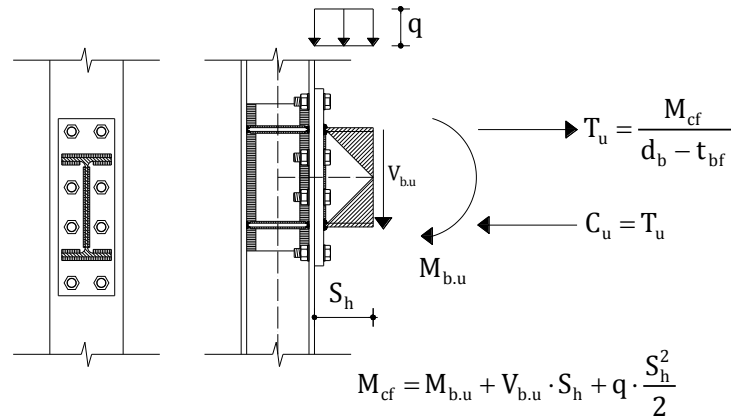


**Fig. 2.6** - Simplified model for the design of the tension zone

According to this model, the design of all the joint components has to guarantee the transmission, at the beam flanges' levels, of a compression force  $C_u$  and of a tensile force  $T_u$  given by:

$$T_u = C_u = \frac{M_{cf}}{d_b - t_{bf}} \quad (2.22)$$

Starting from the knowledge of  $T_u$  and  $C_u$  values occurring when the beam plastic hinges have attained their ultimate flexural resistance, all the geometrical details of the connecting elements can be designed by means of the resistance formulations provided by Eurocode 3 for the joint components. To this aim, a specific sequence of design operations or resistance checks of the joint components has to be followed:

**Step 1:** Evaluation, by means of Eq. (2.11), of the average (because of random material variability) ultimate moment  $M_{b,u}$  which the fully yielded and strain-hardened beam is able to transmit.

**Step 2:** Calculation of bending moment  $M_{cf}$  and shear action  $V_{cf}$  at the column flange and evaluation of compression force  $C_u$  and tensile force  $T_u$  to be transmitted at the beam flanges' levels.

**Step 3:** Design of the bolt diameter accounting for the combined action of shear and tension.

**Step 4:** Design of throat thickness of welds connecting the end-plate to the beam flange and design of throat thickness of welds connecting the end-plate to the beam web assuming that they have to transmit a bending moment proportional to the plastic modulus of the beam web alone.

**Step 5:** Design of the end-plate thickness according by modelling the tension zone by means of an equivalent T-stub and assuming that the distance  $m$  between the bolt axis and the yield line located close to the beam flange is equal to the minimum allowed by the code,  $m=1.2 d_o$  with  $d_o$  equal to the diameter of the hole; the width of the end-plate can be defined considering code requirements concerning the bolt spacing and the edge distances.

**Step 6:** Check of the resistance of the column web in shear and design of supplementary web plates if needed. Eurocode 3 introduces a limitation about the thickness of the supplementary plates. In particular, the shear area  $A_{vc}$  may be increased no more than  $b_{st_{wc}}$ . If a further supplementary web plate is added on the other side of the web, no further increase of the shear area is allowed. The proposed method does not take into account such limitation.

**Step 7:** Check of the resistance of the column web in tension and in compression; if needed continuity plates are added and/or

supplementary web plates are extended to cover also tension and compression zones.

**Step 8:** Check of the resistance of the column flange in bending; if not satisfied, backing plates can be adopted to increase the resistance of the equivalent T-stub modelling the column flange in bending, provided that type 1 mechanism occurs, otherwise (type 2 mechanism) the increase of the bolt diameter is needed and the procedure has to be repeated starting from step 3.

In order to show in detail the design procedure, a worked example has been reported in Annex A.

#### 2.4.2. Validation of the procedure with FEM simulations

Reference is made to the building plan layout depicted in Fig. 2.7.

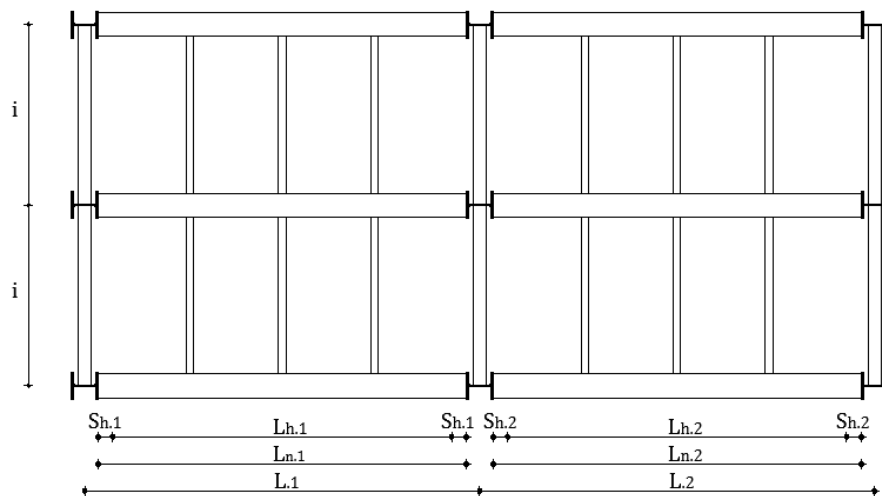


**Fig. 2.7** - Building plan layout of study cases

Three different solutions have been designed with reference to the external joint of the longitudinal inner frame by varying the geometry of the structure. In Table 2.3, the input data for the three cases analysed are reported.

**Table 2.3** - Input data of study cases

	<b>Study case A</b>	<b>Study case B</b>	<b>Study case C</b>
<b>Beam section</b>	IPE 600	IPE450	IPE220
<b>Column section</b>	HE 320M	HE 260 M	HE 200 M
<b>Beam steel grade</b>	S235	S235	S235
<b>Column steel grade</b>	S355	S355	S355
<b>Plate steel grade</b>	S275	S275	S275
<b>Bolt class</b>	10.9	10.9	10.9
<b><math>q</math> [kN/m]</b>	1.25	1.00	0.75
<b><math>F</math> [kN]</b>	65.00	45.00	30.00
<b><math>n_F</math></b>	3	3	3
<b><math>L_n</math> [mm]</b>	8641.00	6332.00	3800.00

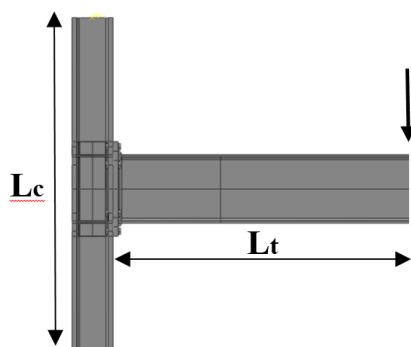
For the three study cases, the results of the proposed design procedure are summarized in Table 2.4. Moreover, in the same table also the results obtained by applying the design rules suggested by Eurocode 8 are presented.

It can be observed that the most important difference occurs for study case C, i.e. in the case of the smallest beam section, where the design bending moment according to the proposed design procedure is about 36.4% greater than the one required according to Eurocode 8. This difference reduces to 26.5% for study case B and to 23.6% for study case A.

**Table 2.4** - Design solutions for analysed study cases

	<b>Study case A</b>		<b>Study case B</b>		<b>Study case C</b>	
	<b>Proposal approach</b>	<b>Eurocode8 approach</b>	<b>Proposal approach</b>	<b>Eurocode8 approach</b>	<b>Proposal approach</b>	<b>Eurocode8 approach</b>
$\gamma_{ov,rm}$	1.15	1.25	1.24	1.25	1.25	1.25
$\gamma_{ov,sh}$	1.28	1.10	1.26	1.10	1.30	1.10
$M_{cf}[kNm]$	1336	1081	663	524	120	88
$V_{cf}[kN]$	405	353	278	239	107	93
$T_u[kN]$	2299	1860	1524	1203	571	417
$d_b[mm]$	36	33	30	27	20	16
$a_f[mm]$	29	23	22	18	14	11
$a_w[mm]$	10	10	9	8	6	5
$t_{ep}[mm]$	55	45	45	35	25	20
$t_s[mm]$	5	-	5	-	5	-
$t_{cp}[mm]$	20	20	15	15	10	10
$a_{cp}[mm]$	8	8	6	6	4	4
$F_{(Rd.1)}/T_u$	2.79	3.56	2.94	3.73	1.67	2.29
$F_{(Rd.2)}/T_u$	1.18	1.39	1.22	1.41	1.03	1.08

In order to investigate the accuracy of the proposed design criteria, numerical simulations by means of advanced finite element models have been performed using ABAQUS 6.13 software.

**Fig. 2.8** - Analysed structural scheme

Since the behaviour of the analysed connections is strongly affected by in-plane and out-of-plane deformations, by contacts between the connecting elements and the profiles of column and beam and by geometrical and material non linearities, the finite element model has been developed adopting a three-dimensional approach based on the following steps: geometrical characterization of the components, definition of material properties, definition of the interactions between the elements, definition of the boundary conditions and choice of the elements and size of the mesh, calibration and application of a proper initial imperfection model. The simulation has been performed considering the scheme depicted in Fig. 2.8, restrained with an hinge at the bottom end of the column and a simple horizontal support at the top end of the column.

The beam end is loaded with a vertical force aiming to provide an internal action distribution similar to that arising under seismic actions. To this aim, the length of the beam has been assumed equal to  $M_{cf}/V_{cf}$ , thus assuring that when the design bending resistance is attained also the corresponding shear action is reached. The length of the column has been assumed equal to 3500 mm, i.e. the interstorey height of the sample building.

Regarding the **geometrical definition** of the components, the model is made up of seven repetitive elements: the column, the beam, the end plate, the bolts, the continuity plates and the additional supplementary web plates (Fig. 2.9).



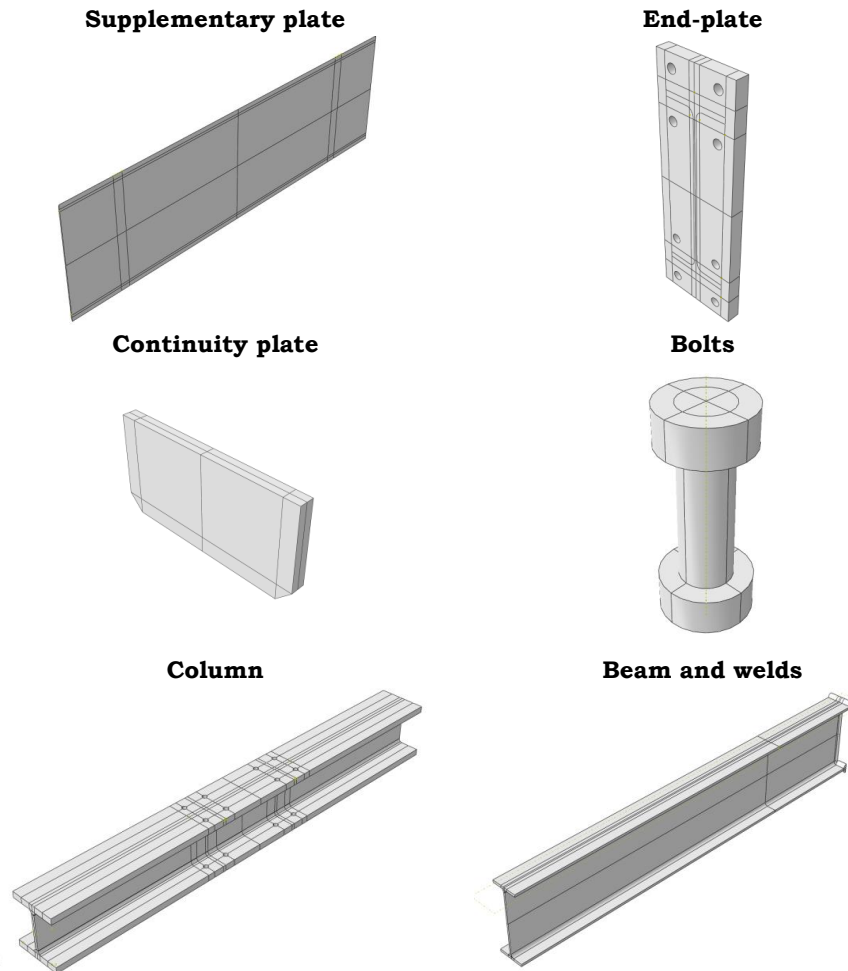


**Fig. 2.9** - Components of the finite element model

The **material properties** of the plate elements and of the profiles have been described by means of an elastic-plastic isotropic model by adopting a quadrilinear true stress-true strain law (Fig. 2.10a). The parameters for different constructional steels are given in Table 2.2.

The behaviour of the material of the bolts has been modelled using a simplified tri-linear model (Fig. 2.10b) based on the yield and ultimate nominal strength according to the bolt class. The strain corresponding to the ultimate resistance and the ultimate strain have been evaluated by means of the following relationships:  $\varepsilon_m = A_r [\%]$  and  $\varepsilon_u = \ln(1/1-Z)$ , where  $A_r$  is elongation at fracture and  $Z$  is the necking ratio given by the ratio between the original cross-sectional area and the minimum cross-sectional area after fracture.

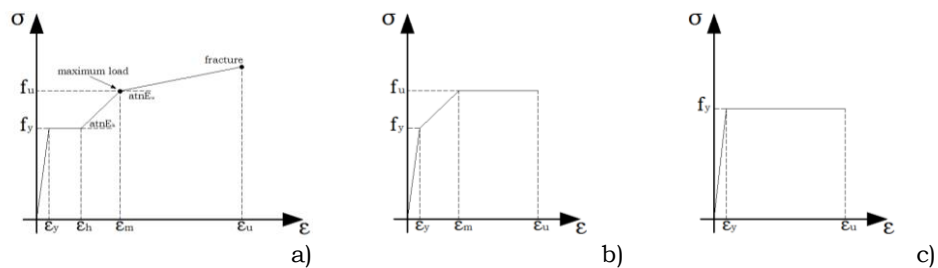


**Fig. 2.10** - Material constitutive laws: a) plates and profiles; b) bolts; c) welds

The values provided by the manufacturer [19] have been adopted. The welds have modelled by means of a bilinear elastic-perfectly plastic law (Fig. 2.10c) with yield strength and ultimate strain defined according to [20]. Regarding the value of the yield strength of all the components, consistently with the design approach which accounts the influence of random material variability considering the average yield strength of the beam flanges, the average value of the yield strength has been adopted for the beam component, while for all others components the nominal characteristic value has been assumed.

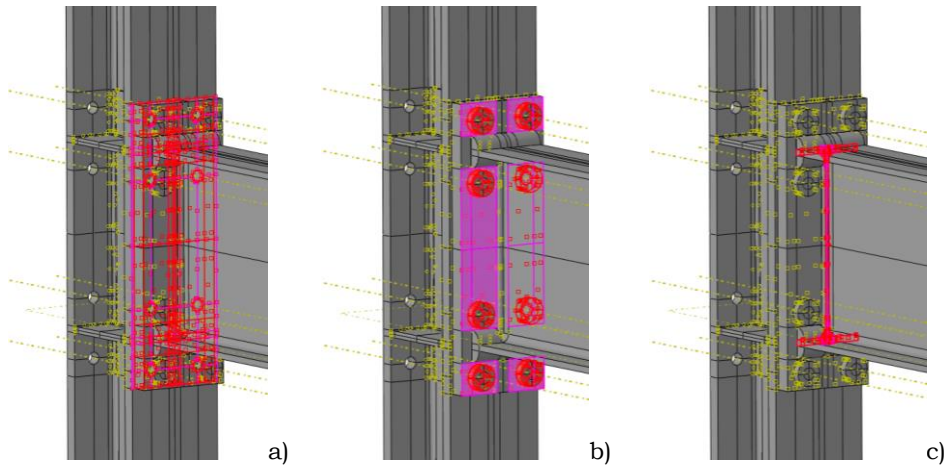


**Fig. 2.11** - Definition of the contacts:

a) end-plate/colum flange; b) bolt head/end-plate; c) end-plate/beam end.

All the **interactions** between the different elements have been defined using the surface-to-surface contact formulation with finite sliding. In particular, the following interactions have been defined (Fig. 2.11): between the end-plate and the column flange, between the bolt head and the end-plate, between the bolt shank and the plate hole, between the bolt shank and the column flange hole, between the end-plate and the beam end. In the normal direction a “hard contact” has been used, while in the tangential direction a friction coefficient equal to 0.20 has been adopted. The latter value of the friction coefficient is provided by Eurocode 3 [1] in case of friction surfaces of class D (surfaces as rolled). Where there was the need to link the rigid kinematic mechanisms of the section to those of a point externally restrained, the constraints have been modelled by introducing at the end of the section of the members a central node and "coupling internal constraints" (Fig. 2.11a).

In order to simulate the application of an axial force, at the top of the column an external pressure equal to 30% of the yield strength of the material has been applied (Fig. 2.11b).

Regarding the **finite element type**, in order to reduce the computational efforts, eight-node brick elements with reduced integration and first order approximation (C3D8R) have been adopted. The end part of the beam close to the column where local buckling phenomena are expected, for a length equal to 2.5 times the beam height, has been modelled with non linear eight-node brick elements with full integration (C3D8). Such elements, as also reported in [21], are particularly accurate for analysis where buckling effects are significant.

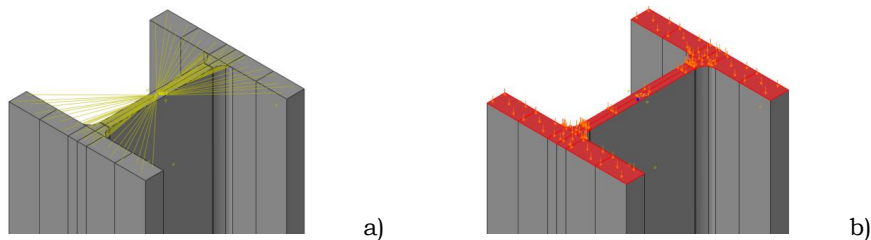


**Fig. 2.12** - a) Coupling internal constraints; b) application of external pressure

Preliminarily, a sensitivity analysis has been performed in order to determine the **mesh dimension**. The parameters that could influence the results are the number of the elements in the thickness of the plates, the dimension of the mesh of the bolts and the dimension of the elements where the local buckling is expected. In order to obtain accurate results, the following “meshing” procedure has been applied: where local buckling is expected the maximum dimension of the elements has been taken as 20 mm, the plates with elements whose dimension is at least 30 mm and with 2 elements in the thickness, the

bolts have been divided using elements with minimum dimension equal to 6 mm with a deviation factor equal to 0.1.

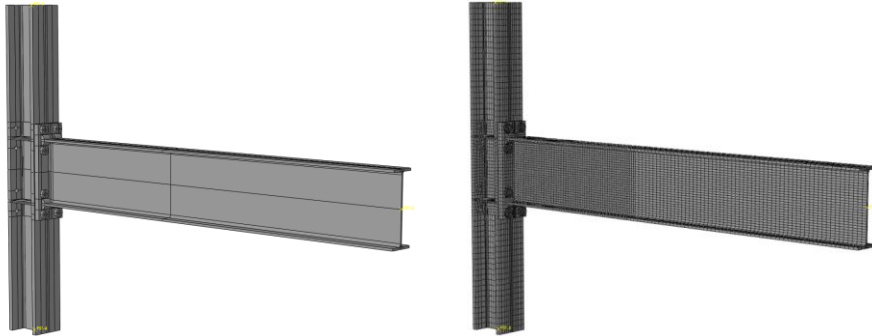


**Fig. 2.13** - ABAQUS Model

In addition, **geometrical imperfections** have been introduced according to the requirements of EN10034, by using a distorted shape of the joint similar to the 1st buckling mode preliminarily evaluated by means of an elastic buckling analysis. The calibration of the distortion of the model has been performed based on the maximum value of the angular distortion of the flanges of steel profiles given by EN 1090-2. The model finalized to the execution of the “linear buckling analysis” is depicted in Fig. 2.13.

The results of the buckling analyses are reported in Fig. 2.14 representing the first four buckling modes. In particular, because of the application of the load downwards, the first and the third buckling mode involve the combined buckling of the bottom flange and the compressed part of the web. Similarly, the second and the fourth mode provide the buckling of the upper flange of the profile when the load is applied upward. Therefore, as the analyses developed in this paper are referred to monotonic downward loading conditions, an imperfection pattern proportional to first buckling mode has been introduced.

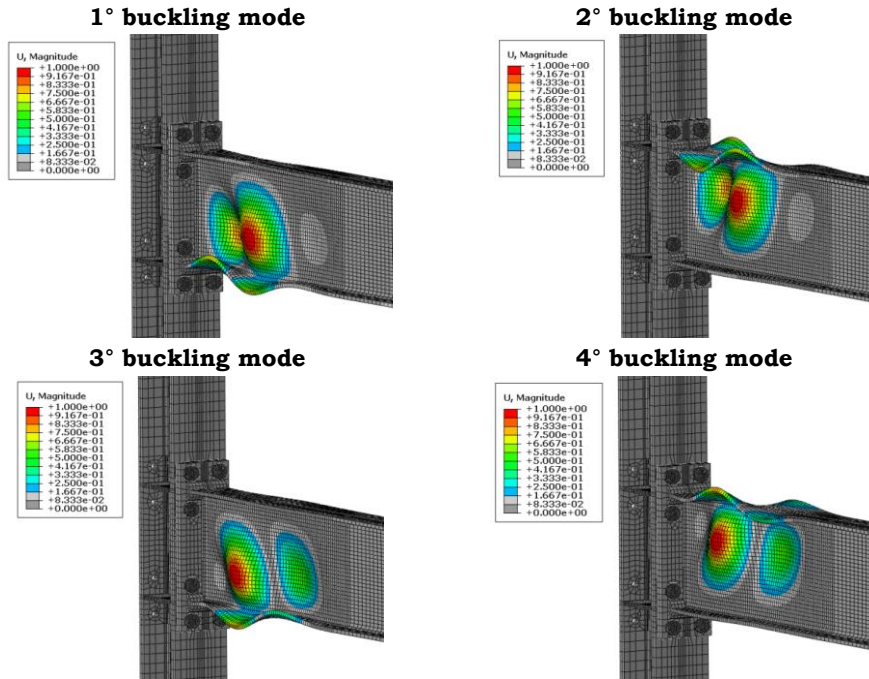


**Fig. 2.14** - Buckling modes of beam-to-column joints

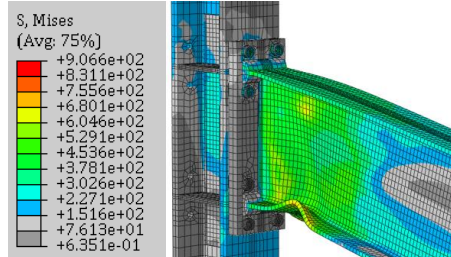
Following this approach, the proportionality coefficient  $k_{(1^{\circ}\text{mode})}$  for scaling the "buckling eigenmode" has been determined as the ratio between the 80% [22] of the maximum manufacturing tolerance (equal to 2% of the width of the flange [23]) and the sum of the beam flange tip displacements  $\delta_f$  in the buckled configuration:

$$k_{1^{\circ}\text{mode}} = \frac{0.8 \times 0.02 \times b_f}{2 \times \delta_f} \quad (2.23)$$

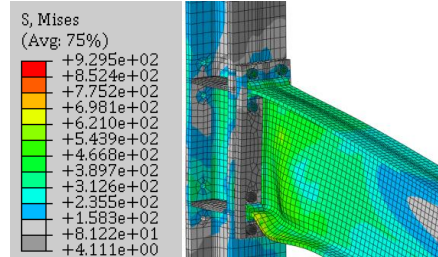
According to the design criteria adopted, it is expected that plastic deformations are mainly located at the beam end.

**STUDY CASE A: IPE 600 BEAM – HEM 320 COLUMN**

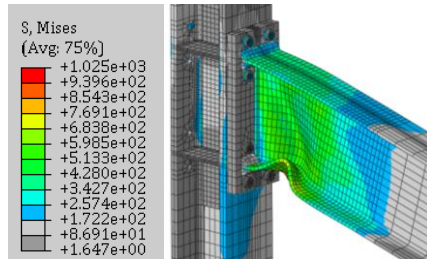
Proposed design approach



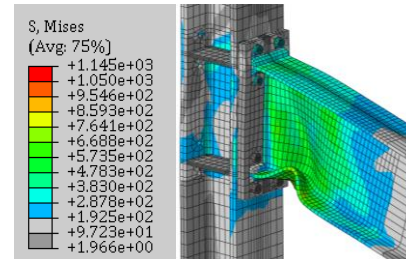
Eurocode 8 design approach

**STUDY CASE B: IPE 450 BEAM – HEM 260 COLUMN**

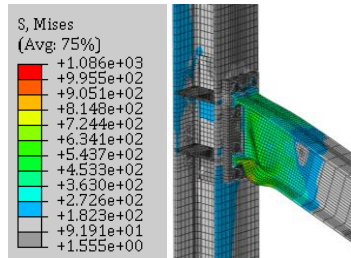
Proposed design approach



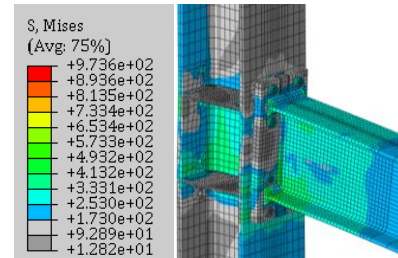
Eurocode 8 design approach

**STUDY CASE C: IPE 220 BEAM – HEM 200 COLUMN**

Proposed design approach



Eurocode 8 design approach

**Fig. 2.15** - Ultimate behaviour of the analysed joints ( Von Mises stresses)

Conversely, the connection components are expected to be subjected to very limited yielding. In fact, it should be noted that, even if the joints have been designed to attain full strength, limited yielding of joint components has to be expected because the formulas used for design,

as suggested by Eurocode 3, are based on the definition of design plastic resistances rather than on elastic design resistances.

From the overall point of view, as expected, FE analyses showed the concentration of the plastic deformations at the beam end with the attainment of a plastic hinge characterized by the development of plastic local buckling of the compressed beam flange, accompanied by the out-of-plane buckling of the compressed part of the web.

The moment-rotation curves of the beam-joint system for all the analysed cases are represented in Figs. 2.16-2.18. The curves have been obtained, in all cases, by multiplying the force applied at the end of the cantilever for  $L_t$  (Fig.2.8) and dividing the displacement evaluated in the same point for the same length.

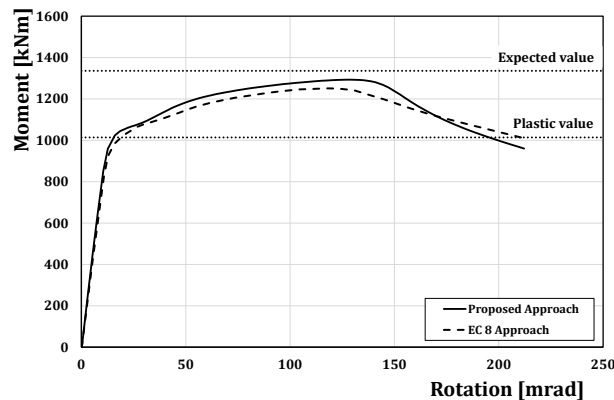


**Fig. 2.16** - Moment-rotation curves (case A)

The curves reported in Fig. 2.16 are referred to the CASE A. As expected, after the initial linear behaviour, at the attainment of the plastic resistance of the section, they provide a non-linear response characterized by an initial increase of the bending moment, due to the



material strain-hardening of the section, which continues up to the attainment of the action which gives rise to the local instability of the beam compressed flange. After the achievement of the maximum bending moment the beam flange starts to buckle providing in terms of moment-rotation response a softening branch. In the two cases (EC8 and proposed procedure), as it is possible to check easily from the figure, the values are very similar and, in particular, equal to 1293 kNm and 1251 kNm. These values are a little bit lower than the design value, evaluated at the column flange level, equal to 1336 kNm.

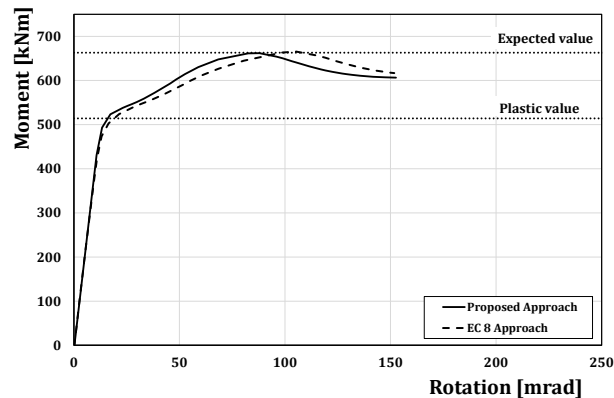


**Fig. 2.17** - Moment-rotation curves (case B)

With reference to the case study B, the shape of the moment-rotation curve is analogous to the previous case and the values of the moment corresponding to the achievement of the local buckling of the beam flange are equal to 662 kNm and 666 kNm in case of the joint designed according to the proposed approach and to Eurocode 8 respectively. These values of the bending moment are practically equal to the

adopted design value (663 kNm) confirming the accuracy of the equations used to predict the overstrength factor  $s$  (Fig. 2.17).

Similarly, in the study case C (Fig. 2.18) the local buckling is achieved in correspondence of a bending moment equal to 115 kNm and 113 kNm respectively in case of the joint designed according to the proposed approach and Eurocode8, that is lower (about 7% in the first case and 8% in the second) than the design value that is equal to 123 kNm

In this case, in terms of rotations, the joint designed according to the Eurocode 8 shows a lower value of the ultimate rotation (131 mrad) while, on the contrary, in case of the joint designed according to the proposed procedure, the ultimate rotation is higher. This difference is due to the brittle failure of the bolts connecting the endplate to the column flange.

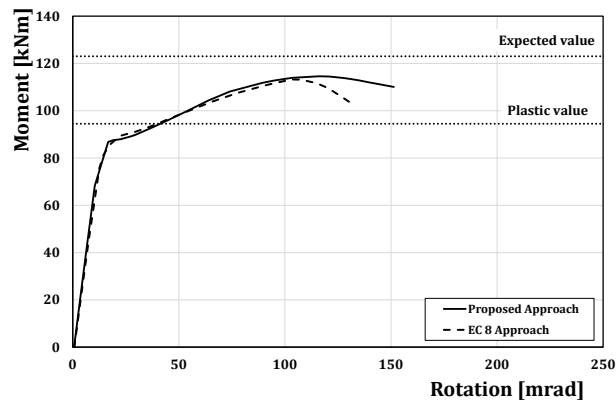


**Fig. 2.18** - Moment-rotation curves (case C)

Therefore, as a conclusion, in terms of global behaviour the comparison between the moment-rotation curves of the joints designed according to the proposed procedure with those designed according to the EC8

provisions are not very different, made exception for case study C where the bolt failure activates, limiting significantly the rotation capacity of the beam-joint system. Such a brittle behaviour, which should not even be in the basic philosophy of EC8, is due to the fact that in many cases, the actual overstrength of the connected member is substantially underestimated by EC8 (as reported in the 4th column of Table 3) and therefore it may happen that the maximum resistance of the beam is such that the bolts' resistance is exceeded even though they are usually oversized adopting a safety factor equal to 1.25.

In any case, due to the fact that the EC8 procedure for connections is not completely rationally addressed, aside from the possible activation of undesired failure modes, it also happens that, in many cases, the plastic engagement of the joint components is significant, meaning that in case of severe seismic events a reparation of many parts of the connection has to be accounted for. Conversely, with the proposed procedure, as far as the beam overstrength is more rationally considered in the design phase, all the joint components are sized for actions which, at most, can achieve the plastic resistance, with a consequent negligible plastic engagement. In order to quantify the damage of the joints' components, a parameter NPPEEQ defined as the ratio between the equivalent plastic deformation (PEEQ) evaluated at the achievement of the rotational capacity of the beam-joint system (i.e. in correspondence of the point on the softening branch where the plastic moment of the beam is achieved) and the elastic deformation has been considered as a measure of damage. To this scope, all the components have been isolated and the corresponding deformation maps have been tracked in order to determine the value of the

equivalent plastic deformation summarized in the Tables 2.5, 2.6 and 2.7.

With reference to the case study A (IPE 600 beam and HEM 320 column), the results provided in Tab. 2.5 evidence that the level of yielding occurring in connection components is very limited when the beam-to-column joint is designed according to the proposed procedure, achieving a maximum value of 5.57 in the welds; conversely, the use of Eurocode 8 design criteria leads to a normalised PEEQ equal to 63.44 in the bolts and 38.46 in the welds.

**Table 2.5** - Damage to joint components expressed as PEEQ and NPEEQ (NPEEQ=PEEQ/ $\epsilon_y$ ) – study case A

	<b>Study case A</b>			
	<b>Proposal approach</b>		<b>Eurocode8 approach</b>	
	<b>PEEQ</b>	<b>NPEEQ</b>	<b>PEEQ</b>	<b>NPEEQ</b>
<b>Beam</b>	0.3577	319.65	0.3577	319.65
<b>Welds</b>	0.0101	<b>5.57</b>	0.0696	<b>38.46</b>
<b>End-Plate</b>	0.0016	1.25	0.0205	15.68
<b>Column</b>	0.0062	3.65	0.0260	15.35
<b>Supplementary plate</b>	0.0007	0.43	-	-
<b>Bolts</b>	0.0177	4.12	0.2719	<b>63.44</b>
<b>Continuity plate</b>	0.0000	0.00	0.0000	0.00

Even in the case study B (IPE 450 beam and HEM 260 column), the maximum normalized PEEQ (Table 2.6) occurs in the welds and is equal to 5.53 for the proposed design procedure while in case of Eurocode 8 the yielding achieves maximum values of normalised PEEQs equal to 23.82 and 21.49 in the bolts and in the welds respectively.

**Table 2.6** - Damage to joint components expressed as PEEQ and NPEEQ  
(NPEEQ=PEEQ/ $\epsilon_y$ ) – study case B

	<b>Study case B</b>			
	<b>Proposal approach</b>		<b>Eurocode8 approach</b>	
	<b>PEEQ</b>	<b>NPEEQ</b>	<b>PEEQ</b>	<b>NPEEQ</b>
<b>Beam</b>	0.8000	714.89	0.9600	857.87
<b>Welds</b>	0.0100	<b>5.53</b>	0.0431	<b>23.82</b>
<b>End-Plate</b>	0.0070	5.35	0.0180	13.75
<b>Column</b>	0.0061	3.61	0.0270	15.97
<b>Supplementary plate</b>	0.0010	0.59	-	-
<b>Bolts</b>	0.0116	2.71	0.0921	<b>21.49</b>
<b>Continuity plate</b>	0.0000	0.00	0.0000	0.00

Finally, in case study C (IPE 220 beam and HEM 200 column), the maximum normalized PEEQs (Table 2.7) in the joint components occur in the welds and is equal to 41.78 in the case of the proposed design procedure while in case of Eurocode 8 occurs in the bolts in tension and is equal to 117.90. Also in this case damage is highly concentrated at the end of the connected beam even though the bolts achieve their ultimate capacity in case of the joint designed according to Eurocode 8.

**Table 2.7** - Damage to joint components expressed as PEEQ and NPEEQ  
(NPEEQ=PEEQ/ $\epsilon_y$ ) – study case C

	<b>Study case B</b>			
	<b>Proposal approach</b>		<b>Eurocode8 approach</b>	
	<b>PEEQ</b>	<b>NPEEQ</b>	<b>PEEQ</b>	<b>NPEEQ</b>
<b>Beam</b>	0.9665	863.68	0.1902	169.97
<b>Welds</b>	0.0756	<b>41.78</b>	0.0540	<b>29.84</b>
<b>End-Plate</b>	0.0016	1.22	0.0231	17.64
<b>Column</b>	0.0041	2.43	0.0370	<b>21.89</b>
<b>Supplementary plate</b>	0.0016	0.95	-	-
<b>Bolts</b>	0.0012	0.28	0.5053	<b>117.90</b>
<b>Continuity plate</b>	0.0000	0.00	0.0037	2.83

In conclusion, the results obtained have confirmed the accuracy of the design approach evidencing, in the same time, some criticisms of the EC8 design procedure. In fact, EC8 provisions do not account rationally for the overstrength due to the beam strain-hardening leading to results that in some cases can be poor and characterized by the development of brittle failure modes. Aside from this, due to the same reason, the design of the joint components, following the EC8 provisions, is carried out with actions lower than the actual ones leading to the development of stresses and plastic deformations in all the joint components which are beyond the plastic limit that should be, instead, the upper bound to be imposed in design.

The effectiveness of the proposed approach has been demonstrated in the work comparing the damage level of the joints' components underlining that, in case of connections designed according to the proposed procedure, the damage is prominently concentrated at the end of the beam which constitutes the main dissipative zone, while all the connections' elements remain practically elastic, or only with very limited plastic deformations. Conversely, in case of joints designed according to the Eurocode 8, the joint components are significantly engaged in plastic range achieving high levels of deformations, certainly beyond the plastic limit. As an example, the developed analyses have demonstrated that following the EC8 design procedure, the welds may damage in plastic range with deformations even equal to 38.46 times the yield strain and, in a similar way, the bolts may fail or, in general, undergo severe damages.

## **2.4. Application of the design procedure to the “dog bone” joint typology**

In the seismic design of moment resisting frames it is universally suggested the use of full-strength connections able to develop sufficient overstrength with respect to the connected beam to allow the complete development of the plastic rotation capacity of the beam. This design goal can be achieved provided that the connection overstrength is properly selected accounting for the strain-hardening occurring before flange local buckling and considering also the influence of random material variability [12]. Such high overstrength significantly affects the connection structural detail requiring strengthening elements such as reinforcing ribs, cover plates, haunches, etc.; which significantly affects the cost of connections. For this reason experimental investigations on the cyclic response of partial strength connections have gained new attention [24,25]. RBS connections can be considered a particular typology within the framework of partial-strength connections, because their flexural resistance is less than the one of the connected beam.

A distinguishing feature of the Reduced Beam Section (RBS) connection, is that portions of the beam flange are trimmed away in the region adjacent to the beam-to-column connection (Fig 2.19a). The result is similar to reinforcement, i.e., the connection is stronger than the beam. The design procedure herein presented, could be easily applied to the “*dog bone*” joint typology.

First of all, the parameters to be designed are the distance of the reduced section zone from the face of the column **a**, the length of the reduced section zone **b** and the flange reduction width **c** (Fig. 2.19b).

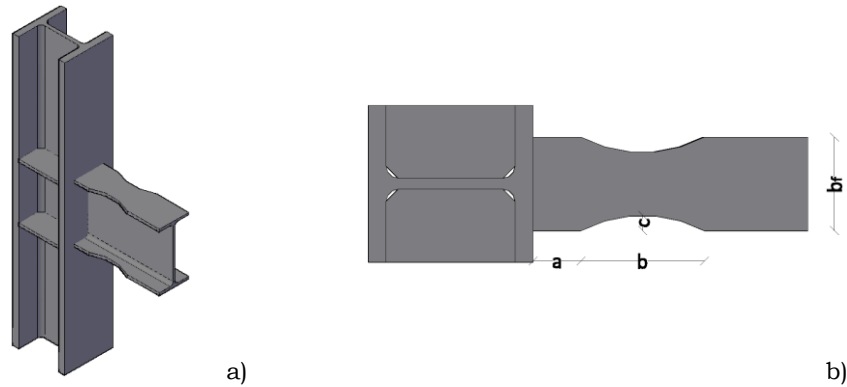


**Fig. 2.19** – Dog bone joint typology: a) Rendering; b) main parameters

It is suggested to use values of the two parameters  $a$  and  $b$  according to the following ranges [26]:

$$\mathbf{a} = (0.5 \div 0.75)b_f \quad \text{and} \quad \mathbf{b} = (0.65 \div 0.85)d_b \quad (2.24)$$

where  $b_f$  is the width of the beam flange and  $d_b$  is the beam depth.

The parameter  $c$  controls the maximum bending moment at the RBS and, as a consequence, the maximum moment at the face of the column flange. This value should be limited in order to obtain at the column face in a range contained in the 85-100% of the beam cross section plastic moment. It is suggested [27,28] to avoid the use of these connections for reductions greater than 50%. In addition,  $c$  must be greater than  $0.25b_f$ . Details about the dimensioning of the flange reduction  $c$  and of the distance between the centre of RBS zone and the face of the column flange is given in Montuori et al.[29].

Once designed the reduced section of the beam, it is possible to design the components of the connections. With reference to the proposed



procedure, the ultimate beam flexural resistance at the plastic hinge location is evaluated as:

$$M_{b,u} = \gamma_{ov.rm} \cdot \gamma_{ov.sh} \cdot \gamma_{M0} \cdot M_{b,RBS,p} \quad (2.25)$$

where:

$$M_{b,RBS,p} = \frac{Z_{b,RBS} \cdot f_{y,b}}{\gamma_{M0}} \quad (2.26)$$

being  $Z_{b,RBS}$  the plastic modulus of the reduced beam section that can be easily determine as:

$$Z_{b,RBS} = Z_b - 2ct_{bf}(d_b - t_{bf}) \quad (2.27)$$

and  $\gamma_{M0}$  the partial safety factor.

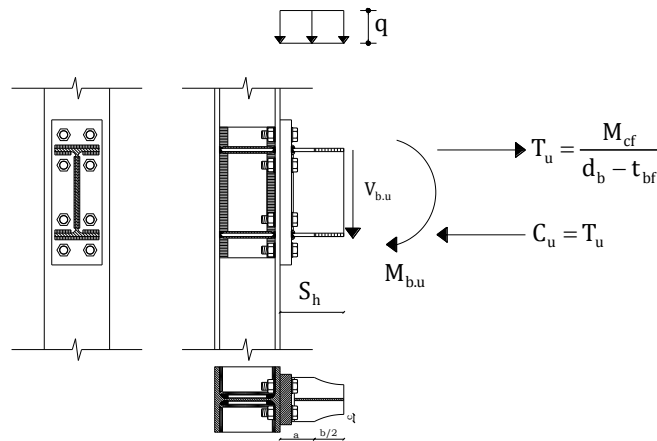


**Fig. 2.20** – Simplified model for the design of the tension zone

The average yield strength of beam flanges is evaluated accounting for the influence of the flange thickness  $t_{bf}$ , as in Eq. (2.13) while the coefficient  $\gamma_{ov,sh}$  accounting for the influence of strain hardening given by Eq. (2.4), can be easily rewritten considering the reduced flange width:

$$s = \frac{1}{0.546 + 1.633\lambda_f^2 + 0.062\lambda_w^2 - 0.602\frac{b_f - 2c}{L_e} + 0.001471\frac{E}{E_h} + 0.007766\frac{\varepsilon_h}{\varepsilon_y}} \leq \frac{f_u}{f_y} \quad (2.28)$$

where  $\lambda_f$  and  $\lambda_w$  are, respectively, the normalized slenderness parameters of the flange and of the web equal to:

$$\bar{\lambda}_f = \frac{b_f - 2c}{2t_f} \sqrt{\frac{f_{ym,f}}{E}} \quad \text{and} \quad \bar{\lambda}_w = \frac{d_w}{2t_w} \sqrt{\frac{f_{ym,w}}{E}} \quad (2.29)$$

where  $b_f - 2c$  is the reduced flange width,  $t_f$  is the flange thickness,  $d_w$  is the compressed part of the beam web,  $t_w$  is the web thickness,  $L_e$  is the shear length of the beam,  $E$  is the Young modulus,  $E_h$  is the hardening modulus,  $\varepsilon_y$  is the strain corresponding to yielding and  $\varepsilon_h$  is the strain corresponding to the end of the yield plateau.

Starting from the average ultimate resistance of the beam provided by Eq. (2.25), assuming the parameter  $S_h$ , i.e. the distance between the plastic hinge and the column flange, equal to  $a + b/2$  (Fig. 2.20), the Eqs. (2.14) to (2.22) are still valid so that, known  $T_u$  and  $C_u$  values occurring when the beam plastic hinges have attained their ultimate flexural resistance, all the geometrical details of the connecting elements can be designed by means of the resistance formulations

provided by Eurocode 3 for the joint components. The specific sequence of design operations or resistance checks of the joint components illustrated in ¶ 2.4.1 has to be followed.

As a validation of the possibility of extending the proposed design procedure to the “dog bone” joint typology, it has been applied, a posteriori, to the already experimentally tested connection [24] starting from the actual values of the mechanical properties of all joint components. In particular, reference is made to connection labelled with ID EEP-DB-CYC03 which is a full strength extended endplate joint designed to force the development of the plastic hinge in the beam by cutting the beam flanges according to the design criteria for reduced beam sections. What the experimental results evidenced during the test, as the main engagement in plastic range of the reduced section of the connected beam but also the effort in plastic range of some other components, is completely justified.

## 2.5. References

- [1] CEN (2005): “Eurocode 3: Design of Steel Structures – Part 1-8: Design of Joints”, EN 1993-1-8.
- [2] D.B. Moore, F. Wald (ed.): “Design of Structural connections to Eurocode 3 – Frequently Asked Questions”, Building Research Establishment Ltd, Watford, 2003, ISBN 80-01-02838-0, Project Continuing Education in Structural Connections, No. CZ/00/B/F/PP-134099, Leonardo Da Vinci, Programme.
- [3] J.P. Jaspart: “Etude de la semi-rigidité des noeuds poutre-colonne et son influence sur la résistance et la stabilité des ossatures en acier” PhD Thesis, University of Liège, Liège, 1991.
- [4] C. Faella, V. Piluso and G. Rizzano: “Structural Steel Semirigid Connections”, CRC Press, Boca Raton, Ann Arbor, London, Tokyo. ISBN 0-8493-7433-2, 1999.
- [5] F.M. Mazzolani and V. Piluso: “Evaluation of the rotation capacity of steel beams and beam-column”, 1st COST C1 Workshop, Strasbourg, 28-30 October, 1992.
- [6] B. Kato: “Rotational Capacity of steel members subject to Local Buckling”, 9th World Conference on Earthquake Engineering, Vol. IV, paper 6-2-3, August 2-9, Tokyo-Kyoto, 1988.
- [7] Y.E. Yee and R.E. Melchers: “Moment-rotation curves for bolted connections”, Journal of Structural Engineering, ASCE, Vol. 112, Issue 3, pp. 615-635, 1986.
- [8] B. Kato: “Deformation Capacity of Steel Structures”, Journal of Constructional Steel Research, pp. 33-94, N.17, 1990.
- [9] A. Girao Coelho: “Characterization of the ductility of bolted extended end plate beam-to-column steel connections”. PhD Thesis: Universidade de Coimbra, 2004.
- [10] CEN, EN 1998-1-1. “Eurocode 8: Design of structures for earthquake resistance - Part 1: General rules, seismic actions and rules for buildings”, European committee for standardization, 2005.
- [11] Ministero delle Infrastrutture: “Norme tecniche per le costruzioni”, NTC2008, 2008.

- [12] V. Piluso and G. Rizzano: “*Random material variability effects on full-strength end-plate beam-to-column joints*”, Journal of constructional steel research, vol.63, 2007.
- [13] G.L. Tucker and R.M. Bennet: “*Reliability Analysis of Partially Restrained Steel Connections*”, Journal of Structural Engineering, ASCE, Vol. 116, No. 4, April, pp. 1090-1101, 1990.
- [14] U.Kuhlmann: “*Definition of Flange Slenderness Limits on the Basis of Rotation Capacity Values*”, Journal of Constructional Steel Research, pp. 21-40, 1989.
- [15] B. Kato: “*Rotation Capacity of H-section members as determined by local buckling*”, Journal of Construction Steel Research, 13, 95-109, 1989.
- [16] R.M. Bennett and F.S. Najem-Clarke: “*Reliability of Bolted Steel Tension Members*”, Journal of Structural Engineering, ASCE, Vol.113, No. 8, pp. 1865-1872, 1987.
- [17] H. Gervásio, L. Simões da Silva and L. Borges: “*Reliability assessment of the post-limit stiffness and ductility of steel joints*”, Third European Conference on Steel Structures, Coimbra, 2002, September 19-20, 2002.
- [18] G. Rizzano: “*New strategies in the seismic design of bolted beam-to-column connections*”, Keynote, X Congresso de Construção Metálica e Mista, Coimbra, Portugal, November 26-27, 2015.
- [19] R.Y. Rubinstein: “*Simulation and the Monte Carlo method*”, John Wiley & Sons, 1981.
- [20] J.W. Fisher, T.V. Galambos, G.L. Kulak and M.K. Ravindra: “*Load and resistance factor design criteria for connection*”, ASCE annual Convention & Exposition, Chicago, October 16-20, 1978.
- [21] Gruppo Fontana, Catalogo Tecnico: Prescrizioni Tecniche, 2004.
- [22] BS-EN-ISO 2560. *Welding consumables: covered electrodes for manual metal arc welding of non-alloy and fine grain steels, Classification*, 2009.
- [23] O.S. Bursi and J.P. Jaspart: “*Calibration of a finite Element model for isolated bolted end-plate steel connections*”, Journal of Constructional Steel Research 44, 1997, 224-262.

- [24] CEN, EN 1993-1-5. “Eurocode 3: Design of steel structures - Part 1-5: Plated structural elements”, European committee for standardization, 2007.
- [25] CEN, EN 10034. “Structural steel I and H sections – Tolerances on shape and dimensions”, European committee for standardization, 1993.
- [26] F. Iannone, M. Latour, V. Piluso, G. Rizzano: “Experimental Analysis of Bolted Steel Beam-to-Column Connections: Component Identification”, Journal of Earthquake Engineering, Vol. 15, (2), 214-244, 2011;
- [27] M. Latour, V. Piluso, G. Rizzano: “Cyclic Modelling of Bolted Beam-to-Column Connections: Component Approach”, Journal of Earthquake Engineering, Vol. 15, (4), pp. 537- 563, 2011;
- [28] K. Moore, J. Malley & M. Engelhardt: “Design of Reduced Beam Section (RBD) Moment Frame Connections”, Steel Tips, 1999.
- [29] M. Engelhardt, T. Winneberger, A. Zekany & T. Potyraj: “The dogbone connections part II”, Modern Steel Constructions, 1996.
- [30] M. Engelhardt, T. Winneberger, A. Zekany & T. Potyraj: “Experimental investigation of dogbone moment connections”, Proceeding of National Steel Constructional Conference, AISC, Chicago, 1997.
- [31] R. Montuori & V. Piluso: “Plastic design of steel frames with dog-bone beam-to-column joints”, 3<sup>rd</sup> International Conference on Behaviour of Steel Structures in Seismic Areas, Montreal, STESSA, 2000.



# **Chapter 3**

**Innovative Partial strength beam-to-column connections and design criteria**





### 3.1. Innovative joints typologies

Structural seismic systems free from damage or easy to replace after the earthquake have received, in recent years, a growing interest by the scientific community. Within this framework, supplemental damping devices able to dissipate a part of the seismic input energy reducing the seismic demand on the structural elements are particularly interesting. In the following, the possibility of providing the structure of supplemental damping devices by means of properly detailed beam-to-column joints, is analysed. A partial strength joint typology particularly appropriate to this purpose is the Double Split Tee Connection (DSTC) in which the connecting elements are clearly identified and easily replaceable. The behaviour of this type of connection is strictly related to that of a T-stub subjected to axial load, which models the top and bottom Tee. In past, many scientific efforts have been devoted to understand and model the behaviour of simple rectangular T-stubs under cyclic loads [1]. Such behaviour, as pointed out in scientific literature, is affected by significant pinching due to many factors, such as the plastic deformation of bolts and contact phenomena. Aiming to increase the energy dissipation capacity of T-stubs, in [2], starting from the results obtained in [1,3-6] concerning monotonic and cyclic behaviour of T-stubs, two different approaches are followed: the first one, aiming to provide the structures of supplemental dampers of yielding type, applies the concepts usually adopted for ADAS devices to the configuration of T-stub flanges; the second approach, in order to provide the structure of supplemental dampers of friction type, is based on the use of proper friction materials. Modern seismic codes are set up

to obtain certain performance levels, providing to check structures to remain elastic in case of ordinary load combinations (Serviceability Limit States) and, eventually, to damage under rare load combinations such as those deriving from the occurrence of destructive seismic events (Ultimate Limit States). Currently, dealing with the ULS design, different possibilities are given to guarantee the failure mode control of the structure governing, in the framework of capacity design, the structural ductility at the local and at the global level. In general, the capacity of the structure to withstand non-linear deformations is based on the development of damage in specific zones which have to be engaged in plastic range in order to absorb the inelastic demand. In case of steel Moment Resisting Frames (MRFs), according to the design procedures suggested by EC8 [7], a first option consists in the formation of the plastic zones in beams, through the adoption of full-strength joints and over-strength columns (continuous frames). As an alternative, a second option consists in the concentration of structural damage in connections, which are designed to be partial-strength [7,8], needing, therefore, specific detailing to guarantee that their rotational capacity is compatible with the seismic demand (semi-continuous frames). Clear criteria to guarantee the correct ductility supply to connections are still under discussion in the research community and, in fact, significant research is being dedicated to this topic also recently [9-14].

Even though the design procedures suggested by EC8 are already validated thanks to the significant work carried out in past decades by many research groups [15-24], it is clear that, independently from the adoption of one or another design strategy, the main drawback of the traditional approaches is the need for the development of structural

damage which, even though on one hand it is used to preserve structural economy and human life, on the other hand represents also the main source of direct and indirect losses in case of rare seismic events. In order to solve this issue in past decades several strategies have been proposed. Among the various possibilities, supplemental energy dissipation systems have been proposed and extensively studied since the 90s, providing a wide set of dissipaters to be inserted in particular zones of the structure, where high relative displacements or velocities are expected under the action of severe ground motions. In this way, the greatest part of the energy dissipation supply is entrusted to dissipative fuses specifically designed for the energy dissipation, while the damage to the main structure is limited, reducing the seismic inelastic demand. Currently, a number of dissipative devices based on this design concept has been proposed, providing systems based on the activation of simple dissipative mechanisms such as yielding of metals, dry friction and viscosity of fluids [25,26]. Nevertheless, also in the case of supplementary energy dissipation design strategies, the introduction of dissipaters improves damping, but the structural damage is not completely avoided because to activate the seismic dissipaters adequate sway displacements of the main structure are still needed.

This is the subject of the FREEDAM project, which is an RFCS project, granted by the European Community, devoted to the development of strategies for the application of such a kind of connections to steel structures.

### 3.2. Friction joints

In order to overcome the drawbacks of the traditional design approaches, recently, the FREEDAM (FREE from DAMage) design strategy has been proposed as a solution able to combine the best features of all the three approaches previously described with the capacity to avoid structural damage both at SLS and ULS, introducing in connections particular types of friction damping devices. In fact, as explained afterwards, the FREEDAM design approach allows, easily, to design rigid frames with fully rigid connections (as in the case of full-strength design, continuous frames) with a resistance very close to the nominal value of the beam resistance (as in case of partial – or equal – strength design) and with high energy dissipation supply (as in the case of supplementary energy dissipation strategies) avoiding, in the same time, the structural damage.

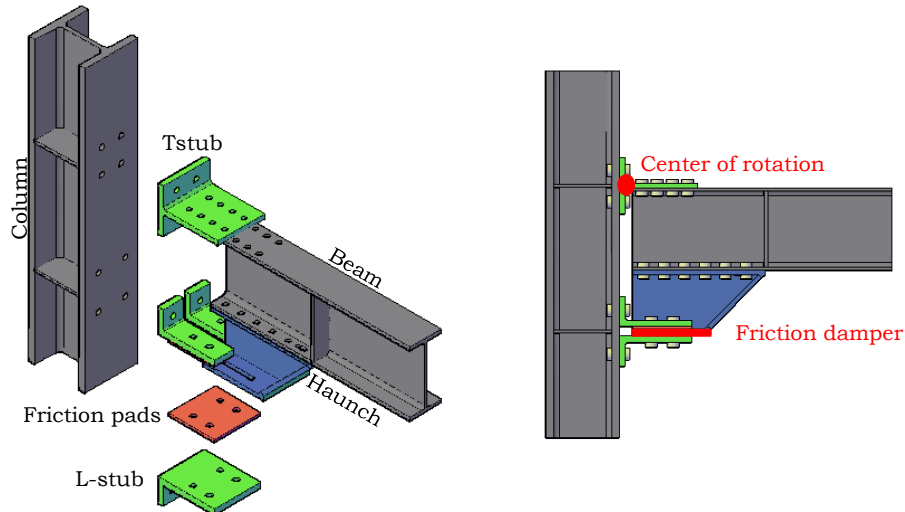


**Fig. 3.1** – FREEDAM connection

In fact, the FREEDAM design approach has as first aim the definition of structural layouts able to dissipate seismic energy avoiding damage both in members and connections, due to the inclusion of friction devices in beam-to-column joints. Such connections, called FREEDAM connections, are detailed to include at the level of the lower beam flange a friction device realized with steel plates and friction pads pre-stressed with high strength bolts. In particular, the typical configuration of a FREEDAM beam-to-column joint consists in a modification of the classical detail of a Double Split Tee Joint (DST) where, the bottom Tee element, is substituted with a symmetrical friction connection [27-30] realized with a slotted haunch which slips on friction shims pre-stressed with high strength bolts (Fig.3.1).

With this connecting system, under bending actions, the joint is forced to rotate around the rotation centre located at the base of the upper T-stub web and the energy dissipation supply is provided by the alternate slippage of the lower beam flange on friction pads. From the design point of view, the FREEDAM approach is extremely simple and it is based only on few steps:

1. design of the FREEDAM friction dampers for the actions deriving from the ULS load combinations. The dampers can be designed, in terms of resistance, both to be partial-strength (less resistant of the connected beam) or equal strength (same resistance of the connected beam) [31-32];
2. design of the non-dissipative parts of the connection, accounting for the maximum over-strength due to random material variability of the friction material. It is worth noting that the part of the over-strength factor related to the strain-hardening is negligible because the friction damper is characterized by a rigid-plastic response. In terms

of stiffness, being the slip resistance of the friction damper uncoupled from the stiffness of the connection, the joints' elements can be designed to achieve a full rigidity, with a clear advantage with respect to the classical semi-continuous design for the serviceability limit state checks [8];

3. design of the columns by means of the adoption of the classical procedures provided by EC8 or even by means of more advanced design procedures, such as the Theory of Plastic Mechanism Control [33], which are able to guarantee the development of a failure mechanism of global type.

In order to govern the resistance of the FREEDAM connections, it is necessary to control the pre-loading force applied with the bolts and to characterize accurately the value of the friction coefficient of the material employed to realize the friction interface. In particular, as already well known, the bolt pre-loading force can be controlled by applying one of the methods already suggested by EN1090-2 (i.e. combined, torque, DTI washers) which are conceived to guarantee the minimum 95% reliability on the tightening required by EN1990 [34]. Conversely, the value of the friction coefficient needs to be characterized experimentally and depends on a plurality of factors. In particular, as already demonstrated in past experimental works, the friction coefficient of an interface strongly depends on the materials employed to realize the friction interface and on the main tribological properties, such as the superficial finishing, micro and macro hardness, shear resistance of the materials and roughness [35,36].

### **3.2.1. Friction materials: experimental tests**

In order to guarantee a correct behaviour of the friction connection both under Serviceability and Ultimate limit states (SLS, ULS), it is necessary to know with a sufficient level of accuracy the value of the static and dynamic friction coefficients and the value of the bolts' preloading. To this scope, an experimental programme consisting of 63 specimens, developed at the STRENGTH laboratory (STRuctural ENgineering Testing Hall) of the University of Salerno, following the guidelines provided by EN 1090-2 and EN 15129 (anti-seismic devices), has been performed. The experimental programme consists of two phases: initially, 13 tests on eight different materials combined with stainless steel plates have been realized in order to evaluate the behaviour of the friction interfaces in terms of static and kinetic friction coefficient and in terms of degradation. In the second phase, the experimental work is mainly devoted to the evaluation of the response of only three different materials of the eight already subject of a preliminary study, applied as a coating on steel plates by means of thermal spray, investigating the influence of the bolt preloading level and of the washer's typology on their response. In particular, the possible influence of the pressure applied to the analysed interfaces is considered carrying out tests at variable values of the pre-loading (between 40% and 100% of the standard pre-loading value), and the influence of the washers' configuration is evaluated performing tests with flat washers and different configurations of series and parallel of Belleville disc springs. The influence of the washer's typology is considered in order to assess the effectiveness of the Belleville disc springs in the reduction of the bolts' loosening during a cyclic test.



In particular, from the analysis of the available technical literature, eight materials that can be applied by means of thermal spray providing corrosion resistance (that is a fundamental requirement for the durability of the damper) and a value of the superficial hardness strongly different from that of steel (much higher or much lower) have been selected. The difference between the superficial hardness of plates in contact is a fundamental feature because as already hypothesized by Bowden and Tabor in [46] the friction coefficient ( $\mu$ ) of a metal interface is related to the ratio between the shear resistance of the weakest material ( $s_0$ ) and to the superficial hardness of the softest material ( $\sigma_0$ ) constituting the interface:

$$\mu = \frac{s_0}{\sigma_0} \quad (3.1)$$

Therefore, in order to obtain a high value of the friction coefficient, a high value of the shear resistance of the weakest material and/or a very low value of the superficial hardness of the softest material are needed. Assuming that the internal surface of the friction damper proposed for the application to the FREEDAM connections is made of stainless steel AISI 304, which is characterized by a superficial hardness of about 130 HV, then the material to be coupled has to be characterized by a much lower or much higher value of the superficial hardness. In order to reach this scope, the materials' selection has been carried out by checking among the materials or alloys commercially available those characterized by very low or very high values of the superficial hardness. In the class of soft materials, five materials composed by non-ferrous pure metals or metal alloys with Vickers Hardness lower than 30 have

been selected and labelled with the ID tags M1-M5. Conversely, in the class of “hard” materials, some carbide alloys produced as powder blends and electroless nickel friction shims produced by 3M Deutschland GmbH have been selected and labelled with labels from M6 to M8. These materials are characterized by superficial hardness higher than 550 HV. In particular, the friction shims produced by 3M are Electroless Nickel shims realized with a particular blend including diamond powder, which is used to obtain a high value of the superficial hardness (600/900 HV). It is useful to note that, following the proposed approach it is expected that, when stainless steel is combined with harder materials, the consumption of the steel plate is promoted and, therefore, the friction coefficient obtained is mainly governed by the ratio between the shear resistance and superficial hardness of the steel plate. Conversely, when steel is combined with a softer material, the wearing of the interface is due essentially to the consumption of the friction shims and the friction coefficient mainly depends on the ratio between shear resistance and superficial hardness of the material employed to coat the friction shim.

#### **3.2.1.1. Experimental layout**

The typical specimen realized to evaluate the value of the friction coefficient of the analysed interfaces is composed by a system of steel plates assembled in order to test the uni-axial behaviour of friction interfaces resulting from the coupling of a stainless steel plate with friction shims coated with one of the eight materials previously described. The tested sub-assembly is inspired to the specimens' layout provided for slip tests by EN1090-2 [33]. In particular, it is constituted

by a slotted steel plate realized in 1.4301 Stainless Steel equivalent to AISI 304 steel, a steel plate with normal holes used to connect the specimen to the testing machine and external steel plates and friction shims pre-stressed with M20 class 10.9 HV bolts [38] (Fig. 3.2).

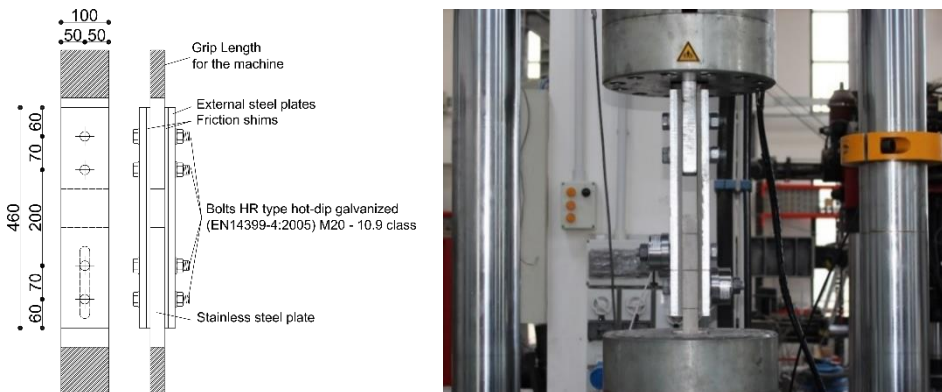


**Fig. 3.2** – a) Typical layout of a specimen; b) specimen in the machine

In order to determine the value of the initial slippage force and its degradation, all the specimens have been tested under cyclic loading conditions following the loading protocol provided by EN15129 (2009) [39], which is the only code currently available devoted to the testing of displacement dependent dissipative devices. In particular, such a code requires to perform the tests under cyclic loading conditions aiming to reproduce the actual working conditions on the devices. To this scope, it suggests to apply to the damper increasing amplitude cycles at 25%, 50% and 100% of the maximum design displacement of the device. For the intermediate amplitudes it provides to perform at least 5 cycles and for the maximum amplitude it provides to perform at least 10 cycles. Therefore, in order to reach displacement amplitudes similar to those occurring in real applications, following the suggestions of EN 15129

(2009), the loading protocol was constituted by 5 cycles at the amplitude of 6.25 mm, 5 cycles at the amplitude of 12.5 mm and 40 cycle at the maximum amplitude of 25 mm. The maximum amplitude was defined by estimating the displacement demand arising at the friction damper level in real applications. Therefore, considering a reference value of the lever arm, i.e. the distance between the upper T-stub of the FREEDAM connection and the mid-centre of the friction damper (Fig. 3.2a), equal to 600 mm and a maximum rotation of 40 mrad (greater than the minimum value required by EC8 equal to 35 mrad for DCH frames), the design displacement demand at the level of the damper has been calculated as equal to  $0.04 \cdot 600 = 24$ , which has been rounded to 25 mm. The cycles were executed at increasing values of the speed that were defined in order to remain in a quasi-static range and according to the capabilities of the available equipment. The cycles' velocity varied from 1 mm/s for the first 10 cycles to 5 mm/s for the cycles at the maximum amplitude. However, it is useful to note that, in order to evaluate the influence of the speed of application of the load on the materials' behaviour, in the FREEDAM project, additional tests considering velocities varying up to values of 200 mm/s are planned. In each test, both the upper and lower M20 high strength bolts have been tightened by means of a torque wrench, in order to reach a percentage of the proof load, equal to  $0.7 \cdot A_{bolt} \cdot f_{ub} = 0.7 \cdot 245 \cdot 1000 = 171500$  N, varying from 40% to 100% depending on the tested specimen, which has been controlled before starting the tests by means of appropriate donut load cells installed in the connection under the nuts of the bolts used to pre-stress the friction interface.

All the tests have been carried out employing a universal testing machine Schenck Hydropuls S56 (Fig. 3.2b). Such a machine is

constituted by a hydraulic piston with loading capacity equal to +/- 630 kN, maximum stroke equal to +/- 125 mm and a self-balanced steel frame used to counteract the axial load. Different sensors have been used before and during the test to control continuously the bolt force, the slippage load, the tightening torque and the displacement. The axial displacements of the device have been read directly from the transducer of the testing machine and, in the same way, the slippage force has been controlled directly exploiting the load cell of the machine. Before the test, the tightening torque has been applied through an hand torque wrench and monitored by means of a torque sensor Futek TAT430 with maximum capacity equal to 680 Nm. At the same time, the pre-tension applied to the bolts has been monitored before and during the test by means of donut load cells Futek LTH500 with maximum capacity of 222 kN. The donut load cell is a particular type of load cell that can be easily used to measure the clamping force applied to the bolts. Such a load cell has the typical structure of a shear beam cell, where the load is applied on a cylinder located in the middle of the load cell and it is transferred to an external cylinder through shear panels. Therefore, considering the structure of the load cell, aiming to preserve the distribution of pressure normally applied by the bolt to the friction interface, a thick and stiff washer with diameter equal to the external diameter of the load cell and a normal washer have been interposed in between the load cell and the external plates of the tested sub-assembly.

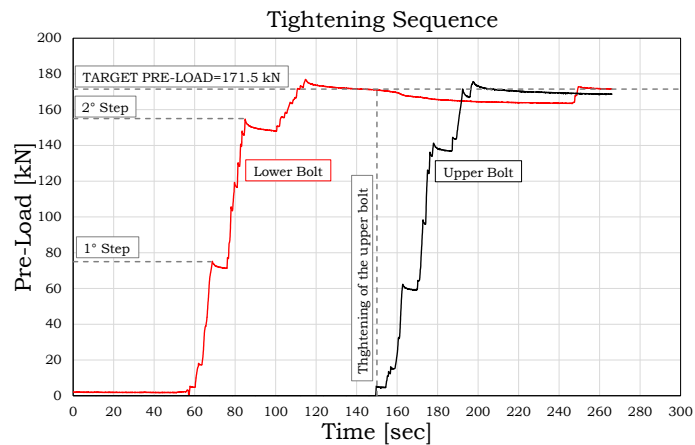


**Fig. 3.3** – Tightening sequence

Before every test, the force has been applied to the bolts by means of a hand torque wrench in order to reach the target pre-load amplified of a factor equal to 1.1. The amplification factor equal to 1.1 has been adopted to provide to the pre-load the meaning of a mean value as intended in EN 1090-2. In particular, the adopted bolts had an average value of the k-factor equal to 0.13.

Therefore, the value of the tightening torque applied to the bolts in each test was approximately equal to  $0.13 \cdot 171.5 \cdot 20 = 446 \text{ Nm}$ . An example of the tightening sequence is reported in Fig. 3.3 where the force versus time diagram is given for the two bolts located in the lower part of the specimen. From this figure, it is possible to note that for each bolt the pre-load was applied in different steps before achieving the target value. At the end of each step, it is also possible to note that after releasing the torque wrench there was always an “instantaneous” loosening of the pre-load of about 5-10%.

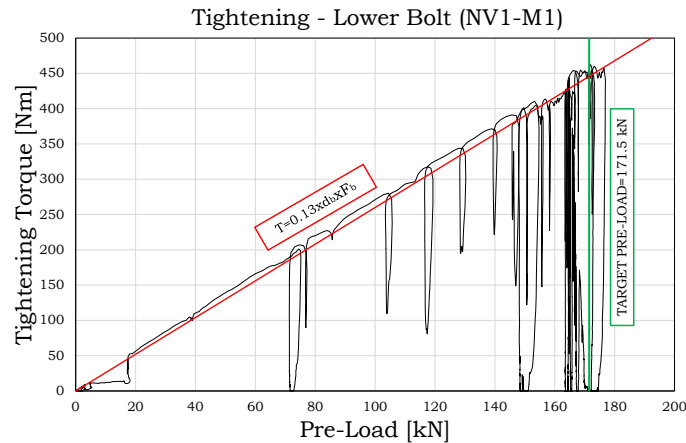


**Fig. 3.4** – Typical Torque vs Pre-load diagram

This is a well-known phenomenon due to the local crushing of microscopic spots of the steel parts in contact (embedment relaxation) that, in order to be exactly quantified, deserves deeper and more specific studies. Another effect that is possible to easily note from Fig. 3.3 is the group effect. In fact, the tightening of the second bolt, mutually influences the pre-loading force already applied in the other bolt.

### 3.2.1.2. Results of the tests - 1<sup>st</sup> phase

For each one of the eight materials previously mentioned two identical tests have been planned.

As aforesaid, in order to evaluate their performance under cyclic loading conditions, several parameters have been monitored during the test. In particular, in order to compare the friction coefficient of the various materials, the values of the slippage force and of the bolt forces read with the donut load cells have been exploited. Starting from the data

acquired during the tests with the measuring devices employed, two different values of the friction coefficient have been characterized: an “effective” value and an “actual” value. In particular, the “effective” value ( $\mu_{effective}$ ) of the friction coefficient has been calculated as the ratio between the slippage force and the sum of the nominal values of the pre-loading forces applied by the bolts (i.e.  $4 \cdot 171.5$  kN). Such an effective value represents the value of the friction coefficient that can be used in seismic design and accounts as a whole both for the degradation of the friction coefficient due to the damage of the surfaces in contact and for the degradation due to the bolts’ loosening. Conversely, the “actual” value of the friction coefficient ( $\mu_{actual}$ ) has been determined as the ratio between the slippage force and the sum of the values of the bolts’ forces read from the load cells during the test. Such an actual value provides the real measure of the friction coefficient, whose degradation is due only to the damage of the surfaces in contact, while the effects coming from bolt loosening are directly measured by means of the donut load cells. In the following a synthesis of the obtained results is reported, describing the main experimental outcomes and providing a comparison between the different materials.

#### **Experimental behaviour of the “Hard” Materials (Carbide M6, Carbide M7, 3M friction shims (M8))**

A synthesis of the results of the tests on the interfaces coupling stainless steel with friction pads coated with the “hard” coatings previously described are delivered in Figs. 3.5 to 3.7, where the hysteretic curves of one of the two identical tests performed on each material are reported. It is worth noting that even though, in order to



simplify the representation of the results, only the hysteretic curve of one of the two tests performed is reported, for all the three analysed materials, a very small scatter of the response for the two tests was observed, evidencing a very low random variability of the friction coefficient for these materials.

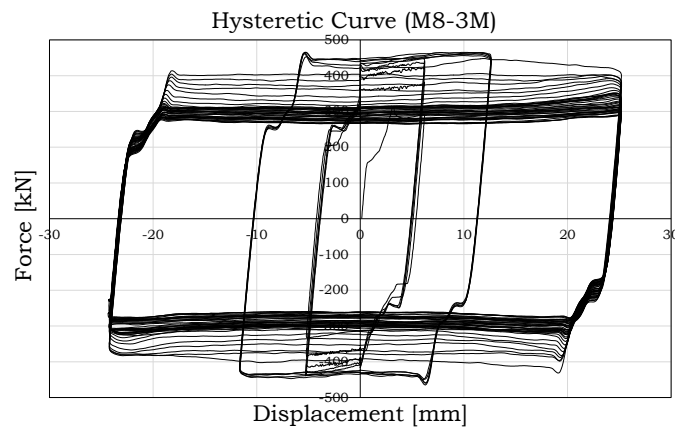


**Fig. 3.5** – Hysteretic behaviour of hard materials: 3M friction shims

In case of M6 carbide coating, the cyclic response has been characterized by the development of an initial value of the slip force equal to about 350 kN, followed by a progressive degradation that, at the end of the test was of about the 20%. During the tests, a peculiar behaviour of this material has been observed. In fact, as it is possible to note from Fig. 3.5, the hysteretic curve was affected by an initial stick-slip phase with the development of a first unstable cycle characterized by jumps of the force and sudden releases of energy.

Nevertheless, after this first cycle, that probably allows to break the initial interatomic attraction between the surfaces in contact (adhesion

component of friction), the slippage occurred regularly leading to a very stable response up to the end of the test.

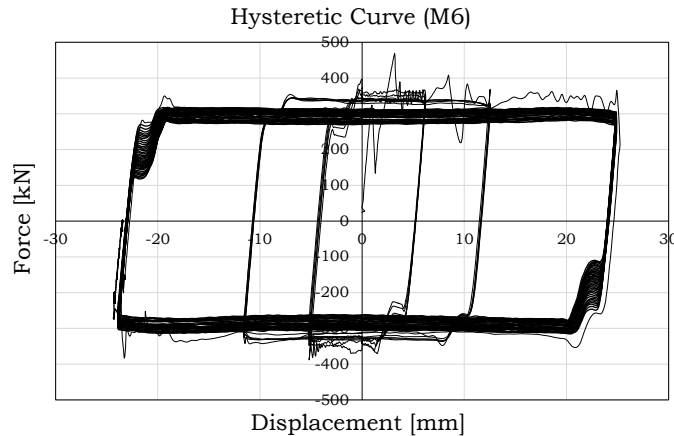


**Fig. 3.6** – Hysteretic behaviour of hard materials: Carbide M6

In case of M7 carbide coating, globally, a similar response was observed. The behaviour, in this case, was characterized by an initial slip force equal to about 250 kN, that after few cycles slightly increased, stabilizing at a value of about 300 kN. After reaching this value, all the cycles were characterized by the same slippage force obtaining, also in this case, a stable and dissipative behaviour. Even though the hysteretic behaviour reported in Fig. 3.6 appears pretty similar to that observed for material M6, in reality, in this case, in order to perform the test it was necessary to significantly reduce the velocity due to the development of a strong stick and slip behaviour, characterized by sudden releases of energy and vibrations. Therefore, to avoid any damage to the equipment, the testing velocity was reduced progressively

up to a value of 0,01 mm/s in order to check if, with a lower value of the velocity, the stick and slip phenomenon disappears.

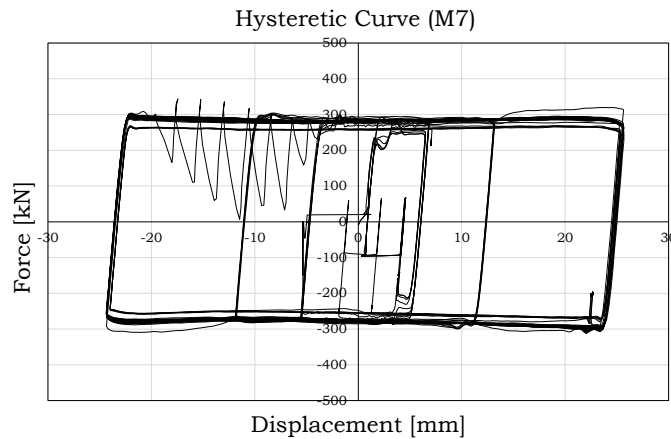


**Fig. 3.7** – Hysteretic behaviour of hard materials: Carbide M7

In particular, the stick-slip is a well-known phenomenon of instability of the friction behaviour that provides the alternate and continuous sticking and slipping of the two surfaces in contact. According to the technical literature, this phenomenon is usually related to an high difference between the static and kinetic value of the friction coefficient which in some cases leads, after the first slippage, to a sudden jump of the velocity resulting in a deceleration until stopping. After stopping, to restart the movement, the interface needs again to reach a higher value of the force in order to overcome the static value of the friction coefficient, but then restarts, decelerates and, due to the same phenomenon, stops again. Usually, as observed in these tests, this behaviour results in a force-displacement response characterized by continuous jumps of the slippage force between the static and kinetic values. Even though the physical interpretation of the stick and slip

behaviour is not easy and it is definitely out from the objectives of this work, it is obvious, from the response reported in Fig. 3.7, that it is a phenomenon not acceptable for the application of such materials in seismic damping devices.

3M friction shims were characterized by a response that, as already observed in the past by the same authors with other materials such as brass or some types of phenolic rubbers [71], was characterized by two different phases of the response. A first phase where the interface provided a strain hardening behaviour characterized by an increase of the slippage resistance of about 60% and a second phase characterized by a reduction of the slippage force which, at the end of the degradation returned to the initial value. In addition, in this case no stick and slip response has been observed and all the cycles have been characterized by a stable value of the slippage force. The initial value of the slippage force has been of about 400 kN.

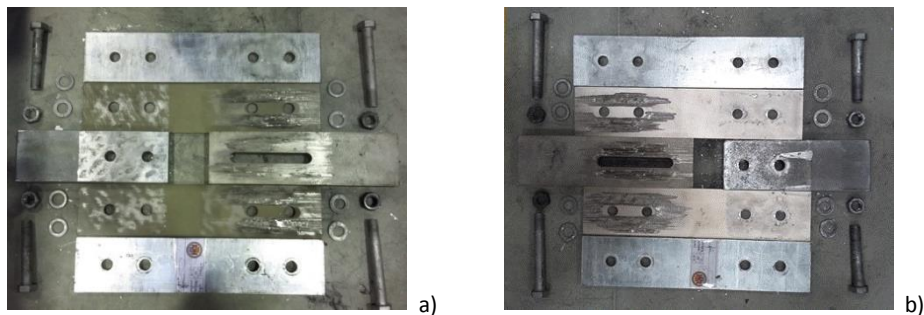


**Fig. 3.8** – Damage of the interfaces: a) M6; b) 3M friction shims

After the tests, the specimens have been opened in order to evaluate the damage of the interfaces. In Figs. 3.8a, 3.8b the damage state of the interface is represented for specimens employing M6 and 3M friction shims. As it is possible to observe from this figure, for these materials,

due to the higher hardness of the coating layer with respect to stainless steel, the greatest part of the damage was concentrated on the stainless steel plate which at the end of the test had many scratches in the zone located under the bolt head. In Fig. 3.9, as an example, the diagram of the bolt forces (monitored by means of the load cells) and of the actual friction coefficient represented versus the cumulative travel done by the damper are reported for the specimen with friction pads coated with M6 carbide.

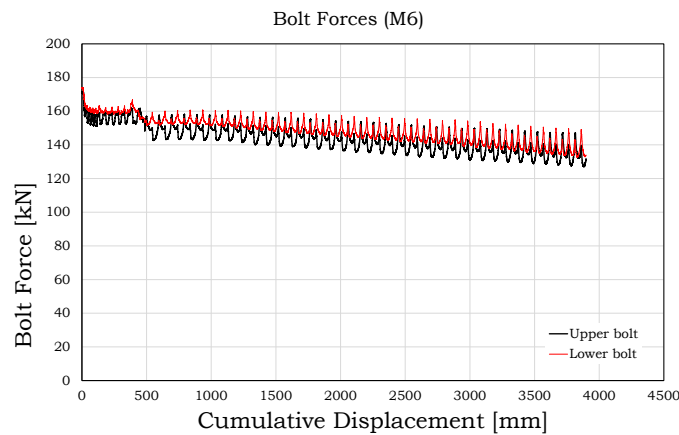


**Fig. 3.9** – Typical diagrams of the bolt forces

From such a figure it is possible to observe that both bolts, which are initially tightened in order to reach the proof load equal to 171.5 kN, after the first cycle of the loading history lose about the 7% of the initial pre-load and afterwards they uniformly loosen during the test reaching at the end a total loss of about the 20%.

Clearly, this initial loss, that seems to occur just after the first sliding of the connection, should be properly accounted for in the design of the damper. From the comparison between Fig. 3.5 and Figs. 3.9, 3.10 it is

possible to note also that the degradation of the sliding force observed during the test is essentially due to the degradation of the bolts' forces. In fact, they both degrade of about the 20% while the "actual" friction coefficient remains constant.

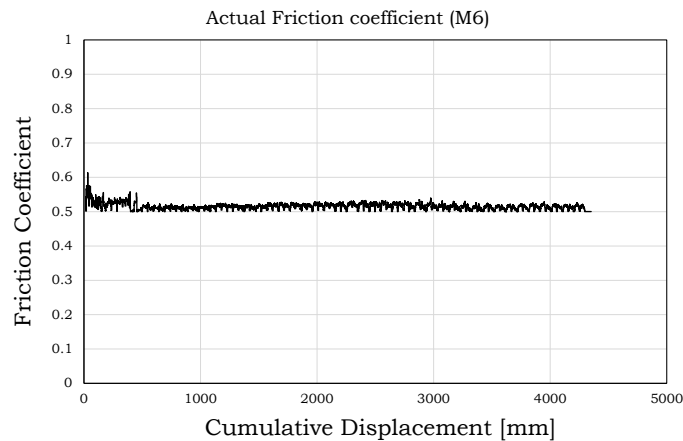


**Fig. 3.10** – "Actual" friction coefficient vs cumulative travel: M6

Even though, for the sake of simplicity, detailed graphs representing the behaviour of the bolts and the degradation of the friction coefficient for the other materials are not reported, analogous results have been obtained for all the other "hard" interfaces. Therefore, also for the other interfaces a correspondence between the bolts' loosening and degradation of the sliding force has been observed.

#### **Experimental behaviour of the "Soft" Materials (M1-M5)**

Similarly to what occurred in case of M7 carbide, also some of the soft materials exhibited a behaviour characterized by the stick-slip phenomenon. This is the case of three of the selected non-ferrous metal, namely M2, M3 and M5, whose response was characterized by alternate

stops and starts of the motion with strong and sudden releases of energy (Figs. 3.11, 3.12). Therefore, also in all these cases the tests have been stopped prematurely in order to prevent damage to the testing equipment.

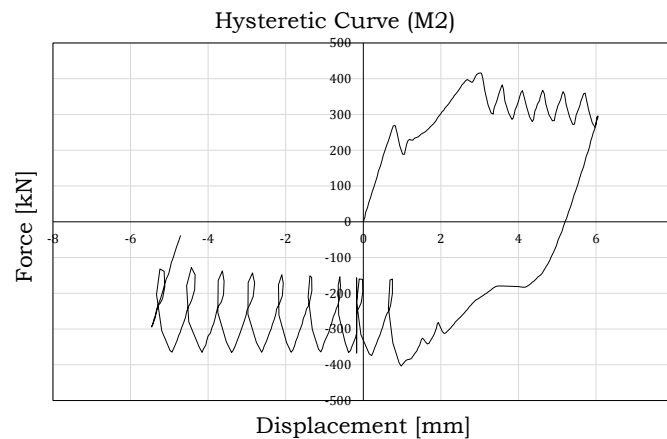


**Fig. 3.11** – Hysteretic behaviour of soft materials: M2

For these materials, as reported in Fig. 3.11, 3.12, the initial slippage force was equal to about 200 kN and was followed by an increase of the slippage resistance up to about 400 kN which corresponds to a value of the friction coefficient equal to about 0.58. After the first sliding, the hysteretic behaviour has been characterized by alternate and continuous jumps of the force from the static to the dynamic values. It is worth noting that, even though the cyclic behaviour of these interfaces is evidently not appropriate for seismic applications, from the results obtained in this experimental analysis it seems that these materials, due to the high value of the friction coefficient, could be still promising for application in friction connections designed for static loads.

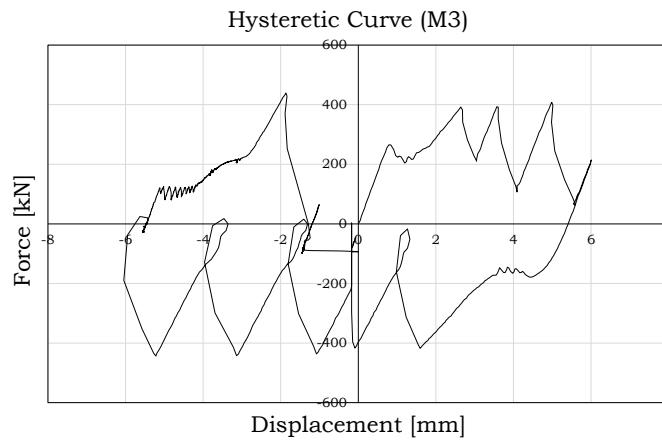


**Fig. 3.12** – Hysteretic behaviour of soft materials: M3

M1 and M4 metals have exhibited a very similar behaviour (Figs. 3.13-3.14).

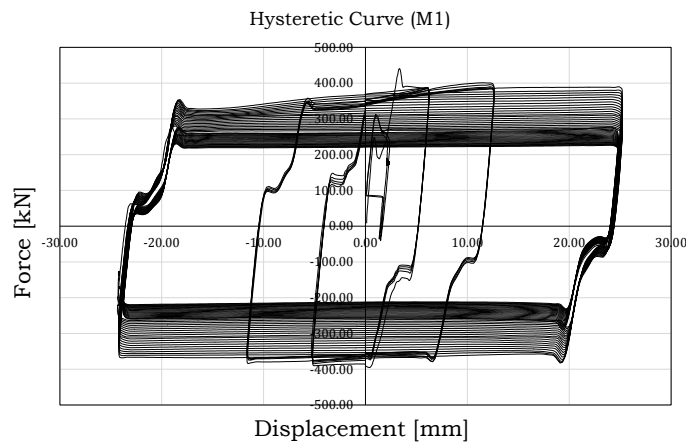


**Fig. 3.13** – Hysteretic behaviour of soft materials: M1

In particular, their hysteretic response has been characterized by a value of the slippage force higher than the corresponding obtained with



the “hard” materials but, on the other hand, they have also provided a more significant degradation due both to the bolt loosening and to the damage occurring in the friction pads. In addition, for both materials the behaviour exhibited in the two identical tests was significantly different showing a random variability of the behaviour of these materials. Such a variability was mainly due to the different behaviour provided by the bolts in the two tests.

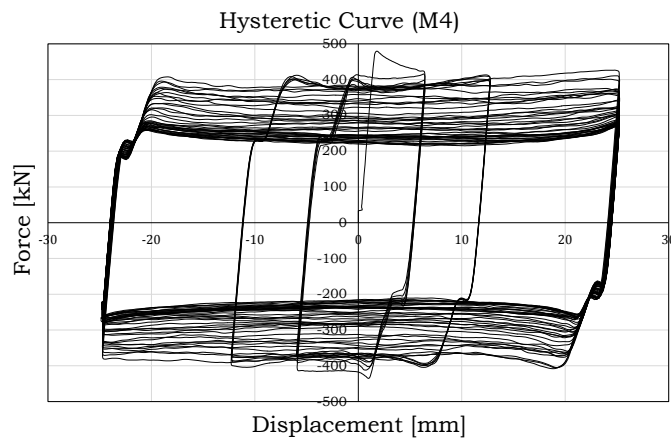


**Fig. 3.14** – Hysteretic behaviour of soft materials: M4

As an example, in Figs. 3.15, 3.16 with red and black lines are represented the results expressed in terms of friction coefficient and bolt forces versus the cumulated travel, for the two tests executed on the specimens with M4 friction pads. From this graphs it is clear that, even though the actual value of the friction coefficient does not varies in the two tests, the bolts provide a significantly different behaviour leading, consequently, to a different response of the whole hysteretic response. In particular, in one of the two tests after the first sliding a

sudden loss of pre-tension in the bolts of about the 15% was observed leading, as a consequence, to a proportional loss of the sliding force.

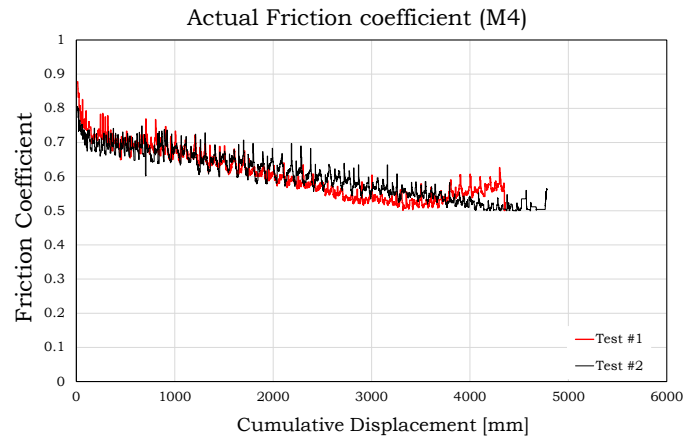


**Fig. 3.15** – Actual friction coefficient – M4

Such a different response of the specimens can be probably due to the imperfections of the coating applied on the friction shims, which in case of soft coatings is completely manual and leads to a non-uniform spread of the coating metal. In case of material M1, the degradation of the initial slippage force at the end of the tests was the 45%, while in case of material M4 it was of about the 50%.

Nevertheless, both materials provided very high values of the friction coefficient and, in particular, the initial friction coefficient of materials M1 and M4 were equal to about 0.55/0.65 and 0.7/0.9 respectively. As in previous cases, also the specimens realized with soft materials were opened after the test, in order to evaluate the damage of the interfaces.

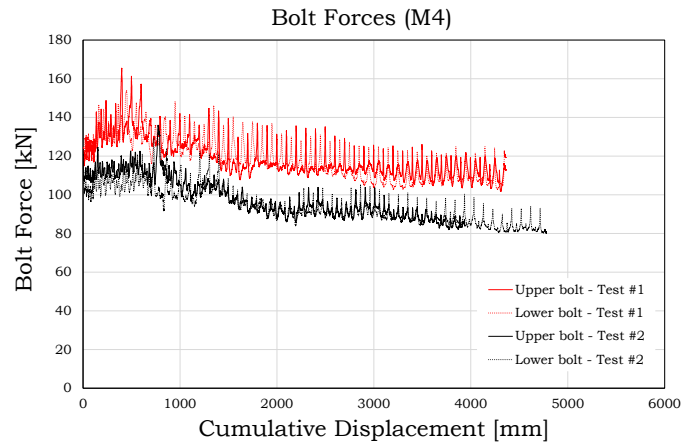


**Fig. 3.16** – Bolt forces – M4

As it is possible to note from Fig. 3.17, as expected, in these cases the damage was mainly concentrated on the friction shims, while the stainless steel plates after the test were practically undamaged.

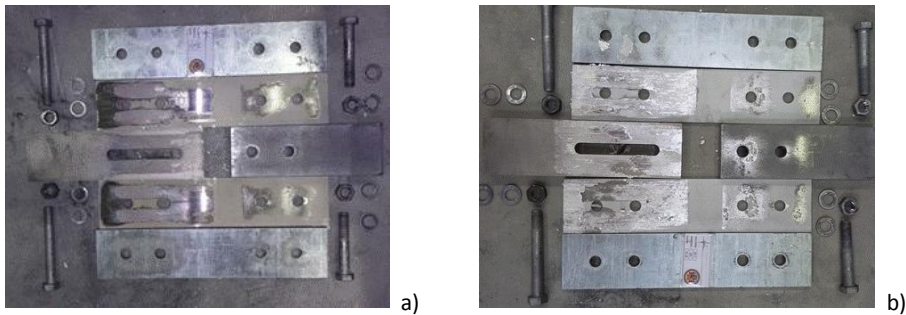


**Fig. 3.17** – Damage of the interfaces: a) M1; b) M4

Finally, it should be underlined that in all the tests the temperature of all the elements of the connection significantly increased, supposedly even over 100 °C. Provided that the influence of temperature on the behaviour of the friction damper deserves further investigations,

including the measurement of temperature of the connection' elements and the development of thermo-mechanical models, it could be said that, from what observed in this experimental activity, it seems that in the initial phases of the tests, due a problem of heat transfer, there is a difference between the temperature of the bolt and the temperature of the plates of the specimen. This behaviour seems evidenced, in some cases, by an initial increase of the bolt forces (e.g. Fig. 3.16). In view of this, in the second phase of the experimental programme, the thermal state of the specimens has been monitored during the tests by means of two thermocouples, one placed on the external plate surface on the side of the lower bolt, another placed on the bolt head.

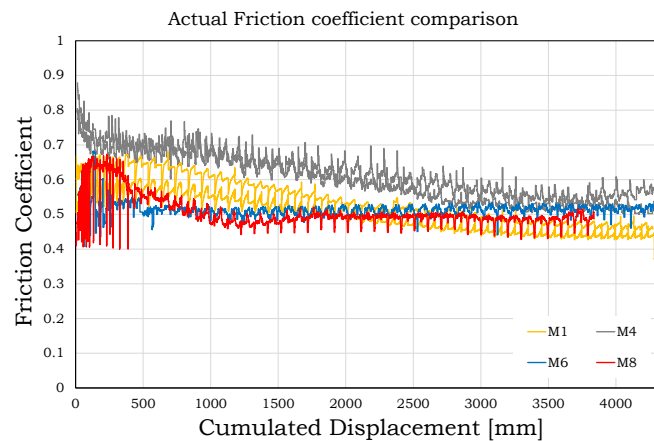


**Fig. 3.18** – Comparisons: “Actual” friction coefficient vs cumulated displacement

In conclusion, a first quantitative comparison of the response of the tested materials has been carried out by plotting on the same diagram the effective and actual values of the friction coefficients obtained in the different tests (Figs. 3.18, 3.19). From such diagrams, it is possible to

note that hard materials (M6 and 3M) have provided, in general, a lower value of the initial friction coefficient with respect to soft materials. The friction coefficient under cyclic loads, in case of M6 has been very stable, while in case of 3M friction shims it has been characterized by an initial increase of about 60% and, afterwards, by a continuous decrease up to the initial value of the friction coefficient. In addition, as reported in previous Sections, hard materials have provided a response practically coincident for the two analysed specimens, evidencing a low variability of their response which, from the practical point of view, may result in the possibility to predict with a higher accuracy the value of the friction coefficient to be used in design.

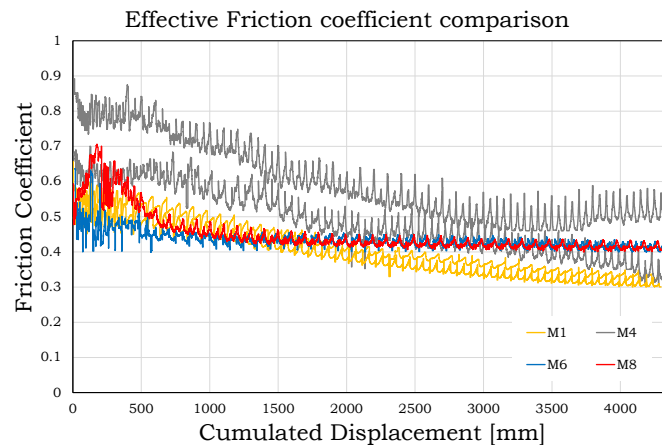


**Fig. 3.19** – Comparisons: “Effective” friction coefficient vs cumulated displacement

The higher reliability of these interfaces, probably is due to the production process of these coatings, which as a difference with respect to soft materials is completely industrialized and allows to obtain an high level of control of the distribution of the coating layer applied to the

friction shims. In fact, usually, in these applications it has been observed that the coating layer, due to the higher control of the application process, is normally uniformly distributed over the plate and with a very low variability of the coating thickness.

Conversely, soft materials (M1 and M4), even though, on one hand, have provided a better response in terms of initial value of the friction coefficient, on the other hand have also provided a higher variability of the response for the two tested specimens. In fact, in case of material M4, the value of the effective friction coefficient was significantly different for the two tests (0.90 and 0.70). In a similar way, also in case of material M1, the actual value of the friction coefficient was significantly different in the two tests. In fact in one test it was equal to 0.55, while in the other test it was equal to 0.65. Probably, the scatter obtained with the specimens employing soft coatings, can be linked to the production process that is typically performed by means of arc wire spray, which is a procedure completely manual that strongly relies on the individual capacity of the workman and on his experience. In fact, with arc wire spray, the coating is manually applied in different passes obtaining, at the end of the application process, a significant variability of the thickness of the coating layer. Such an inhomogeneous distribution of the coating thickness can be, normally, clearly observed also with the unaided eye.

In conclusion, from the results reported in Figs. 3.20, 3.21 it seems that soft materials are able to provide an higher initial value of the friction coefficient with respect to hard materials. Conversely, hard materials are able to provide a low degradation under cyclic loading histories and a very low variability of the response. Only in case of friction shims coated with 3M electroless nickel, a strong increase of the friction

coefficient initially occurs and, successively, a strong decrease of the friction coefficient can be observed. Probably, this high overstrength with respect to the initial slippage value is a disadvantage of this coating because, in seismic design, the adoption of this material would require a significant oversize of the non-dissipative parts of the frame and of the connections in order to allow the complete development of the dissipative mechanism in the FREEDAM connections. In terms of energy dissipation, all the four materials under consideration provided a significant capacity but, as it is possible to see from Fig. 3.19 their energy dissipation capacity, due to the degradation of the friction coefficient under cyclic loading histories, is not constant and depends on the considered value of the cumulative displacement.

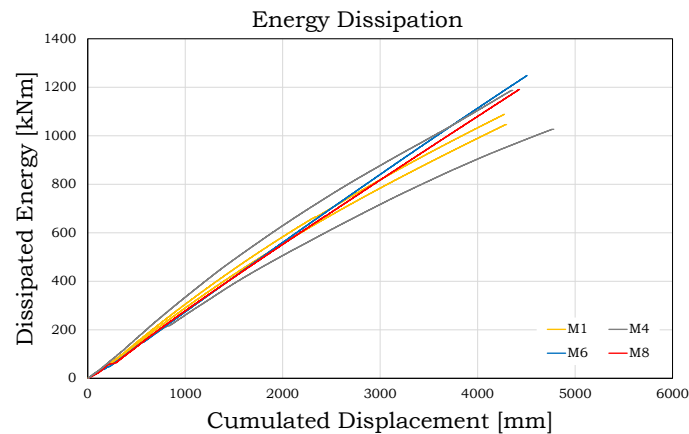


**Fig. 3.20** – Energy dissipation capacity

In fact, from Fig. 3.20 it is easy to note that, up to a value of the cumulative displacement approximately equal to about 1700 mm, the materials which are able to dissipate the highest amount of energy are the soft materials. Conversely, for higher values of the cumulative

displacement, hard materials are able to provide a higher value of the energy dissipation. Therefore, in order to understand what is the best material for application to the FREEDAM beam-to-column connections, from this point of view it would be necessary to fix a target design value of the cumulative displacement that the friction damper of the FREEDAM connection have to sustain under destructive seismic events. To this scope, a wide set of incremental dynamic analyses on case study buildings will be carried out in a subsequent phase of the work to be developed within the FREEDAM project in order to establish the maximum cumulative displacement expected under the action of real earthquakes.

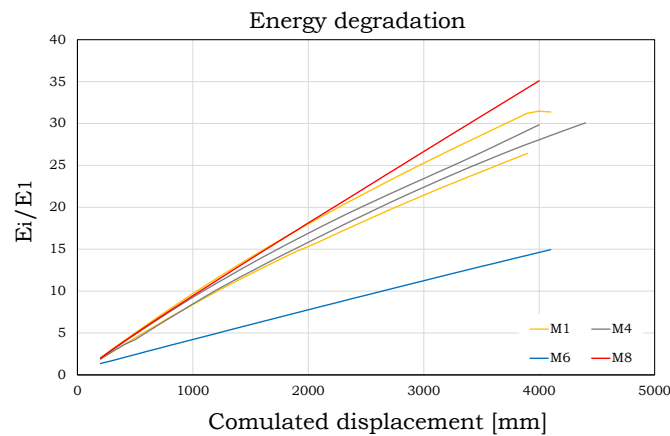


**Fig. 3.21** – Energy degradation

In Fig. 3.21, considering only the set of cycles at maximum amplitude, the degradation of the dissipated energy is represented. From such a figure, as expected from the test results previously reported, it is possible to note that, in terms of degradation, all the materials exhibited a similar behaviour made exception for Carbide M6. In fact for this



material, the degradation rate is much lower, practically half of all the other materials.

A summary of the tests performed is reported in Table 3.1.

**Table 3.1** - Summary of the tests – 1<sup>st</sup> phase

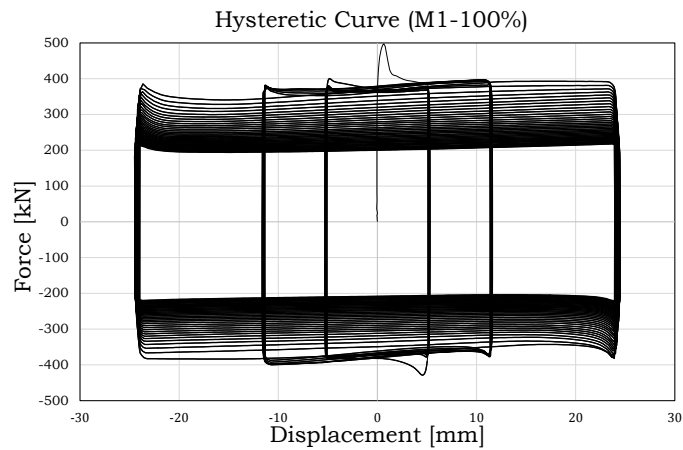
Specimen code	Material code	Test performed
NV - 1	M1	x
NV - 2		x
NV - 3	M2	x
NV - 4		
NV - 5	M3	x
NV - 6		
NV - 7	M4	x
NV - 8		x
NV - 9	M5	x
NV - 10		
NV - 11	M6	x
NV - 12		x
NV - 13	M7	x
NV - 14		x
NV - 15	M8	x
NV - 16		x

### 3.2.1.3. Results of the tests – 2<sup>nd</sup> phase

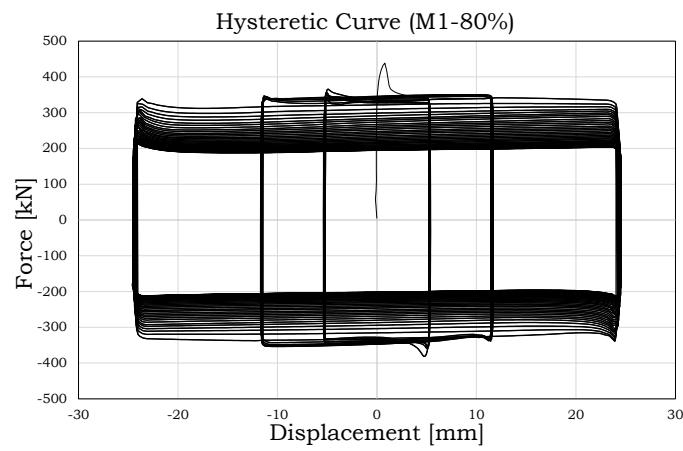
As aforementioned, 21 tests out of 51 have been executed to evaluate the influence of the bolts' pre-load and disc springs configuration over the friction coefficient, bolts' force degradation and effective damping deterioration. While, 30 tests (10 for each coating material) were executed in order to evaluate the random variation of the friction coefficient during whole test. For every test, exploiting the data acquired through the measuring devices previously described different graphical representations of the results have been made.

***Influence of the bolts' preload***

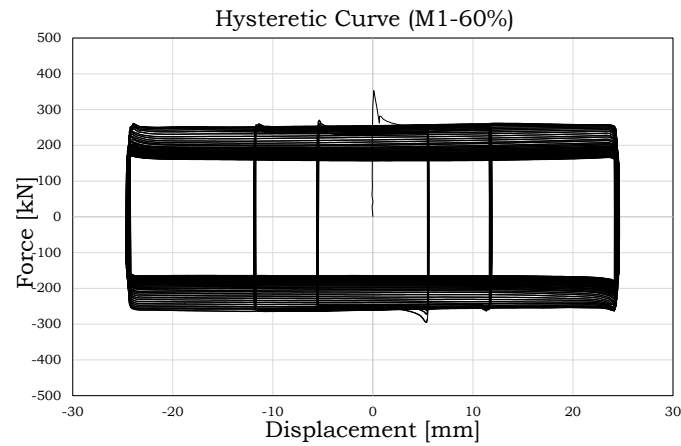
A representation of the typical force-displacement curves as dependent on the variation of the bolts' preloading force is reported, as an example, in Figs.3.22 to 3.24 for the three examined materials.



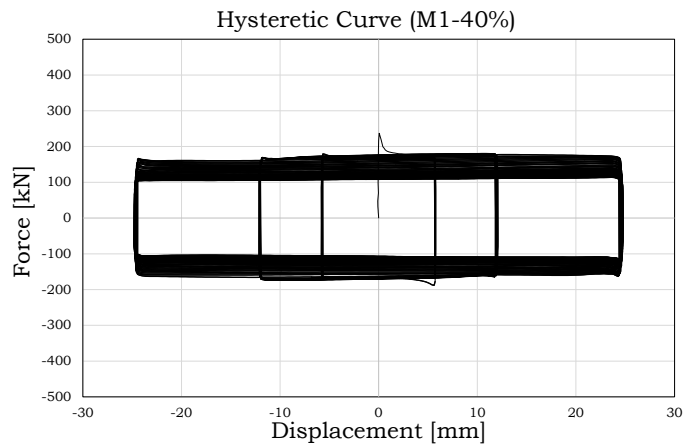
a)



b)



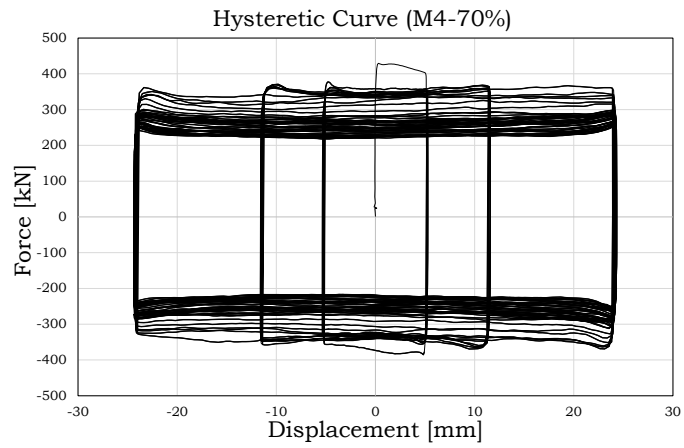
c)



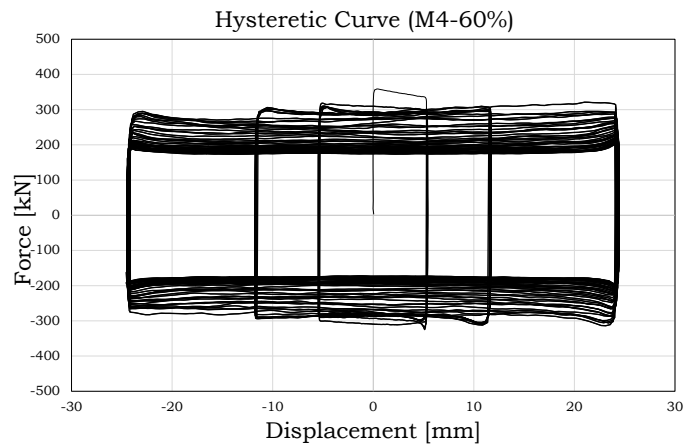
d)

**Fig. 3.22** – Influence of the bolts’ pre-load over the force-displacement hysteretic response (M1)

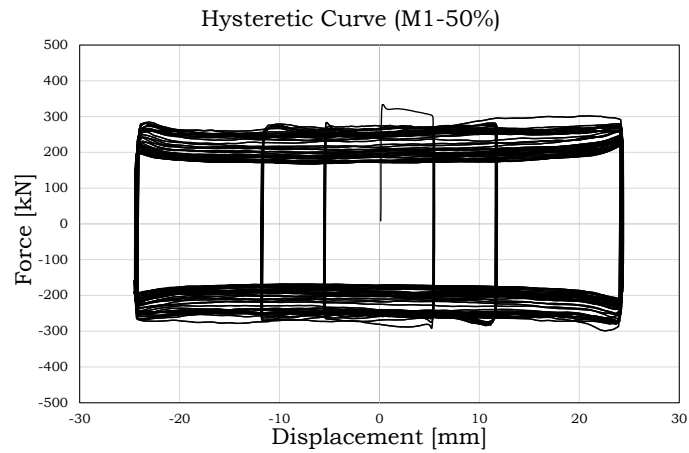
As it is possible to note from Fig.3.22 to 3.24, the tests are, in general, characterized by a force-slippage behaviour with very high initial stiffness until the achievement of the value of the static friction coefficient that, in all the analysed cases, was higher than the dynamic friction coefficient obtained in the first stabilized cycle.



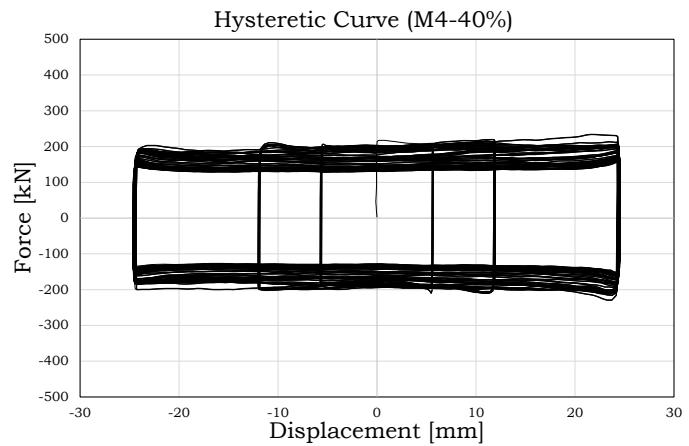
a)



b)



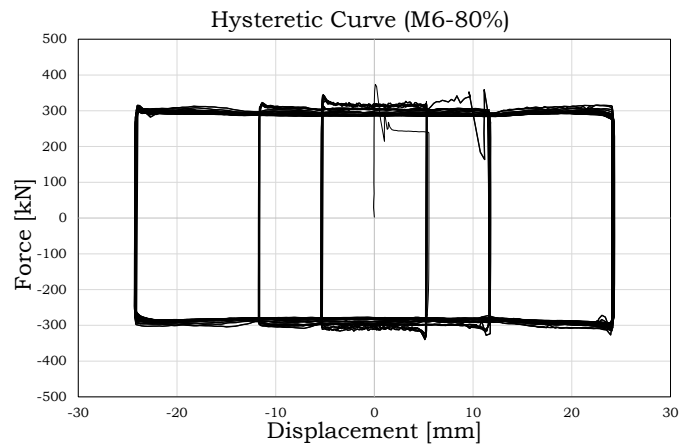
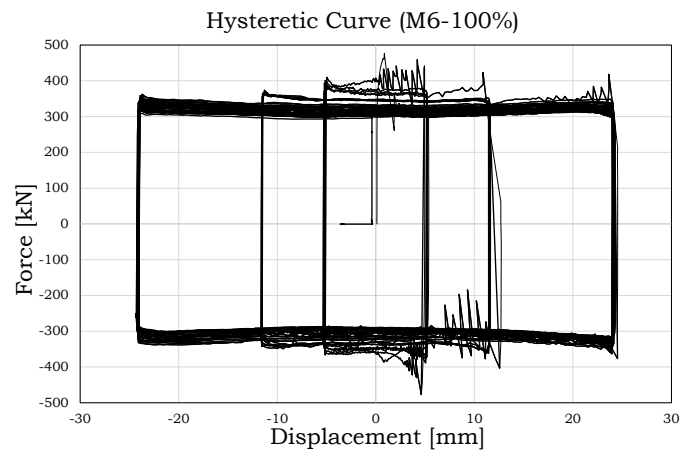
c)

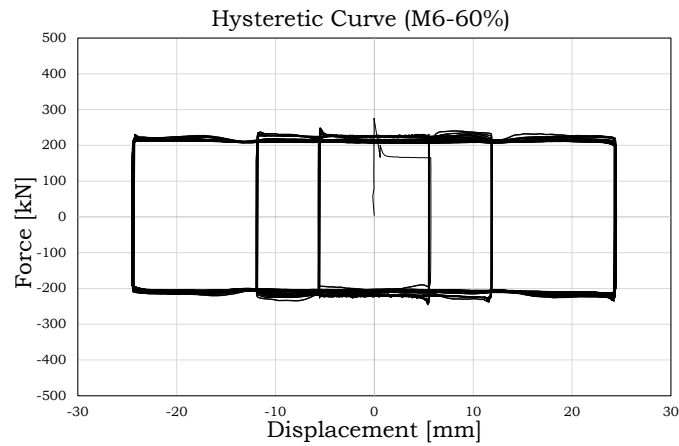


d)

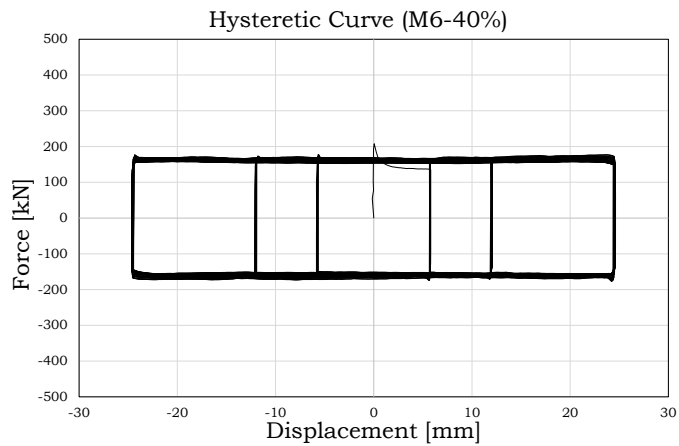
**Fig. 3.23** – Influence of the bolts’ pre-load over the force-displacement hysteretic response (M4)

All the materials exhibited a very high energy dissipation with hysteresis loops almost rectangular. In terms of force-displacement response, the only material providing a particular behaviour was material M6 which, as already explained in the previously, is an hard coating material whose behaviour is characterized, at high pressures, by a first cycle exhibiting a slight stick-slip response.





c)

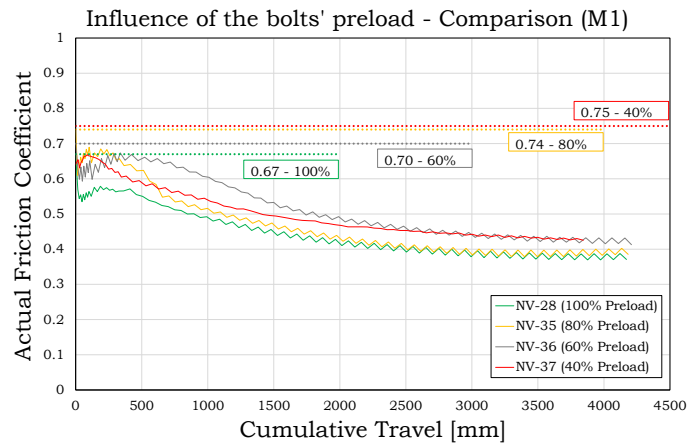


d)

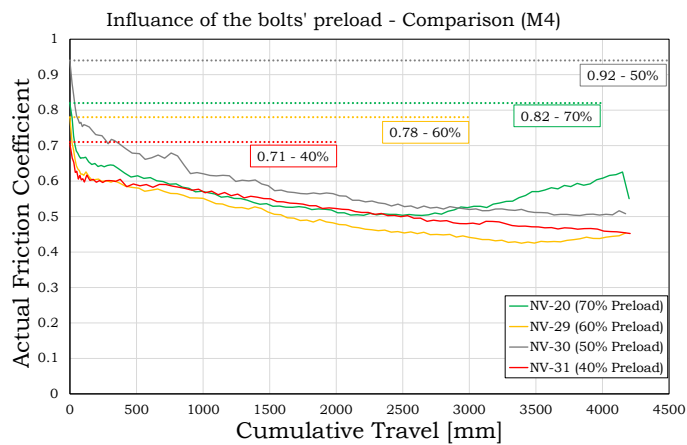
**Fig. 3.24** – Influence of the bolts’ pre-load over the force-displacement hysteretic response (M6)

Such a stick-slip is due to adhesion forces arising between the interfaces in contact and results in alternate stops and starts of the motion. As reported in Figs.3.21 to 3.23, one of the most important things observed with this session of testing is that, for this specific coating material, the stick-slip response tended to disappear when the pre-load applied to the bolts was reduced, revealing that the stick-slip

behaviour strongly depends on the contact pressure generated on the interface.



a)



b)



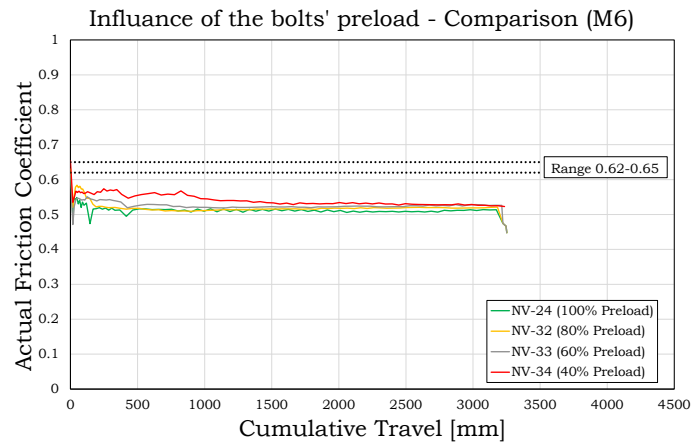
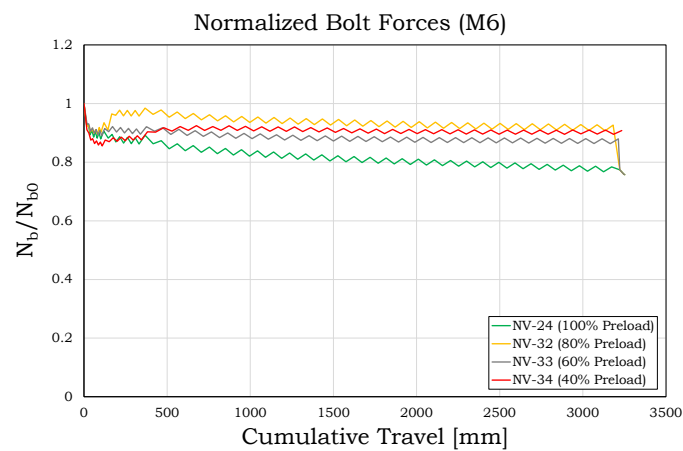


**Fig. 3.25** – Influence of the bolts' pre-load over the actual friction coefficient

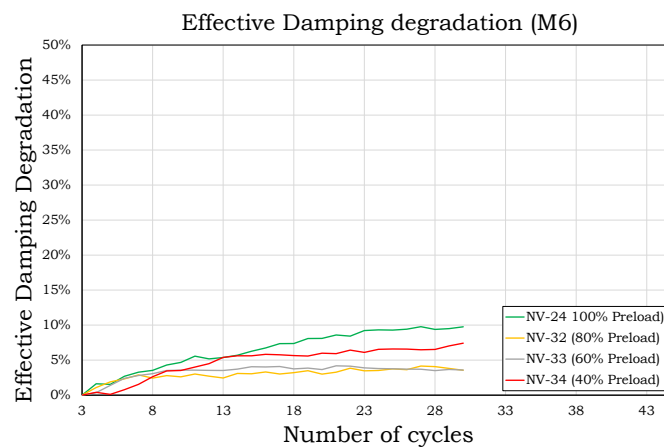
In terms of friction coefficient, as reported in synthesis in Fig.3.24 the three analysed materials did not show a strong variation and, as it will be hereinafter reported, the variation of the friction coefficient observed in this testing session was practically within the normal range of variation of the friction coefficient observed for these materials in the session of tests aimed at the evaluation of the random variability of the static and dynamic friction coefficients. In fact, the initial value of the friction coefficient for material M1 ranged from 0.67 to 0.75, for material M4 from 0.71 to 0.94 and for material M6 from 0.62 to 0.65 (not showing a clear tendency with respect to the applied preload), while the normal statistical range of variation of the same parameter is, as demonstrated hereinafter, equal to 0.62-0.81 for material M1, 0.69-0.84 and 0.52-0.68 for material M6.

Therefore, the tests at variable value of the preloading force did not point out a clear correlation between the friction coefficient and bolts' force for the three analysed coating materials. Conversely, the

representation of the bolts' forces, normalized with respect to the initial preload, versus the cumulative travel and the effective damping degradation versus the number of cycles for the maximum amplitude cycles, seemed to reveal that a reduction of the preloading force, as expected, results in a lower loss of bolt's preload and lower energy degradation.



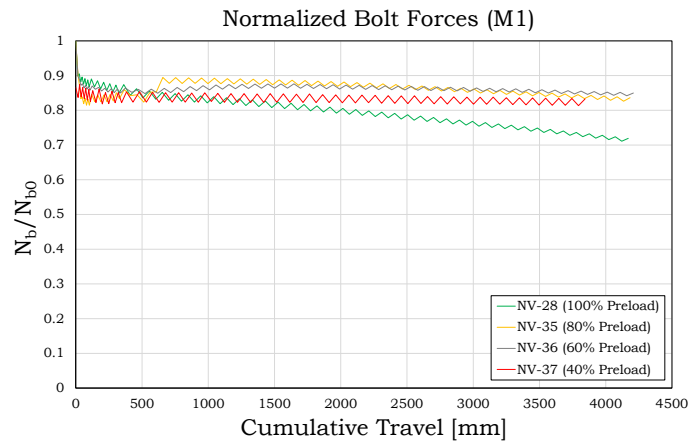
a)



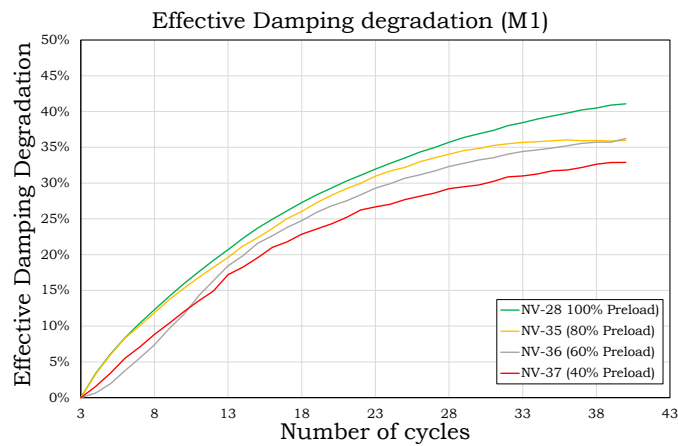
b)

**Fig. 3.26** – Bolts' preloading and effective damping for material M6

Additionally, the analysis of all the data of the test results (not reported extensively for reasons of length) revealed that for the hard material (M6) the effective damping degradation at the 10th cycle was always lower than the 10% as required by EN15129. Conversely, for materials M1 (Fig.3.26) and M4 (Fig.3.27) (soft materials) the analysis of the results revealed that this minimum requirement can be met only if the load pressure is limited to the 60% of the proof load.



a)



b)

**Fig. 3.27** – Bolts’ preloading and effective damping for material M1

In conclusion, on one hand stick and slip reasons and on the other hand minimum requirements in terms of effective damping degradation seem to suggest to limit the preload, for all the analysed interfaces, to a maximum value equal to the 60% of the proof load codified in EC3 part 1.8.

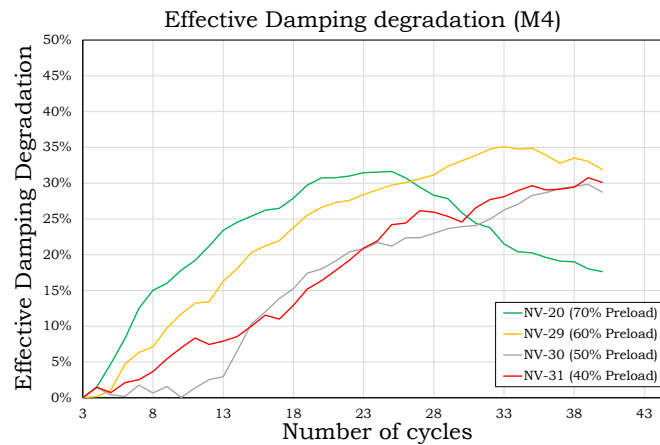
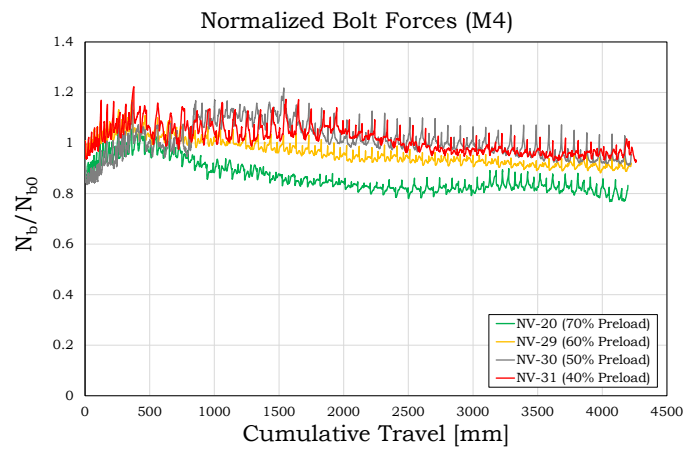


**Fig. 3.28** – Bolts' preloading and effective damping for material M4

### ***Influence of the Disc-Springs' Configuration***

The disc-springs are particular type of conical annular washers, also often referred as Belleville, which are able to compress elastically until reaching a threshold value beyond which they show a significant increase of stiffness until complete flattening.

Their main feature is that they can be arranged one over the other (parallel stack) in order to double the resistance or face-to-face (series stack) in order to double the deformability or, again, in combinations of series and parallels in order to obtain contemporarily a system of washers with desired values of stiffness and resistance. Their presence, in technical literature, is usually considered beneficial in all those cases where it is needed to maintain constant the pre-load in bolts over the life-time of a connection and especially in the cases where vibrations, creep or elastic interactions between bolts may be expected. Their possible effect is explained briefly in Fig.3.28 where the behaviour of a system with normal washers and another with disc springs are compared.

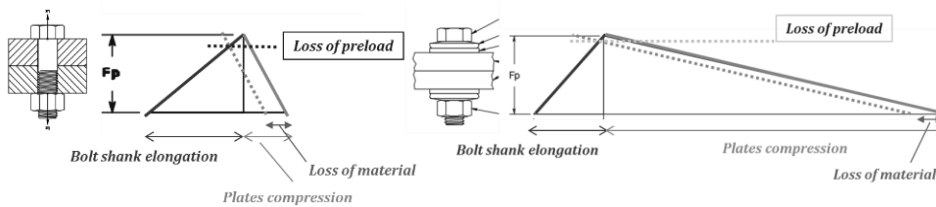
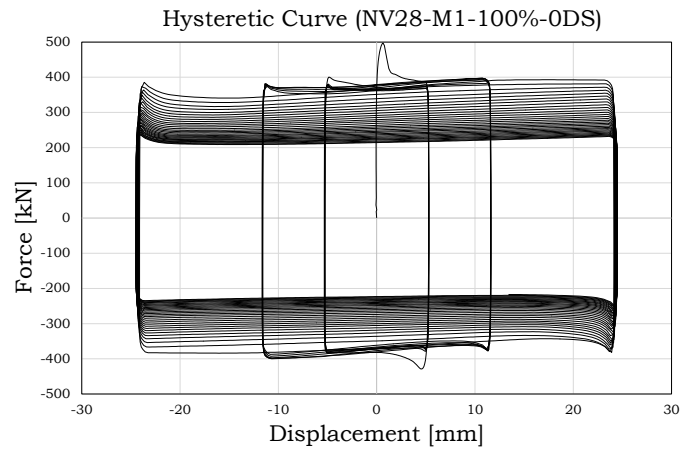
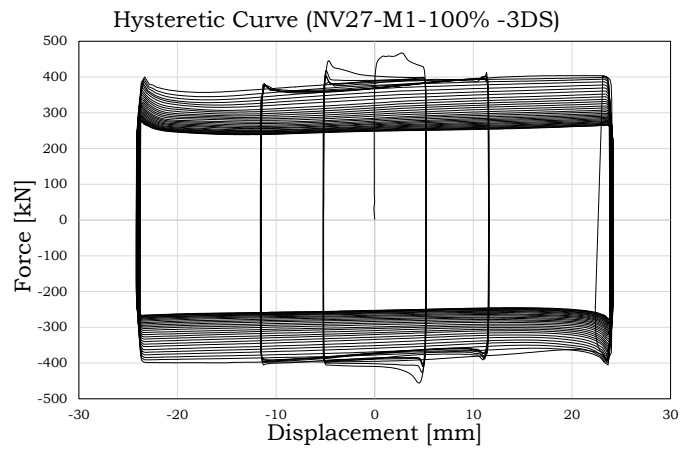


**Fig. 3.29** – Effect of disc springs

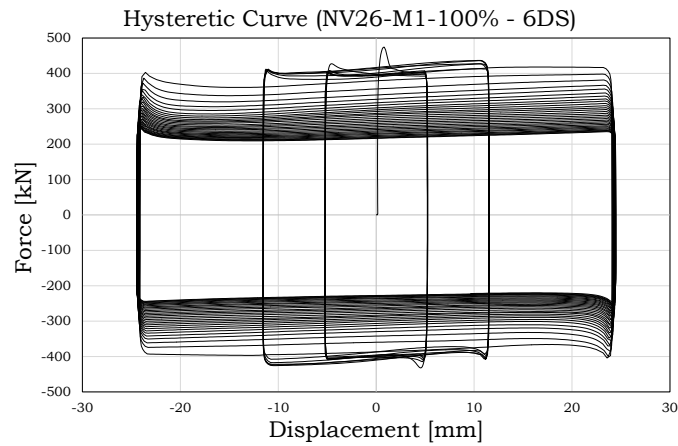
As before, the test results are summarized only for one material but negligible differences in the behaviour were observed for the three different materials. Therefore, what commented hereinafter for material M1 can be totally extended also to materials M4 and M6.



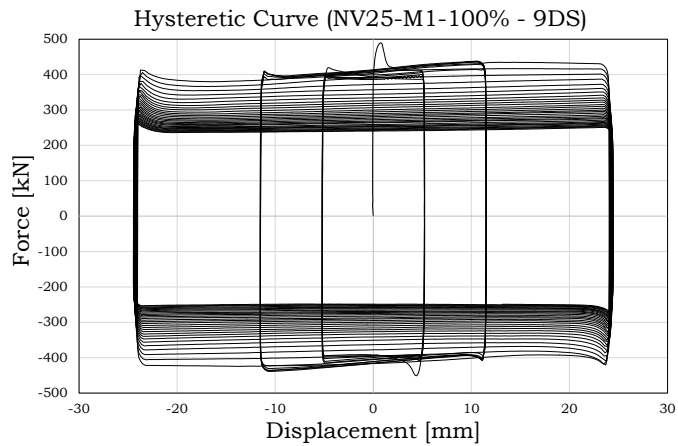
a)



b)



c)

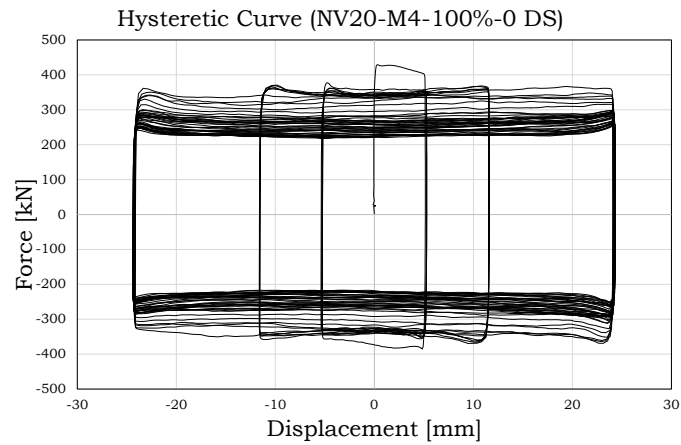


d)

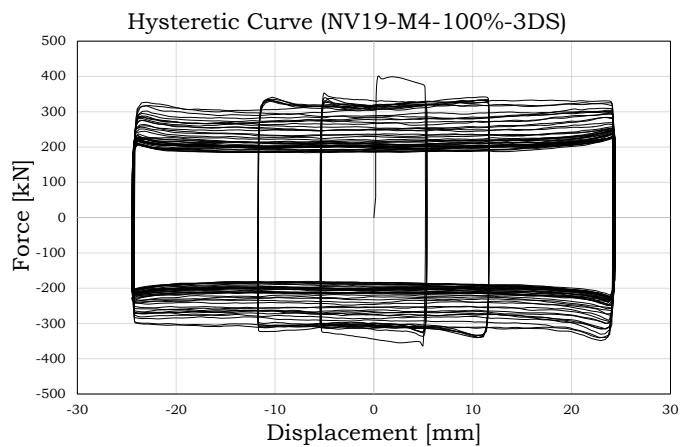
**Fig. 3.30** – Influence of the disc spring configuration over the hysteretic response (M1)

Considering as an example material M1, it is easy to understand immediately from Fig.3.29 that the configuration of disc springs, globally, did not seem to provide a significant influence over the hysteretic response. In fact, all the tests started with an initial slippage force of about 400 kN and ended with a force of about 200 kN and

rather, in contrast with the expected response, in the case with higher number of disc springs, the response was even slightly worse (Fig.3.28).

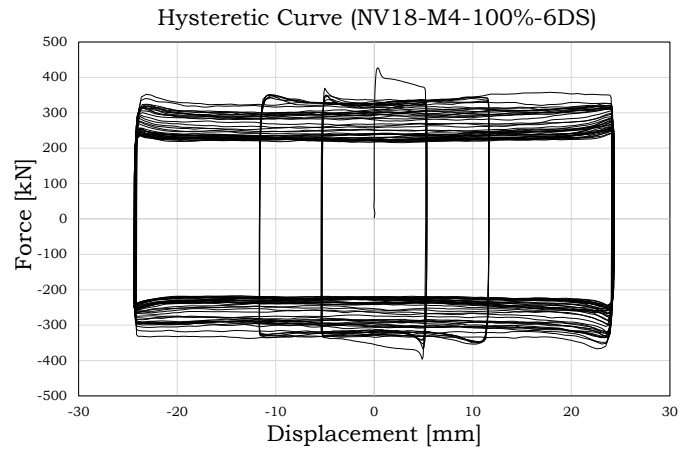


a)

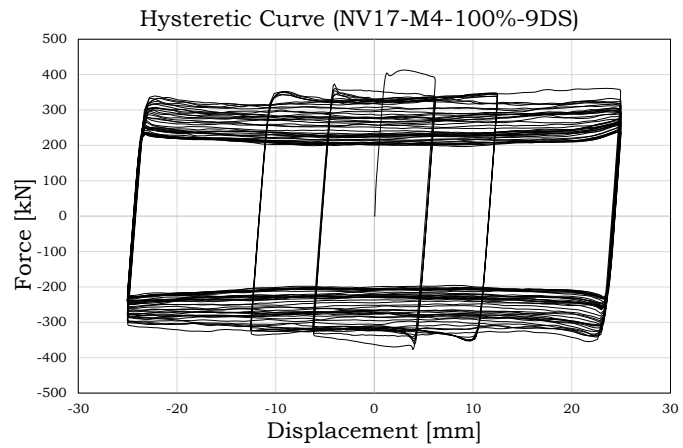


b)





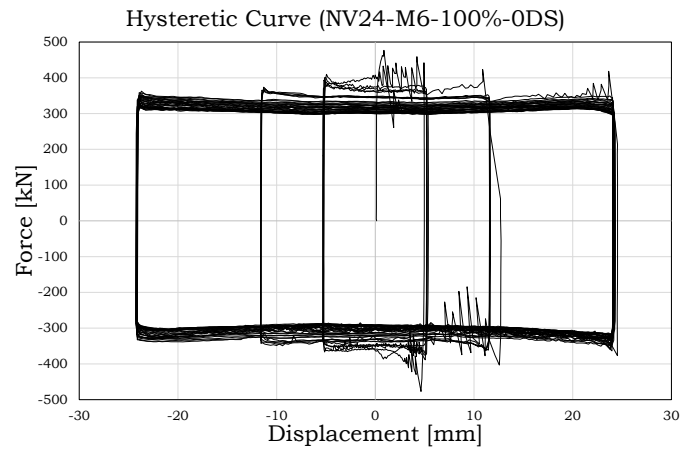
c)



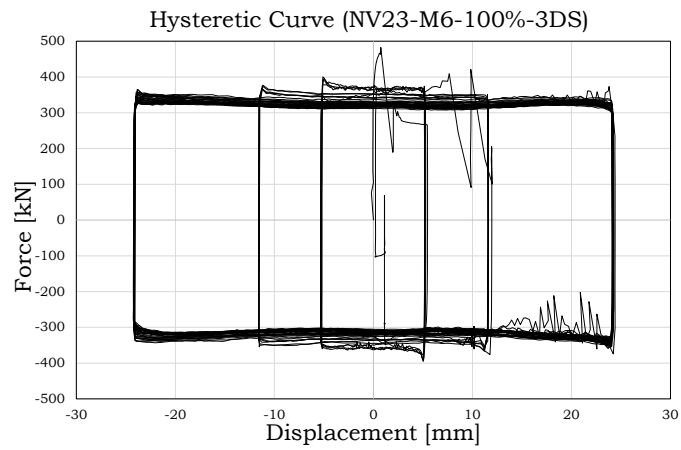
d)

**Fig. 3.31** – Influence of the disc spring configuration over the hysteretic response (M4)

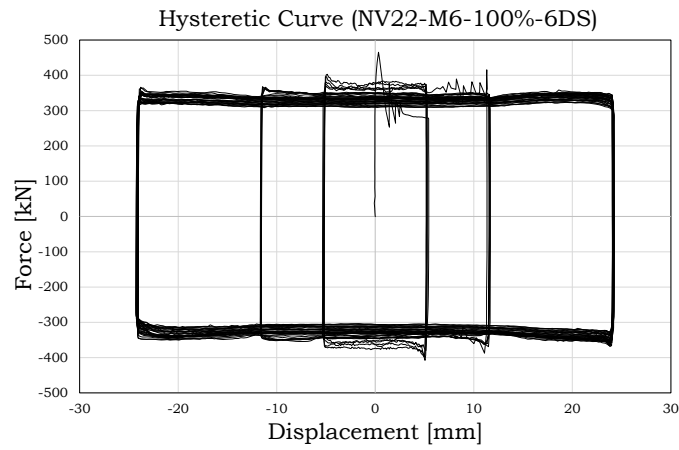
This result, from the point of view of the global behaviour points out the inefficiency of the disc springs in improving the response of the specimen.



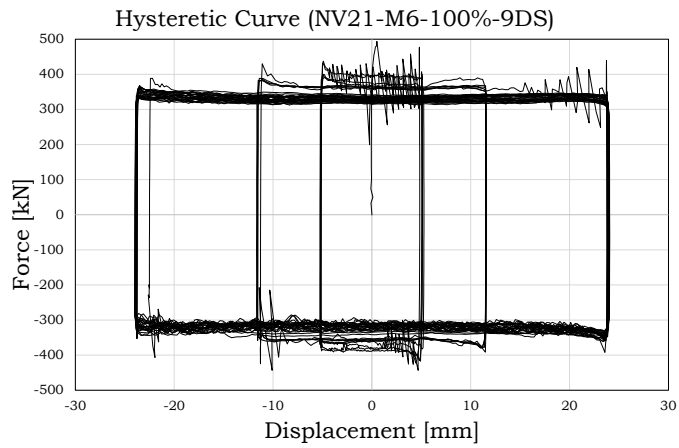
a)



b)



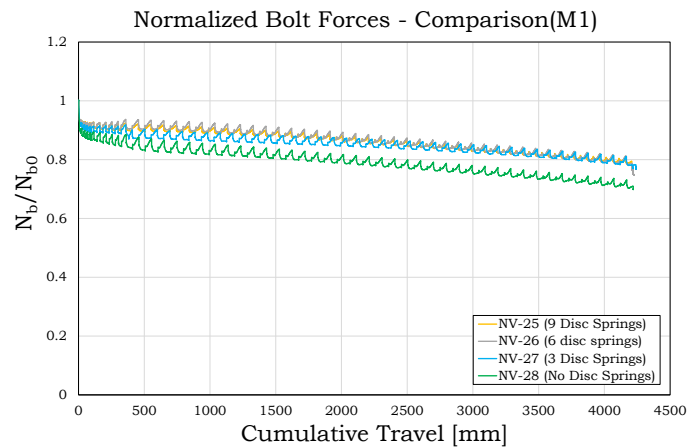
c)



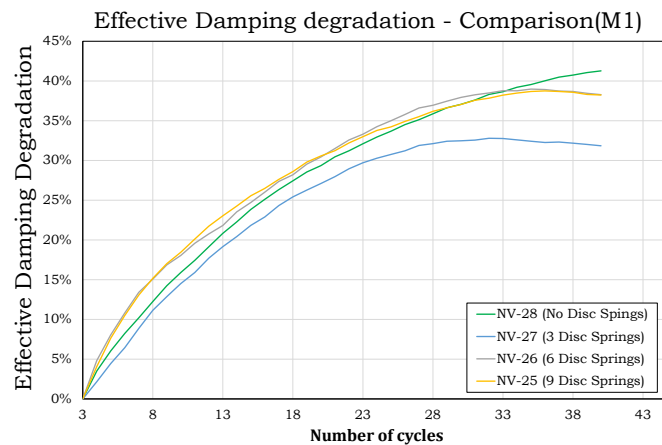
d)

**Fig. 3.32** – Influence of the disc spring configuration over the hysteretic response (M6)

Additionally even though on one hand it seems somehow unexpected and illogical, on the contrary it can be explained observing the representations of the bolts' forces during the test and the effective damping degradation diagram (Fig.3.32 to Fig.3.34).



a)

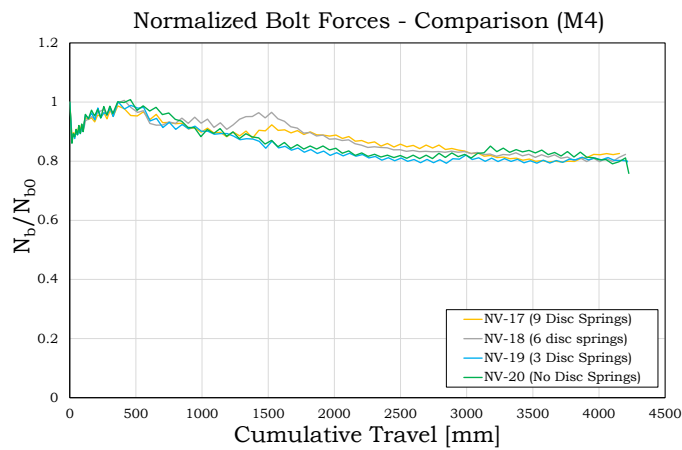


b)

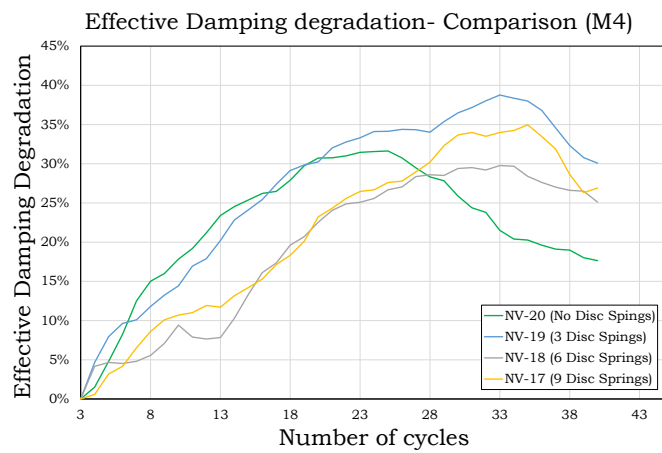
**Fig. 3.33** – Bolts' preloading and effective damping for material M1

In particular, the tension in the bolts' read with the load cells, when comparing the case with disc springs with the case with normal washers reveals that, indeed, the disc springs are able to maintain the preload in the bolts pretty constant during the test but, probably, in the same time the higher preload results also in a higher wearing of the coating material resulting, globally, in a higher degradation of the

slippage force. In fact, also the energy degradation diagram seems to show that, even varying the disc springs' configuration the energy dissipation supply tends to reduce showing higher deterioration with a higher number of disc springs.



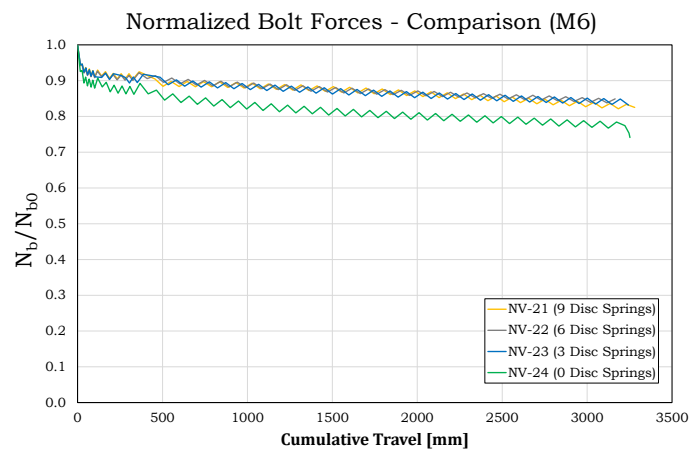
a)



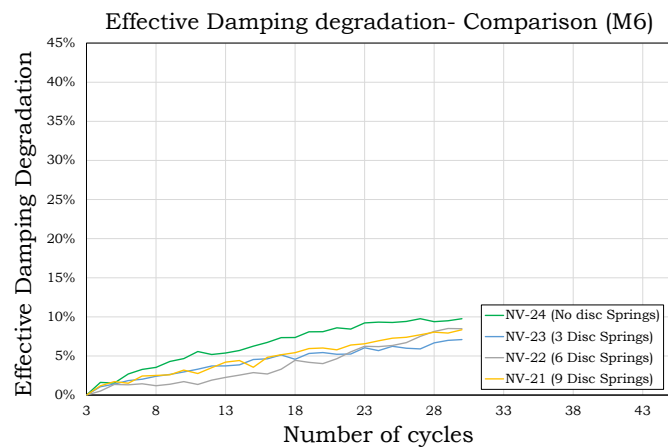
b)

**Fig. 3.34** – Bolts' preloading and effective damping for material M4

As a conclusion, the results of this analysis show, therefore, that the disc spring are effective in maintaining the pre-load constant over the friction interface but, from the point of view of the cyclic uniaxial behaviour they are not able to provide a significant improvement (and rather they seem to slightly worsen the response).



a)



b)

**Fig. 3.35** – Bolts' preloading and effective damping for material M6

Therefore, while their role may be significant in order to limit other effects, such as those related to the long-term response, vibrations or thermal effects, in the same time their effectiveness seems negligible in terms of improvement of the cyclic response in uni-axial tests.

### ***Influence of Randomness over the friction coefficient***

Following the two previous sessions of testing, other tests were planned with the main objective to evaluate the cyclic response of the three analysed interfaces in order to determine a statistical range of variation of the values of the friction coefficients to be used in design. In fact, it is easy to observe also just from the previous results that the examined coating materials are affected by a random variation that needs to be accounted for to individuate the main design parameters. In particular, as explained subsequently, for SLS and ULS checks are needed the following values of the friction coefficient:

- 1) characteristic value of the static friction coefficient for SLS checks;
- 2) characteristic value of the dynamic friction coefficient to be used in the ULS design of the dissipative components;
- 3) upper bound value of the static friction coefficient to be used, in the framework of capacity design, for the design of the non-dissipative part of the connection and of the structure (design of columns). This upper bound value is represented by the 95% fractile of the static friction coefficient which provides the maximum force that the damper can transfer to the structure before the activation of the sliding motion occurs. This series of test has been executed, for each coating material, on ten equal specimens, all preloaded at the recommended maximum value of the 60% (as it comes out, for different reasons, from the tests at variable pre-load) adopting a

configuration of disc springs with 2 in parallel 2 times in series (Table 3.2).

**Table 3.2** - Summary of the tests – 2<sup>nd</sup> phase (The round brackets represent the disc springs configuration, n° of parallel or series)

	Specimen code	Material code	Preload kN	% of PL/1.1	Spring configuration
<i>Different DS Configuration</i>	NV - 17	M4	134.75	70%	3X3 )))((0))
	NV - 18				3X3 )))(((
	NV - 19				3X3 )))
	NV - 20				NONE
	NV - 21	M6	188.65	100%	3X3 )))((0))
	NV - 22				3X3 )))(((
	NV - 23				3X3 )))
	NV - 24				NONE
	NV - 25	M1	188.65	100%	3X3 )))((0))
	NV - 26				3X3 )))(((
	NV - 27				3X3 )))
	NV - 28				NONE
<i>Variable Pre-load</i>	NV - 29	M4	113.19	60%	NONE
	NV - 30		94.33	50%	
	NV - 31		75.46	40%	
	NV - 32	M6	150.92	80%	NONE
	NV - 33		113.19	60%	
	NV - 34		75.46	40%	
	NV - 35	M1	150.92	80%	NONE
	NV - 36		113.19	60%	
	NV - 37		75.46	40%	

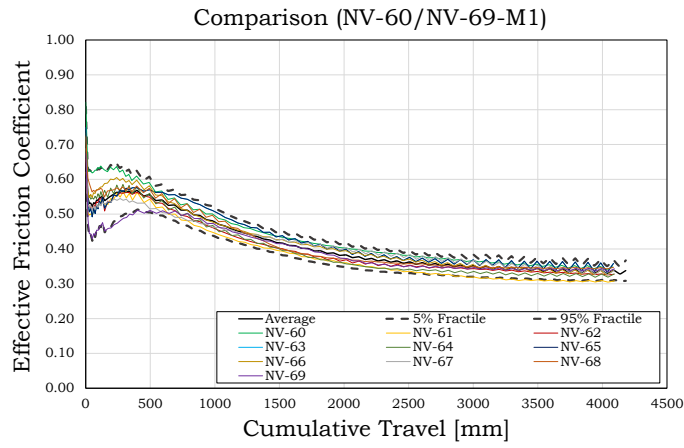


<i>Random variation Friction Coefficient</i>	NV - 38	M4	113.19	60%	2+3 ))((()
	NV - 39				
	NV - 40				
	NV - 41				
	NV - 42				
	NV - 43				
	NV - 44				
	NV - 45				
	NV - 46				
	NV - 47				
<i>Random variation Friction Coefficient</i>	NV - 49	M6	113.19	60%	2+3 ))((()
	NV - 50				
	NV - 51				
	NV - 52				
	NV - 53				
	NV - 54				
	NV - 55				
	NV - 56				
	NV - 57				
	NV - 58				
<i>Random variation Friction Coefficient</i>	NV - 60	M1	113.19	60%	2+3 ))((()
	NV - 61				
	NV - 62				
	NV - 63				
	NV - 64				
	NV - 65				
	NV - 66				
	NV - 67				
	NV - 68				
	NV - 69				

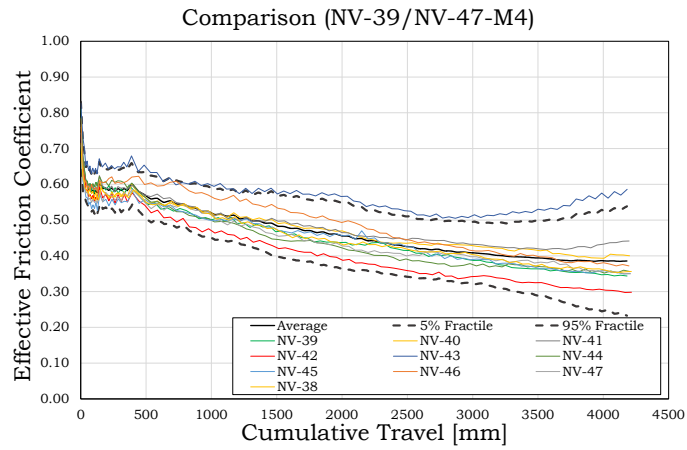
For every test, the same diagrams previously reported have been depicted. In particular, the main result of interest for the seismic design is related to the effective friction coefficient represented as a function of

the cumulative travel. This, as also explained before, represents the ratio between the sliding force measured during the test divided by the sum of the initial pre-loading forces multiplied for the number of interfaces (two in the current case).

In particular, in the diagrams of Fig.3.35 a synthesis of the friction coefficient obtained in all the tests, represented versus the cumulative travel is reported, indicated in the same diagrams the mean value (continuous line) and the 5% and 95% fractiles (lower and upper dashed lines) evaluated for each value of the cumulative travel subtracting or adding to the mean value  $k$  times the coefficient of variation. To account for the narrowness of the sample (10 specimens for each material), the value of  $k$  has been determined according to the approach suggested by EC0 in section D7.2, namely it has been assumed equal to 1.92 under the assumption of normal distribution. From Fig.3.35 it is possible to observe that, in general, for the whole loading history material M6 (the hard coating) provided a much more predictable response, while materials M1 and M4 (the soft coatings) provided a higher dispersion. Such a dispersion, clearly evident in the representations reported in Fig.3.35, it is not so strong if evaluated only on the initial peak value, namely the static slippage force. This aspect is better detailed in next section. In order to provide a fast tool for the design or modelling of devices with the three coating materials here described, a regression analysis of the data (mean and fractiles) has been carried out.



a)



b)

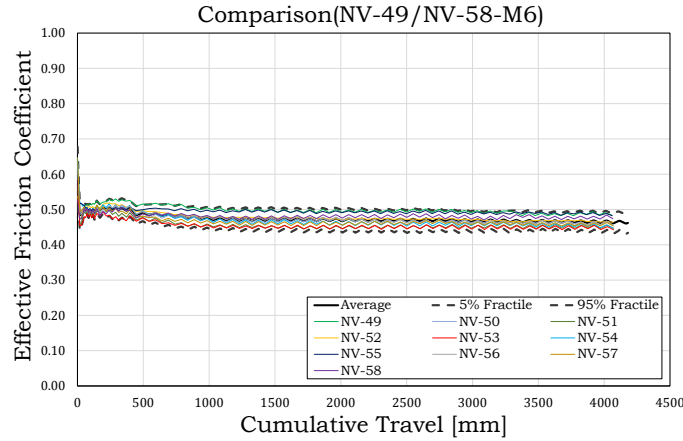


**Fig. 3.36** – Influence of the disc spring configuration over the preload and effective friction coefficient

This is reported for material M4:

*Regression analysis - characteristic values vs cumulative travel:*

$$\begin{aligned}
 \mu_{eff,k} &= 6.35 \cdot 10^{-5} \delta_t^2 - 6.35 \cdot 10^{-3} \delta_t + 0.69 && \text{if } \delta_t < 50 \text{ mm} \\
 \mu_{eff,k} &= 0.53 && \text{if } 50 < \delta_t < 400 \text{ mm} \\
 \mu_{eff,k} &= -1.233 \cdot 10^{-4} \delta_t + 0.579 && \text{if } 400 < \delta_t < 1500 \text{ mm} \\
 \mu_{eff,k} &= -5.32 \cdot 10^{-5} \delta_t + 0.474 && \text{if } 1500 < \delta_t < 4000 \text{ mm}
 \end{aligned} \quad (3.2)$$

*Regression analysis - mean values vs cumulative travel:*

$$\begin{aligned}
 \mu_{eff,ave} &= 7.34 \cdot 10^{-5} \delta_t^2 - 7.34 \cdot 10^{-3} \delta_t + 0.76 && \text{if } \delta_t < 50 \text{ mm} \\
 \mu_{eff,ave} &= 0.58 && \text{if } 50 < \delta_t < 400 \text{ mm} \\
 \mu_{eff,ave} &= -9.096 \cdot 10^{-5} \delta_t + 0.616 && \text{if } 400 < \delta_t < 1500 \text{ mm} \\
 \mu_{eff,ave} &= -4.41 \cdot 10^{-5} \delta_t + 0.545 && \text{if } 1500 < \delta_t < 4000 \text{ mm}
 \end{aligned} \quad (3.3)$$

*Regression analysis - upper bound values vs cumulative travel:*

$$\begin{aligned}
 \mu_{eff,95\%} &= 7.93 \cdot 10^{-5} \delta_t^2 - 7.934 \cdot 10^{-3} \delta_t + 0.84 && \text{if } \delta_t < 50 \text{ mm} \\
 \mu_{eff,ave} &= 0.64 && \text{if } 50 < \delta_t < 400 \text{ mm} \\
 \mu_{eff,95\%} &= -7.37 \cdot 10^{-5} \delta_t + 0.669 && \text{if } 400 < \delta_t < 1500 \text{ mm} \\
 \mu_{eff,95\%} &= -3.09 \cdot 10^{-5} \delta_t + 0.604 && \text{if } 1500 < \delta_t < 4000 \text{ mm}
 \end{aligned} \quad (3.4)$$

### **3.2.2. Design procedure**

Starting from the results obtained in previous sections, the main parameters to be used for the design of FREEDAM connections with the three materials described in this work have been derived. As aforementioned, the design of a friction device requires mainly three different values of the friction coefficient. The value to be used for serviceability limit states check, the value to design the resistance of dissipative component of the structure, namely the friction damper, and the upper bound value of the friction coefficient to design the non-dissipative elements of the structure. For SLS checks it has to be mainly guaranteed that the friction connections do not slip under the occurrence of static loading conditions or under the occurrence of moderate seismic events. In all these load combinations, *the characteristic value of the static friction coefficient* has to be used. For the energy dissipaters, in order to size the number of bolts required and their tightening torque, it is needed to consider the *lowest expected value of the dynamic friction coefficient*, namely the characteristic value of the dynamic friction coefficient. Additionally, for the non-dissipative parts of the structure, that in case of a FREEDAM frame are the beams, the columns and the connecting elements, the highest expected value of the static friction coefficient has to be considered, namely the *95% fractile of the static friction coefficient*.

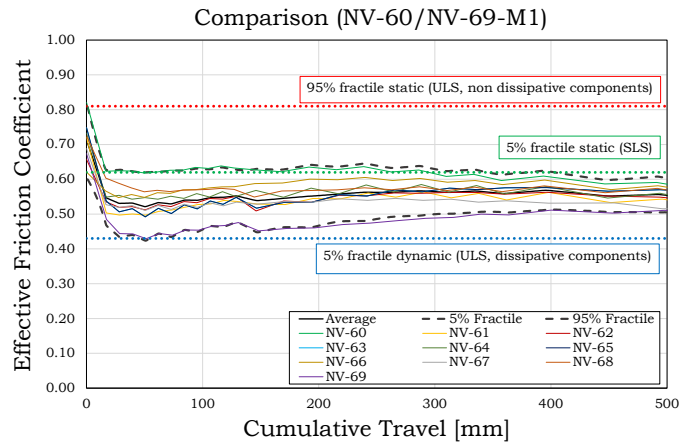
In fact, this is the maximum possible value that, from a statistical point of view, the non-dissipative elements have to withstand before that sliding of the damping devices occurs. With this aim, for each material, for every set of 10 data, the effective and actual values of the static

friction coefficients have been evaluated, summarizing the results in Table 3.3.

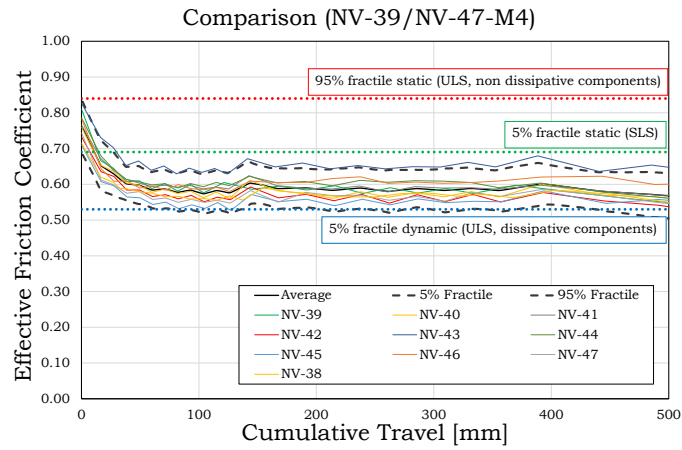
**Table 3.3** - Static friction coefficients for every tests

Material <b>M1</b>				Material <b>M4</b>				Material <b>M6</b>			
Test n°	$\mu_{0,eff}$	$\mu_{0,act}$		Test n°	$\mu_{0,eff}$	$\mu_{0,act}$		Test n°	$\mu_{0,eff}$	$\mu_{0,act}$	
NV	60	0.82	0.84	NV	39	0.64	0.65	NV	49	0.64	0.65
NV	61	0.72	0.73	NV	40	0.63	0.63	NV	50	0.63	0.63
NV	62	0.66	0.67	NV	41	0.57	0.57	NV	51	0.57	0.57
NV	63	0.75	0.77	NV	42	0.54	0.55	NV	52	0.54	0.55
NV	64	0.73	0.75	NV	43	0.59	0.59	NV	53	0.59	0.59
NV	65	0.75	0.77	NV	44	0.65	0.65	NV	54	0.65	0.65
NV	66	0.62	0.62	NV	45	0.58	0.59	NV	55	0.58	0.59
NV	67	0.69	0.70	NV	46	0.64	0.65	NV	56	0.64	0.65
NV	68	0.72	0.74	NV	47	0.65	0.65	NV	57	0.65	0.65
NV	69	0.67	0.69	NV	48	0.53	0.53	NV	58	0.53	0.53
MEAN		0.71	0.73	MEAN		0.76	0.79	MEAN		0.60	0.61
DEV ST		0.06	0.061	DEV ST		0.04	0.041	DEV ST		0.05	0.047
CV		0.08	0.084	CV		0.05	0.052	CV		0.08	0.077
Fractile 5%		0.62	0.61	Fractile 5%		0.69	0.72	Fractile 5%		0.52	0.52
Fractile 95%		0.81	0.85	Fractile 95%		0.84	0.87	Fractile 95%		0.68	0.70

As described previously, these values together with the 5% fractile of the dynamic friction coefficient evaluated in correspondence of the first stabilized cycle represent the value needed to design the friction connections.



a)



b)

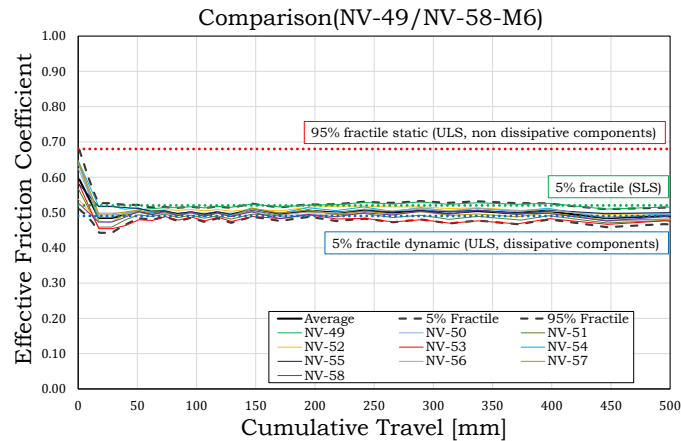


**Fig. 3.37** – Design values of the friction coefficient (static or dynamic) for the three materials

The meanings of these friction coefficients are represented in Fig.3.36, while for the sake of simplicity they are summarized in Table 3.4.

**Table 3.4** - Design values of the friction coefficients

Material <b>M1</b>		Material <b>M4</b>		Material <b>M6</b>	
Design FC	$\mu_{0,d}$	Design FC	$\mu_{0,d}$	Design FC	$\mu_{0,d}$
Static 5% fractile	0.62	Static 5% fractile	0.69	Static 5% fractile	0.52
Static 95% fractile	0.81	Static 95% fractile	0.84	Static 95% fractile	0.68
Dynamic 5% fractile	0.43	Dynamic 5% fractile	0.53	Dynamic 5% fractile	0.49

In the design procedure also the random variation of the bolts' tightening and, as a consequence, the preload force has to be taken into account. In fact, the tightening of the bolts is a sensitive process that introduces uncertainties, both in the construction phase and during the life time of the structure (relaxation). According to the EN 1090-2 [33], the torque method is, basically, a force (torque) control method and it is



divided into two steps: during the first one the torque applied to the bolts is equal to 0.75 times the torque reference value (i.e.  $T_r = 0.7 \cdot A_b \cdot f_{ub} \cdot k \cdot d_b$ ), during the second phase the torque applied is equal to 1.1 times the torque reference value, which corresponds, implicitly, to a target mean value equal to  $(1 + 1.64V_{comb})0.7 \cdot A_b \cdot f_{ub} \cdot k \cdot d_b$  with a combined coefficient of variation including the variation of the tools used for testing and installation. This increase of the 10% of the nominal preload value is meant to consider the random variation of the bolts' tightening in order to guarantee contemporarily that the 5% fractile of the pre-load (lower bound value) is higher than the nominal preload ( $0.7 \cdot A_b \cdot f_{ub}$ ) and that the 95% fractile (upper bound value) is lower than the nominal bolt resistance ( $0.9 \cdot A_b \cdot f_{ub}$ ) (this to prevent unexpected bolts' failures).

In particular, in Table 3.5 the coefficients of variation are reported:

**Table 3.5** – Coefficient of variation for the preload force

Coefficient of variation $k$ -factor ( $V_k$ ) for bolt assemblies EN-14399-3	A	0.06
Coefficient of variation $k$ -factor ( $V_k$ ) for testing tools: EN-14399-2		
- the required accuracy of the bolt force measuring device	B	0.02
- the repeatability of the bolt force measuring device	C	0.01
- the required accuracy of the torque	D	0.01
- the repeatability of the torque	E	0.01
Coefficient of variation $k$ -factor ( $V_k$ ) for installation tools: EN-1090-2		
- the required accuracy of the torque in the second step	F	0.04

The combined  $k$ -factor is defined as:

$$V_{comb} = \sqrt{(A^2 + B^2 + C^2 + D^2 + E^2 + F^2)} \quad (3.5)$$

The difference between the static and the dynamic friction coefficient and the randomness of the two variables has to be accounted for, especially for the hierarchy of the elements. The simplest way to do this is to consider the overstrength coefficient  $\gamma_{ov}$  that is given by the ratio between the 95% fractile of the static friction force and the 5% fractile of the dynamic friction force:

$$\gamma_{ov} = \frac{F_{stat,95\%} \cdot n_b \cdot n_s}{\mu_{d,k} \cdot F_{p,k} \cdot n_b \cdot n_s} \quad (3.6)$$

With reference to the three tested materials, the values of the overstrength factor are summarized in Table 3.6:

**Table 3.6** – Values of the overstrength factor  $\gamma_{ov}$

	M1	M4	M6
$\gamma_{ov}$	2.02	1.70	1.48

Starting from the results of the preliminary tests on the joint component, the design of dissipative DST connections with friction pads has been performed. The two different joint details proposed provides to modify the classical detail of a double split Tee joint by substituting the lower T-stub with a friction damper composed by a stack of metallic plates in which, one or more layers of friction materials are interposed. In particular two different configurations of the friction device have been considered: an haunch composed by horizontal steel plates with normal holes except the inner plate realized in 1.4301 Stainless Steel equivalent to AISI 304 steel and bolted to the pre-stressed friction shims with M20

class 10.9 HV bolts (Fig. 3.37a). The second configuration of the device is characterized by a plate bolted to the bottom beam flange and welded to the vertical slotted Stainless Steel plate that, even in this case, has to be bolted to the friction shims with M20 class 10.9 HV bolts (Fig.3.37b).

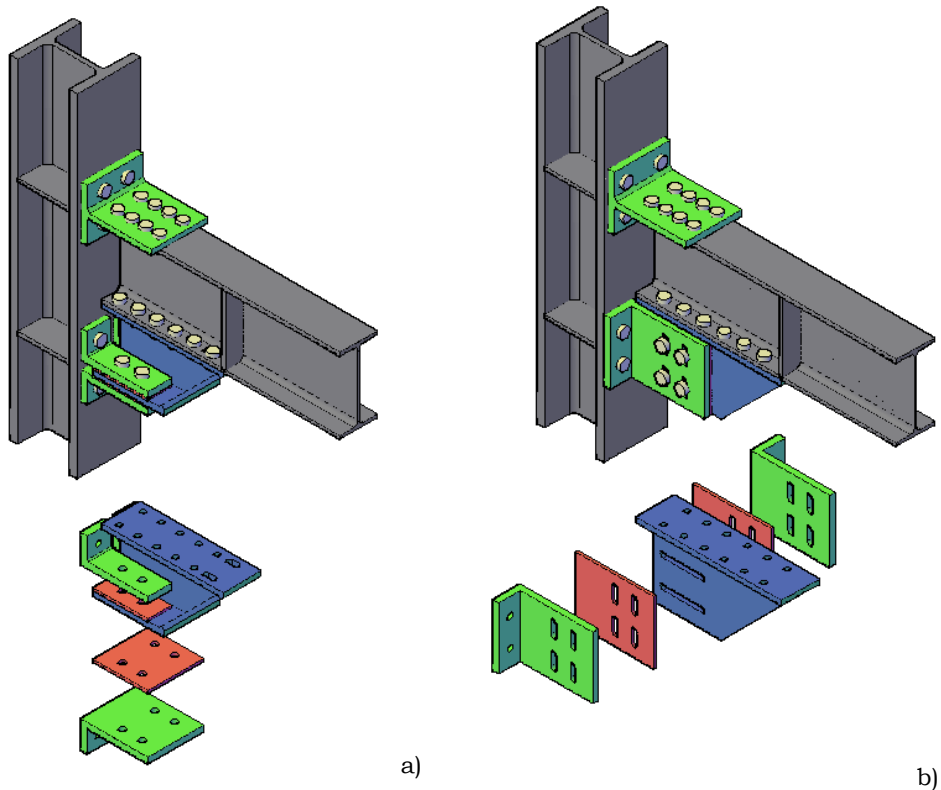


**Fig. 3.38** – FREEDAM joint configurations: a) horizontal friction device;  
b) vertical friction device

In the former configuration, the friction shims and the angles have to present vertical slotted holes in order to accommodate the rotation of the beam. In this way, the energy dissipation supply of the beam-joint system is provided by the friction damper, while all the other elements

of the connection and the beam are designed in order to be completely free from damage. This strategy, as already demonstrated in some preliminary studies on different prototypes, allows the development of beam-to-column connections with high energy dissipation able to accommodate the required displacements without any damage. A significant advantage of these joint configurations is that, by controlling the tightening torque applied to the bolts, it is possible to calibrate the exact amount of force that is transmitted to the column obtaining a flexural capacity very close to the nominal bending resistance of the connected beam. In such a way, the beam section is fully exploited, but both the oversizing of the other joint components (usually requiring supplementary web plates, reinforcing ribs, cover plates, increased bolt diameter, etc.) and the column oversizing (because of beam-column hierarchy criterion) are significantly limited.

With regards to the proposed connections the following components have to be designed: the shear panel, the column web panels in tension and compression, the T-stub/Angles and the friction damper. In order to obtain a joint where the only component providing energy dissipation is the friction damper, the steel parts have been oversized with respect to the maximum force that the friction damper is able to transmit. According to this hierarchy, the geometry of all the elements composing the joint has been defined by exploiting the formulations provided by literature models or by means of the formulations given in EC3 [8].

The connections have to be designed for a bending moment value greater to beam plastic resistance, given by the Eq. 2.12, because of the possibility to exploit the additional strengthening resulting from the haunched end. As the ratio between the bending moment that the joint is able to withstand before the slippage of the friction damper and the

beam plastic resistance is strongly dependent on the geometrical properties of the haunch, that are not known a priori, the design of the joint is performed by means of a very simple iterative procedure described in the following.

### ***Design of the friction damper***

In the FREEDAM connections, due to the high simplification of the structural detail (even with respect to some of the most common types of beam-to-column connections), the bending moment transferred from the beam to the column can be controlled only by calibrating the slippage force of the friction damper, which is the result of the product of the friction coefficient (arising between the friction pads and the steel composing the internal plate of the haunch), multiplied for the number of friction interfaces (two in case of a symmetrical damper) and for the sum of the pre-tightening forces applied with the bolts.

Starting from the given value of the beam plastic resistance  $M_{p,b}$  and the lever arm  $h$ , the device has to withstand to the design friction force evaluated as:

$$F_{slip,Ed} = \frac{M_{p,b}}{h} \quad (3.7)$$

The lever arm is defined as the distance between the upper T-stub of the FREEDAM connection and the mid-centre of the friction damper, that in configuration n.1 (Fig. 3.38a) is given by:

$$h_1 = h_b + h_h \quad (3.8)$$

where  $h_b$  is the beam depth and  $h_h$  is the height of the haunch.

In the joint configuration n.2 (Fig. 3.38b), mid-centre of the friction damper results to be coincident with the axis of the bolts so that the lever arm is defined as:

$$h_2 = h_b + t + \frac{h_h}{2} \quad (3.9)$$

where  $t$  is the distance between the upper bound of friction pads and the lower beam flange and  $h_b$  and  $h_h$  are the parameters previously defined.

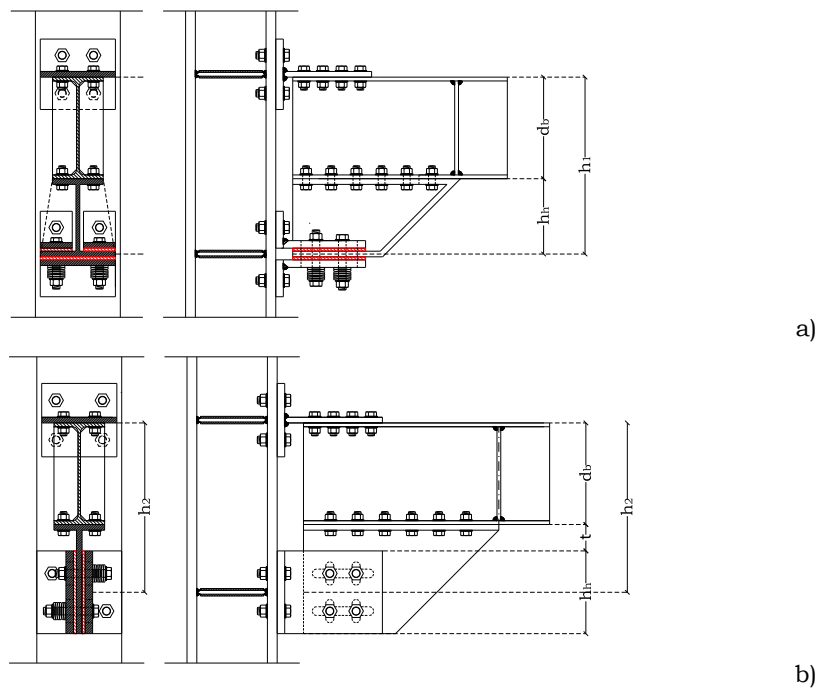


**Fig. 3.39** – Lever arm of friction joints: a) configuration n.1; b) configuration n.2

The sliding force  $F_{sliding}$  could be determined by means of the relationship between the dynamic friction coefficient  $\mu_d$  of the chosen friction material, the bolt preloading force  $F_p$ , the number of bolts  $n_b$  and the number of surfaces in contact  $n_s$ :

$$F_{sliding} = \mu_d \cdot F_p \cdot n_b \cdot n_s \quad (3.10)$$

Therefore, equating the design friction force and the sliding force, the minimum number of the bolts can be evaluated:

$$n_{b,min} = \frac{M_{p,b}}{h \cdot \mu_{d,5\%} \cdot F_p \cdot n_s} \quad (3.11)$$

In particular, in order to evaluate the minimum value of the force that allows the slippage of the friction damper, the 5% fractile of the dynamic friction coefficient  $\mu_{d,5\%}$  has to be considered.

The input data results to be the diameter of the preloaded bolts, the number of the surfaces in contact (equal to two in both joint configurations), and the value of the bolt preload that is evaluated according to [8]. Once evaluated the number of the bolts, it is possible to easily determine, applying the Coulomb equation, the design friction resistance:

$$F_{friction,Rd} = \mu_{d,5\%} \cdot F_p \cdot n_b \cdot n_s \quad (3.12)$$

and the correspondent value of the bending moment:

$$M_{friction,Rd} = F_{friction,Rd} \cdot h \quad (3.13)$$

The other parameter to be controlled in the design is the length of the slots made on the haunch which allows the movement of the beam on the friction material. In particular, this parameter governs the rotational capacity of the connection and, as a consequence, it can be selected starting from the knowledge of the minimum required value of the rotational capacity, by using the following equation:

$$L_{slot} = (n_b - 1)p + d_b + 2\phi h \quad (3.14)$$

where  $d_b$  is the bolts diameter,  $n_b$  is the number of bolt rows used to fasten the web of the L-stub to the haunch,  $p$  is the bolt pitch,  $\phi$  is the assumed value of the rotational capacity and  $h$  is the lever arm of joints.

#### ***Design of the non-dissipative components***

Starting from the evaluation of the minimum length of the slots, it is possible to determine the horizontal overall dimension of the haunch on the basis of technological considerations and, as a consequence, the distance  $a$  between the beam section where the plastic hinge could develop and the column flange (Fig. 3.39).

As aforementioned, for the non-dissipative parts of the structure, the highest expected value of the static friction coefficient has to be considered. Starting from this concept, applying the basic principles of “capacity design”, the maximum bending moment at the column face  $M_{cf.cd}$  can be determined as:



$$M_{cf.cd} = \gamma_{ov} \cdot M_{friction,Rd} \tag{3.15}$$

As previously said, the bending moment  $M_{cf.cd}$  is greater than the plastic resistance of the beam because of the possibility to exploit the additional strengthening resulting from the haunch end. Therefore, it is essential to evaluate the bending moment achievable in correspondence of the axis of the beam plastic hinge that has to be smaller than the plastic resistance of the beam:

$$M_b = M_{cf.cd} \cdot \frac{L_e - a}{L_e} \leq M_{b,p} \tag{3.16}$$

where  $L_e$  is the shear length of the beam, already defined in section 2.3.

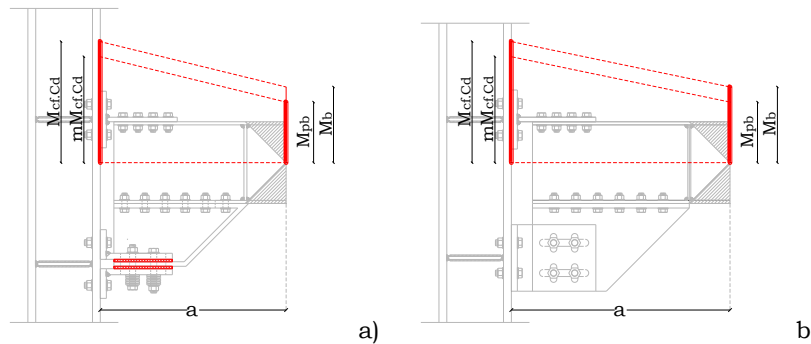


**Fig. 3.40** – Distance between the axis of the beam plastic hinge and the column flange: a) configuration n.1; b) configuration n.2

If the disequation given by the Eq.(3.16) is not satisfied, the bending moment of the connection  $M_{cf.cd}$  has to be reduced. It can be easily calibrated by controlling the tightening torque of the bolts of the friction damper in order to ensure that the beam remains in elastic range. How

reduce the tightening torque can be evaluated identifying a parameter  $m$  that is the ratio between the bending moment  $M_b$  previously defined and the plastic resistance of the beam:

$$m = \frac{M_{b,p}}{M_b} \quad (3.17)$$

The design friction resistance given by the Eq. 3.12 has to be recalculated as:

$$F_{friction,Rd} = \mu_{d,5\%} \cdot (m \cdot F_p) \cdot n_b \cdot n_s \quad (3.18)$$

In this way, the force that the joint has to withstand before that the slippage of the friction damper occurs, results to be equal to:

$$\frac{m \cdot M_{cf,cd}}{h} = F_{cf,cd} = \frac{m \cdot M_{friction,Rd} \cdot \gamma_{ov}}{h} \quad (3.19)$$

According to the principles of the “capacity design”, the non dissipative components, namely the T-stub and angles in bending, the haunch, the column web in tension and compression, the column flange in bending, have to be designed in order to transmit the maximum force that the dissipative component is able to exhibit, i.e. the maximum static force evaluated by means of the Eq. 3.15.

To this aim, a sequence of design operations or resistance check of the joint components has to be followed:

**Step 1:** Evaluation, considering the lowest expected value of the dynamic friction coefficient, namely the characteristic value of

the dynamic friction coefficient, of the design friction resistance  $F_{friction,Rd}$  of the dissipative component, i.e. the friction device, by means of Eq. (3.12).

**Step 2:** Design of the length of the slots made on the haunch in order to evaluate the overall dimension of the reinforced part of the joint.

**Step 3:** Calculation of bending moment  $M_{cf,cd}$  at the column flange, considering the maximum expected value of the static friction coefficient, namely 95% fractile of the static friction coefficient, and check of the resistance of the beam in bending; if not satisfied, the tightening torque of the bolts of the friction damper has to be reduced in order to reduce the force that the joint has to withstand before the slippage of the friction damper.

**Step 4:** Design of the bolt diameter.

**Step 5:** Design of the T-stub and L-stubs.

**Step 6:** Design of the bolts connecting the lower flange of the beam and the flange of the haunch. In order to avoid the slippage of the two surfaces in contact, the bolts have to be preloaded considering the proof value of the tightening torque.

**Step 7:** Check of the resistance of the column web in shear and design of supplementary web plates if needed. Eurocode 3 introduces a limitation about the thickness of the supplementary plates. In particular, the shear area  $A_{vc}$  may be increased no more than  $b_{stwc}$ . If a further supplementary web plate is added on the other side of the web, no further increase of the shear

area is allowed. The proposed method does not take into account such limitation.

**Step 8:** Check of the resistance of the column web in tension and in compression; if needed continuity plates are added and/or supplementary web plates are extended to cover also tension and compression zones.

**Step 9:** Check of the resistance of the column flange in bending by modelling the tension zone by means of an equivalent T-stub.

### 3.3. References

- [1] V. Piluso, G. Rizzano: “*Experimental analysis and modelling of bolted T-stubs under cyclic loads*”. *Journal of Constructional Steel Research*, vol. 64, pp. 655–669, 2008.
- [2] M. Latour, V. Piluso and G. Rizzano: “*Experimental analysis of innovative dissipative bolted double split tee beam-to-column connections*”, *Steel Construction*, Vol. 4, pp. 53-64, 2011.
- [3] V. Piluso, C. Faella, G. Rizzano: “*Ultimate Behaviour of Bolted T-stubs – I. Theoretical Model*”. *Journal of Structural Engineering*, ASCE, vol. 127, pp. 686–693, 2001.
- [4] V. Piluso, C. Faella, G. Rizzano: “*Ultimate Behaviour of Bolted T-stubs – II. Experimental Analysis*”. *Journal of Structural Engineering*, ASCE, vol. 127, No. 6, pp. 694–704, 2001.
- [5] M. Latour and G. Rizzano: “*Monotonic Modelling, Cyclic Behaviour and Fatigue Life of Dissipative T-stubs*”. ICASS 2009, Hong Kong, 2009.
- [6] M. Latour, V. Piluso and G. Rizzano: “*Cyclic behaviour of Friction Dissipative Double Split Tee Connections*”. STESSA 2011, Santiago de Chile, 2011.
- [7] CEN, 2005c. “*Eurocode 8: Design of structures for earthquake resistance - Part 1: General rules, seismic actions and rules for buildings*”. s.l.:s.n.
- [8] CEN, 2005b. “*Eurocode 3: Design of steel structures - Part 1-8: Design of joints*”. s.l.:s.n.
- [9] D. Beg, E. Zupancic and I. Vayas: “*On the Rotation Capacity of Moment Connections*”. *Journal of Constructional Steel Research*, 60, pp.601-20, 2004.
- [10] A.M. Girao Coelho, F. Bijlaard and L. Simoes Da Silva: “*Experimental Assessment of the Ductility of Extended End Plate Connections*”. *Engineering Structures*, 26, pp.1185-206, 2004.
- [11] J.P. Jaspart, 2002: “*Design of Structural Joints in Building Frames. Progress in Structural Engineering and Materials*”, Vol.4(18-34), 2002.

- [12] A.T. Myers, A.M. Kanvinde, G.G. Deierlein and B.V. Fell: "*Effect of weld details on the ductility of steel column baseplate connections*". Journal of Constructional Steel Research, 65, pp. 1366-73, 2009.
- [13] L. Simoes Da Silva and A.G. Coelho: "*A Ductility Model for Steel Connections*". Journal of Constructional Steel Research, 57(1), pp.45-70, 2001.
- [14] M. Latour M and G. Rizzano: "*A theoretical model for predicting the rotational capacity of steel base joints*". Journal of Constructional Steel Research, 91, pp.89.99, 2013.
- [15] M. Latour M and G. Rizzano: "*Full Strength Design of Column Base Connections accounting for Random Material Variability*". Engineering Structures.48:458-471, 2013.
- [16] F.M. Mazzolani and V. Piluso: "*Theory and Design of Seismic Resistant Steel Frames*". London: E & FN Spon, an Imprint of Chapman & Hall; 1996.
- [17] M. D'Aniello, R. Landolfo, V. Piluso and G. Rizzano: "*Ultimate behavior of steel beams under non-uniform bending*". Journal of Constructional Steel Research.78:144-158, 2012.
- [18] D. Grecea, F. Dinu, D. Dubina D: "*Performance Criteria for MR Steel Frames in Seismic Zones*". Journal of Constructional Steel Research. 60:739-749, 2004.
- [19] C.J. Carter and N. Iwankiw: "*Improved ductility in seismic steel moment frames with dogbone connections*". Journal of Constructional Steel Research.46(1-3):253, 1998.
- [20] M.D. Engelhardt, T. Winneberger, A.J. Zekany and T.J. Potyraj: "*Experimental investigation of dogbone moment connections*". Paper presented at: Proceedings of National Steel Construction Conference, Chicago, 1997.
- [21] F. Iannone, M. Latour M, V. Piluso and G. Rizzano: "*Experimental Analysis of Bolted Steel Beam-to-Column Connections: Component Identification*". Journal of Earthquake Engineering.15(2):214-244, 2011.

- [22] J.P. Jaspart and J.F. Demonceau: “*European Design recommendations for simple joints in steel structures*”. Journal of Constructional Steel Research.64/7(8):822-832, 2008.
- [23] J.P. Jaspart and J.F. Demonceau: “*Simple Connections*”. Publ.126 ed. Brussels: ECCS Press; 2009.
- [24] J.M. Castro, A.Y Elghazouli and B.A. Izzudin: “*Modelling of the panel zone in steel and composite moment frames*”. Engineering Structures.27:129-144, 2005.
- [25] C. Christopoulos and A. Filiatrault (2006): “*Principles of Passive Supplemental Damping and Seismic Isolation*”. Pavia: IUSS PRESS, 2006.
- [26] T.T. Soong and Jr B.F. Spencer: “*Supplemental Energy Dissipation: State-of-the-Art and State-of-the-Practice*”. Engineering Structures. 2002;24:243-259, 2002.
- [27] H. Khoo, G. Clifton, G. Macrae and S. Ramhormozian: “*Proposed design models for the asymmetric friction connection*”. Earthquake Engineering & Structural Dynamics. Vol. 44(8):1309-132, 2014.
- [28] H. Khoo, C. Clifton C, J. Butterworth, G. MacRae, S. Gledhill and G. Sidwell: “*Development of the self-centering Sliding Hinge Joint with friction ring springs*”. Journal of Constructional Steel Research, 78:201-211, 2012.
- [29] H. Khoo, C. Clifton C, J. Butterworth and G. MacRae: “*Experimental Study of Full-Scale Self-Centering Sliding Hinge Joint Connections with Friction Ring Springs*”. Journal of Earthquake Engineering. September (17):972-997, 2013.
- [30] J. Borzouie, G. Macrae and J. Chase: “*Cyclic Performance of Asymmetric Friction Connections*”. The Bridge and Structural Engineer. March;45(1), 2015.
- [31] M. D’aniello, R. Tartaglia, S. Costanzo and R. Landolfo: “*Seismic design of extended stiffened end-plate joints in the framework of Eurocodes*”. Journal of Constructional Steel Research, January, 128; pp.512-527, 2017.

- [32] M. D'aniello, D. Cassiano and R. Landolfo: "*Monotonic and cyclic inelastic tensile response of European preloadable gr10.9 bolt assemblies*". Journal of Constructional Steel Research, January, 124; pp.77-90, 2009.
- [33] EN 1090-2: "*Execution of steel structure and aluminium structure: Technical requirements for steel structures. Annex G: Test to determine slip factor*". 2008.
- [34] CEN, 2005. "*Eurocode 0: Basis of Structural Design*".
- [35] M. Latour, V. Piluso and G. Rizzano: "*Experimental Analysis of Friction Materials for supplemental damping devices*". Construction and Building Materials, 2014.
- [36] G. Ferrante Cavallaro, A.B. Francavilla, M. Latour, V. Piluso and G. Rizzano: "*Experimental behaviour of innovative thermal spray coating materials for FREEDAM joints*". Composites Part B Engineering, 2016.
- [37] F. Bowden and D. Tabor: "*The Friction and Lubrication of Solids: part I*". Oxford: Oxford University Press, 1950.
- [38] EN10088-1, 2005. "*Part 1: List of stainless steels*".
- [39] EN 15129, (2009): "*Anti-seismic devices*".
- [40] M. Latour, V. Piluso and G. Rizzano: "*Free from damage beam-to-column joints: Testing and design of DST connections with friction pads*". Engineering Structures.85:219-233, 2015.





# **Chapter 4**

**Cyclic behaviour of external beam-to-  
column joints with friction pads:  
experimental tests**



## 4.1. Introduction

The aim of the work presented in this chapter is the investigation of the behaviour of the FREEDAM joints described in the previous chapter, in terms of rotational response when subject to cyclic loads. In particular, it is pointed out how the typology of the hysteresis loops is mainly governed by the weakest joint component.

The specimens have been designed by exploiting, for the components different from the friction pad, the already available models contained in Eurocode 3 part 1-8 and, for the new component, i.e. the friction damper, the results coming from the experimental activities described in the previous chapter. In particular, the tests on the friction materials at high velocities have demonstrated that the materials M1 and M6 can develop a slight stick-slip behaviour which may induce vibrations with consequent problems to the structure, therefore their use has been excluded while M4 material seems to perform adequately for FREEDAM joints so that its use has been considered. The experimental activity has been carried out with reference to external beam-to-column connections. The following joints have been experimentally analysed:

- **FREEDAM-CYC01** is a joint equipped with friction device (Fig.4.1a) realized by means of a haunch composed by horizontal steel plates with normal holes except the inner plate realized in 1.4301 Stainless Steel and bolted to the pre-stressed friction shims with M20 class 10.9 HV bolts and 6 disc springs (2s+3p);
- **FREEDAM-CYC02** is a joint equipped with friction device (Fig.4.1b) characterized by a plate bolted to the bottom beam flange and welded

to the vertical slotted Stainless Steel plate that, even in this case, has to be bolted to the friction shims with M20 class 10.9 HV bolts and 6 disc springs (2s+3p);

- **FREEDAM-CYC03** is the same configuration of test n°1, without disc springs;
- **FREEDAM-CYC04** is the same configuration of test n°2, without disc springs.

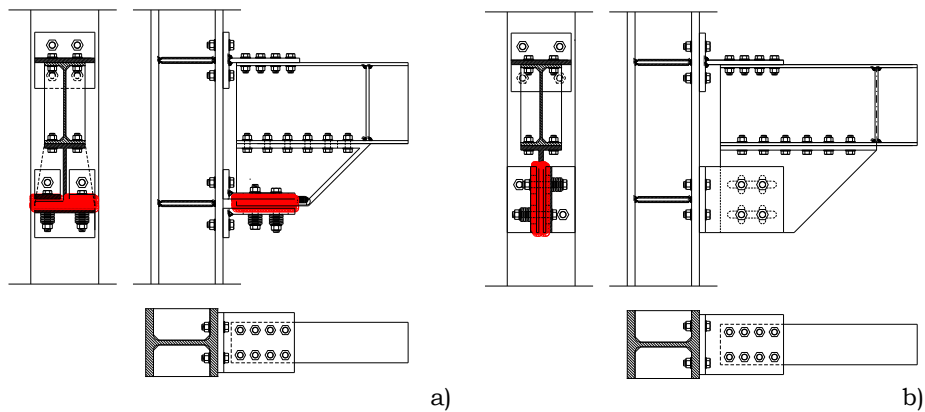


**Fig. 4.1** – Typologies of joints: a) FREEDAM-CYC01/03;  
b) FREEDAM-CYC02/04

## 4.2. Description of the test setup

All the experimental tests have been developed at the STRENGTH laboratory (STRuctural ENgineering Testing Hall) of the University of Salerno. The tests setup is constituted by instruments and machines that could be regroup in three macro categories: constraining devices, loading machines and measurement instruments.

In fact, in order to counteract the actions due to the loading machines, constrains devices are used. These devices are used in order to obtain the desired structural scheme and to avoid the arise of undesired effects, as

the lateral torsional buckling of a steel member. In the STRENGTH laboratory, the main constrain devices is represented by the laboratory strong floor characterized by the presence of holes, with a diameter of 80mm, spaced according to 1mx1m grid.

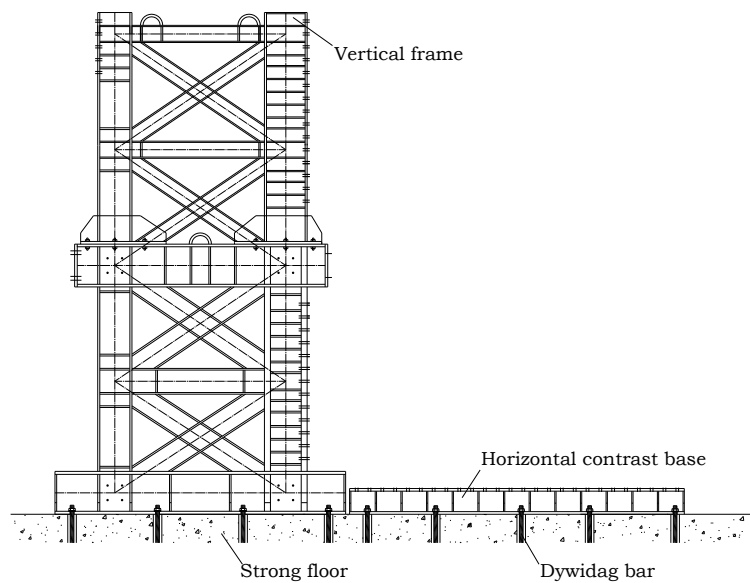


**Fig. 4.2** – Constraining devices used in the experimental campaign

The holes allow to fix the structures by means of high strength dywidag bars. For the performed cyclic tests on the joints, an additional constrain structures have been used: a rigid and strong vertical frame and an horizontal base sleigh, both realized assembling fully welded steel plates and structural members (Fig. 4.2).

In order to simulate the structural scheme, shown in the next section, two steel hinges, designed to resist shear actions of 2000kN and bolted to the base sleigh, have been adopted. One of the two hinges has been detailed to absorb shear and axial actions by means of a pin and of

calibrated holes. The second one has been designed in order to allow the slippage in the horizontal direction and to resist displacements in the orthogonal direction by means of a pin and slotted holes. Finally, an horizontal counteract frame is in charge of avoid the development of lateral-torsional buckling phenomena of the steel members during the experimental tests.

With regards to the loading machines, in the experimental campaign two different MTS 243 hydraulic actuators have been used. In order to simulate the axial load in the column, a MTS 243.60 actuator, operating under load control, has been utilised. Its maximum loading capacity is equal to 667kN in tension and compression with a piston stroke of +/- 126mm. The other actuator, MTS 243.35, has a maximum load capacity equal to 245 kN in compression and 365 kN in tension with a piston stroke of +/- 508mm and is exploited to apply, under displacement control, the desired displacement history at the end of the beam.



**Fig. 4.3** – MTS hydraulic actuator

As measurement instrumentations, displacements transducers LVDT have been used (Fig. 4.4). In these devices, a magnetic flux coupling between two coils is altered by movement of a ferromagnetic shaft within the flux path and subsequently converted into voltage. In this way, LVDTs

allow to acquire linear displacements by means of the movement of a metallic shaft. The advantages of the LVDTs are several: the sensor is a non-contact device with very little friction resistance, output impedance is very low, there is a low susceptibility to noise and interfaces and its construction is solid and robust.



**Fig. 4.4** – Displacement transducer LVDT

These instruments have been used so as to acquire during the tests the desired displacements and, as a consequence, the angles. In particular, during the experimental campaign, the displacements of beam and column and of the element composing the connection, especially the friction damper, have been monitored.

As aforementioned, the experimental tests have been executed using two hydraulic actuators, the bottom actuator has been governed under force control in order to impose a constant axial compression load equal to 650 kN which corresponds to 12.5% of the column squash load. The top actuator has been connected to the top of the beam in order to apply the displacement history (Fig. 4.4).



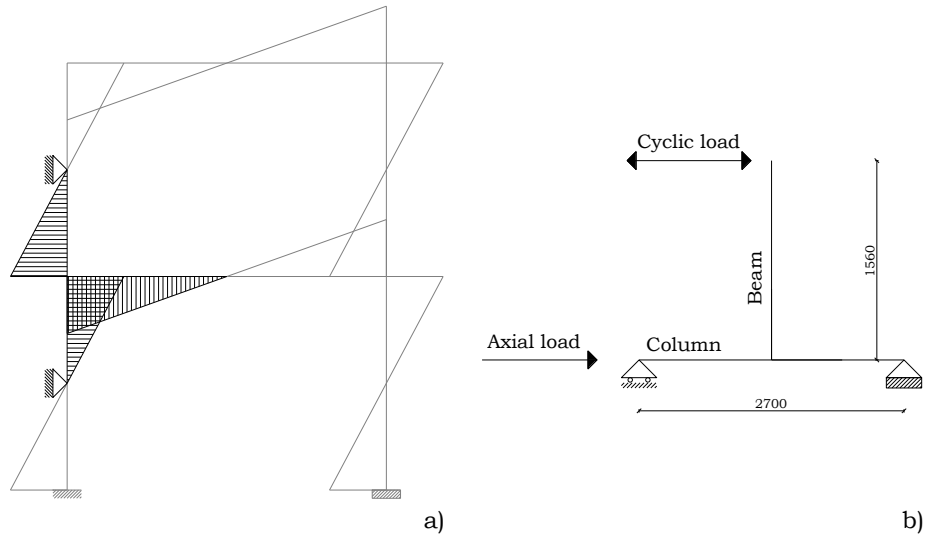


**Fig. 4.5** – Structural scheme: a) action in a frame due to the seismic loads;  
b) reproduced scheme in the laboratory

According to AISC provision [1], in terms of drift angle, the loading history is given in Fig. 4.5.

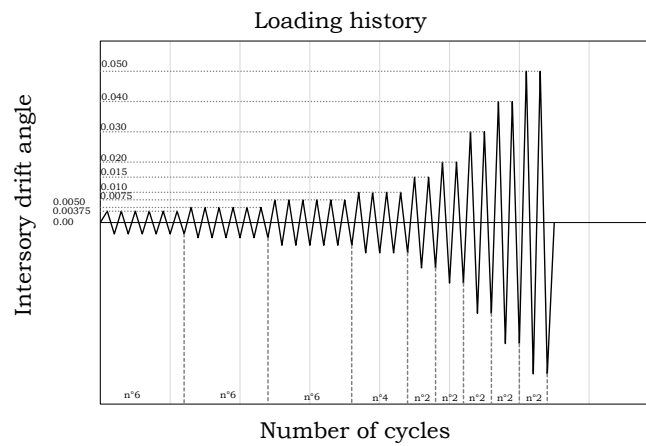


**Fig. 4.6** – AISC loading history for beam-to-column joints

- 6 cycles at  $\theta = 0.00375$  rad
- 6 cycles at  $\theta = 0.0050$  rad
- 6 cycles at  $\theta = 0.0075$  rad
- 4 cycles at  $\theta = 0.0100$  rad
- 2 cycles at  $\theta = 0.0150$  rad
- 2 cycles at  $\theta = 0.0200$  rad
- 2 cycles at  $\theta = 0.0300$  rad
- 2 cycles at  $\theta = 0.0400$  rad
- 2 cycles at  $\theta = 0.0500$  rad

Therefore, starting from the knowledge of code requirement, is possible to obtain the displacement history at the top of the beam (Tab.4.1).

**Table 4.1** – Loading displacement history

$v$ [mm/s]	step	$\theta$ [rad]	# cycles	$\delta$ [mm]	$t_r$ [s]	$t_c$ [s]	$t_{step}$ [s]
0.5	1	0.00375	6	5.835	11.67	46.68	280.08
	2	0.0050	6	7.780	15.56	62.24	373.44
1	3	0.0075	6	11.67	11.67	46.68	280.08
	4	0.010	4	15.56	11.67	62.24	248.96
2	5	0.015	2	23.34	11.67	46.68	93.36
	6	0.020	2	31.12	15.56	62.24	124.48
	7	0.030	2	46.68	23.34	93.36	186.72
4	8	0.040	2	62.24	15.56	62.24	124.48
	9	0.050	2	77.80	19.45	77.80	155.60

During the tests many parameters have been monitored and acquired, in order to get the test machine history imposed by the top actuator and the displacements of the different joint components.

In particular, in FREEDAM CYC-01 joint (Fig.4.6a):

- LVDTs n.02, 03 and 07 measure the relative displacement between the T-stub/angles flanges and the column flange;
- LVDT n. 05 measure the eventual displacements between the haunch and the beam;
- LVDTs n. 06 measure the displacement of the friction device;
- LVDT n. 01 provide eventual slips of the web of the T-stub with respect to the beam flange.

in FREEDAM CYC-02 joint (Fig.4.6b):

- LVDTs n.01, 03 and 05 are able to measure the relative displacement between the T-stub/angles flanges and the column flange;
- LVDT n. 02 measure the eventual displacements between the haunch and the beam;
- LVDTs n. 04 and 06 measure the displacement of the two bolt rows of the friction device;
- LVDT n. 07 provide eventual slips of the web of the T-stub with respect to the beam flange.

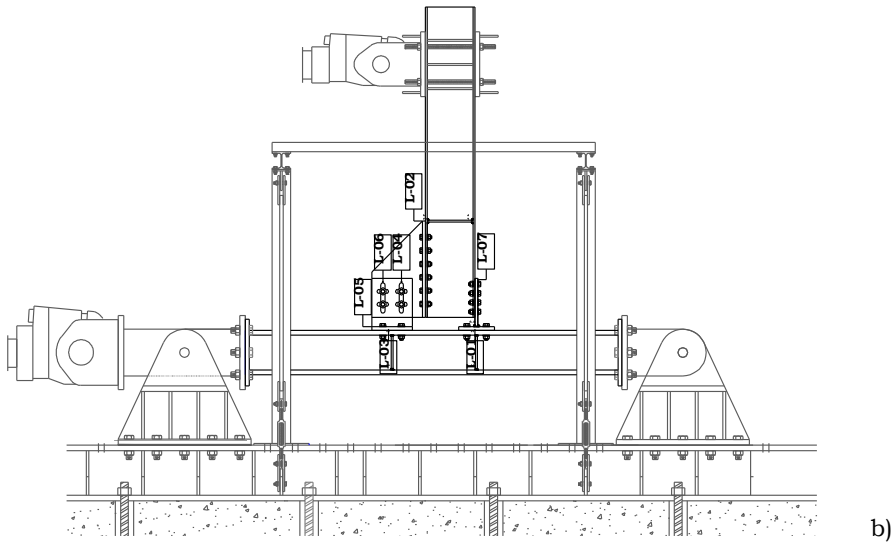
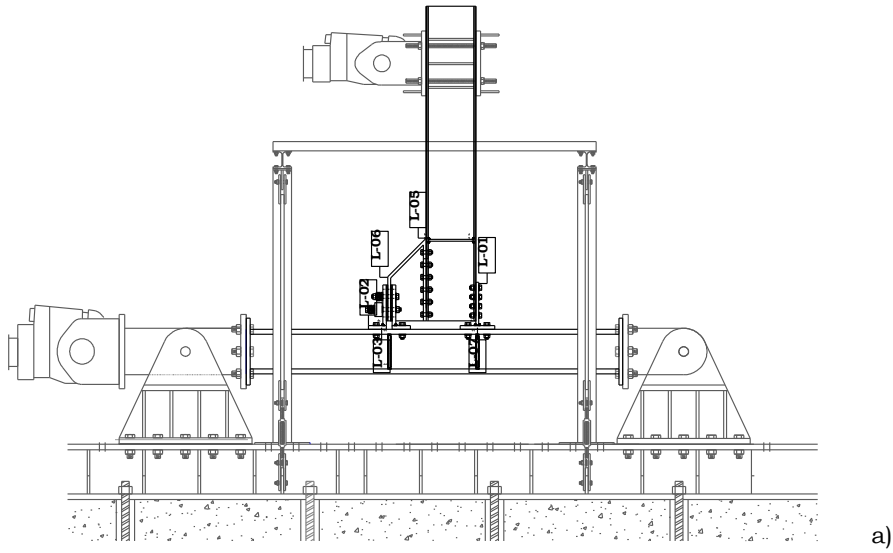
in FREEDAM CYC-03 joint (Fig.4.6c):

- LVDTs n.02, 03 and 04 are able to measure the relative displacement between the T-stub/angles flanges and the column flange;
- LVDT n. 05 measure the eventual displacements between the haunch and the beam;
- LVDTs n. 07 measure the displacement of the friction device;

- LVDT n. 01 provide eventual slips of the web of the T-stub with respect to the beam flange.

and in FREEDAM CYC-04 joint (Fig.4.6d):

- LVDTs n.03, 04 and 05 are able to measure the relative displacement between the T-stub/angles flanges and the column flange;
- LVDTs n. 02 and 07 measure the displacement of the two bolt rows of the friction device;
- LVDT n. 01 provide eventual slips of the web of the T-stub with respect to the beam flange.



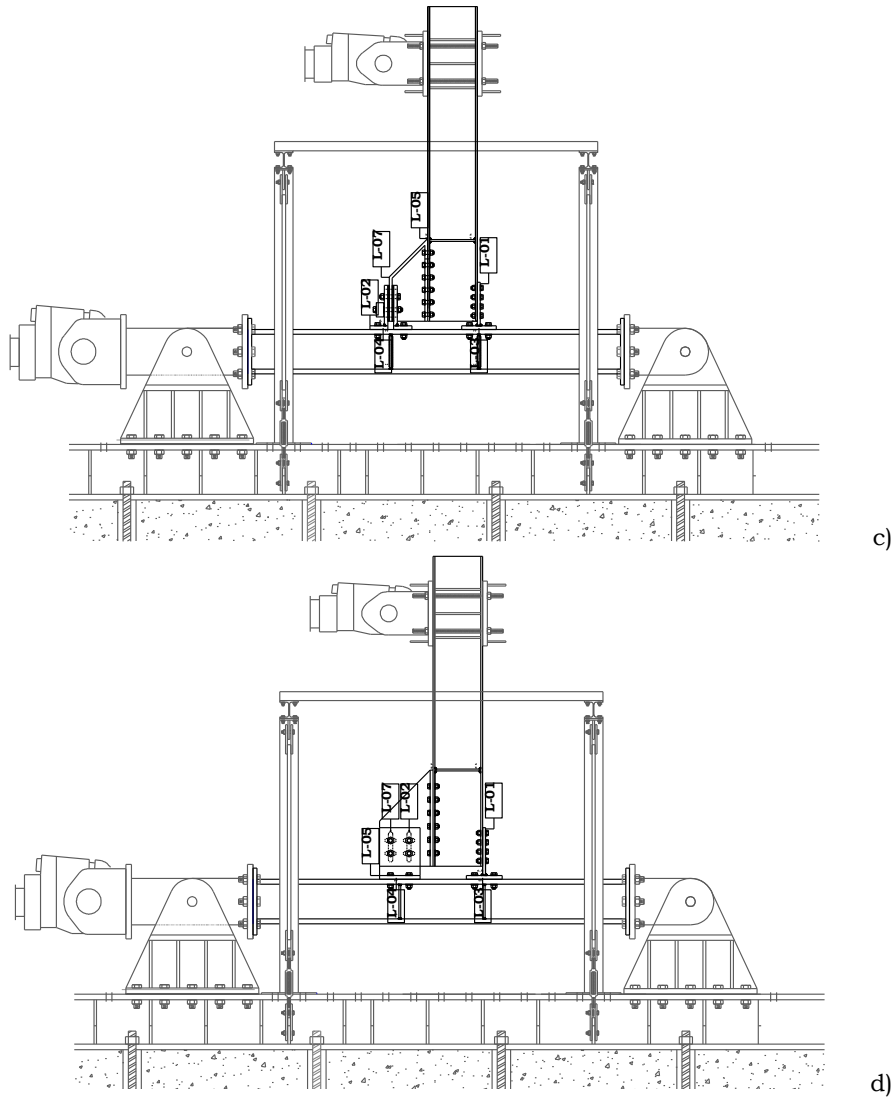


**Fig. 4.7** – Position of the LVDTs: a) FREEDAM-CYC01; b) FREEDAM-CYC02;  
c) FREEDAM-CYC03; d) FREEDAM-CYC04

In addition, the pre-tension applied to two of the four bolts of the friction device has been monitored before and during the test by means of donut load cells Futek LTH500 labelled RC-03 and RC-04.

With the aim of evaluation of the beam-to-column joint rotational behaviour only  $\delta_j$ , the displacements measured at the top of the beam, in correspondance of the load application, have been corrected by subtracting the elastic part due to the beam and to the column flexural deformability.

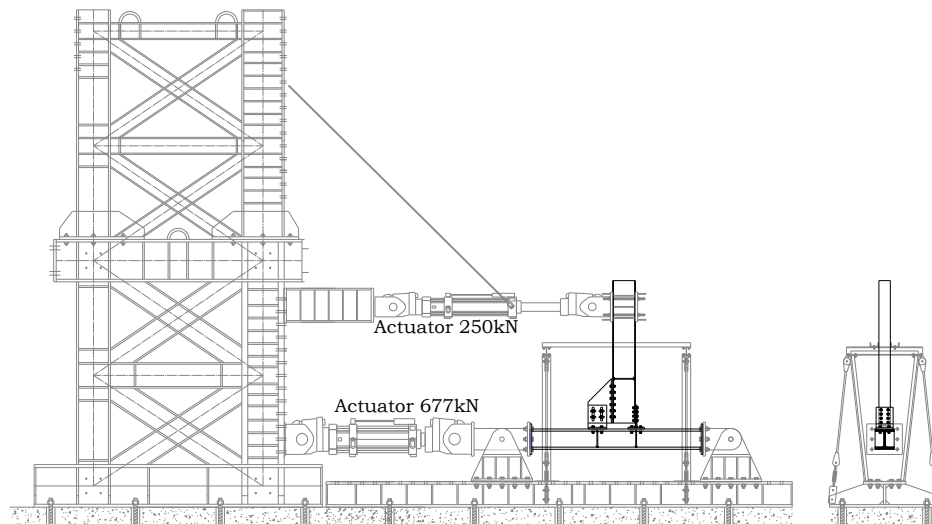


**Fig. 4.8** – Experimental layout

### **4.3. Description of the specimens**

As described in the previous chapters, the overall behaviour of the joints is strictly affected by the basic behaviour of the single components so that, in case of the FREEDAM joints, the flexural resistance and the dissipative capacity is governed by the behaviour of the friction damper and then by the chosen friction material. In the following, the design of the tested joints will be reported. In particular, reference is made to the friction material M4 while for the design of joint components the concepts introduced by EC3 [2] have been applied. Since the employment of disc springs not influence the design procedure of the joint, in the following the design of only the specimens FREEDAM-CYC01 and FREEDAM-CYC02 has been detailed. All the tested specimens are constituted by an IPE 270 beam and an HE 220 M column made both of S355 steel so as the plates and the bolts are class 10.9 HV.

#### **4.3.1. Design of the specimen FREEDAM-CYC01**

The FREEDAM joint labelled with the ID tags CYC01 is characterized by the presence of an haunch composed by horizontal steel plates with normal holes except the inner plate realized in 1.4301 Stainless Steel equivalent to AISI 304 steel and bolted to the pre-stressed friction shims with M20 class 10.9 HV bolts (Fig. 4.7).

With reference to the design of the joint, the sequence of operations or resistance check of the joints components listed in the previous chapter has been followed.



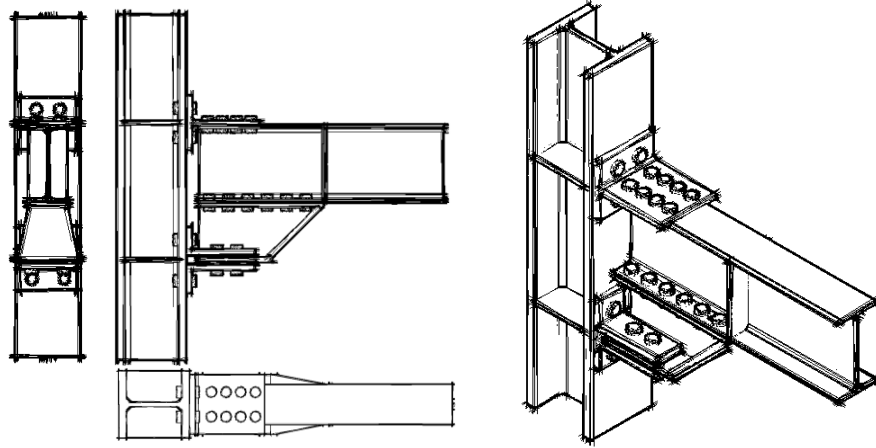


Fig. 4.9 – FREEDAM-CYC01 joint configuration

**Step 1: Evaluation of the design friction resistance  $F_{friction,Rd}$  of the dissipative component, i.e. the friction device.**

Starting from the given value of the beam plastic resistance  $M_{p,b}$  and the lever arm  $h$ , the device has to withstand to the design friction force evaluated as:

$$F_{slip.Ed} = \frac{M_{b,p}}{h} = \frac{171.82}{0.47} = 365.57kN \quad (4.1)$$

taking into account the height of the haunch equal to 220mm.

Equating the slip force and the sliding force  $F_{sliding}$  given by:

$$F_{sliding} = \mu_d \cdot F_p \cdot n_b \cdot n_s \quad (4.2)$$

the minimum number of friction device bolts can be evaluated:

$$n_{b,min} = \frac{F_{slip.Ed}}{\mu_{d,5\%} \cdot F_p \cdot n_s} = \frac{365.57}{0.53 \cdot 171.50 \cdot 2} = 2.01 \quad \rightarrow n_b = 4 \quad (4.3)$$

Once evaluated the number of the bolts, it is possible to easily determine, in order to obtain the sliding force evaluated by means of the Eq. (4.3), the reduced value of the bolts preload:

$$F_{p,red} = \frac{F_{slip.Ed}}{\mu_{d,5\%} \cdot n_b \cdot n_s} = \frac{365.57}{0.53 \cdot 4 \cdot 2} \cong 86.21kN \cong 50\% F_p \quad (4.4)$$

Once evaluated the number of the bolts and the reduced preload force, the design friction resistance, whose value results to be equal to  $F_{slip.Ed}$ , is easily determined as:

$$F_{friction,Rd} = \mu_{d,5\%} \cdot F_{p,red} \cdot n_b \cdot n_s = 0.53 \cdot 86.21 \cdot 4 \cdot 2 = 365.57 kN \quad (4.5)$$

and the correspondent value of the bending moment:

$$M_{friction,Rd} = F_{friction,Rd} \cdot h = 365.57kN \cdot 0.47m = 171.82kNm \quad (4.6)$$

**Step 2: Design of the length of the slots made on the haunch in order to evaluate the overall dimension of the reinforced part of the joint.**

The other parameter to be controlled in the design is the length of the slots made on the haunch which allows the movement of the beam on the friction material. In particular, this parameter governs the rotational capacity of the connection and, consequently, it can be selected starting

from the knowledge of the minimum required value of the rotational capacity, by using the following equation:

$$L_{slot} = \left(\frac{n_b}{2} - 1\right) \cdot p + d_b + 2\phi h = \quad (4.7)$$

$$= (2 - 1)70 + 20 + 2 \cdot 0.06 \cdot 470 = 146.50mm \rightarrow L_{slot} = 150mm$$

Starting from the evaluation of the minimum length of the slots, the horizontal overall dimension of the haunch based on technological considerations and, as a consequence, the distance  $a$  between the beam section where the plastic hinge could develop and the column flange have been determined.

**Step 3: Calculation of bending moment  $M_{cf,Cd}$  at the column flange and check of the resistance of the beam in bending.**

As mentioned in the chapter 3, for the non-dissipative parts of the structure, the highest expected value of the static friction coefficient has to be considered. Starting from this concept, applying the basic principles of "capacity design", the maximum bending moment at the column face  $M_{cf,Cd}$  can be determined as:

$$M_{cf,Cd} = M_{friction,Rd} \cdot \gamma_{ov} = 171.82kNm \cdot 1.70 = 292.09kNm \quad (4.8)$$

As previously said, the bending moment at the column flange  $M_{cf,Cd}$  is greater than the plastic bending resistance of the beam because of the possibility to exploit the additional strengthening resulting from the haunched end. Therefore, is essential to evaluate the bending moment

achievable in correspondance of the axis of beam plastic hinge  $M_b$  that has to be smaller than the plastic resistance of the beam:

$$M_b = M_{cf,cd} \cdot \frac{L_e - a}{L_e} = 292.09kNm \cdot \frac{2890 - 615}{2890} = 229.86kNm \quad (4.9)$$

$$> M_{b,p} = 171.82kNm$$

where  $L_e$  is the shear length of the beam equal to 2.89m. Reference is made to the length of the spans, equal to 6.00m, of the reference frames analysed in the following sections.

Resulting the bending moment  $M_b$  greater than the plastic beam resistance, the bending moment of the connection  $M_{cf,cd}$  has to be reduced by calibrating the tightening torque of the bolts of the friction damper. The  $m$  parameter results to be equal to:

$$m = \frac{M_{b,p}}{M_b} = \frac{171.82}{229.86} = 0.75 \quad (4.10)$$

and the reduced design friction resistance is given by:

$$F_{friction,Rd} = \mu_{d,5\%} \cdot (m \cdot F_{p,red}) \cdot n_b \cdot n_s \quad (4.11)$$

$$= 0.53 \cdot (0.75 \cdot 86.21) \cdot 4 \cdot 2 = 273.25kN$$

In this way, the force that the joint has to withstand before that the slippage of the friction damper occurs, result to be equal to:

$$F_{cf,cd} = \frac{0.75 \cdot 171.82 \cdot 1.70}{0.47} = 464.53kN \quad (4.12)$$

According to the principles of the “capacity design”, the non dissipative components, namely the T-stub and angles in bending, the haunch, the column web in tension and compression, the column flange in bending, have to be designed in order to transmit the maximum force that the dissipative component is able to exhibit, i.e. the maximum static force evaluated by means of the Eq. (4.12).

**Step 4: Design of the diameter of bolts connecting the Tee element and the angles to the column.**

For the design of the diameter of the bolts in tensile side the following actions have to be considered:

$$\begin{aligned} F_{t,Ed} &= \frac{F_{cf,Cd}}{n_{b,t}} = \frac{464.53}{4} \cong 116.13 \text{ kN} \\ F_{v,Ed} &= \frac{F_v}{2 n_b} = \frac{250}{2 \cdot 4} = 31.25 \text{ kN} \end{aligned} \quad (4.13)$$

where  $F_v$  is the maximum shear action transmitted by the adopted actuator.

Therefore, according to Eurocode 3, the check under combined shear and tension lead to determine a first minimum value of the resistant area of the bolts. In particular, for 10.9 class:

$$\begin{aligned} A_{res} &\geq \frac{\gamma_{M2}}{f_{tb}} \left( \frac{F_{v,Ed}}{\alpha_v} + \frac{F_{t,Ed}}{1.26} \right) \\ A_{res} &\geq \frac{1.25}{1000} \left( \frac{31250}{0.5} + \frac{116130}{1.26} \right) \cong 193.33 \text{ mm}^2 \end{aligned} \quad (4.14)$$

According to Eurocode 3, in any case, the resistant area of the bolts has to be greater than the value determined considering only the tension action:

$$A_{res} \geq \frac{\gamma_{M2} F_{t,Ed}}{0.9 f_{tb}} = \frac{1.25 \cdot 116130}{0.9 \cdot 1000} \cong 161.30 \text{ mm}^2 \quad (4.15)$$

Consequently, bolts M20 have been chosen.

#### **Step 5: Design of the T-stub and L-stubs.**

Considering the design criteria already adopted for the bolts, failure mechanism type 3 can be excluded. Therefore, only the resistance formulations for mechanism type 1 and mechanism type 2 have to be considered to check the T-stub and the L-stubs in bending.

#### Design of the T-stub

It is assumed that the distance  $m$  between the bolt axis and the plastic hinge located close to the beam flange is equal to 43mm so as the distance  $n$  between the bolt line and the end of the plate.

The horizontal distance between the bolts  $w$  has to satisfy the following limitations:

$$\begin{aligned} w_{\min} &\cong t_{cw} + 2 r_c + 1.8 = 26 + 2 \cdot 18 + 1.8 \cdot 21.5 = 100.7 \text{ mm} \\ w_{\max} &= b_{cf} - 2.4 d_0 = 226 - 2.4 \cdot 21.5 = 174.4 \text{ mm} \end{aligned} \quad (4.16)$$

where  $t_{cw}$  is the thickness of the column web,  $r_c$  the root radius,  $d_0$  the diameter of the hole and  $b_{cf}$  the column width. According to the above limitations, the T-stub bolt spacing is taken equal to  $w_0 = 103.4 \text{ mm}$ .

Regarding the width of the T-stub, it should be greater than:

$$\begin{aligned} b_{T\text{-stub}} &= \max\{w + 2.4 d_0; b_{bf}\} = \\ &= \max\{103.4 + 2.4 \cdot 21.5; 135\} = 155 \text{ mm} \end{aligned} \quad (4.17)$$

and, anyway, smaller than the width of the column that is equal to 226 mm, consequently the width of the end plate is taken equal to 200mm.

For the evaluation of the effective length of the T-stub  $b_{eff}$ , it is considered the half part of the geometrical length, i.e. equal to 100mm.

The thickness of the T-stub  $t_{Tstub.1}$  required to avoid the collapse of the equivalent T-stub according to type-1 mechanism is:

$$\begin{aligned} F_{1,Rd} &= 2 \frac{b_{eff} t_{Tstub}^2 f_{y,Tstub}}{m \gamma_{M0}} = F_{cf,Cd} \rightarrow \\ t_{Tstub.1} &= \sqrt{\frac{m F_{cf,Cd} \gamma_{M0}}{2 \cdot b_{eff,Tstub} \cdot f_{y,Tstub}}} = \sqrt{\frac{43 \cdot 464530 \cdot 1.05}{2 \cdot 100 \cdot 355}} \cong 16.77 \text{ mm} \end{aligned} \quad (4.18)$$

where  $f_{y,Tstub}$  is the yielding resistance of the plate.

Similarly, to avoid the collapse of the T-stub according to type-2 mechanism the required thickness  $t_{Tstub.2}$  is:

$$\begin{aligned} F_{2,Rd} &= 2 \frac{\frac{f_{y,Tstub} b_{eff} t_{Tstub}^2}{2} + 2 F_{t,Rd} n}{m + n} = F_{cf,Cd} \rightarrow \\ t_{Tstub.2} &= \sqrt{\frac{2 \gamma_{M0}}{b_{eff,ep} f_{y,Tstub}} \left[ \frac{F_{cf,Cd}(m+n)}{2} - 2 F_{t,Rd} n \right]} = \\ &= \sqrt{\frac{2 \cdot 1.05}{100 \cdot 355} \left[ \frac{464530 (43 + 43)}{2} - 2 \cdot 176400 \cdot 43 \right]} \cong 16.45 \text{ mm} \end{aligned} \quad (4.19)$$

Therefore, the thickness of the T-stub flange has been assumed equal to 20mm. With regards to the T-stub web, taking into account that its thickness has to be greater than the that of the beam flange (equal to 10.2 mm) it is assumed equal to 15mm.

Subsequently, the  $n_{b,s}$  bolts connecting the T-stub web and the beam flange have to absorb the shear force transmitted by the upper beam flange that is equal to  $F_{cf,c,d}$ . According to Eurocode 3, the shear resistance of the bolts can be evaluated as:

$$F_{V,Rd} = n_{b,s} \frac{\alpha_v \cdot A_{res} \cdot f_{tb}}{\gamma_{M2}} = F_{cf,c,d} \quad \rightarrow \quad n_{b,s} = \frac{F_{cf,c,d} \cdot \gamma_{M2}}{\alpha_v \cdot A_{res} \cdot f_{tb}} \quad (4.20)$$

where  $A_{res}$  is the nut area,  $f_{tb}$  the ultimate resistance,  $\alpha_v$  a coefficient depending on the bolt class and  $\gamma_{M2}$  a partial factor.

Consistent with the beam size, the maximum diameter of the holes on the flange is equal to 19mm therefore, M18 bolts have been considered and the minimum number is evaluated:

$$n_{b,s} = \frac{464530 \cdot 1.25}{0.5 \cdot 193 \cdot 1000} = 6.02 \quad \rightarrow \quad n_{b,s} = 8 \quad (4.21)$$

Anyway, aiming to avoid any slippage between the surfaces in contact, namely the T-stub web and the beam flange, the bolts will be pre-tightened in order to obtain a friction resistance greater than the action  $F_{cf,c,d}$ :

$$F_{fric,Tstub,w} = \mu \cdot F_p \cdot n_s \cdot n_b = 0.5 \cdot 135.10 \cdot 1 \cdot 8 = 540.40kN > F_{cf,c,d} \quad (4.22)$$



### Design of the L-stubs

In FREEDAM joints the internal angles are different from the external one because of the different width. For sake of simplicity, and because on safe side, the resistance of the lower L-stubs has been evaluated as double of that of the inner angles. It is assumed that the distance  $m$  between the bolt axis and the plastic hinge located close to the beam flange is equal to 35mm and the distance  $n$  between the bolt line and the end of the plate is equal to 43mm. The horizontal distance between the bolts  $w$  has to satisfy the following limitations:

$$\begin{aligned} w_{\min} &\cong t_{cw} + 2 r_c + 1.8 d_0 = 26 + 2 \cdot 18 + 1.8 \cdot 21.5 + 15 \\ &= 100.7 \text{ mm} \\ w_{\max} &= b_{cf} - 2.4 d_0 = 226 - 2.4 \cdot 21.5 = 174.4 \text{ mm} \end{aligned} \quad (4.23)$$

According to the above limitations, the L-stub bolt spacing is taken equal to  $w_0 = 115 \text{ mm}$ .

Regarding the width of the L-stub, it should be greater than:

$$\begin{aligned} b_{L\text{-stub}} &= \max \left\{ \frac{w + 2.4 d_0 - t_{hw}}{2}; \frac{b_{bf}}{2} \right\} = \\ &= \max \left\{ \frac{115 + 2.4 \cdot 21.5 + 10}{2}; \frac{135}{2} \right\} = 67.5 \text{ mm} \end{aligned} \quad (4.24)$$

and, anyway, smaller than:

$$b_{L\text{-stub}} = \frac{b_c - t_{hw}}{2} = \frac{226 - 10}{2} = 108 \text{ mm} \quad (4.25)$$

consequently the width of the L-stub, that is coincident with the effective length, is taken equal to 85mm.

The thickness of the L-stab flange required to avoid the collapse of the equivalent T-stub according to type-1 mechanism is:

$$F_{1,Rd} = \frac{b_{eff} t_{Lstub}^2 f_{y,Lstub}}{2 \cdot m \gamma_{M0}} = \frac{F_{cf,Cd}}{4} \rightarrow$$

$$t_{Lstub.1} = \sqrt{\frac{m F_{cf,Cd} \gamma_{M0}}{2 \cdot b_{eff,Lstub} \cdot f_{y,Lstub}}} = \sqrt{\frac{35 \cdot 464530 \cdot 1.05}{2 \cdot 85 \cdot 355}} \cong 16.82 \text{ mm} \quad (4.26)$$

Similarly, to avoid the collapse of the L-stub according to type-2 mechanism the required thickness is:

$$F_{2,Rd} = \frac{\frac{f_{y,Lstub} b_{eff} t_{Lstub}^2}{\gamma_{M0}} + F_{t,Rd} n}{m + n} = \frac{F_{cf,Cd}}{4} \rightarrow$$

$$t_{Lstub.2} = \sqrt{\frac{4 \gamma_{M0}}{b_{eff,ep} f_{y,Lstub}} \left[ \frac{F_{cf,Cd}(m + n)}{4} - F_{t,Rd} n \right]} =$$

$$= \sqrt{\frac{4 \cdot 1.05}{85 \cdot 355} \left[ \frac{464530 (35 + 43)}{4} - 176400 \cdot 43 \right]} \cong 14.32 \text{ mm} \quad (4.27)$$

Therefore, the thickness of the L-stub flange/web has been assumed equal to 20mm.

**Step 7: Design of the bolts connecting the lower flange of the beam and the flange of the haunch.**

For the design of the bolts connecting the upper flange of the haunch to the lower flange of the beam, the following actions have to be considered:

$$F_{t,Ed} = \frac{F_{cf,c,d} \cdot h_h}{\sum_i d_i^2} \cdot d_i \quad F_{v,Ed} = \frac{F_{cf,c,d}}{n_{b,h}} \quad (4.28)$$

where  $d_i$  is the distance of the  $i^{th}$  bolt from the centre of rotation.

The position of the bolts is defined on the basis of the code requirements for bolt spacing and of technological conditions. The most stressed bolt, whose diameter is equal to 18mm, is the one further from the column face and is subjected to the following actions values:

$$F_{t,Ed} = \frac{F_{cf,c,d} \cdot h_h}{\sum_i d_i^2} \cdot d_i = \frac{464530 \cdot 200}{324595} \cdot 370 = 52950N$$

$$F_{v,Ed} = \frac{F_{cf,c,d}}{n_{b,h}} = \frac{464530}{2 \cdot 6} = 37710N \quad (4.29)$$

Therefore, according to Eurocode 3, the check under combined shear and tension lead to determine a first minimum value of the resistant area of the bolts. In particular:

$$A_{res} \geq \frac{\gamma_{M2}}{f_{tb}} \left( \frac{F_{v,Ed}}{\alpha_v} + \frac{F_{t,Ed}}{1.26} \right) \quad (4.30)$$

$$A_{res} \geq \frac{1.25}{1000} \left( \frac{37710}{0.5} + \frac{52950}{1.26} \right) \cong 149.30 \text{ mm}^2 > 193 \text{ mm}^2 = A_{res,M18}$$

**Step 8: Check of the resistance of the column web in shear and design of supplementary web plates if needed.**

The shear resistant area of the column section is given by:

$$\begin{aligned}
 A_{vc} &= A - 2 b_{cf} t_{cf} + (t_{cw} + 2r_c)t_{cf} = \\
 &= 14940 - 2 \cdot 226 \cdot 26 + (15.5 + 2 \cdot 18) \cdot 26 = 4527 \text{ mm}^2
 \end{aligned} \tag{4.31}$$

The resistance of the column web panel, without continuity and/or supplementary plates, is:

$$V_{wp,Rd} = \frac{0.9 \cdot A_{vc} \cdot f_{y,cw}}{\sqrt{3} \cdot \gamma_{M0}} = \frac{0.9 \cdot 4527 \cdot 355}{\sqrt{3} \cdot 1.05} \cong 835 \text{ kN} \tag{4.32}$$

whereas the shear resistance of the column web panel is greater than the action  $F_{cf,cd}$ , supplementary web plates are not needed.

**Step 9: Check of the resistance of the column web in tension and in compression.**

The resistance of the column web in compression can be determined as follows:

$$\begin{aligned}
 F_{cwc,Rd} &= \omega \cdot k_{wc} \cdot b_{eff,cwc} \cdot t_{cw} \cdot \frac{f_{y,cw}}{\gamma_{M0}} = \\
 &= \frac{0.67 \cdot 1 \cdot 280 \cdot 15.5 \cdot 355}{1.05} \cong 938 \text{ kN}
 \end{aligned} \tag{4.33}$$

where  $b_{eff,cwc}$  is the effective length of the column web given by:

$$\begin{aligned}
 b_{eff,cwc} &= t_{Lstub,w} + 5(t_{fc} + r_c) + 2 t_{T-Lstub} = \\
 &= 20 + 5(26 + 18) + 2 \cdot 20 = 280 \text{ mm}
 \end{aligned} \tag{4.34}$$

and the coefficients  $\omega$ , accounts for the possible effects of interaction with shear in the column web panel, and  $k_{wc}$ , accounts for the effect of the longitudinal compressive stress  $\sigma_{com,Ed}$  due to the axial force and the

bending moment on the column on the compression column web resistance, are given by:

$$\omega = \frac{1}{\sqrt{1 + 1.3 \left( \frac{b_{eff.cwc} \cdot t_{cw}}{A_{vc}} \right)^2}} = \frac{1}{\sqrt{1 + 1.3 \left( \frac{280 \cdot 15.5}{4527} \right)^2}} = 0.67 \quad (4.35)$$

$$k_{wc} = 1 \quad \text{when} \quad \sigma_{com,Ed} \leq 0.7f_{y,wc}$$

Since the resistance is greater than the action  $F_{cf,cd}$ , continuity plates are not required.

**Step 10: Check of the resistance of the column flange in bending by modelling the tension zone by means of an equivalent T-stub.**

In bolted connections, an equivalent T-stub in tension may be used to model the design resistance of the column flange in bending. Excluding failure mode according to mechanism type-3 because of the design criterion adopted for the bolts, the design resistances for mechanism type-1 and type-2 have to be evaluated. In particular, the following equation has to be considered:

$$F_{1,Rd} \geq F_{cf,cd} \quad F_{2,Rd} \geq F_{cf,cd} \quad (4.36)$$

where:

$$F_{1,Rd} = 2 \frac{b_{eff} t_{cf}^2 f_{y,cf}}{m \gamma_{M0}} \quad \text{and} \quad F_{2,Rd} = 2 \frac{\frac{f_{y,cf} b_{eff} t_{cf}^2}{\gamma_{M0}} + 2 F_{t,Rd} n}{m + n} \quad (4.37)$$

According to Eurocode 3 the effective length, in absence of transverse stiffeners, is given by:

$$\begin{aligned} b_{eff} &= \min\{2\pi m_c; 4m_c + 1.25e; p\} = \\ &= \min\{2\pi \cdot 26; 4 \cdot 26 + 1.25 \cdot 61.3; 101\} \cong 101 \text{ mm} \end{aligned} \quad (4.38)$$

Thereafter, the design resistances for mechanisms type-1 and type-2 are given by:

$$\begin{aligned} F_{1,Rd} &= 2 \frac{f_{y,cf} b_{eff,cfb} t_{cf}^2}{\gamma_{M0} m_c} = 2 \frac{355 \cdot 101 \cdot 20^2}{1.05 \cdot 26} \cong 1051 \text{ kN} \geq F_{cf,Cd} \\ F_{2,Rd} &= 2 \frac{f_{y,cf} \frac{b_{eff,cfb} t_{cf}^2}{2} + 2 F_{t,Rd} n}{\gamma_{M0} (m_c + n)} = \\ &= 2 \frac{355 \frac{101 \cdot 20^2}{2} + 2 \cdot 176400 \cdot 32.5}{1.05(26 + 32.5)} \cong 607 \text{ kN} \geq F_{cf,Cd} \end{aligned} \quad (4.39)$$

where  $n = \min\{e; e_{Lstubb}; 1.25m_c\} = \min\{61.3; 48.3; 1.25 \cdot 26\} = 32.5 \text{ mm}$ .

Since the both design resistances are greater than the action  $F_{cf,Cd}$ , derived by means of capacity design principles, the check of the column flange in bending is satisfied. Anyway, continuity plates have been inserted in order to reduce the column deformation capacity.

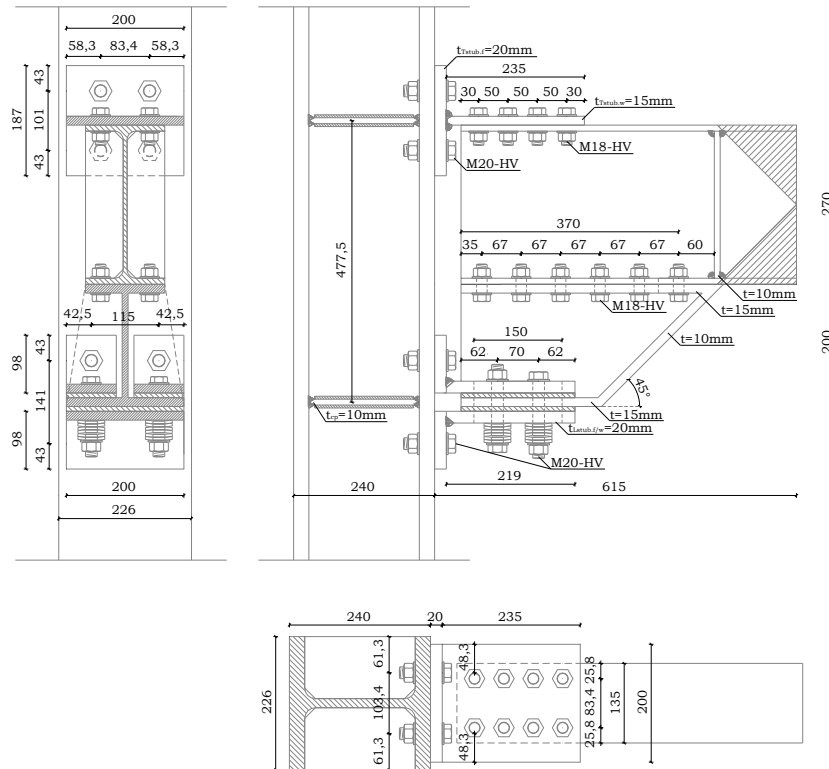


**Fig. 4.10** – Geometry of the specimen FREEDAM-CYC01

### 4.3.2. Design of the specimen FREEDAM-CYC02

The FREEDAM joint labelled with the ID tag CYC02 is characterized by a plate bolted to the bottom beam flange and welded to the vertical slotted Stainless Steel plate that, even in this case, has to be bolted to the friction shims with M20 class 10.9 HV bolts (Fig.4.11). In this configuration, the friction shims and the angles have to present vertical slotted holes in order to accommodate the rotation of the beam.

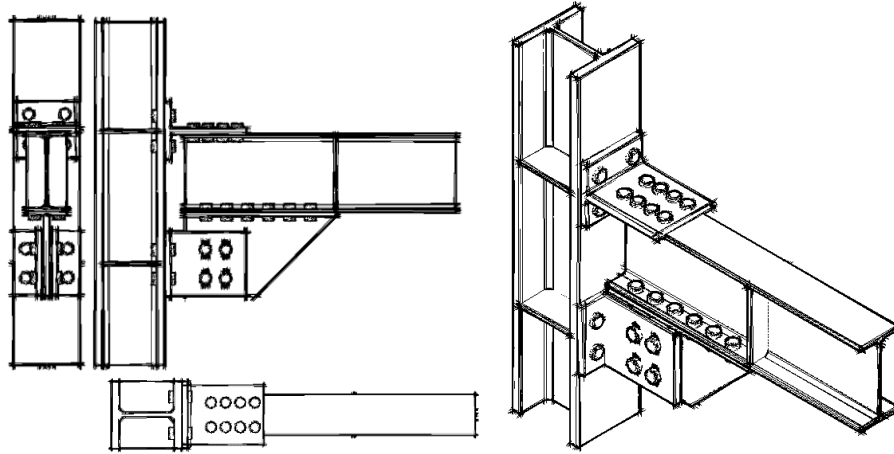


**Fig. 4.11** – FREEDAM-CYC02 joint configuration

The design procedure for the joints in the second configuration is exactly the same followed in the previous section. Nevertheless, with reference to the specimens FREEDAM-CYC02, the procedure will be reported because of the different value of the lever arm and, as a consequence, the static and dynamic values of the friction resistance.

**Step 1: Evaluation of the design friction resistance  $F_{friction,Rd}$  of the dissipative component, i.e. the friction device.**

The device has to withstand to the design friction force evaluated as:

$$F_{slip.Ed} = \frac{M_{b,p}}{h} = \frac{171.82}{0.45} = 381.82kN \quad (4.40)$$

taking into account the height of the haunch equal to 200mm.

Equating the slip force and the sliding force  $F_{sliding}$  given by:



$$F_{sliding} = \mu_d \cdot F_p \cdot n_b \cdot n_s \quad (4.41)$$

the minimum number of friction device bolts can be evaluated:

$$n_{b,min} = \frac{F_{slip.Ed}}{\mu_{d,5\%} \cdot F_p \cdot n_s} = \frac{381.82}{0.53 \cdot 171.50 \cdot 2} = 2.10 \rightarrow n_b = 4 \quad (4.42)$$

Once evaluated the number of the bolts, it is possible to easily determine, in order to obtain the sliding force evaluated by means of the Eq. (4.40), the reduced value of the bolts preload:

$$F_{p,red} = \frac{F_{slip.Ed}}{\mu_{d,5\%} \cdot n_b \cdot n_s} = \frac{381.82}{0.53 \cdot 4 \cdot 2} \cong 90.05kN \cong 53\% F_p \quad (4.43)$$

Once evaluated the number of the bolts and the reduced preload force, the design friction resistance, whose value result to be equal to  $F_{slip.Ed}$ , is easily determined as:

$$F_{friction,Rd} = \mu_{d,5\%} \cdot F_{p,red} \cdot n_b \cdot n_s = 0.53 \cdot 90.05 \cdot 4 \cdot 2 = 381.82 kN \quad (4.44)$$

and the correspondent value of the bending moment:

$$M_{friction,Rd} = F_{friction,Rd} \cdot h = 381.82kN \cdot 0.45m = 171.82kNm \quad (4.45)$$

Therefore, the two different configurations, even though the different dimension of the haunch and then of the lever arm, have the same design flexural resistance.

**Step 2: Design of the length of the slots made on the haunch in order to evaluate the overall dimension of the reinforced part of the joint.**

In this case, the other parameters to be controlled in the design is the length of the horizontal slots made on the haunch which allow the movement of the beam on the friction material but also the vertical slots made on the L-stubs. In particular, these parameters govern the rotational capacity of the connection and, as a consequence, they can be selected starting from the knowledge of the minimum required value of the rotational capacity, by using the following equations:

$$L_{slot,h} = \left(\frac{n_b}{2} - 1\right) \cdot p + d_b + 2\phi h_h = \quad (4.46)$$

$$= (2 - 1)70 + 20 + 2 \cdot 0.06 \cdot 500 = 150mm \rightarrow L_{slot} = 163mm$$

$$L_{slot,v} = d_b + 2\phi h_v = \quad (4.47)$$

$$= 20 + 2 \cdot 0.06 \cdot 210 = 45.2. mm \rightarrow L_{slot} = 61.5mm$$

where  $h_h$  is the distance between the center of compression, namely the flange-to-web connection of the T-stub, and the bolts positioned in the bottom row in the friction device while  $h_v$  is defined as the vertical distance between the upper T-stub of the FREEDAM connection and the farthest bolt from it (Fig.4.9).

Starting from the evaluation of the minimum length of the slots, the horizontal overall dimension of the haunch on the basis of technological considerations and, as a consequence, the distance  $a$  between the beam section where the plastic hinge could develop and the column flange have been determined.

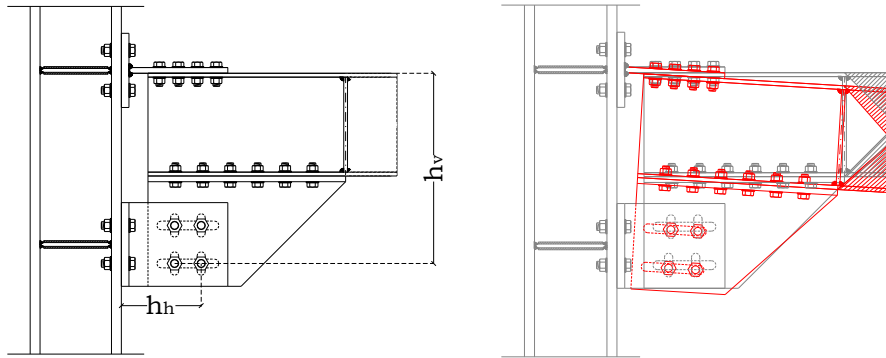


**Fig. 4.12** – Rigid deformation of the FREEDAM-CYC02 joint

**Step 3: Calculation of bending moment  $M_{cf,Cd}$  at the column flange and check of the resistance of the beam in bending.**

As mentioned in the chapter 3, for the non-dissipative parts of the structure, the highest expected value of the static friction coefficient has to be considered. Starting from this concept, applying the basic principles of "capacity design", the maximum bending moment at the column face  $M_{cf,Cd}$  can be determined as:

$$M_{cf,Cd} = M_{friction,Rd} \cdot \gamma_{ov} = 171.82kNm \cdot 1.70 = 291.38kNm \quad (4.48)$$

As previously said, the bending moment at the column flange  $M_{cf,Cd}$  is greater than the plastic bending resistance of the beam because of the possibility to exploit the additional strengthening resulting from the haunched end. Therefore, is essential to evaluate the bending moment achievable in correspondance of the axis of beam plastic hinge  $M_b$  that has to be smaller than the plastic resistance of the beam:

$$M_b = M_{cf,cd} \cdot \frac{L_e - a}{L_e} = 291.38 \text{ kNm} \cdot \frac{2890 - 725}{2890} = 218.21 \text{ kNm} \quad (4.49)$$

$$> M_{b,p} = 178.82 \text{ kNm}$$

where  $L_e$  is the shear length of the beam equal to 2.89m. Resulting the bending moment  $M_b$  greater than the plastic beam resistance, the bending moment of the connection  $M_{cf,cd}$  has to be reduced by calibrating the tightening torque of the bolts of the friction damper. The  $m$  parameter results to be equal to:

$$m = \frac{M_{b,p}}{M_b} = \frac{171.82}{218.21} = 0.79 \quad (4.50)$$

and the reduced design friction resistance is given by:

$$F_{friction,Rd} = \mu_{d,5\%} \cdot (m \cdot F_{p,red}) \cdot n_b \cdot n_s \quad (4.51)$$

$$= 0.53 \cdot (0.79 \cdot 90.05) \cdot 4 \cdot 2 = 300.65 \text{ kN}$$

In this way, the force that the joint has to withstand before that the slippage of the friction damper occurs, result to be equal to:

$$F_{cf,cd} = \frac{0.79 \cdot 171.82 \cdot 1.70}{0.47} = 509.86 \text{ kN} \quad (4.52)$$

According to the principles of the “capacity design”, the non dissipative components, namely the T-stub and angles in bending, the haunch, the column web in tension and compression, the column flange in bending, have to be designed in order to transmit the maximum force that the

dissipative component is able to exhibit, i.e. the maximum static force evaluated by means of the Eq. (4.52).

**Step 4: Design of the diameter of bolts connecting the Tee element and the angles to the column.**

For the design of the diameter of the bolts in tensile side the following actions have to be considered:

$$\begin{aligned} F_{t,Ed} &= \frac{F_{cf,Cd}}{n_{b,t}} = \frac{509.86}{4} \cong 127.46 \text{ kN} \\ F_{v,Ed} &= \frac{F_v}{2 n_b} = \frac{250}{2 \cdot 4} = 31.25 \text{ kN} \end{aligned} \quad (4.53)$$

where  $F_v$  is the maximum shear action transmitted by the adopted actuator.

Therefore, according to Eurocode 3, the check under combined shear and tension lead to determine a first minimum value of the resistant area of the bolts. In particular, for 10.9 class:

$$\begin{aligned} A_{res} &\geq \frac{\gamma_{M2}}{f_{tb}} \left( \frac{F_{v,Ed}}{\alpha_v} + \frac{F_{t,Ed}}{1.26} \right) \\ A_{res} &\geq \frac{1.25}{1000} \left( \frac{31250}{0.5} + \frac{127460}{1.26} \right) \cong 204.57 \text{ mm}^2 \end{aligned} \quad (4.54)$$

According to Eurocode 3, in any case, the resistant area of the bolts has to be greater than the value determined considering only the tension action:

$$A_{res} \geq \frac{\gamma_{M2} F_{t,Ed}}{0.9 f_{tb}} = \frac{1.25 \cdot 127460}{0.9 \cdot 1000} \cong 177.04 \text{ mm}^2 \quad (4.55)$$

Consequently, bolts M20 have been chosen.

**Step 5: Design of the T-stub and L-stubs.**

Considering the design criteria already adopted for the bolts, failure mechanism type 3 can be excluded. Therefore, only the resistance formulations for mechanism type 1 and mechanism type 2 have to be considered to check the T-stub and the L-stubs in bending.

Design of the T-stub

It is assumed that the distance  $m$  between the bolt axis and the plastic hinge located close to the beam flange is equal to 45mm so as the distance  $n$  between the bolt line and the end of the plate.

The horizontal distance between the bolts  $w$  has to satisfy the following limitations:

$$\begin{aligned} w_{\min} &\cong t_{cw} + 2 r_c + 1.8 d_0 = 26 + 2 \cdot 18 + 1.8 \cdot 21.5 = 100.7 \text{ mm} \\ w_{\max} &= b_{cf} - 2.4 d_0 = 226 - 2.4 \cdot 21.5 = 174.4 \text{ mm} \end{aligned} \quad (4.56)$$

According to the above limitations, the T-stub bolt spacing is taken equal to  $w_0 = 123.4 \text{ mm}$ .

Regarding the width of the T-stub, it should be greater than:

$$\begin{aligned} b_{T\text{-stub}} &= \max\{w + 2.4 d_0; b_{bf}\} = \\ &= \max\{123.4 + 2.4 \cdot 21.5; 135\} = 175 \text{ mm} \end{aligned} \quad (4.57)$$

and, anyway, smaller than the width of the column that is equal to 226 mm, consequently the width of the end plate is taken equal to 200mm.

For the evaluation of the effective length of the T-stub, it is considered the half part of the geometrical length, i.e. equal to 100mm.

The thickness of the T-stub required to avoid the collapse of the equivalent T-stub according to type-1 mechanism is:

$$F_{1,Rd} = 2 \frac{b_{eff} t_{Tstub}^2 f_{y,Tstub}}{m \gamma_{M0}} = F_{cf,Cd} \rightarrow$$

$$t_{Tstub.1} = \sqrt{\frac{m F_{cf,Cd} \gamma_{M0}}{2 \cdot b_{eff,Tstub} \cdot f_{y,Tstub}}} = \sqrt{\frac{45 \cdot 509860 \cdot 1.05}{2 \cdot 100 \cdot 355}} \cong 17.98 \text{ mm} \quad (4.58)$$

Similarly, to avoid the collapse of the T-stub according to type-2 mechanism the required thickness is:

$$F_{2,Rd} = 2 \frac{\frac{f_{y,Tstub} b_{eff} t_{Tstub}^2}{2} + 2 F_{t,Rd} n}{m + n} = F_{cf,Cd} \rightarrow$$

$$t_{Lstub.2} = \sqrt{\frac{2 \gamma_{M0}}{b_{eff,ep} f_{y,Tstub}} \left[ \frac{F_{cf,Cd}(m+n)}{2} - 2 F_{t,Rd} n \right]} =$$

$$= \sqrt{\frac{2 \cdot 1.05}{100 \cdot 355} \left[ \frac{509680 (45 + 45)}{2} - 2 \cdot 176400 \cdot 45 \right]} \cong 19.95 \text{ mm} \quad (4.59)$$

Therefore, the thickness of the T-stub flange has been assumed equal to 20mm. With regards to the T-stub web, taking into account that its thickness has to be greater than the that of the beam flange (equal to 10.2 mm) it is assumed equal to 15mm.

Subsequently, the  $n_{b,s}$  bolts connecting the T-stub web and the beam flange have to absorb the shear force transmitted by the upper beam

flange that is equal to  $F_{cf,cd}$ . According to Eurocode 3, the shear resistance of the bolts can be evaluated as:

$$F_{V,Rd} = n_{b,s} \frac{\alpha_v \cdot A_{res} \cdot f_{tb}}{\gamma_{M2}} = F_{cf,cd} \quad \rightarrow \quad n_{b,s} = \frac{F_{cf,cd} \cdot \gamma_{M2}}{\alpha_v \cdot A_{res} \cdot f_{tb}} \quad (4.60)$$

Consistent with the beam size, the maximum diameter of the holes on the flange is equal to 19mm therefore M18 bolts have been considered and the minimum number is evaluated:

$$n_{b,s} = \frac{509680 \cdot 1.25}{0.5 \cdot 193 \cdot 1000} = 6.60 \quad \rightarrow \quad n_{b,s} = 8 \quad (4.61)$$

Anyway, aiming to avoid any slippage between the surfaces in contact, namely the T-stub web and the beam flange, the bolts will be pre-tightened in order to obtain a friction resistance greater than the action  $F_{cf,cd}$ :

$$F_{fric,Tstub,w} = \mu \cdot F_p \cdot n_s \cdot n_b = 0.5 \cdot 135.10 \cdot 1 \cdot 8 = 540.40kN > F_{cf,cd} \quad (4.62)$$

#### Design of the L-stubs

In this FREEDAM joint configuration it is assumed that the distance  $m$  between the bolt axis and the plastic hinge located close to the beam flange is equal to 37mm and the distance  $n$  between the bolt line and the end of the plate is equal to 40.5mm.

The horizontal distance between the bolts  $w$  has to satisfy the following limitations:



$$\begin{aligned}
w_{\min} &\cong t_{cw} + 2 r_c + 1.8 d_0 = 26 + 2 \cdot 18 + 1.8 \cdot 21.5 + 15 \\
&= 100.7 \text{ mm} \\
w_{\max} &= b_{cf} - 2.4 d_0 = 226 - 2.4 \cdot 21.5 = 174.4 \text{ mm}
\end{aligned} \tag{4.63}$$

According to the above limitations, the L-stub bolt spacing is taken equal to  $w_0 = 145 \text{ mm}$ . The width of the L-stub, that is coincident with the effective length, is taken equal to 110mm.

The thickness of the L-stub flange required to avoid the collapse of the equivalent T-stub according to type-1 mechanism is:

$$\begin{aligned}
F_{1,Rd} &= \frac{b_{eff} t_{Lstub}^2 f_{y,Lstub}}{2 \cdot m \gamma_{M0}} = \frac{F_{cf,Cd}}{4} \rightarrow \\
t_{Lstub.1} &= \sqrt{\frac{m F_{cf,Cd} \gamma_{M0}}{2 \cdot b_{eff,Lstub} \cdot f_{y,Lstub}}} = \sqrt{\frac{37 \cdot 509860 \cdot 1.05}{2 \cdot 110 \cdot 355}} \cong 15.54 \text{ mm}
\end{aligned} \tag{4.64}$$

Similarly, to avoid the collapse of the L-stub according to type-2 mechanism the required thickness is:

$$\begin{aligned}
F_{2,Rd} &= \frac{\frac{f_{y,Lstub} b_{eff} t_{Lstub}^2}{\gamma_{M0}} + F_{t,Rd} n}{m + n} = \frac{F_{cf,Cd}}{4} \rightarrow \\
t_{Lstub.2} &= \sqrt{\frac{4 \gamma_{M0}}{b_{eff,ep} f_{y,Lstub}} \left[ \frac{F_{cf,Cd}(m+n)}{4} - F_{t,Rd} n \right]} = \\
&= \sqrt{\frac{4 \cdot 1.05}{110 \cdot 355} \left[ \frac{509680 (37 + 40.5)}{4} - 176400 \cdot 40.5 \right]} \cong 16.74 \text{ mm}
\end{aligned} \tag{4.65}$$

Therefore, the thickness of the L-stub flange/web has been assumed equal to 20mm.

**Step 7: Design of the bolts connecting the lower flange of the beam and the flange of the haunch.**

For the design of the bolts connecting the upper flange of the haunch to the lower flange of the beam, the following actions have to be considered:

$$F_{t,Ed} = \frac{F_{cf,Cd} \cdot h_h}{\sum_i d_i^2} \cdot d_i \quad F_{v,Ed} = \frac{F_{cf,Cd}}{n_{b,h}} \quad (4.66)$$

The position of the bolts is defined on the basis of the code requirements for bolt spacing and of technological conditions. The most stressed bolt, whose diameter is equal to 18mm, is the one further from the column face and is subjected to the following actions values:

$$F_{t,Ed} = \frac{F_{cf,Cd} \cdot h_h}{\sum_i d_i^2} \cdot d_i = \frac{509680 \cdot 180}{473055} \cdot 432.6 = 41960N$$

$$F_{v,Ed} = \frac{F_{cf,Cd}}{n_{b,h}} = \frac{509680}{2 \cdot 6} = 42490N \quad (4.67)$$

Therefore, according to Eurocode 3, the check under combined shear and tension lead to determine a first minimum value of the resistant area of the bolts. In particular:

$$A_{res} \geq \frac{\gamma_{M2}}{f_{tb}} \left( \frac{F_{v,Ed}}{\alpha_v} + \frac{F_{t,Ed}}{1.26} \right) \quad (4.68)$$

$$A_{res} \geq \frac{1.25}{1000} \left( \frac{42490}{0.5} + \frac{41960}{1.26} \right) \cong 147.90 \text{ mm}^2 > 193 \text{ mm}^2 = A_{res,M18}$$

**Step 8: Check of the resistance of the column web in shear and design of supplementary web plates if needed.**

The shear resistant area of the column section is given by:

$$\begin{aligned} A_{vc} &= A - 2 b_{cf} t_{cf} + (t_{cw} + 2r_c)t_{cf} = \\ &= 14940 - 2 \cdot 226 \cdot 26 + (15.5 + 2 \cdot 18) \cdot 26 = 4527 \text{ mm}^2 \end{aligned} \quad (4.69)$$

The resistance of the column web panel, without continuity and/or supplementary plates, is:

$$V_{wp,Rd} = \frac{0.9 \cdot A_{vc} \cdot f_{y,cw}}{\sqrt{3} \cdot \gamma_{M0}} = \frac{0.9 \cdot 4527 \cdot 355}{\sqrt{3} \cdot 1.05} \cong 835 \text{ kN} \quad (4.70)$$

Whereas the shear resistance of the column web panel is greater than the action  $F_{cf,cd}$ , supplementary web plates are not needed.

**Step 9: Check of the resistance of the column web in tension and in compression.**

The resistance of the column web in compression can be determined as follows:

$$\begin{aligned} F_{cwc,Rd} &= \omega \cdot k_{wc} \cdot b_{eff,cwc} \cdot t_{cw} \cdot \frac{f_{y,cw}}{\gamma_{M0}} = \\ &= \frac{0.68 \cdot 1 \cdot 275 \cdot 15.5 \cdot 355}{1.05} \cong 978 \text{ kN} \end{aligned} \quad (4.71)$$

where  $b_{eff,cwc}$  is the effective length of the column web given by:

$$\begin{aligned} b_{eff,cwc} &= t_{Tstub,w} + 5(t_{fc} + r_c) + 2 t_{Tstub} = \\ &= 15 + 5(26 + 18) + 2 \cdot 20 = 275 \text{ mm} \end{aligned} \quad (4.72)$$

and the coefficients  $\omega$ , accounts for the possible effects of interaction with shear in the column web panel, and  $k_{wc}$ , accounts for the effect of the longitudinal compressive stress  $\sigma_{com,Ed}$  due to the axial force and the bending moment on the column on the compression column web resistance, are given by:

$$\omega = \frac{1}{\sqrt{1 + 1.3 \left( \frac{b_{eff,cwc} \cdot t_{cw}}{A_{vc}} \right)^2}} = \frac{1}{\sqrt{1 + 1.3 \left( \frac{275 \cdot 15.5}{4527} \right)^2}} = 0.68 \quad (4.73)$$

$$k_{wc} = 1 \quad \text{when} \quad \sigma_{com,Ed} \leq 0.7f_{y,wc}$$

Since the resistance is greater than the action  $F_{cf,cd}$ , continuity plates are not required.

**Step 10: Check of the resistance of the column flange in bending by modelling the tension zone by means of an equivalent T-stub.**

In bolted connections, an equivalent T-stub in tension may be used to model the design resistance of the column flange in bending. Excluding failure mode according to mechanism type-3 because of the design criterion adopted for the bolts, the design resistances for mechanism type-1 and type-2 have to be evaluated. In particular, the following equation has to be considered:

$$F_{1,Rd} \geq F_{cf,cd} \quad F_{2,Rd} \geq F_{cf,cd} \quad (4.74)$$

where:

$$F_{1,Rd} = 2 \frac{b_{eff} t_{cf}^2 f_{y,cf}}{m \gamma_{M0}} \quad \text{and} \quad F_{2,Rd} = 2 \frac{\frac{f_{y,cf} b_{eff} t_{cf}^2}{\gamma_{M0}} + 2 F_{t,Rd} n}{m + n} \quad (4.75)$$

According to Eurocode 3 the effective length, in absence of transverse stiffeners, is given by:

$$\begin{aligned} b_{eff} &= \min\{2\pi m_c; 4m_c + 1.25e; p\} = \\ &= \min\{2\pi \cdot 36; 4 \cdot 36 + 1.25 \cdot 51.3; 105\} \cong 105 \text{ mm} \end{aligned} \quad (4.76)$$

Thereafter, the design resistances for mechanisms type-1 and type-2 are given by:

$$\begin{aligned} F_{1,Rd} &= 2 \frac{f_{y,cf} b_{eff,cfb} t_{cf}^2}{\gamma_{M0} m_c} = 2 \frac{355 \cdot 105 \cdot 20^2}{1.05 \cdot 36} \cong 789 \text{ kN} \geq F_{cf,Cd} \\ F_{2,Rd} &= 2 \frac{\frac{f_{y,cf} b_{eff,cfb} t_{cf}^2}{\gamma_{M0}} + 2 F_{t,Rd} n}{m_c + n} = \\ &= 2 \frac{355 \frac{105 \cdot 20^2}{2} + 2 \cdot 176400 \cdot 38.3}{1.05(36 + 38.3)} \cong 729 \text{ kN} \geq F_{cf,Cd} \end{aligned} \quad (4.77)$$

where  $n = \min\{e; e_{Tstub}; 1.25m_c\} = \min\{51.3; 38.3; 1.25 \cdot 36\} = 38.3 \text{ mm}$ .

Since the both design resistances are greater than the action  $F_{cf,Cd}$ , derived by means of capacity design principles, the check of the column flange in bending is satisfied. Anyway, continuity plates have been inserted in order to reduce the column deformation capacity.

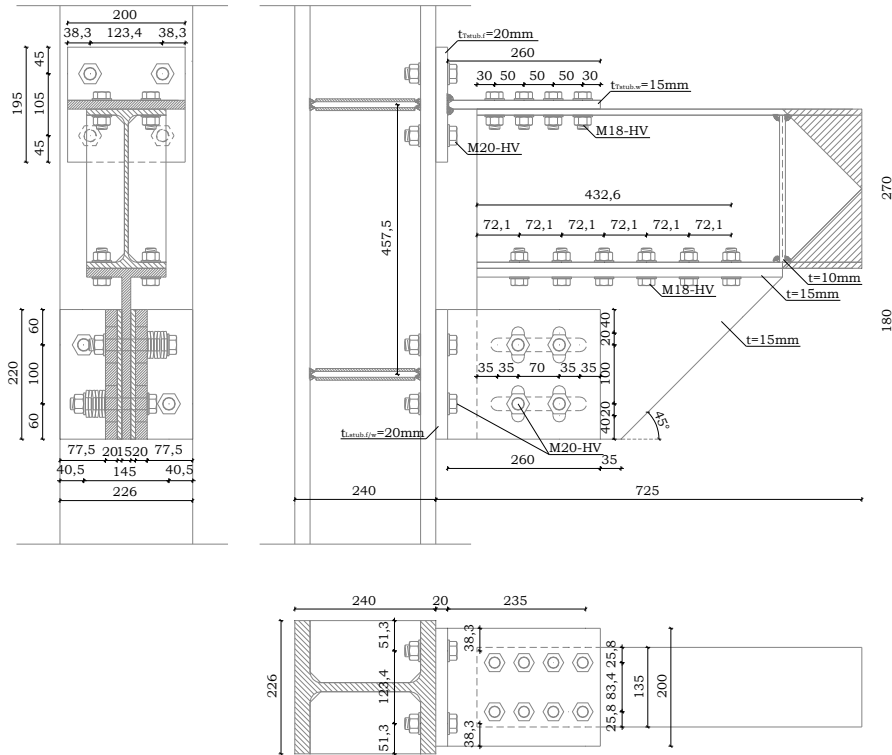


**Fig. 4.13** – Geometry of the specimen FREEDAM-CYC02

## 4.4. Results of the experimental tests

### 4.4.1. Test FREEDAM-CYC01

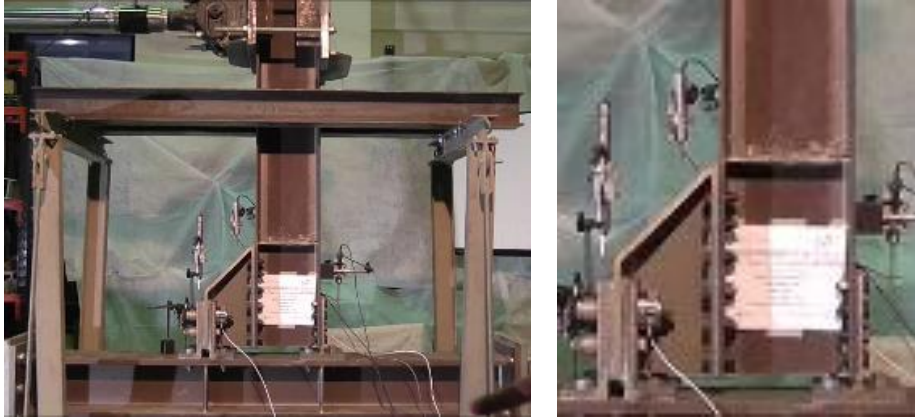


**Fig. 4.14** – FREEDAM-CYC01 specimen

The test FREEDAM-CYC01 has exhibited a global behaviour in line with the prevision. In fact, according to the adopted design criteria, the non dissipative components remained in elastic range. The joint behaviour is stable and without strength degradation but exhibits a hardening behaviour once the sliding has been activated (Fig.4.14). In addition, it could be possible to note that the maximum bending moment exhibited during the test is greater than the plastic resistance of the beam equal to 171.82 kNm. It means that the bending moment corresponding to the slippage resistance results to be greater than the maximum nominal value of the plastic resistance of the connected beam. In other words, by using a friction device, an appropriate value of the tightening torque of the bolts and increasing the lever arm, it is possible to design a full strength joints that are, at the end, FREE from DAMAge.

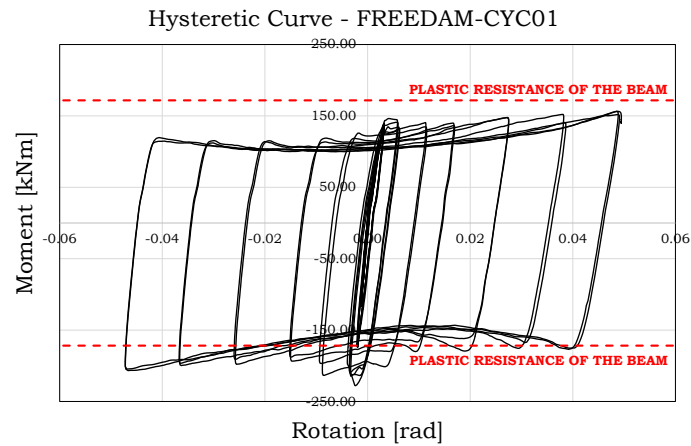


**Fig. 4.15** – Hysteretic curve of the specimen FREEDAM-CYC01

The static friction moment evaluated in correspondence of the column flange is equal to 145.73kNm in case of sagging moment and equal to 227.80kNm when hogging moment occurs.

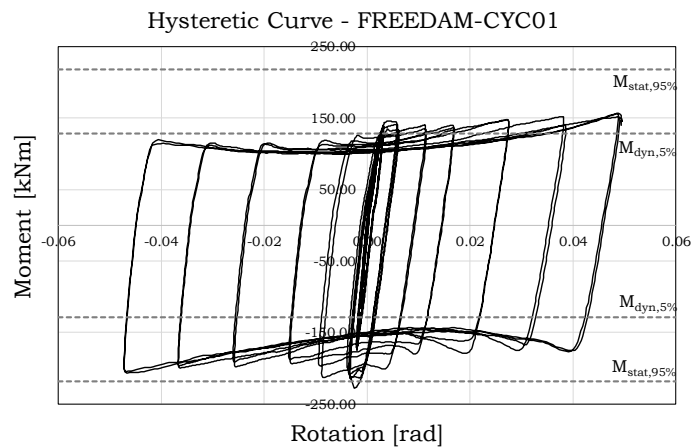


**Fig. 4.16** – Moment-rotation curve of the specimen FREEDAM-CYC01



In fact, the response of the joint is strongly asymmetric under the two loading conditions, reaching values up to 36% smaller under sagging moment. The asymmetry is due to a parasite bending of the plates of the friction damper and variation of the bolt forces under hogging/sagging moments. The dynamic friction moment, i.e. the moment corresponding to the slippage of the friction device, is equal to about 138.06kNm and 196.64kNm in case of sagging and hogging moment respectively, reaching values up to 30% smaller under sagging moment (Fig. 4.16).

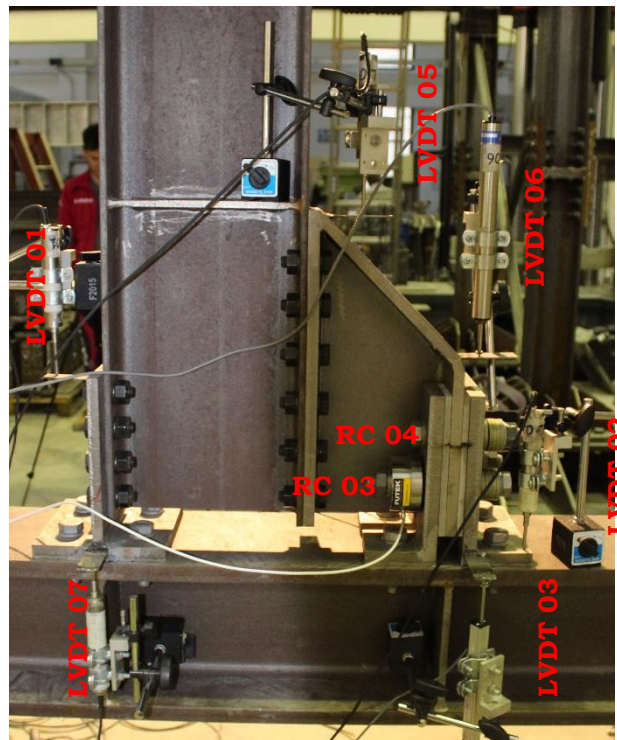


**Fig. 4.17** – Position of the instruments – FREEDAM-CYC01

The value of the bolts preload, and its variation during the tests, has been monitored by means of the two cell loads RC-03 and RC-04 and is

reported in Fig. 4.18. It is possible to observe that initially, at first sliding as already detected in the shear lap tests, there is a settlement of the bolts with a loosening that increases as far as the loading cycles increase. This loosening occurs up to the achievement of high displacement cycles in which the bending effects developing in the dampers' bolt lines lead to a significant oscillation of the bolt forces which, at the peak, achieve, again, practically the initial force.

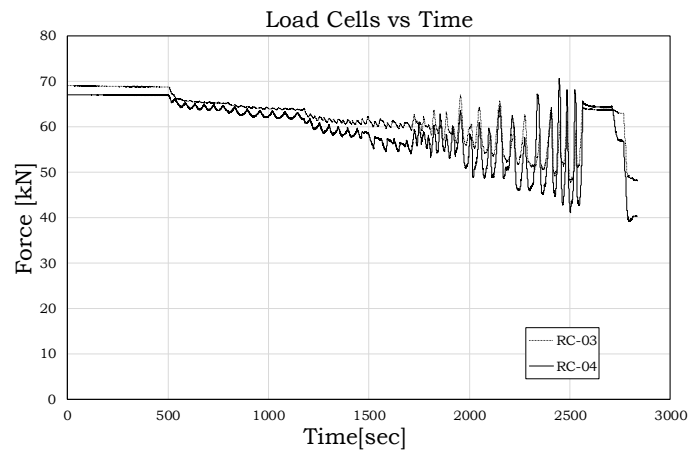


**Fig. 4.18** – Preload force in the bolts of the friction damper

Assuming that the centre of compression is located at the centreline of the damper and that the tension force is located in correspondence of the T-stub, in the following, representations of the local measures obtained with the LVDTs are made reporting the measured displacement versus the local force acting in the joint components. In particular, positive values of the forces corresponds to tensile stress in the joint components.

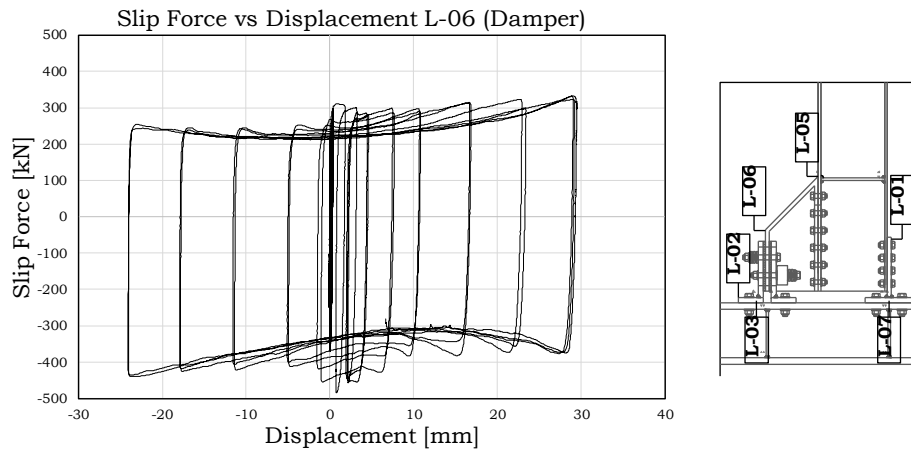


**Fig. 4.19** – Slip force vs displacement curve of the friction damper

Using the displacements recorded by the LVDT 06 (Fig.4.17), the force versus displacement of the friction damper has been determined (Fig. 4.19). It can be easily observed that the hysteretic loops in this case are practically rectangular with a significant energy dissipation capacity and almost no degradation both in terms of stiffness and resistance.

As shown in Figs. 4.20 to 4.23, the other joint components almost remain in the elastic range.

LVDT 01 measures the slip of the web of the T-stub with respect to the beam flange that are about 2.5mm (Fig.4.20). The holes of the bolts connecting the T-stub web and beam flange are greater than the minimum required by the code in order to accommodate the assembly of the all components.

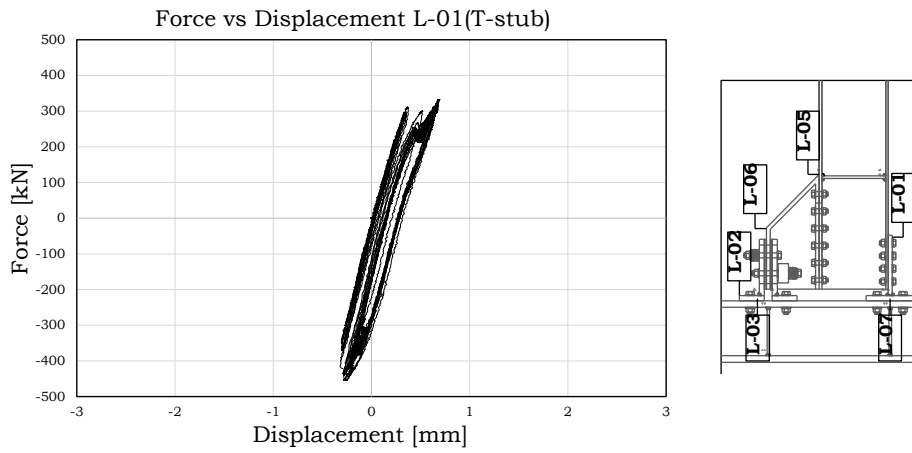


**Fig. 4.20** – Compression force vs displacement curve (T-stub web-beam flange)

LVDT 02 provide the displacements of the edge of the L-stub flange with respect to the column flange that are close to zero (Fig.4.21).

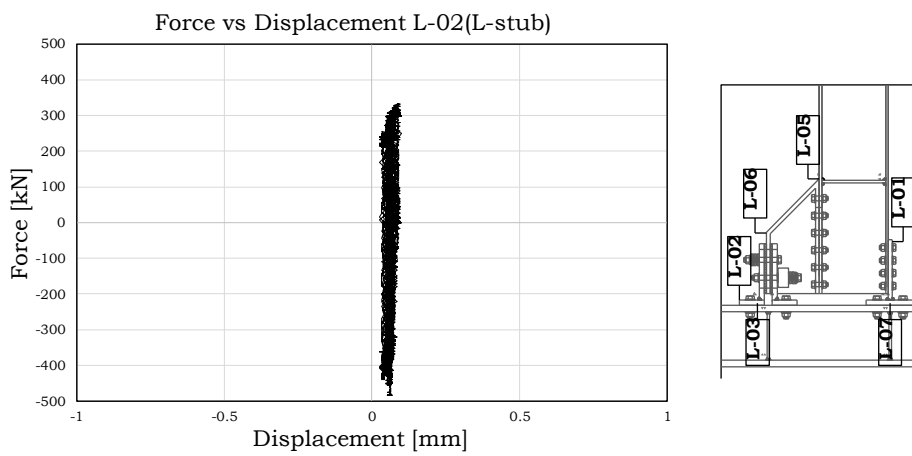


**Fig. 4.21** – Force vs displacement curve (T-stub flange)

LVDTs 03 and 07 provide the eventual deformations of the column web panel that are close to zero (Fig.4.22).

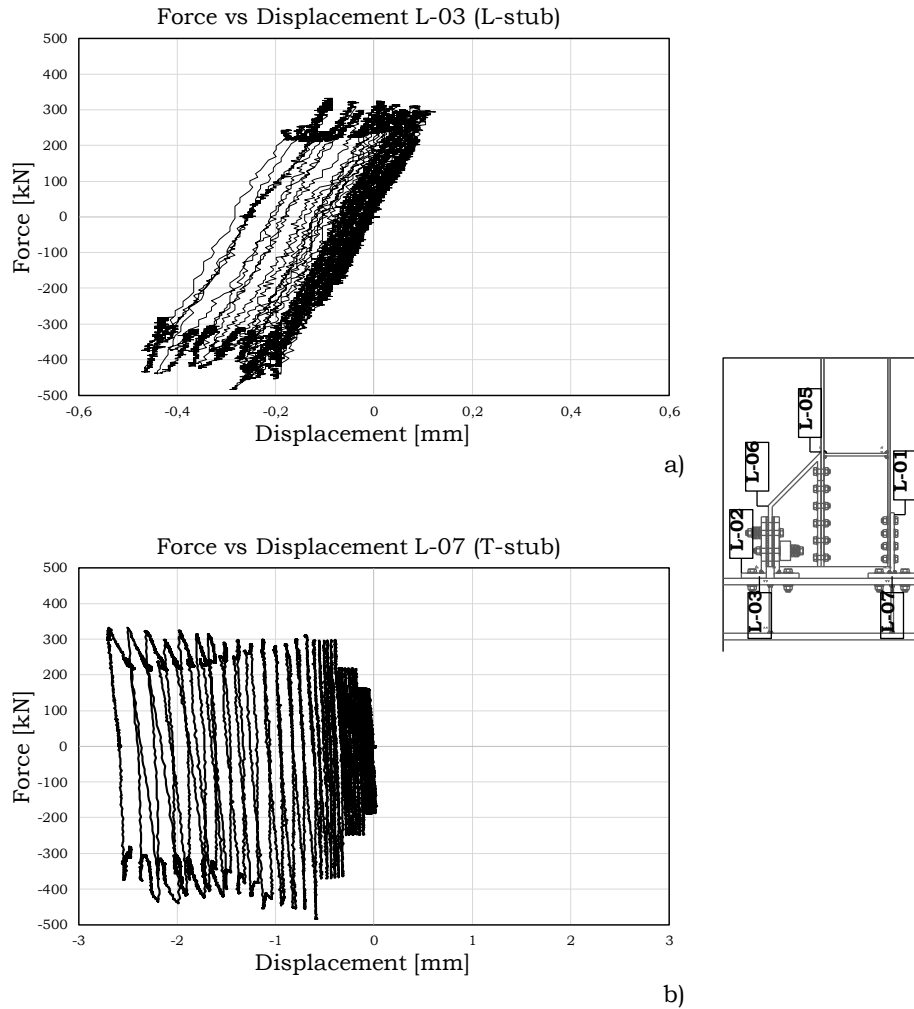


**Fig. 4.22** – Force vs displacement curve: a) L-stub flange/column flange;  
b) T-stub flange/column flange

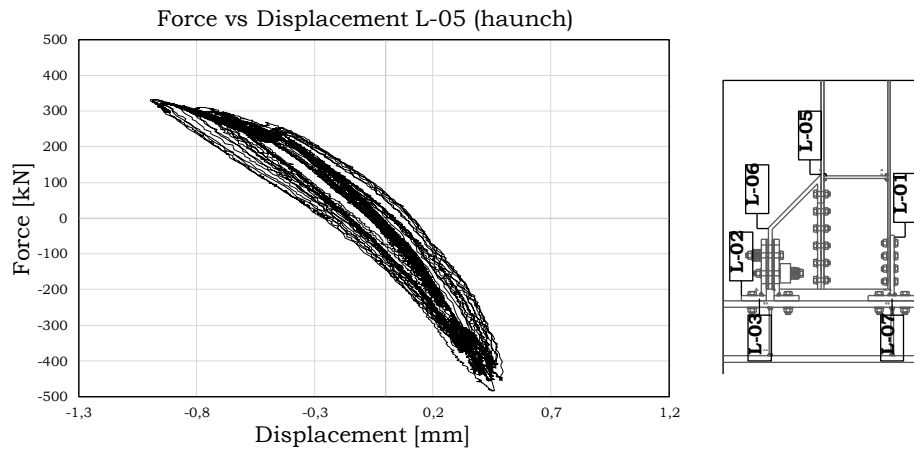


**Fig. 4.23** – Force vs displacement curve (haunch)

The relative displacements of the haunch and the flange of the beam are provided by LVDT 05. These displacements are quite small but it should be underlined that, in case of sagging moment, there is a detachment of the two surfaces in contact (Fig.4.23).

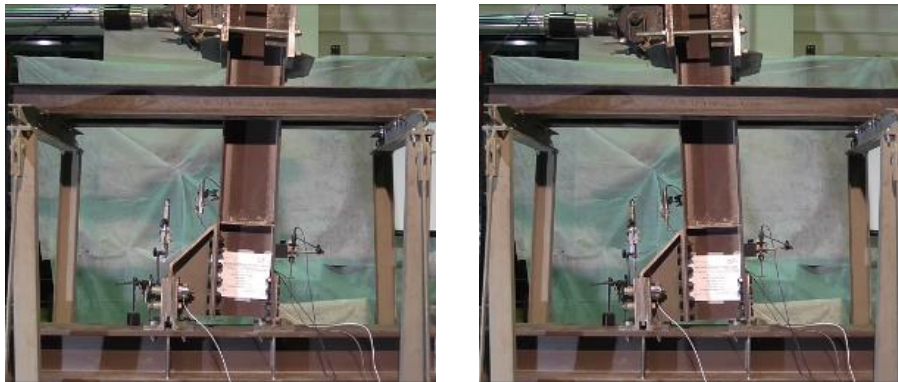


**Fig. 4.24** – FREEDAM-CYC01 specimen in the deformed configuration

Fig. 4.24 shows the specimen when subjected to sagging and hogging moment.

#### 4.4.2. Test FREEDAM-CYC02

Specimen FREEDAM-CYC02 (Fig. 4.25) has been designed in order to behave similarly to specimen FREEDAM-CYC01.



**Fig. 4.25** – FREEDAM-CYC02 specimen

As described in the previous section, in order to reach the design goal, the preload force of the bolts connecting the friction shims to the stainless steel plate has to be greater than that applied in the first specimen. Also the second specimen has exhibited a global behaviour in line with the prevision. The joint behaviour is stable, without strength degradation and with a hardening behaviour once the sliding has been activated (Fig.4.26). Even in this case, it is possible to note that the obtained flexural strength is greater than the plastic resistance of the connected beam, so that practically full-strength connections are obtained without providing any damage to the beam ends (Fig.4.26). The value of the moment corresponding to the achievement of the maximum static slip force is equal to 185.45kNm and 210.41kNm in case of sagging and hogging moment respectively.

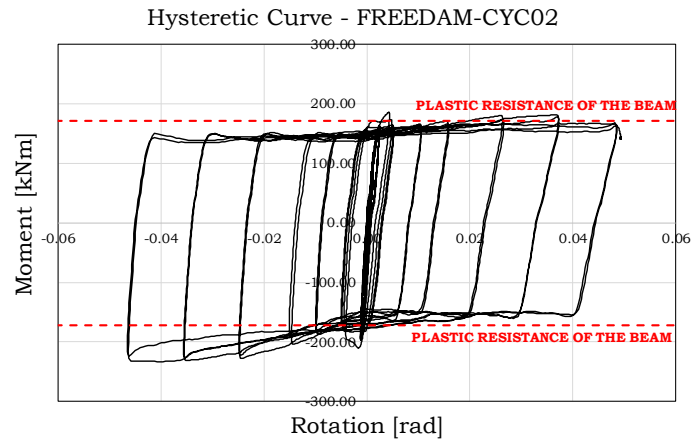


**Fig. 4.26** – Hysteretic curve of the specimen FREEDAM-CYC02

In fact, the response of the joint is still strongly asymmetric under the two loading conditions reaching a sagging moment 13% smaller than the hogging one. The experimental value of the moment corresponding to the slippage of the friction damper is equal to 170.71kN in case of sagging moment and equal to 182.26 in case of hogging moment therefore the difference is negligible being approximately equal to 6% (Fig.4.27).

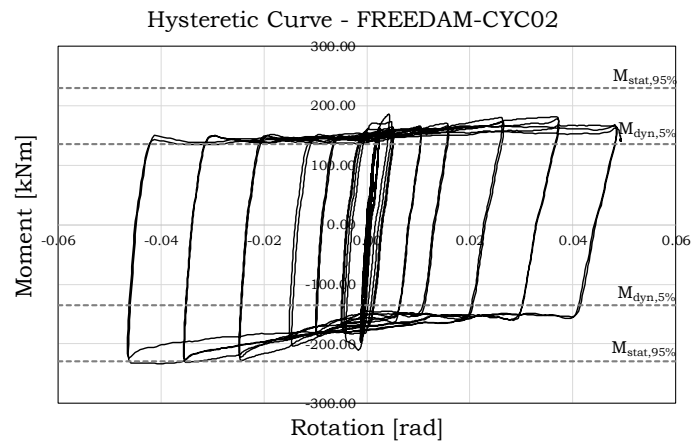


**Fig. 4.27** – Moment-rotation curve of the specimen FREEDAM-CYC02



However, the value of the moment corresponding to the slippage of the friction damper is even greater if considering, especially in case of hogging moment, the increase of the rotation amplitude.

The position of the LVDTs and the load cells used in the monitoring of the local deformation and forces is represented in Fig. 4.28.

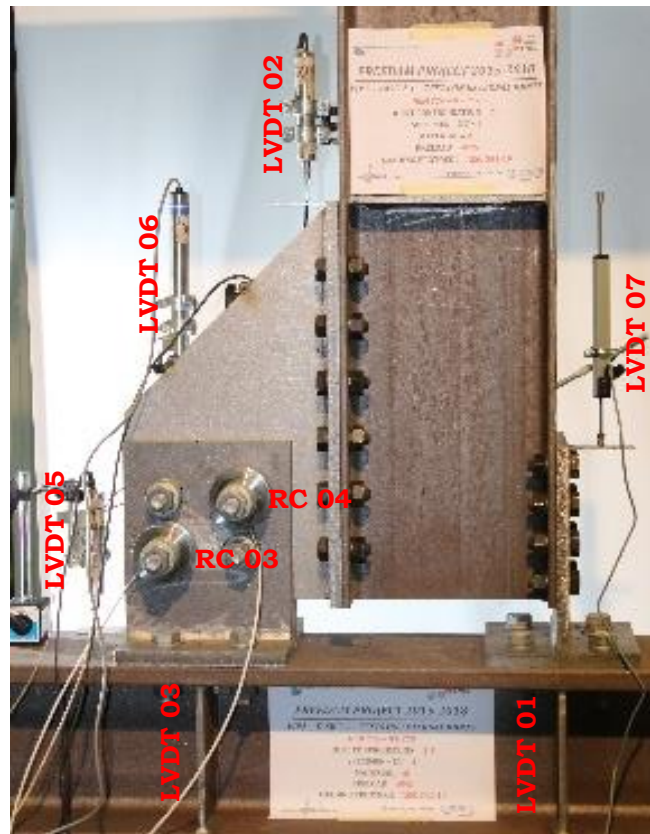


**Fig. 4.28** – Position of the instruments – FREEDAM-CYC02

The variation of the bolts preload during the tests, has been monitored by means of the two cell loads RC-03 and RC-04. The considerations done before are still valid: immediately there is a loosening that increases as

far as the loading cycles increase. Follows a significant oscillation of the bolt forces which, at the peak, achieve, again, practically the initial value.

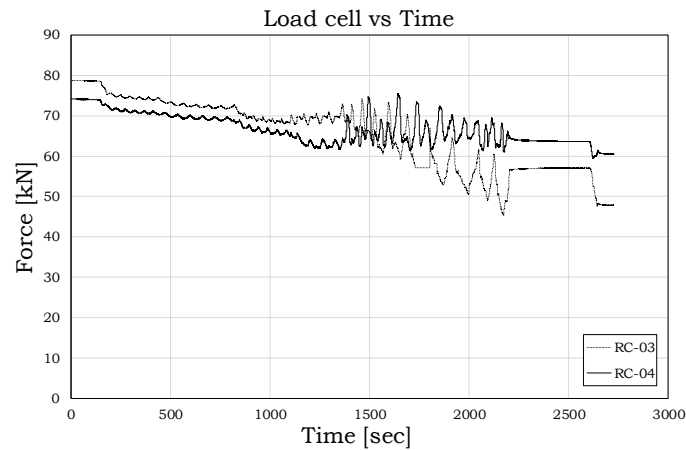


**Fig. 4.29** – Preload force in the bolts of the friction damper

The displacements recorded by the LVDTs 04 and 06 against the slip of the friction damper has been determined (Fig. 4.30).

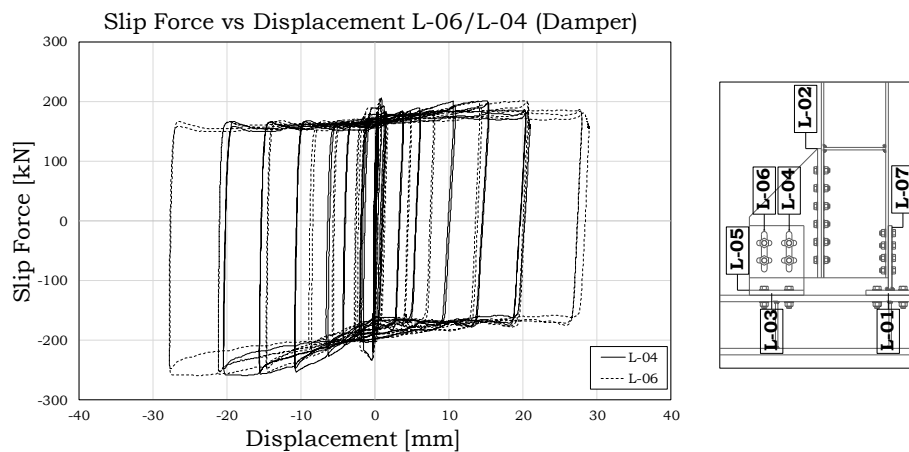


**Fig. 4.30** – Slip force vs displacement curve of the friction damper

Even in this case it can be easily observed that the behaviour of the friction damper strongly affects the whole behaviour of the joint.

Figs. 4.31 to 4.34 show the behaviour of the other joint components, that essentially remain in the elastic range.

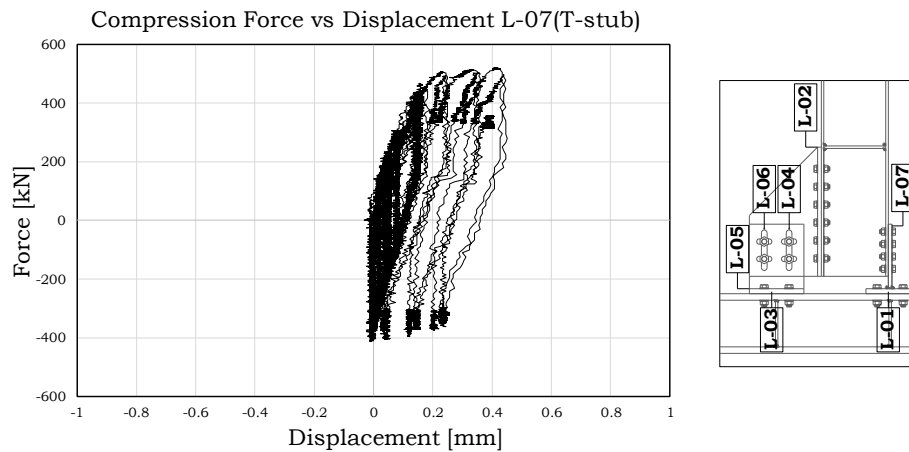


**Fig. 4.31** – Compression force vs displacement curve (T-stub web-beam flange)

LVDT 07 (Fig. 4.31) measures the slips of the web of the T-stub with respect to the beam flange when subjected to a compression/tension force; that displacements results to be no more than 0.5 mm. The displacements of the edge of the L-stub flange with respect to the column flange, provided by LVDT 05, are close to zero (Fig. 4.32).

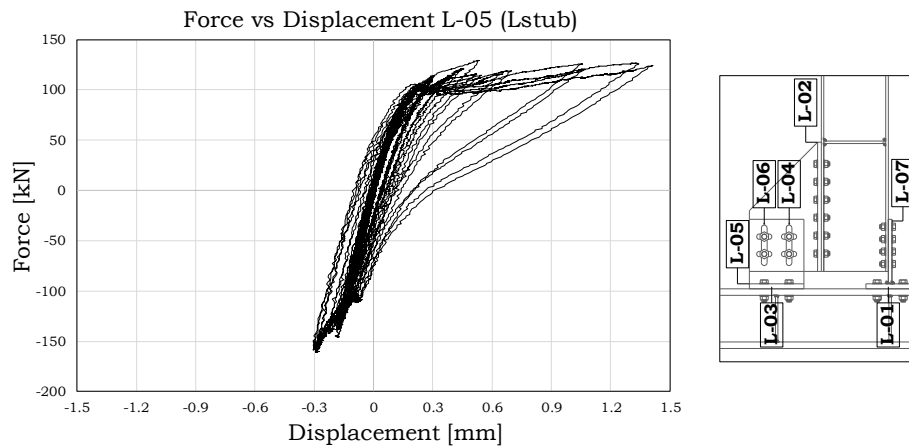


**Fig. 4.32** – Force vs displacement curve (L-stub flange)

LVDT 02 provides the relative displacements between the haunch and the flange of the beam that are less than 1mm even though there is a detachment of the two surfaces in contact in case of sagging moment (Fig. 4.33).

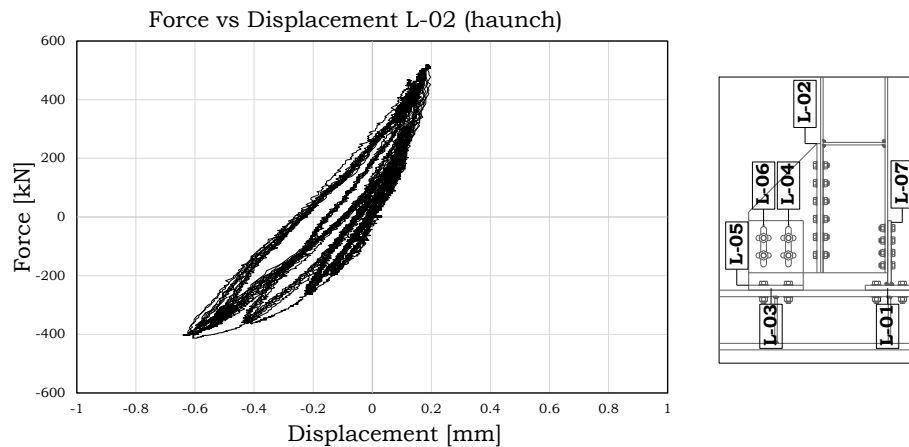


**Fig. 4.33** – Force vs displacement curve (haunch)

Finally, LVDTs 01 and 03 provide the eventual deformations of the column web panel that are close to zero (Fig. 4.34).

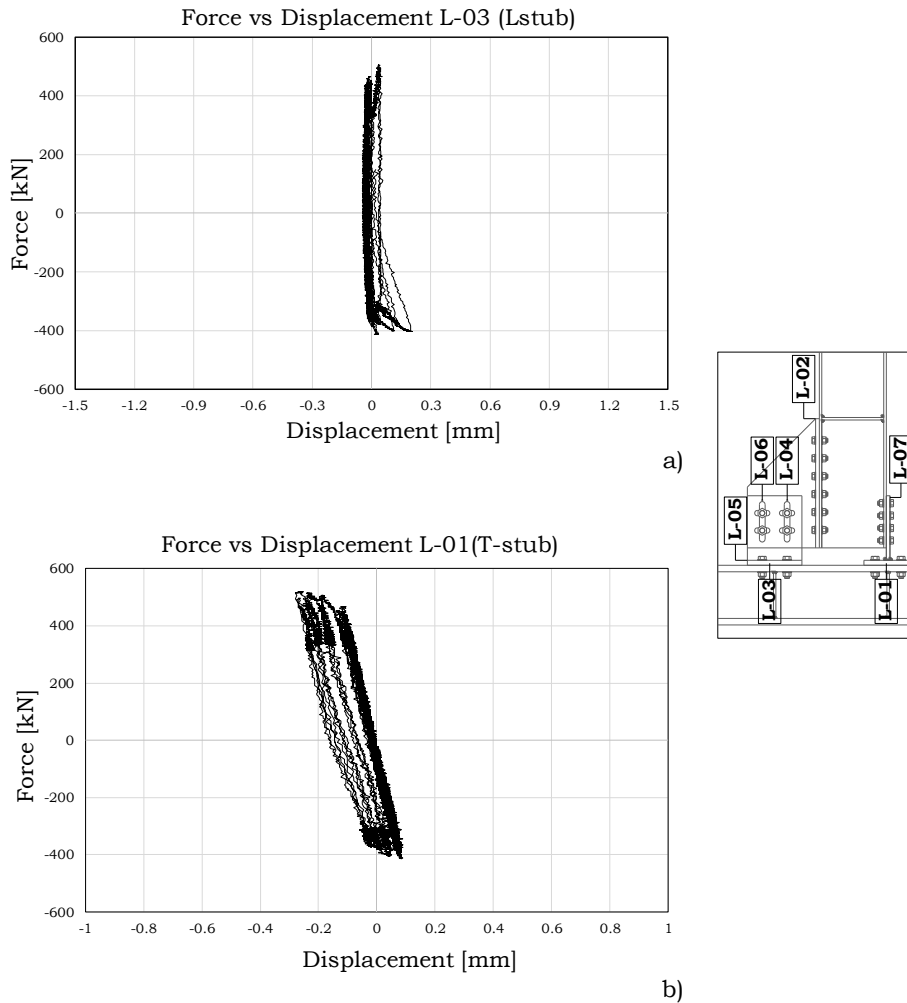


**Fig. 4.34** – Force vs displacement curve: a) L-stub flange/column flange; b) T-stub flange/column flange

The specimen FREEDAM-CYC 02 when subjected to sagging and hogging moment has been depicted in Fig.4.35.

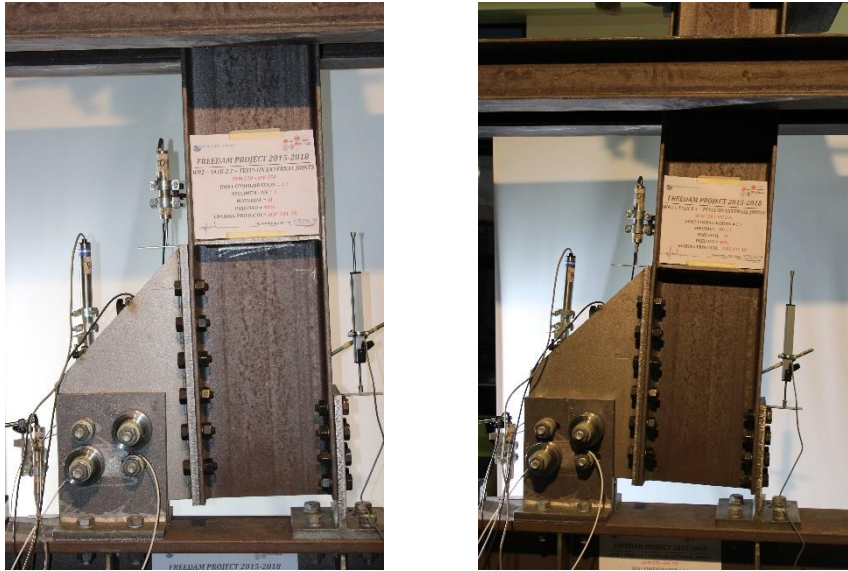


**Fig. 4.35** – FREEDAM-CYC02 specimen in the deformed configuration

#### 4.4.3. Test FREEDAM-CYC03

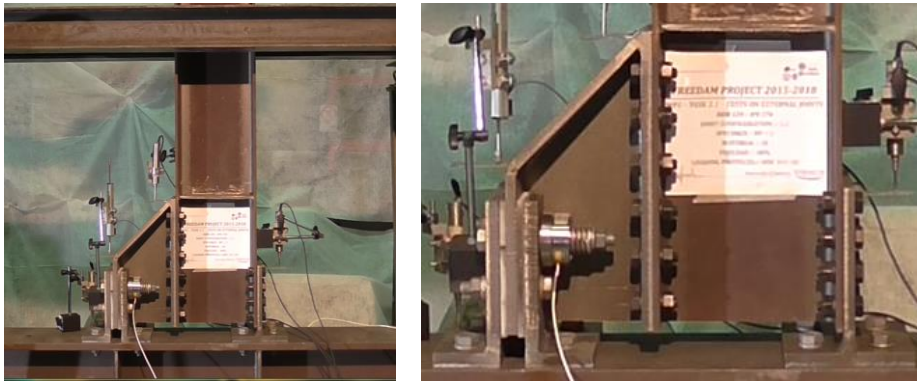


**Fig. 4.36** – FREEDAM-CYC03 specimen

---

*Robustness and seismic behaviour of structures equipped with traditional and innovative beam-to-column connections*

The test FREEDAM-CYC03 is the same configuration of test n°1, without disc springs. The results, in terms of moment-rotation, evidence that the disc springs did not seem to provide a substantial benefit. In fact, even in this configuration, the specimen has exhibited a global behaviour in line with the prevision. The static friction moment evaluated in correspondence of the column flange is equal to 117.58kNm in case of sagging moment and equal to 161.78kNm when hogging moment occurs. As in case of the specimen FREEDAM-CYC01, the response of the joint is strongly asymmetric under the two loading conditions, reaching values up to 27% smaller under sagging moment.

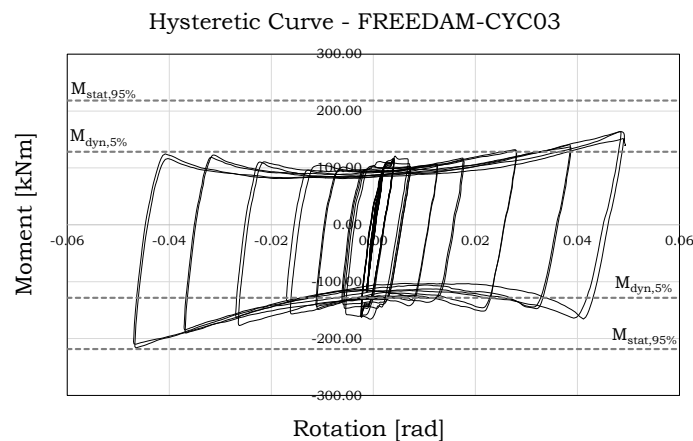
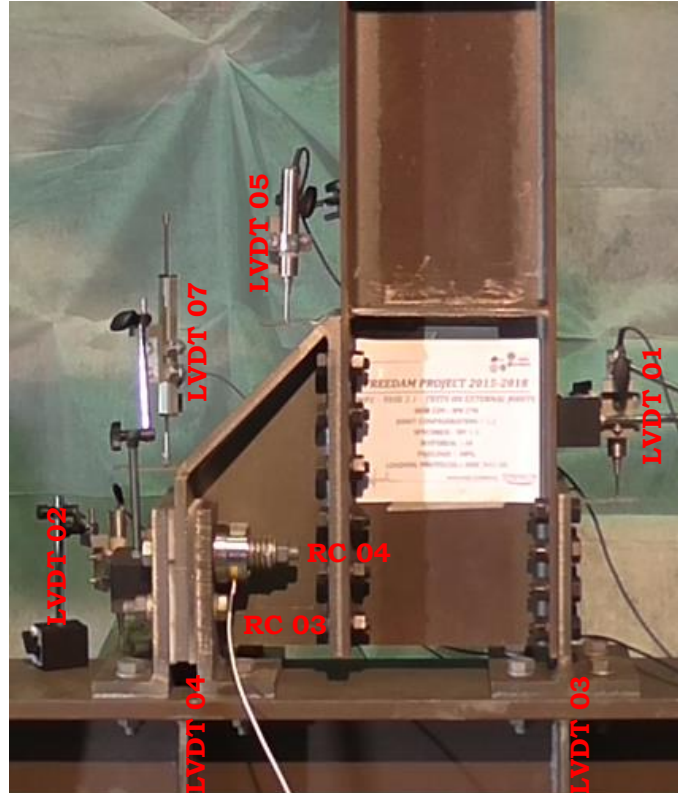


**Fig. 4.37** – Moment-rotation curve of the specimen FREEDAM-CYC03

The dynamic friction moment, i.e. the moment corresponding to the slippage of the friction device, is equal to about 112.57kNm and 158.35kNm in case of sagging and hogging moment respectively, reaching values up to 29% smaller under sagging moment (Fig. 4.37).

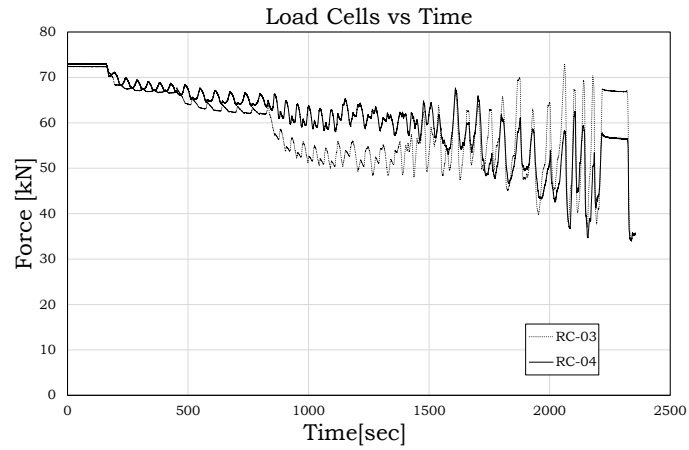
The local measures obtained with the LVDTs and the load cells (Fig. 4.38) are made and the measured displacement versus the local force acting in

the joint components have been reported in Figs. 4.39 to 4.44. This figures show that, according to the design procedure, the non dissipative components remain in elastic range.

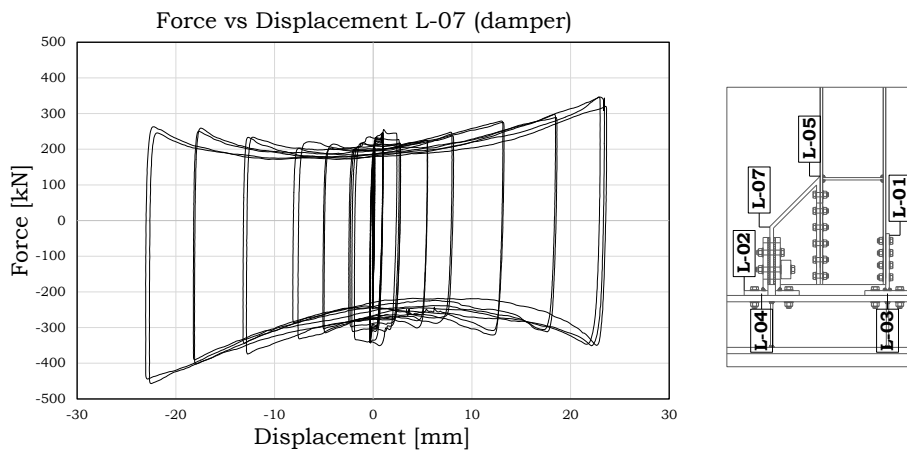


**Fig. 4.38** – Position of the instruments – FREEDAM-CYC03

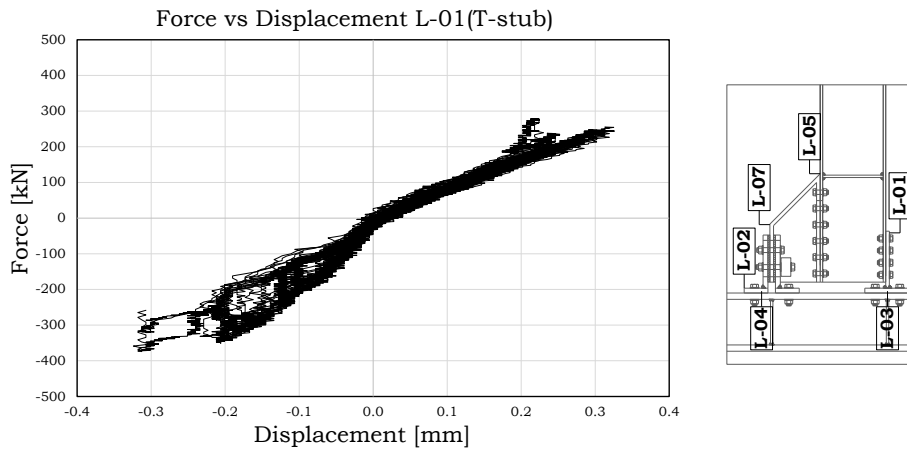




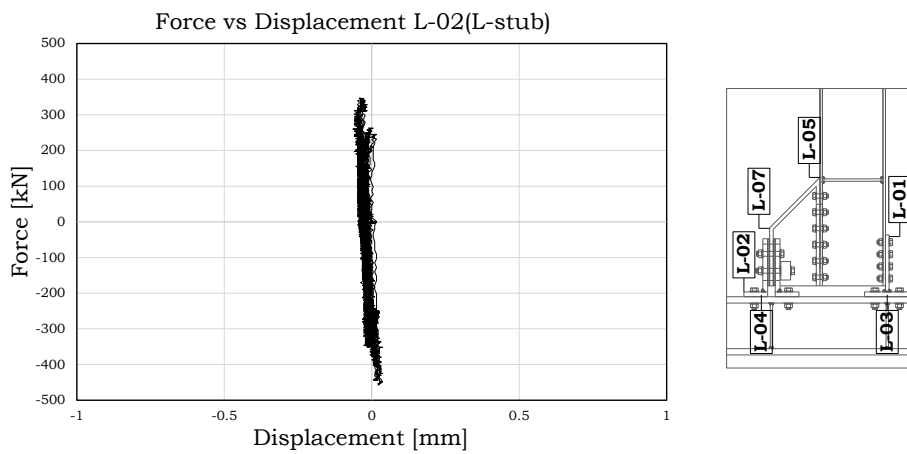
**Fig. 4.39** – Preload force in the bolts of the friction damper



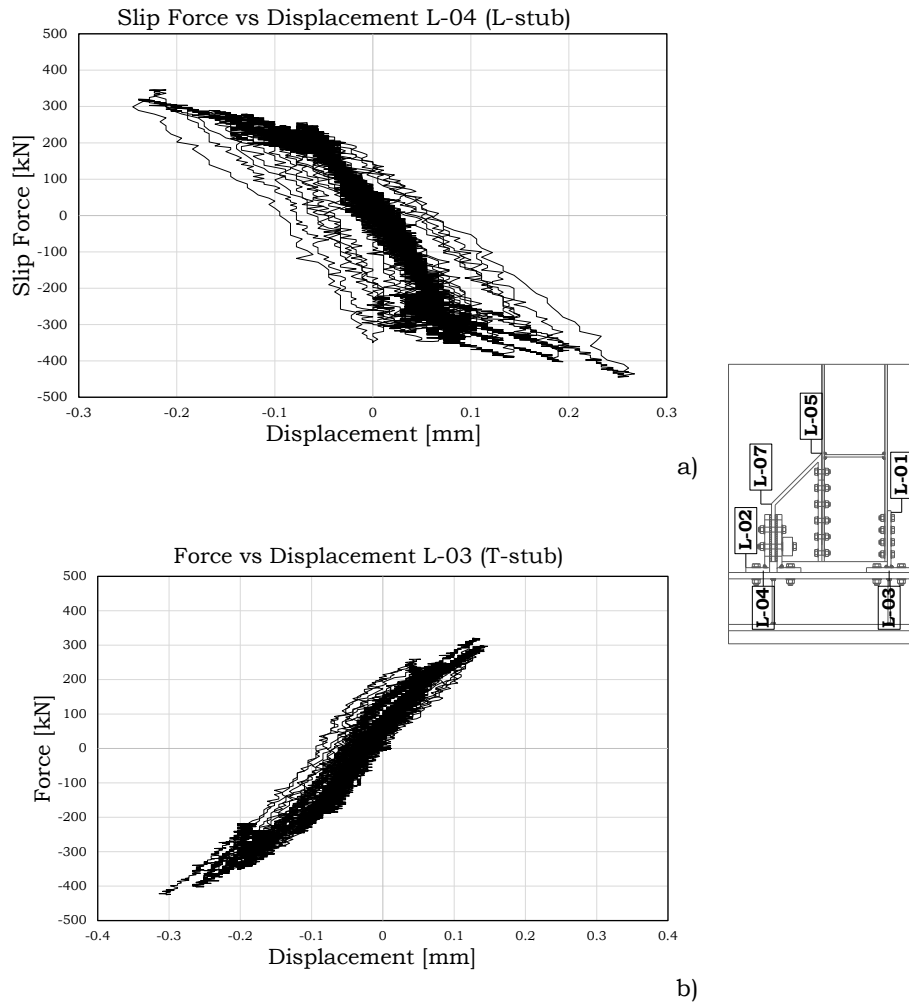
**Fig. 4.40** – Slip force vs displacement curve of the friction damper



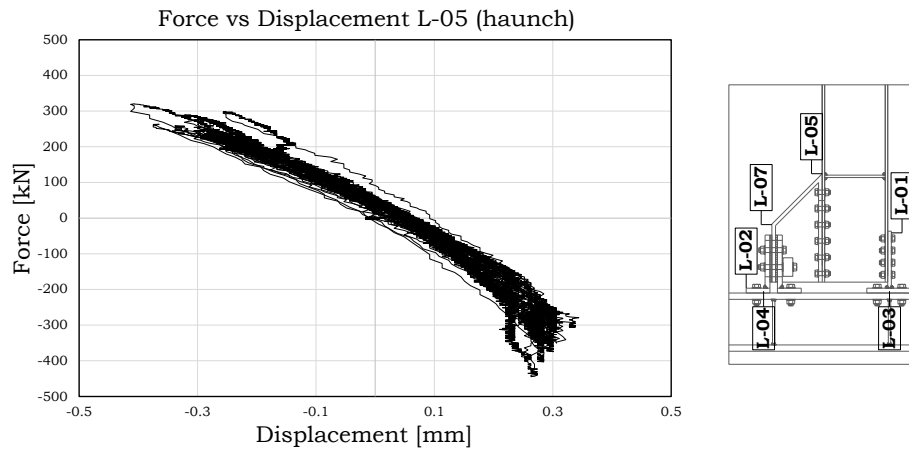
**Fig. 4.41** – Compression force vs displacement curve (T-stub web-beam flange)



**Fig. 4.42** – Force vs displacement curve (L-stub flange)

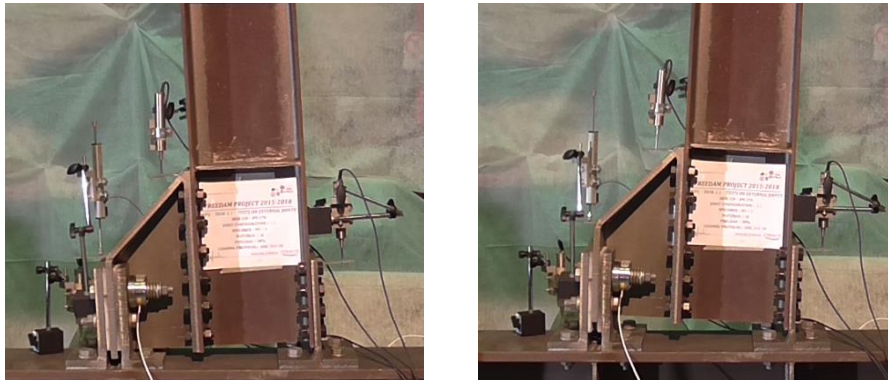


**Fig. 4.43** – Force vs displacement curve: a) L-stub flange/column flange;  
b) T-stub flange/column flange



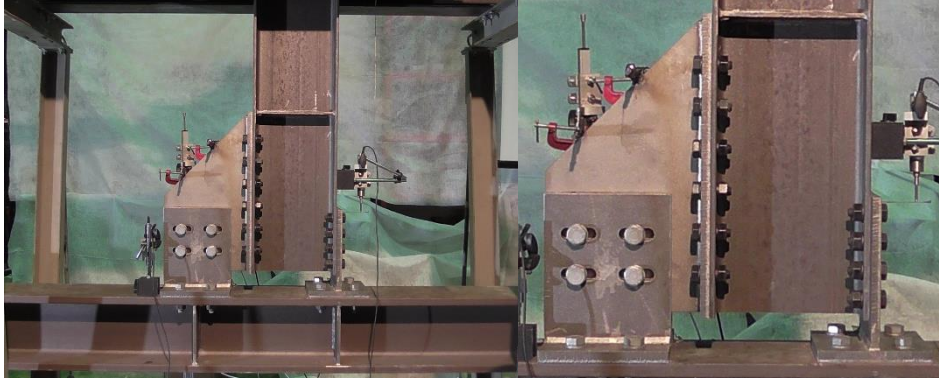
**Fig. 4.44** – Force vs displacement curve (haunch)

Fig. 4.45 shows the specimen when in the deformed configuration.



**Fig. 4.45** – FREEDAM-CYC03 specimen in the deformed configuration

#### 4.4.4. Test FREEDAM-CYC04



**Fig. 4.46** – FREEDAM-CYC04 specimen

Specimen FREEDAM-CYC04 (Fig. 4.46) differs from specimen FREEDAM-CYC 02 because of the absence of the Belleville disc springs. The hysteretic behaviour of the two specimen is quite similar evidencing that, even in the joint configuration n.2, the disc springs did not seem to provide a substantial benefit. The joint behaviour is stable, without strength degradation and with a hardening behaviour once the sliding has been activated (Fig.4.47).

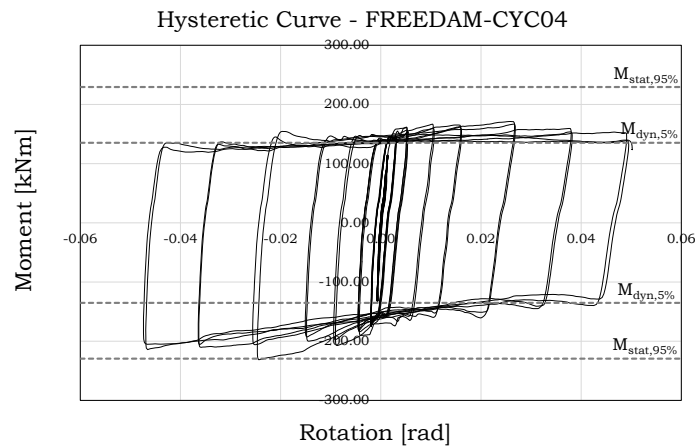


**Fig. 4.47** – Hysteretic curve of the specimen FREEDAM-CYC04

The value of the moment corresponding to the achievement of the maximum static slip force is equal to 159.80kNm and 181.48kNm in case of sagging and hogging moment respectively. In fact, it is easily possible to note from Fig. 4.47 that the difference between the maximum bending moment due to hogging or sagging actions was equal to about the 13%. In the following, representations of the local measures obtained with the LVDTs and the load cells (Fig. 4.48) are made reporting the measured displacement versus the local force acting in the joint components (Figs. 4.49 to 4.53). The acquired measurements evidence that the non dissipative components remain in elastic range accordingly to the design criteria.

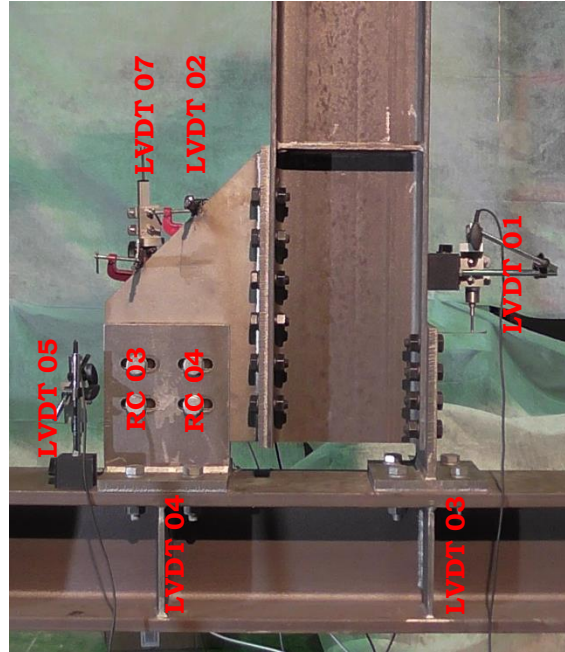


**Fig. 4.48** – Position of the instruments – FREEDAM-CYC04

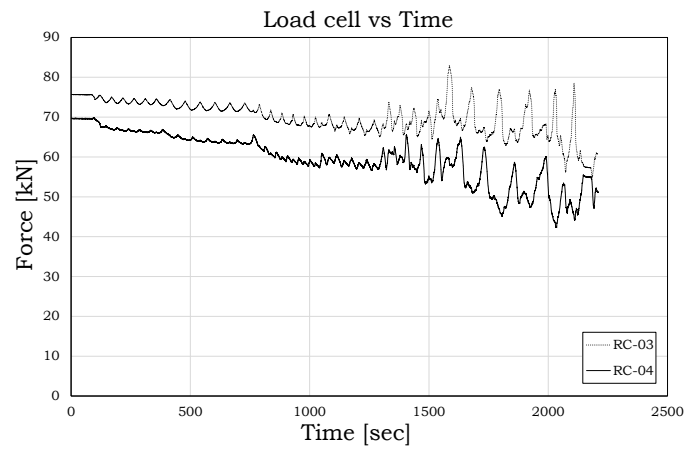


**Fig. 4.49** – Preload force in the bolts of the friction damper

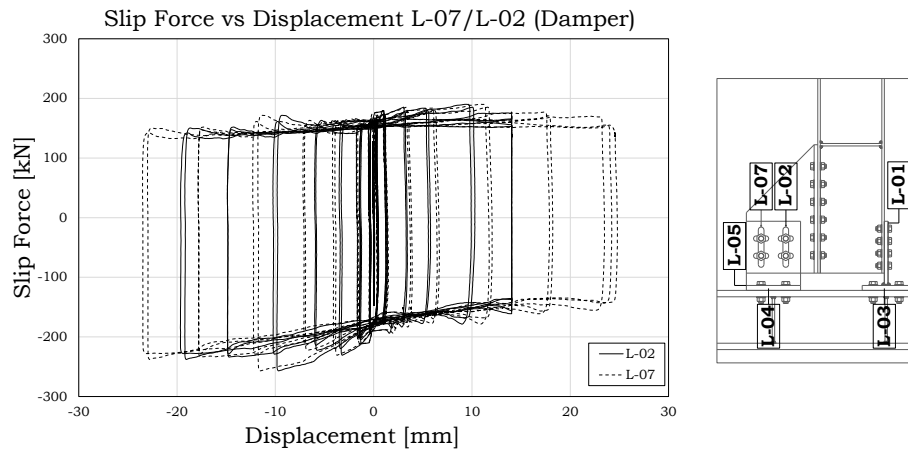


**Fig. 4.50** – Slip force vs displacement curve of the friction damper

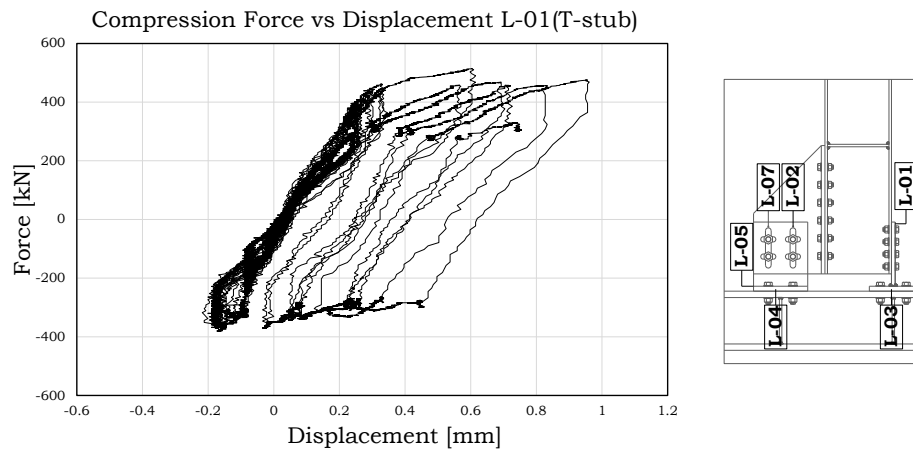


**Fig. 4.51** – Compression force vs displacement curve (T-stub web-beam flange)



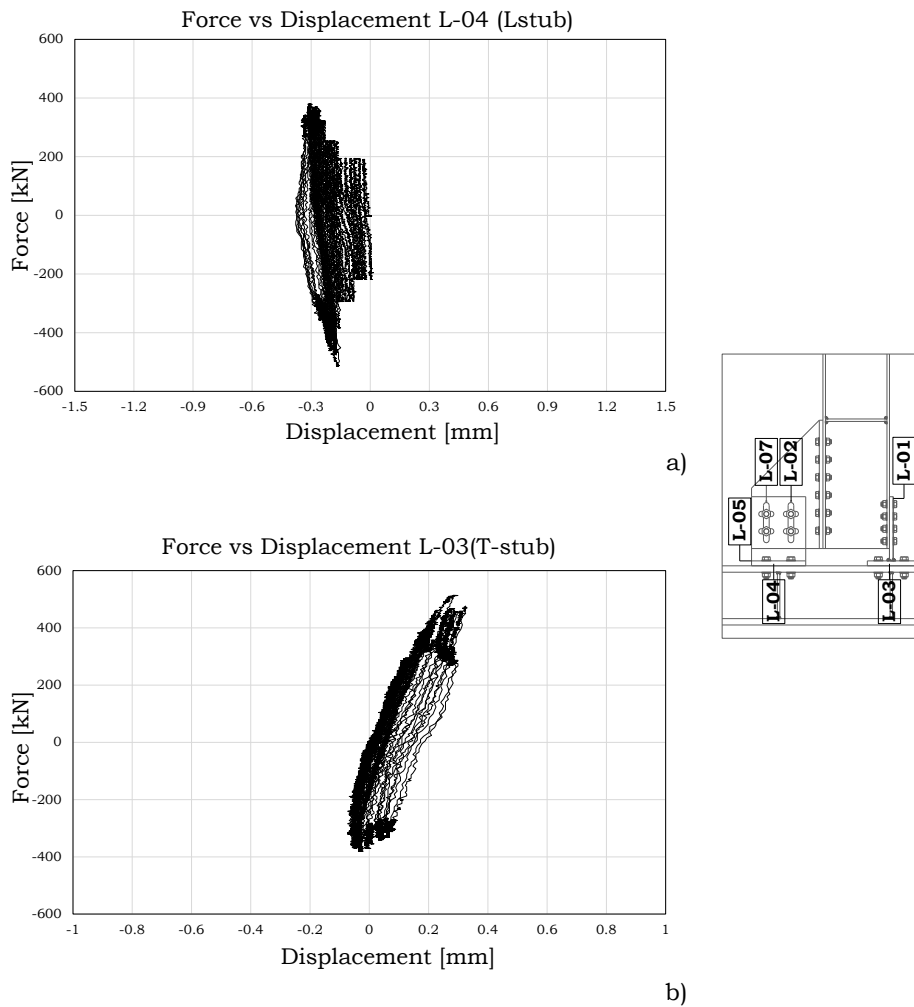


**Fig. 4.52** – Force vs displacement curve: a) L-stub flange/column flange; b) T-stub flange/column flange

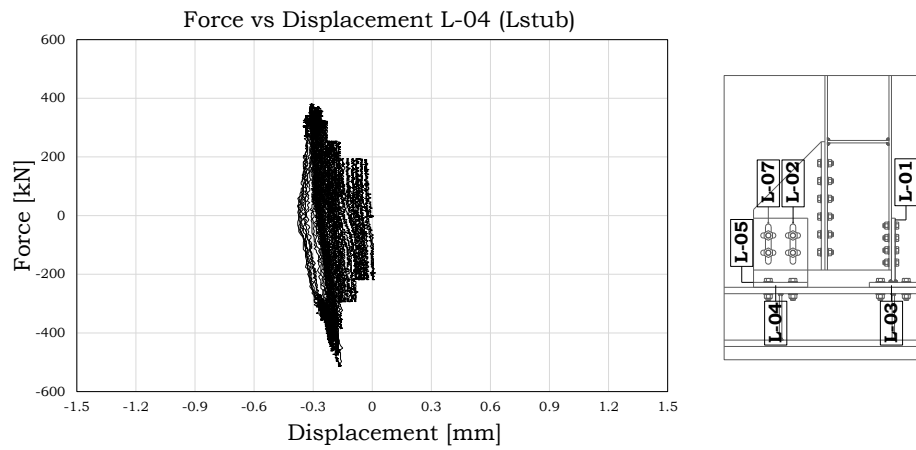


**Fig. 4.53** – Force vs displacement curve (L-stub flange)

The specimen FREEDAM-CYC 04 when subjected to sagging and hogging moment has been depicted in Fig.4.54.

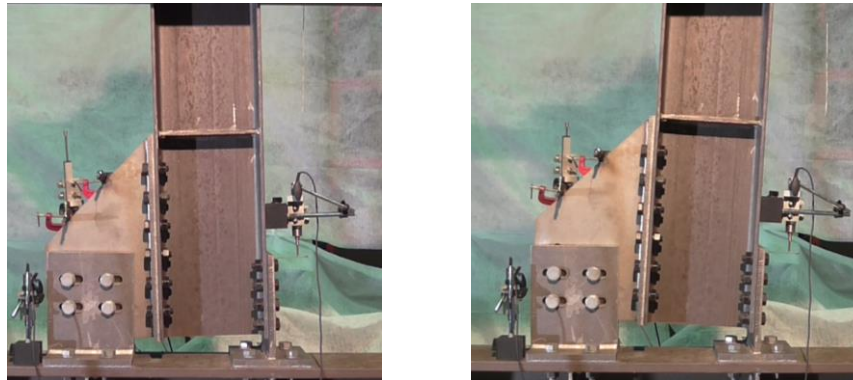


**Fig. 4.54** – FREEDAM-CYC04 specimen in the deformed configuration

## **4.5. Comparison among the tests**

The experimental results are in line with the outcomes of the tests on the friction interfaces pointing out that, as expected, the cyclic behaviour of the joint is mainly governed by the cyclic behaviour of the weakest joint component, i.e. the friction damper. In fact, in all the experimental tests the response has been very similar to that exhibited during the uniaxial tests on the interface. When the force applied at the end of the cantilever beam reached a value approximately equal to the design bending moment divided by the beam length, the slippage of the friction dampers started (Figs. 4.16, 4.27, 4.37, 4.47). Observing the hysteretic loops of the two configurations, different shapes can be noticed. While configuration n.1 exhibits a more smooth nonlinear behaviour from the beginning up to the end of loading/reloading cycles, the second configuration has a more saw-teeth behaviour. From the comparison with the response of the tests on the simple friction dampers, it is worth noting that the shape of the hysteresis cycle of the friction DST joint differs from that observed during the uni-axial tension test. This difference is mainly due to the role played by the beam rotation in the kinematic mechanism. In fact, the beam rotation causes two effects that give rise to an increase of the bending moment as far as the beam rotation increases. On one hand, there is an increase of the local pressure on the friction pads due to the reaction force provided by the T-stub webs that behave in a way similar to a pocket foundation. On the other hand, minor yielding of the tee stems at the web-to-flange attachment contributes to the total bending resistance of the joint. Both of these effects lead to the hardening behaviour experimentally observed. Another thing that was pointed out in this experimental phase is that the Belleville disc springs did not seem to

provide a substantial benefit in terms of hysteretic behaviour. This result seems to confirm the observations already made in chapter 3.

An important feature of the proposed connection is that, as confirmed by the experimental results, it is able to provide a high dissipative capacity also under values of the rotation significantly greater than the minimum value equal to 35 mrad required by EC3 for frames in High Ductility Class. Furthermore, it is possible to observe from Figs. 4.16, 4.27, 4.37 and 4.47, that the resistances of the joints and of the dampers approximately correspond to the design ones, confirming the accuracy of the design procedure previously described. A comparison between the actual structural performance and the specimens design values is provided in Table 4.2. In particular, the experimental values of the bending moment reached during the loading process and the design values evaluated considering the nominal, the average and the 95% fractile of the friction coefficients are reported.

**Table 4.2** – Comparison between experimental and design values of friction moments

	<b>FREEDAM-CYC01</b>	<b>FREEDAM-CYC03</b>	<b>FREEDAM-CYC02</b>	<b>FREEDAM-CYC04</b>
<b>M<sub>stat,exp</sub> [kNm]</b>	+145.73 -227.80	+117.58 -161.78	+185.45 -210.41	+159.80 -181.48
<b>M<sub>stat,d</sub> [kNm]</b>	179.34 ( $\mu_{stat,5\%}$ )		170.52 ( $\mu_{stat,5\%}$ )	
	197.54 ( $\mu_{stat,k}$ )		207.59 ( $\mu_{stat,k}$ )	
	218.33 ( $\mu_{stat,95\%}$ )		229.44 ( $\mu_{stat,95\%}$ )	
<b>M<sub>dyn,exp</sub> [kNm]</b>	+130.06 -196.64	+112.57 -158.35	+170.71 -182.26	+145.82 -171.97
<b>M<sub>dyn,d</sub> [kNm]</b>	128.43 ( $\mu_{dyn,5\%}$ )		135.29 ( $\mu_{dyn,5\%}$ )	
	140.54 ( $\mu_{dyn,k}$ )		148.06 ( $\mu_{dyn,k}$ )	
	155.08 ( $\mu_{dyn,95\%}$ )		163.37 ( $\mu_{dyn,95\%}$ )	

With reference to all the specimens, it is possible to note that the experimental values of the flexural resistance are in between the range of design values and in particular result to be quite similar to the average static and dynamic resistances. The differences between design and actual values of the static flexural resistances could be attributed to the random variability of the friction coefficient but also to the randomness of the bolt preload. Conversely, in terms of dynamic resistance, the forecast is more accurate.

## **4.6. References**

- [1] American Institute of Steel Construction, ANSI/AISC 341-10, AISC, 2010.
- [2] CEN: “Eurocode 3: Design of Steel Structures – Part 1-8: Design of Joints”, EN 1993-1-8, 2005.

# **Chapter 5**

**Influence of the beam-to-column joints on  
the seismic behaviour of steel MRFs**





## 5.1. Introduction

With the aim to develop more accurate methods for evaluating the seismic response of the structures equipped with innovative connections, in this chapter, starting from the knowledge of the their cyclic rotational behaviour, the influence of the beam-to-column joints on the seismic response of the steel structures has been investigated. The performances of the MRF equipped with FREEDAM connections, and in particular with FREEDAM-CYC 01 joint (considering its more smooth nonlinear behaviour from the beginning up to the end of loading/reloading cycles), have been analysed.

In particular, incremental dynamic analyses and pushdown analyses have been performed in order to evaluate the benefits on the global behaviour of the structures when equipped with innovative beam-to-column connections. To this aim, the seismic response and the structural robustness of the frame where the friction connections have been adopted, have been compared to the performance of the same MRF equipped with a traditional double split tee connection (Fig.5.1a) TS-CYC04 (partial strength joints) and with the dobgone connection (Fig.5.1b) EEP-DB-CYC03 (full strength joints) whose cyclic response have been experimentally analysed in the past years at the University of Salerno and herein reported in terms of Moment-rotation in Fig.5.2.

The scope of that experimental campaign was the evaluation of the performances of different joint typologies under seismic loading conditions and the reliability of the available design approach to configure the joints' details for obtaining a desired value of stiffness, strength and ductility [1-3].

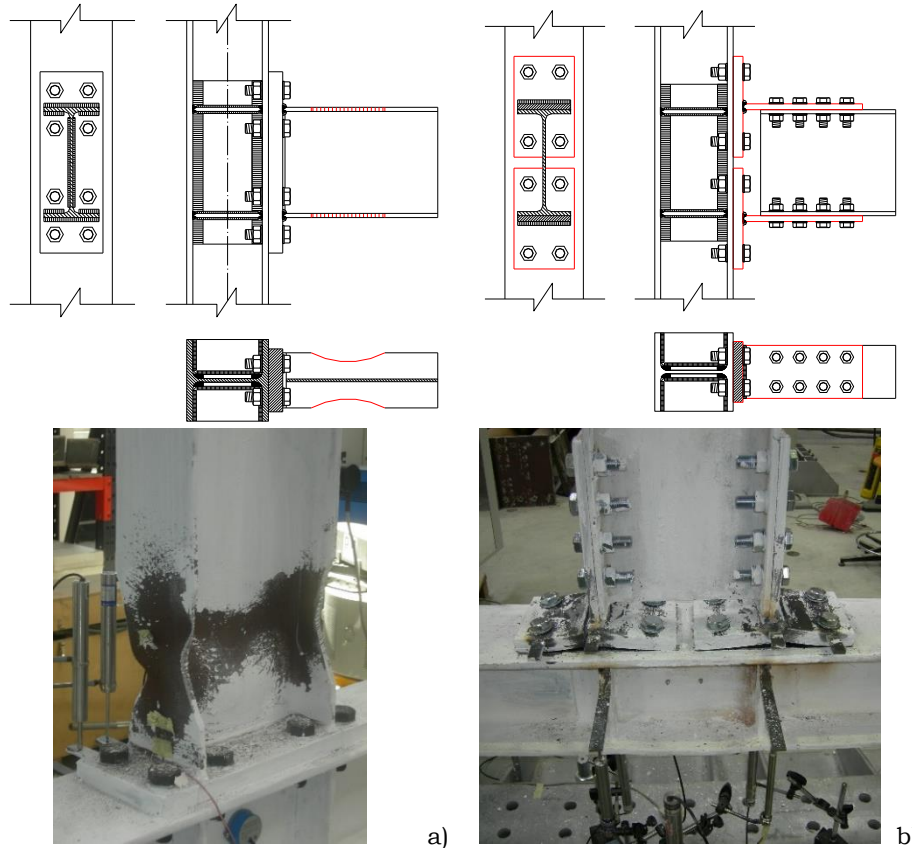
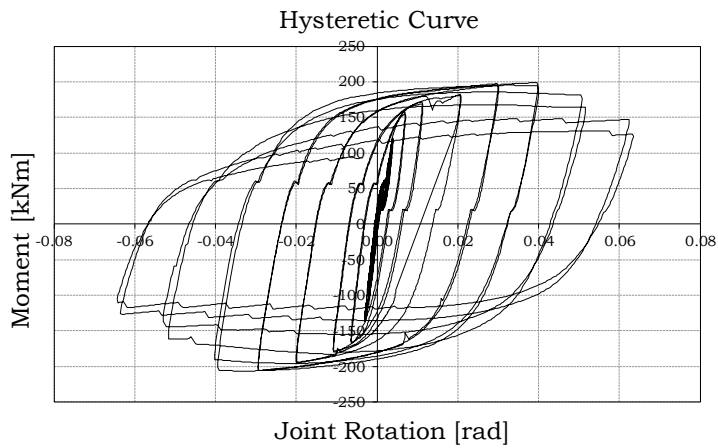
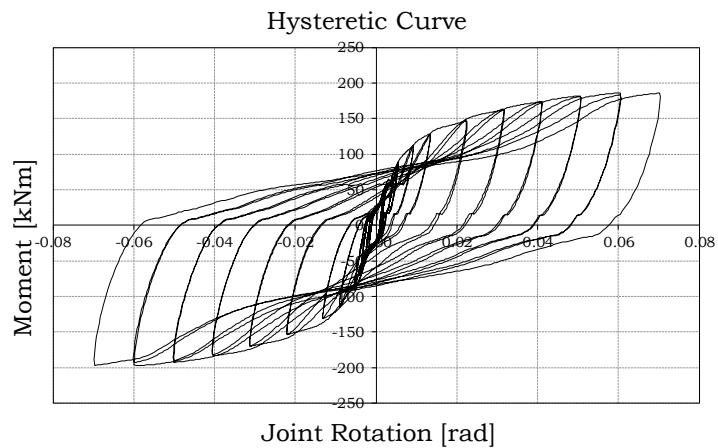


**Fig. 5.1** – Typologies of joints: a) EEP-DB-CYC03; b) TS-CYC04

In case of EEP-DB-CYC 03, the shape of the cycles of the whole joint is wide and stable guaranteeing a good energy dissipation capacity and significant plastic rotation supply (Fig.5.2a). The TS-CYC 04 joint has provided a very good plastic rotation supply and a good amount of energy dissipation. The hysteretic loops is obviously affected by pinching phenomena (Fig.5.2b).



a)



b)

**Fig. 5.2** – Hysteretic curve: a) EEP-DB-CYC03; b) TS-CYC04

The main advantage of this kind of connection, provided that the weakest component is constituted by the tee elements, is due to the fact that the beam end does not exhibit any yielding, so that after a seismic event only the tee elements have to be substituted.

## **5.2. Seismic design of the frame by Theory of Plastic Mechanism Control (TPMC)**

As it is known, a fundamental principle of capacity design of MR-Frames is that plastic hinge formation in columns during an earthquake should be avoided, in order to make sure that the seismic energy is dissipated by the beams only. Therefore, the optimisation of the energy dissipation capacity of structures is achieved when a collapse mechanism of global type develops [4-5]. In order to decrease the probability of plastic hinge formation in columns, MR-Frames must be designed to have strong columns and weak beams. To this scope, different simplified design criteria have been such as the so-called beam-column hierarchy criterion has been introduced in Eurocode 8 [6]. However, Eurocode 8 is only able to avoid soft storey mechanism but it does not assures the development of a collapse mechanism of global type. There are a number of reasons why the beam-column hierarchy criterion cannot achieve the above mentioned design goal but, probably the most important and difficult to be accounted for in a simplified design approach, is the shifting of the contraflexure point in columns during the seismic excitation. This considerable shifting leads to a bending moment distribution substantially different from that resulting from code-prescribed design rules. The shift of the contraflexure point is caused by the formation of hinges in beams adjacent to the column and even in part of the columns. All these factors alter the stiffness of beam-column subassemblage, hence the moment distribution.

The main reason why the above issue cannot be accounted for by means of a simplified design rule, such as the beam-column hierarchy criterion, is that the second principle of capacity design cannot be easily applied in

case of multiple resisting mechanisms not located in series. In fact, according to the second principle of capacity design, non-dissipative zones (i.e. the columns in case of MR-Frames) need to be designed considering the maximum internal actions which the dissipative zones (i.e. the beam ends in case of MR-Frames) are able to transmit at their ultimate conditions. For this reason, a rigorous design procedure, based on the kinematic theorem of plastic collapse, has been presented in 1997 [4], aiming to assure a collapse mechanism of global type where plastic hinges develop at the beam ends only, while all the columns remain in elastic range. Obviously, exception is made for base section of first storey columns, leading to a kinematic mechanism. Starting from this first work, the Theory of Plastic Mechanism Control has been outlined as a useful tool for the seismic design of steel structures. It consists on the extension of the kinematic theorem of plastic collapse to the concept of mechanism equilibrium curve. In fact, for any given structural typology, the design conditions to be applied in order to prevent undesired collapse mechanisms can be derived by imposing that the mechanism equilibrium curve corresponding to the global mechanism has to be located below those corresponding to all the other undesired mechanisms up to a top sway displacement level compatible with the local ductility supply of dissipative zones. The original TPMC [4] was based on an iterative procedure; thanks to new considerations regarding collapse mechanism typologies, a closed form solution has been recently provided [5]. Starting from the abovementioned background, in the following sections closed form solution of the TPMC is briefly summarized. According to [4-5] the collapse mechanisms can be considered as belonging to three main typologies (Fig. 5.3). They have to be considered undesired, because they do not involve all the dissipative zones. The global mechanism,

representing the design goal, is a particular case of type-2 mechanism involving all the storeys. However, the simple application of the kinematic theorem of plastic collapse is not sufficient to assure the desired collapse mechanism, because high horizontal displacements occur before the complete development of the kinematic mechanism. These displacements give rise to significant second order effects that cannot be neglected in the seismic design of structures, particularly in case of moment-resisting steel frames.

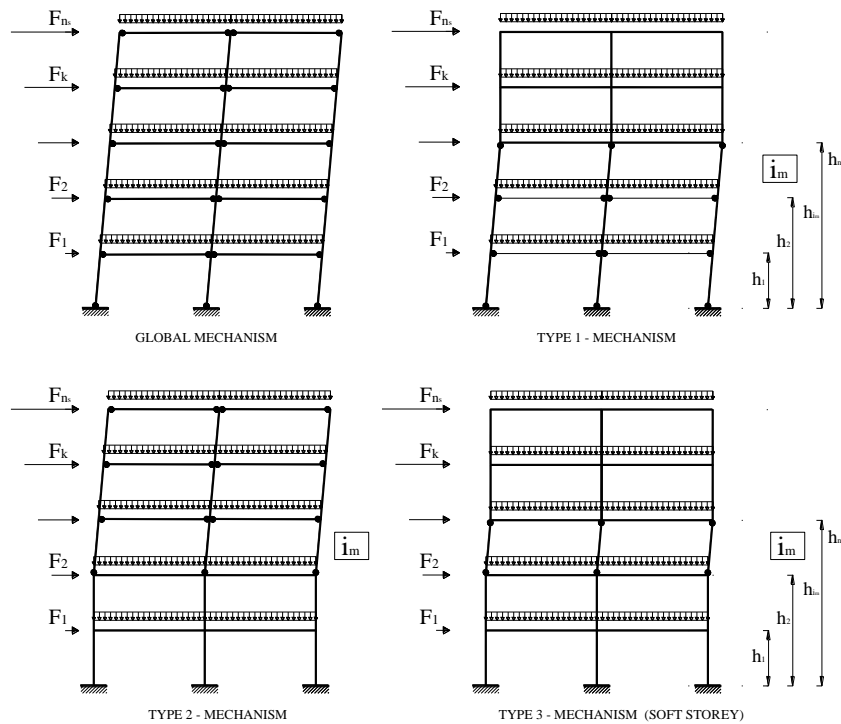


**Fig. 5.3** – Collapse mechanism typologies for MRFs

Therefore, the basic principle of TPMC is essentially constituted by the extension of the kinematic theorem of plastic collapse to the concept of

mechanism equilibrium curve. Within the framework of a kinematic approach, for any given collapse mechanism, the mechanism equilibrium curve can be easily derived by equating the external work to the internal work due to the plastic hinges involved in the collapse mechanism, provided that the external second-order work due to vertical loads is also evaluated [4].

The linearized mechanism equilibrium curve is expressed as:

$$\alpha = \alpha_0 - \gamma\delta \quad (5.1)$$

Being  $\alpha_0$  the kinematically admissible multiplier of horizontal forces and  $\gamma$  the slope of the curve, given by:

$$\gamma^{(g)} = \frac{\mathbf{V}^T \mathbf{S}}{\mathbf{F}^T \mathbf{S}} \cdot \frac{1}{H_0} \quad (5.2)$$

In the following, with reference to the notation given in the Table 5.1, both the kinematically admissible multiplier and the slope of the mechanism equilibrium curve are provided for the analysed collapse mechanism typologies.

**Table 5.1 – Notation**

---

$b$	Beam;
$c$	Column;
$i$	Column index;
$i_m$	Mechanism index;
$j$	Bay index;
$k$	Storey index;
$s$	Storey;
$h_k$	Storey height of the $k^{\text{th}}$ storey;

---

- $n_c$  Number of columns for each storey;  
 $n_b$  Number of beam for each storey;  
 $n_s$  Number of storey;  
 $\delta$  Top sway displacement;  
 $\theta$  Rotation;  
 $H_0$  Sum of the interstorey heights of the storeys involved by the generic mechanism;  
 $L_j$  Bay length;  
 $M_{c,ik}$  Plastic moment reduced due to the interaction with axial force of  $i^{\text{th}}$  column of the  $k^{\text{th}}$  storey;  
 $M_{b,jk}$  Moment resistance of the beam-to-column connection of the  $j^{\text{th}}$  beam of the  $k^{\text{th}}$  storey;  
 $q_{jk}$  Uniform vertical load acting on the  $j^{\text{th}}$  beam of the  $k^{\text{th}}$  storey;  
 $x_{jk}$  Abscissa of the second plastic hinge of the  $j^{\text{th}}$  beam of the  $k^{\text{th}}$  storey, given by:

$$x_{jk} = L_j - \sqrt{\left(\frac{2M_{b,jk}(\bar{m}_{r,jk} + 1)}{q_{jk}}\right)}$$

for

$$q_{jk} > \frac{2M_{b,jk}}{L_j^2} \left\{ (2 + \bar{m}_{r,jk} + \bar{m}_{l,jk}) + 2\sqrt{[(\bar{m}_{r,jk} + 1)(1 - \bar{m}_{l,jk})]} \right\}$$

while  $x_{jk} = 0$  in the opposite case;

- $\alpha$  Kinematically admissible multiplier of horizontal forces;  
 $\alpha^{(g)}$  Kinematically admissible multiplier of horizontal forces corresponding to the global mechanism;  
 $\alpha_{im}^{(t)}$  Kinematically admissible multiplier of horizontal forces corresponding to  $i^{\text{th}}$  mechanism of  $t^{\text{th}}$  type;  
 $i^{(g)}$  Slope of the mechanism equilibrium curve corresponding to the global-type mechanism;  
 $\gamma_{im}^{(t)}$  Slope of the mechanism equilibrium curve corresponding to the  $i^{\text{th}}$  mechanism of  $t^{\text{th}}$  type;  
 $F^T$  Vector of the design horizontal forces equal to  $\{F_1, F_2, \dots, F_k, \dots, F_{n_s}\}$  where  $F_k$  is the horizontal force applied to the  $k^{\text{th}}$  storey;  
 $h^T$  Vector of the storey heights equal to  $\{h_1, h_2, \dots, h_k, \dots, h_{n_s}\}$  where  $h_k$  is the height of the  $k^{\text{th}}$  storey;  
 $s^T$  Shape vector of the storey horizontal virtual displacements equal to  $\{s_1, s_2, \dots, s_k, \dots, s_{n_s}\}$ ;



- $\mathbf{V}^T$  Vector of the storey vertical loads equal to  $\{V_1, V_2, \dots, V_k, \dots, V_{n_s}\}$  where  $V_k$  is total load acting at  $k^{\text{th}}$  storey;
- $\mathbf{M}_{ck}^T$  Vector of the plastic moments of the columns of  $k^{\text{th}}$  storey, reduced due to the interaction with the axial force
- $\mathbf{I}$  Identity matrix
- $\mathbf{B}$  Matrix of order  $n_b \times n_s$  accounting for the location of the plastic hinges within the beams;
- $\mathbf{C}$  Matrix of order  $n_c \times n_s$  whose elements  $C_{ik}$  are equal to the column plastic moments
- $\mathbf{R}_b$  Matrix of order  $n_b \times n_s$  whose coefficient  $R_{b,jk}$  are related to the participation of the  $j^{\text{th}}$  beam of the  $k^{\text{th}}$  storey to the collapse mechanism; this coefficient represents the magnitude of the rotations of the beam plastic hinges for  $\theta = 1$ :

$$R_{b,jk} = \frac{L_j}{L_j - x_{jk}}$$

when the  $j^{\text{th}}$  beam of the  $k^{\text{th}}$  storey participates to the collapse mechanism while  $R_{b,jk} = 0$  in the opposite case;

- $\mathbf{R}_c$  Matrix of order  $n_c \times n_s$  whose coefficient  $R_{c,jk}$  account for the participation of the  $i^{\text{th}}$  column of the  $k^{\text{th}}$  storey to the collapse mechanism, where:  
 $R_{c,jk} = 2$  when the column is yielded at both ends;  
 $R_{c,jk} = 1$  when only one column end is yielded;  
 $R_{c,jk} = 0$  when the column does not participate to the collapse mechanism;
- $\mathbf{D}_v$  Matrix of order  $n_b \times n_s$  whose coefficient are related to the external work of the uniform load acting on the  $j^{\text{th}}$  beam of the  $k^{\text{th}}$  storey given by:

$$D_{v,jk} = \frac{L_j \cdot x_{jk}}{2}$$

when the  $j^{\text{th}}$  beam of the  $k^{\text{th}}$  storey participates in the collapse mechanism otherwise  $D_{v,jk} = 0$ ;

- $\mathbf{q}$  Matrix of order  $n_b \times n_s$  of the uniform loads acting on the beams.

In the case of global type mechanism, as shown in Fig. 5.3, all the storeys participate to the collapse mechanism, therefore the shape vector of the horizontal displacements is given by  $\mathbf{s}^{(g)} = \mathbf{h}$ . The kinematically admissible multiplier of horizontal forces can be expressed as:

$$\alpha_0^{(g)} = \frac{[\mathbf{M}_{c,1}^T \mathbf{I} + 2tr(\mathbf{B}^T \mathbf{R}_b^{(g)}) - tr(\mathbf{q}^T \mathbf{R} \mathbf{D}_v^{(g)})]}{\mathbf{F}^T \mathbf{s}^{(g)}} \quad (5.3)$$

Furthermore, because all the storeys participate to the global mechanism,  $H_0$  is equal to  $h_{ns}$ , and the slope  $\gamma^{(g)}$  is obtained from Eq. (5.2) for  $\mathbf{s} = \mathbf{s}^{(g)} = \mathbf{h}$  and  $H_0 = h_{ns}$ :

$$\gamma^{(g)} = \frac{\mathbf{V}^T \mathbf{s}^{(g)}}{\mathbf{F}^T \mathbf{s}^{(g)}} \cdot \frac{1}{h_{ns}} \quad (5.4)$$

With reference to the  $i_m^{th}$  mechanism of type-1, the shape vector of the horizontal displacements can be written as:

$$\mathbf{s}_{im}^{(1)T} = \{h_1, h_2, \dots, h_{im}, \dots, h_{im}\} \quad (5.5)$$

Where the first element equal to  $h_{im}$  correspond to the  $i_m^{th}$  component. The kinematically admissible multiplier of horizontal forces corresponding to the  $i_m^{th}$  mechanism of type-1 is given by:

$$\alpha_{0.im}^{(1)} = \frac{[\mathbf{M}_{c,1}^T \mathbf{I} + 2tr(\mathbf{B}^T \mathbf{R}_{b,im}^{(1)}) + \mathbf{M}_{c,im}^T \mathbf{I} - tr(\mathbf{q}^T \mathbf{R} \mathbf{D}_{v,im}^{(1)})]}{\mathbf{F}^T \mathbf{s}_{im}^{(1)}} \quad (5.6)$$

In addition, only the first  $i_m$  storeys participate to the collapse mechanism, so that  $H_0 = h_{im}$ . As a consequence, the slope of the mechanism equilibrium curve is still computed through Eq. (5.2), but assuming  $\mathbf{s} = \mathbf{s}_{im}^{(1)}$  and  $H_0 = h_{im}$ :

$$\gamma_{im}^{(1)} = \frac{\mathbf{V}^T \mathbf{s}_{im}^{(1)}}{\mathbf{F}^T \mathbf{s}_{im}^{(1)}} \cdot \frac{1}{h_{im}} \quad (5.7)$$

With reference to the  $i_m^{th}$  mechanism of type-2, the shape vector of the horizontal displacements can be written as:

$$\mathbf{s}_{im}^{(2)T} = \{0, 0, 0, \dots, h_{im} - h_{im-1}, h_{im+1} - h_{im-1}, \dots, h_{ns} - h_{im-1}\} \quad (5.8)$$

Where the first element different from zero is the  $i_m^{th}$  one.

The kinematically admissible multiplier corresponding to the  $i_m^{th}$  mechanism of type-2 is given by:

$$\alpha_{0.im}^{(2)} = \frac{[\mathbf{M}_{C,im}^T \mathbf{I} + 2tr(\mathbf{B}^T \mathbf{R}_{b,im}^{(2)}) - tr(\mathbf{q}^T \mathbf{R} \mathbf{D}_{v,im}^{(2)})]}{\mathbf{F}^T \mathbf{s}_{im}^{(2)}} \quad (5.9)$$

Furthermore, since the  $i_m^{th}$  storey and those above it participate to the collapse mechanism, the slope of the mechanism equilibrium curve is obtained by Eq. (5.2) with  $\mathbf{s} = \mathbf{s}_{im}^{(2)}$  and  $H_0 = h_{ns} - h_{im-1}$ :

$$\gamma_{im}^{(2)} = \frac{\mathbf{V}^T \mathbf{s}_{im}^{(2)}}{\mathbf{F}^T \mathbf{s}_{im}^{(2)}} \cdot \frac{1}{h_{ns} - h_{im-1}} \quad (5.10)$$

Finally, with reference to the  $i_m^{th}$  mechanism of type-3 the shape vector of horizontal displacements can be written as:

$$\mathbf{s}_{im}^{(2)T} = \{0, 0, 0, \dots, 1, 1, 1\} (h_{im} - h_{im-1}) \quad (5.11)$$

where the first term different from zero is the  $i_m^{th}$  one. The kinematically admissible multiplier of horizontal forces for the  $i_m^{th}$  mechanism of type-3 is given by:

$$\alpha_{0.im}^{(3)} = \frac{2M_{C,im}^T I}{F^T \mathbf{s}_{im}^{(3)}} \quad (5.12)$$

In addition, as the  $i_m^{th}$  storey only is involved in the kinematic mechanism, the corresponding slope of the mechanism equilibrium curve can be obtained by substituting  $H_0 = h_{im} - h_{im-1}$  in Eq. (5.2) where also  $\mathbf{s} = \mathbf{s}_{im}^{(3)}$  has to be assumed:

$$\gamma_{im}^{(3)} = \frac{V^T \mathbf{s}_{im}^{(3)}}{F^T \mathbf{s}_{im}^{(3)}} \cdot \frac{1}{h_{im} - h_{im-1}} \quad (5.13)$$

According to the upper bound theorem of plastic design, cross-sections of columns have to be defined so that the kinematically admissible horizontal force multiplier corresponding to the global type mechanism is the minimum among all the kinematically admissible multipliers. This condition is sufficient to guarantee the desired global mechanism only in the case of rigid-plastic behaviour of the structural material, where no displacements are develop and until the collapse mechanism is completely developed. Conversely, the actual behaviour of structures is elastic-plastic, and it is characterized by significant displacements before a kinematic mechanisms completely developed. These displacements are responsible of second order effects, so that as far as the top sway displacement increases, the horizontal force multiplier decreases unless significant strain-hardening occurs. The design process cannot neglect this issue.

It means that the upper bound theorem of plastic design has to be satisfied for each displacement level. Therefore, to account for second order effects, the design conditions have to be defined by imposing that

the mechanism equilibrium curve corresponding to the global-type mechanism equilibrium curve has to be located below those corresponding to all the other mechanisms up to the selected ultimate displacement  $\delta_u$  compatible with the plastic rotation capacity of members (Fig. 5.4).

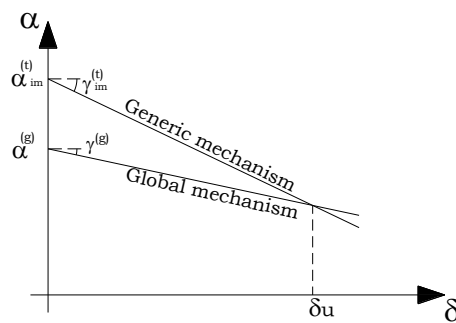


**Fig. 5.4** – Design requirement concerning mechanism equilibrium curves

Consequently, the design conditions can be translated into the following relationships:

$$\alpha_0^{(g)} - \gamma^{(g)} \delta_u \leq \alpha_{i_m}^{(t)} - \gamma_{i_m}^{(t)} \delta_u \quad i_m = 1, 2, 3, \dots, n_s \quad t = 1, 2, 3 \quad (5.14)$$

that constitutes the statement of TPMC. This means that there are  $3n_s$  design condition to be satisfied in the case of a frame having  $n_s$  storeys.

Substituting the values of  $\alpha_0^{(g)}$ ,  $\gamma^{(g)}$ ,  $\alpha_{0.i_m}^{(1)}$  and  $\gamma_{i_m}^{(1)}$  in Eq. (5.14), the following  $n_s$  conditions to avoid undesired mechanisms are obtained:

$$\begin{aligned} & \frac{[M_{c,1}^T I + 2tr(\mathbf{B}^T \mathbf{R}_b^{(g)}) - tr(\mathbf{q}^T \mathbf{R} \mathbf{D}_v^{(g)})]}{F^T \mathbf{s}^{(g)}} - \frac{V^T \mathbf{s}^{(g)}}{F^T \mathbf{s}^{(g)}} \cdot \frac{1}{h_{ns}} \delta_u \leq \\ & \frac{[M_{c,1}^T I + 2tr(\mathbf{B}^T \mathbf{R}_{b,im}^{(1)}) + M_{c,im}^{(1)T} I - tr(\mathbf{q}^T \mathbf{R} \mathbf{D}_{v,im}^{(1)})]}{F^T \mathbf{s}_{im}^{(1)}} - \frac{V^T \mathbf{s}_{im}^{(1)}}{F^T \mathbf{s}_{im}^{(1)}} \cdot \frac{1}{h_{im}} \delta_u \end{aligned} \quad (5.15)$$

needed to avoid type-1 mechanism

$$\begin{aligned} & \frac{[M_{c,1}^T I + 2tr(\mathbf{B}^T \mathbf{R}_b^{(g)}) - tr(\mathbf{q}^T \mathbf{R} \mathbf{D}_v^{(g)})]}{F^T \mathbf{s}^{(g)}} - \frac{V^T \mathbf{s}^{(g)}}{F^T \mathbf{s}^{(g)}} \cdot \frac{1}{h_{ns}} \delta_u \leq \\ & \frac{[M_{c,im}^{(2)T} I + 2tr(\mathbf{B}^T \mathbf{R}_{b,im}^{(2)}) - tr(\mathbf{q}^T \mathbf{R} \mathbf{D}_{v,im}^{(2)})]}{F^T \mathbf{s}_{im}^{(2)}} - \frac{V^T \mathbf{s}_{im}^{(2)}}{F^T \mathbf{s}_{im}^{(2)}} \cdot \frac{1}{h_{ns} - h_{im-1}} \delta_u \end{aligned} \quad (5.16)$$

needed to avoid type-2 mechanism

$$\begin{aligned} & \frac{[M_{c,1}^T I + 2tr(\mathbf{B}^T \mathbf{R}_b^{(g)}) - tr(\mathbf{q}^T \mathbf{R} \mathbf{D}_v^{(g)})]}{F^T \mathbf{s}^{(g)}} - \frac{V^T \mathbf{s}^{(g)}}{F^T \mathbf{s}^{(g)}} \cdot \frac{1}{h_{ns}} \delta_u \leq \\ & \frac{2M_{c,im}^{(3)T} I}{F^T \mathbf{s}_{im}^{(3)}} - \frac{V^T \mathbf{s}_{im}^{(3)}}{F^T \mathbf{s}_{im}^{(3)}} \cdot \frac{1}{h_{im} - h_{im-1}} \delta_u \end{aligned} \quad (5.17)$$

needed to avoid type3 mechanism.

However, by observing that, type-1 mechanism at first storey ( $i_m = 1$ ) and type-3 mechanism at first storey ( $i_m = 1$ ) are perfectly coincident Eq. (5.15) and Eq. (5.17) for  $i_m = 1$  provide the same design condition. In fact, they both represent the condition to avoid the “soft storey” mechanism at

first storey. Eq. (5.15) and Eq. (5.17) can be easily rearranged in the following form:

$$\frac{\left[ 2\text{tr}(\mathbf{B}^T \mathbf{R}_b^{(g)}) + \text{tr}(\mathbf{q}^T \mathbf{R} \mathbf{D}_{v,1}^{(1)}) \Delta_1^{(1)} - \text{tr}(\mathbf{q}^T \mathbf{R} \mathbf{D}_v^{(g)}) + \left( \frac{\mathbf{V}^T \mathbf{s}_1^{(1)} \Delta_1^{(1)}}{h_1} - \frac{\mathbf{V}^T \mathbf{s}^{(g)}}{h_{ns}} \right) \delta_u \right]}{2\Delta_1^{(1)} - 1} \leq \mathbf{M}_{c,1}^T \mathbf{I} \quad (5.18)$$

where the function  $\Delta_1^{(1)}$  is the ratio between the external work which the horizontal forces develop in the global mechanism and that developed in the  $i_m^{\text{th}}$  type-1 mechanism.

$$\Delta_1^{(1)} = \frac{\mathbf{F}^T \mathbf{s}^{(g)}}{\mathbf{F}^T \mathbf{s}_1^{(1)}} \quad (5.19)$$

In addition, type-2 mechanism at first storey ( $i_m = 1$ ) is perfectly coincident with global mechanism, for this reason, the condition expressed in Eq. (5.16) does not make sense.

### **Design algorithm**

The TPMC algorithm is developed according to the following steps:

- a) Selection of the design top sway displacement, i.e. the displacement up to which the equilibrium curve of the global mechanism has to be located below those corresponding to all the undesired mechanisms. The ultimate top sway displacement has to be compatible with the ultimate rotation  $\theta_{pu}$  which the beam-to-column connections and the column-base connections are able to accommodate. It can be evaluated as  $\delta_u = \theta_{pu} h_{ns}$ ;

- b) Computation of the axial load acting at collapse state in the columns starting from the shear action transmitted by the beams;
- c) Computation of the slopes  $\gamma_{im}^{(t)}$  of the equilibrium curves of the considered mechanisms, given by Eqs. (5.7), (5.10) and (5.13);
- d) Computation of the required moment of columns at first storey by means of Eq. (5.18);
- e) Design of first storey columns accounting for axial load at the collapse state (step b)) and computation of the obtained moment of column at first storey namely  $M_{c,1}^* I$
- f) Computation of the required moment of columns at each storey ( $i_m > 1$ ) by rearranging Eq. (5.15), (5.16) and (5.17) in the following way:

$$M_{c,1}^* I \left( \frac{1}{\Delta_{im}^{(1)}} - 1 \right) + \frac{2tr(\mathbf{B}^T \mathbf{R}_b^{(g)})}{\Delta_{im}^{(1)}} - 2tr(\mathbf{B}^T \mathbf{R}_{b,im}^{(1)}) + tr(\mathbf{q}^T \mathbf{R} \mathbf{D}_{v,im}^{(1)}) - \frac{tr(\mathbf{q}^T \mathbf{R} \mathbf{D}_v^{(g)})}{\Delta_{im}^{(1)}} + \left( \frac{\mathbf{V}^T \mathbf{s}_{im}^{(1)}}{h_{im}} - \frac{\mathbf{V}^T \mathbf{s}^{(g)}}{h_{ns} \Delta_{im}^{(1)}} \right) \delta_u \leq M_{c,im}^{(1)T} I \quad (5.20)$$

$$\frac{M_{c,1}^* I}{\Delta_{im}^{(2)}} + \frac{2tr(\mathbf{B}^T \mathbf{R}_b^{(g)})}{\Delta_{im}^{(2)}} - 2tr(\mathbf{B}^T \mathbf{R}_{b,im}^{(2)}) + tr(\mathbf{q}^T \mathbf{R} \mathbf{D}_{v,im}^{(2)}) - \frac{tr(\mathbf{q}^T \mathbf{R} \mathbf{D}_v^{(g)})}{\Delta_{im}^{(2)}} + \left( \frac{\mathbf{V}^T \mathbf{s}_{im}^{(2)}}{h_{ns} - h_{im-1}} - \frac{\mathbf{V}^T \mathbf{s}^{(g)}}{h_{ns} \Delta_{im}^{(2)}} \right) \delta_u \leq M_{c,im}^{(2)T} I \quad (5.21)$$

$$\frac{M_{c,1}^* I}{2 \Delta_{im}^{(3)}} + \frac{tr(\mathbf{B}^T \mathbf{R}_b^{(g)})}{\Delta_{im}^{(3)}} - \frac{tr(\mathbf{q}^T \mathbf{R} \mathbf{D}_v^{(g)})}{2} + \left( \frac{\mathbf{V}^T \mathbf{s}_{im}^{(3)}}{h_{im} - h_{im-1}} - \frac{\mathbf{V}^T \mathbf{s}^{(g)}}{h_{ns} \Delta_{im}^{(3)}} \right) \frac{\delta_u}{2} \leq M_{c,im}^{(3)T} I \quad (5.22)$$



where  $\Delta_{im}^{(1)}$ ,  $\Delta_{im}^{(2)}$  and  $\Delta_{im}^{(3)}$  are the ratio between the external work which the horizontal forces develop in the global mechanism and that developed in the  $i_m^{th}$  type-1, type-2 and type-3 mechanism, respectively.

- g) Computation of the required sum of the reduced plastic moments of columns at each storey as the maximum value among those coming from the above design conditions:

$$M_{C,im}^T I = \max\{M_{C,im}^{(1)} I, M_{C,im}^{(2)} I, M_{C,im}^{(3)} I\} \quad i_m > 1 \quad (5.23)$$

- h) The sum of the required plastic moment of columns at each storey, reduced for the contemporary action of the axial force, is distributed among all the storey columns, proportionally to the axial force acting at collapse state.
- i) If necessary, a technological condition is imposed by requiring, starting from the base, that the column sections cannot increase along the building height. If this condition requires the change of column sections at first storey then the procedure needs to be repeated from point e).

Column sections provided by TPMC are the one necessary to assure the development of a collapse mechanism of global type.

### **Study case**

Applying the procedure described above, a four bays – six storeys frame have been designed. The interstorey heights are equal to  $3.20m$  except for the first storey whose height is equal to  $3.50m$  while the bay span  $L$  is equal to  $6.00m$ . Regarding the design loads, a uniform dead load  $g_k = 4.00 \text{ kN/m}^2$  and a uniform live load  $q_k = 2 \text{ kN/m}^2$  (value given by the code

for residential buildings) have been considered. Since the analysed frame is the perimeter one and the transversal bay span  $L_t$  is equal to  $6.00m$ , a uniform dead load  $G_k = g_k \cdot \frac{L_t}{2} = 12.00 \text{ kN/m}$  and a uniform live load  $Q_k = q_k \cdot \frac{L_t}{2} = 6 \text{ kN/m}$  have been considered so that the design vertical load distribution has been determined, in accordance with EC8, i.e.  $q = 1.35G_k + 1.5Q_k = 25.20 \text{ kN/m}$ . With reference to the seismic load combination,  $q = G_k + \psi_2 Q_k + E_d$  (where  $\psi_2$  is the coefficient for the quasi-permanent value of the variable actions, equal to 0.3 for residential buildings), the applied vertical load is  $q = 12 + 0.3 \cdot 6 = 13.8 \text{ kN/m}$  (Fig.5.5). Finally, in the dynamic analyses, the considered seismic masses have been evaluated starting from the uniform distributed loads.

In order to withstand vertical loads, a design value of the beam plastic moment approximately equal to  $qL^2/8$  has been chosen and IPE270 profiles made of S275 steel grade have been adopted for the beams. The column sections has been selected by adopting the design procedure previously described assuring a global collapse mechanism. The whole procedure has been carried out with reference to S275 steel grade ( $f_{yk} = 275 \text{ MPa}$ ). The design horizontal forces have been determined according to Eurocode 8 [6], assuming a peak ground acceleration equal to 0.35 g, a seismic response factor equal to 2.5, a behaviour factor equal to 6. In addition, an horizontal force distribution according to the first vibration mode is assumed.

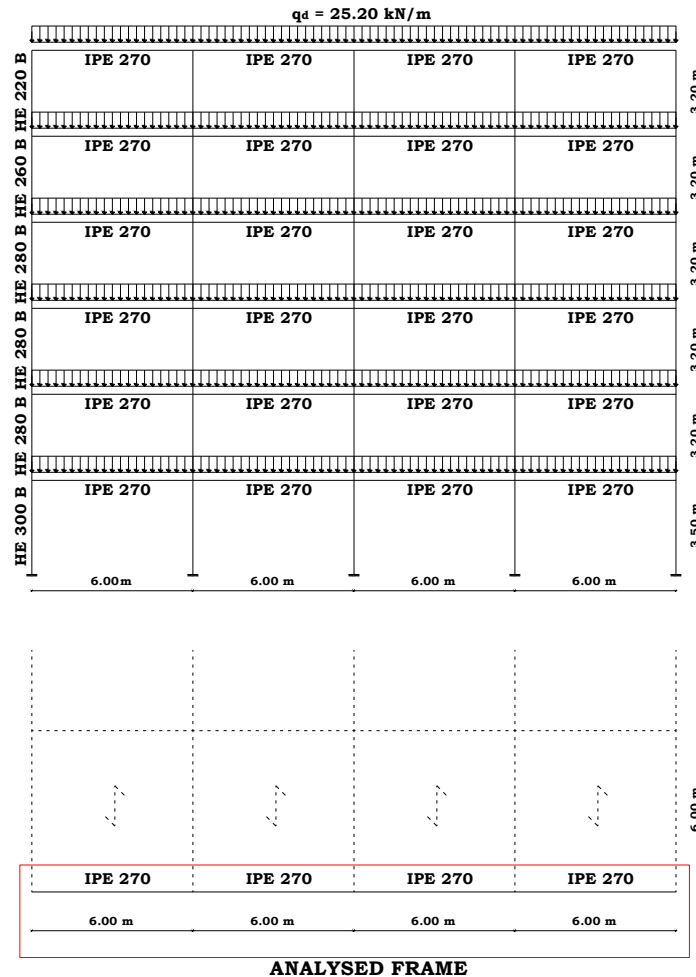


**Fig. 5.5** – Analysed frame

Aiming to assure a frame structural response consistent with the joint rotational behaviour obtained from experimental tests, the values of column and beam material mechanical properties adopted in IDA are assumed equal to the nominal values. For beam and column elements, a

bilinear elastic-perfectly plastic model characterized by an hysteretic behaviour without any degradation have been adopted. Once defined the material constitutive laws, in the SeismoStruct 2016 computer program, the elements have been modelled as:

- **Beams and Columns:** *infrmDB elements*. This is the displacement-based 3D beam-column element type capable of modelling members of space frames with geometric and material nonlinearities. The sectional stress-strain state is obtained through the integration of the nonlinear uniaxial material response of the individual fibres in which the section has been subdivided, fully accounting for the spread of inelasticity along the member length and across the section depth. In order to approximate nonlinear element response, constant axial deformation and linear curvature distribution are enforced along the element length, which is exact only for prismatic linear elastic elements. Consequently, *infrmDB* should be employed with members of small length, leading to the need for a mesh refinement, in order to achieve good accuracy in the case of higher order distributions of deformations. In order to post-process nodal displacements/rotation and to estimate the members chord-rotations, 4 elements per structural member has been defined; the number of section fibres used in equilibrium computations carried out at each of the element's integration sections is equal to 200;
- **Beam-to-column connections:** *link elements*. These are the 3D link elements with uncoupled axial, shear and moment actions that can be used to model, for instance, pinned or flexible beam-column connections. The link elements connect two initially coincident structural nodes and require the definition of an independent force-

displacement (or moment-rotation) response curve for each of its local six degrees of freedom (F1, F2, F3, M1, M2, M3). Several types of link are available in the used software such as the *linear symmetric curve* – *lin\_sym*, *linear asymmetric curve* – *lin\_asm*, *bilinear symmetric curve* – *bl\_sym*, *bilinear asymmetric curve* – *bi\_asm*, *bilinear kinematic hardening curve* – *bl\_kin* and so on. In this work, the *smooth curve* – *smooth* whose parameters have been widely discussed in following section, has been adopted;

- **Seismic masses:** *lmass elements*. The lumped mass element is a single-node mass element, characterised by three translational and three rotational inertia values. The latter are defined by means of the mass moment of inertia (not to be confused with the second moment of area, commonly named also as moment of inertia). The inertia mass values are to be defined with respect to the global reference system (X, Y and Z), and lead to a diagonal 6x6 element mass matrix.
- **Damping:** *Rayleigh damping*. In nonlinear dynamic analysis, hysteretic damping, which usually is responsible for the dissipation of the majority of energy introduced by the earthquake action, is already implicitly included within the nonlinear fibre model formulation of the inelastic frame elements or within the nonlinear force displacement response curve formulation used to characterise the response of link elements. Traditionally, such modest energy dissipation sources have been considered through the use of Rayleigh damping [7,8] with equivalent viscous damping values  $\xi$  varying from 1% to 8%, depending on structural type, materials used, non-structural elements, period and magnitude of vibration, mode of vibration being considered, etc [9]. For Rayleigh damping definition is asked to enter

the period  $T_1$  and  $T_2$  and damping values  $\xi_1$  and  $\xi_2$  of the first and last mode of interest. The mass-proportional  $\alpha_M$  and the stiffness-proportional  $\alpha_K$  matrices multiplying coefficients are then computed by the program, using the expressions given below, which ensure that true Rayleigh damping is obtained:

$$\alpha_M = 4\pi \cdot \frac{\xi_1 T_1 - \xi_2 T_2}{T_1^2 - T_2^2} \quad \text{and} \quad \alpha_K = \frac{T_1 \cdot T_2}{\pi} \cdot \frac{\xi_1 T_1 - \xi_2 T_2}{T_1^2 - T_2^2} \quad (5.24)$$

In Table 5.2 the values of the period  $T_1$  and  $T_2$  and damping values  $\xi_1$  and  $\xi_2$  of the first and second mode of the frame equipped with the three different beam-to-column connections have been reported.

**Table 5.2** – Parameters used for the definition of the Rayleigh damping

Joint	$T_1$	$T_2$	$\xi_1 = \xi_2$
<b>EEP-DB-CYC 03</b>	1.59	0.48	
<b>TS-CYC 04</b>	1.79	0.52	5%
<b>FREEDAM-CYC 01</b>	1.53	0.46	

### 5.3. Cyclic modelling and calibration of the parameters: implementation of genetic algorithm

The hysteretic joint behaviour has been modelled by adopting a Smooth Hysteretic Model (SHM) which allowed a better numerical convergence during the analyses with respect to the Polynomial Hysteretic Model. The parameters of the hysteretic moment-rotation law of the analysed joints have been experimentally calibrated performing the best curve fitting. In

order to calibrate the parameters, a simple portal frame has been implemented in SeismoStruct performing cyclic pushover analyses under displacement control with the same loading history of the experimental tests on joints described in chapter 4. The minimization of the scatter in terms of dissipated energy and bending moment between the spring moment-rotation curves provided by SeismoStruct and those obtained by experimental tests allowed to calibrate the joint model parameters.

Calibration (or parameter identification) of a numerical model means finding the set of parameters  $\tilde{\mathbf{p}}$  such that the computed response given by a simulation of a test  $\mathbf{y}_c(\mathbf{p})$  is as close as possible to the experimental response  $\mathbf{y}_{exp}$ . This implies solving the optimisation problem:

$$\tilde{\mathbf{p}} = \arg \min_{\mathbf{p}} \omega(\mathbf{y}_{exp}, \mathbf{y}_c(\mathbf{p})) \quad (5.25)$$

where  $\omega(\mathbf{y}_{exp}, \mathbf{y}_c(\mathbf{p})) = \omega(\mathbf{p})$  is a suitable cost function measuring the inconsistency between the experimental and computed quantities. One of the simplest and most widespread formulation for the cost function, adopted in this work, is:

$$\omega(\mathbf{p}) = \frac{1}{\omega_{ref}} \|\mathbf{y}_{exp} - \mathbf{y}_c(\mathbf{p})\| \quad (5.26)$$

where the operator  $\|\cdot\|$  represents the Euclidean norm of a vector and  $\omega_{ref} = \|\mathbf{y}_{exp}\|$  is a scaling factor needed to make  $\omega$  non-dimensional. The minimisation of  $\omega$  may be accomplished by using gradient-based methods (Trust region [10], Sequential Quadratic Programming [11]), or zero-order methods (Nelder–Mead algorithm [12], Genetic Algorithms [13]). In the

context of parameter identification, it is useful to remark the difference between *calibration* and *validation* test [14,15]. The former is the test introduced in Eq. (5.25) to estimate the model parameters  $\mathbf{p}$ . The a-posteriori comparison between the experimental results and the best model simulation serves as a preliminary assessment of the result. If the comparison fails, i.e. the two responses are found too different, this may be due to a problem either in the optimisation procedure (the real optimum has not been reached) or in the choice of the numerical model (the optimum has been attained, but the model cannot properly simulate the experimental response). If this check is positively passed, the calibration result has to be verified as regards its predictive capability. This is the objective of a *validation* test. The reasoning under this additional test is twofold. Firstly, it is very unlikely that, from a mathematical viewpoint, the relationship between parameters and response is bijective. Most often, the inverse problem of estimating parameters from the response is ill-posed, meaning that more than one solution corresponds to the same response fitting. When applied to a different loading condition, these multiple solutions may give responses significantly different from each other. Secondly, the mathematical model is always imperfect, and it may be accurate in predicting the response of a structure under some conditions, yet give poor approximation of the response in a different case. A test with different loading conditions is thus useful to investigate the applicability of the previously calibrated model. The cost function defined in Eq. (5.26) is related to a single test. When  $N$  calibration tests are performed, the problem of how to collect information from different sources arises. The optimisation problem (5.25) becomes in this case:



$$\tilde{\mathbf{p}} = \arg \min_{\mathbf{p}} \{\omega_1(\mathbf{p}), \dots, \omega_N(\mathbf{p})\} \quad (5.27)$$

where  $\omega_i(\mathbf{p})$  represents the cost function value of the  $i^{\text{th}}$  test.

In the context of multi-objective optimisation, the concept of Pareto optimality replaces the usual notion of optimality [16]. In a minimisation problem, a solution  $\mathbf{p}_1$  is said to dominate a solution  $\mathbf{p}_2$  if and only if:

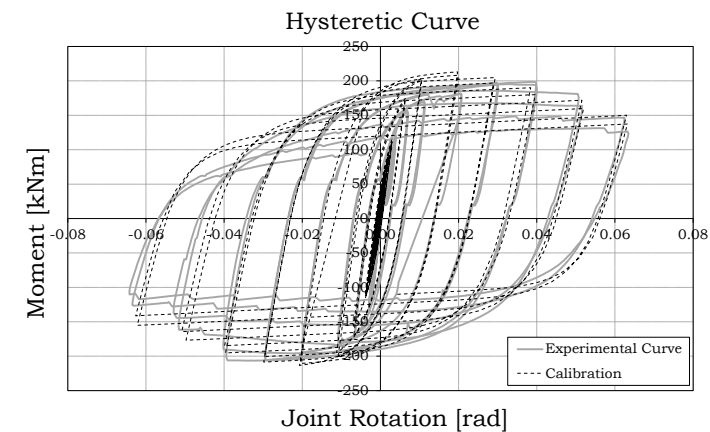
$$\begin{aligned} \omega_i(\mathbf{p}_1) &\leq \omega_i(\mathbf{p}_2) \quad \forall i = 1, \dots, N \\ \omega_i(\mathbf{p}_1) &< \omega_i(\mathbf{p}_2) \quad \exists i = 1, \dots, N \end{aligned} \quad (5.28)$$

A solution is referred to as Pareto optimal if it is not dominated by any other solution. The set of Pareto optimal solutions, called Pareto Front (PF), represents the general solution of the problem (5.27). Most methods for solving multi-objective optimisation problems, such as the Weighted Sum Method [17], convert them into simpler problems, in which a scalar function of the objectives is minimised or maximised.

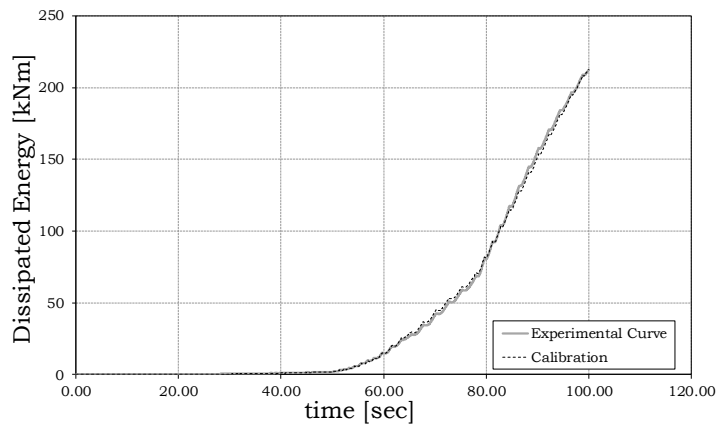
Under some assumptions, this gives a solution belonging to PF and is an acceptable compromise between all (possibly conflicting) objectives. However, the definition of “acceptable compromise” is left to the user, who must carefully define the objective weights a priori. On the contrary, in the context of Genetic Algorithms, it is possible to track the whole Pareto Front without deciding the weight to assign to each objective a priori and postponing instead the choice of a unique solution if needed by the user. Genetic Algorithms [13] are a zero-order, population-based meta-heuristic widely used to solve difficult optimisation problems. They mimic the optimum search as observed in nature, where living species evolve through recombination of their genetic pool. The algorithm starts with a

population of randomly (or quasi-randomly) generated solutions, of which the fitness function is evaluated. The *chromosome* of a solution (individual) is represented by the vector  $\mathbf{p}$ , while its fitness is the value  $\omega(\mathbf{p})$ . The individuals in a population are then ranked based on their fitness and an intermediate population is created by rearranging the previous one. High-fitness individuals may be duplicated, and poor-performing individuals may disappear. Individuals in the intermediate population are selected to mate, and, by recombination (*crossover*) of the parents' chromosomes, new individuals (*offspring*) are generated. These new individuals are the basis for the generation of a new population, which is evaluated after application of *mutation* with low probability (random changes in some genes, to increase exploration capability of the algorithm) and *elitism* (best individuals of the parent population may remain in the new population, to avoid losing promising solutions). The new population is in average better than the previous, and after evaluation undergoes the same operators described, i.e. ranking, selection, crossover, mutation, elitism. The iterative process is stopped when some condition is met. In the problems described in this paper, the termination condition consisted of a fixed number of generations. Thanks to population processing, multi-objective optimisation may be effectively handled by a GA without the need of defining a scalar measure of the objective vector  $\boldsymbol{\omega}=[\omega_1, \dots, \omega_M]^T$ . The key concept of the Non-dominated Sorting Genetic Algorithm-II (NSGA-II, [18]) is that the evolution should be driven by two overall purposes: a) search for the PF and b) avoiding premature convergence. This is achieved by slight modification of the operators described above. Objective a) is obtained with ranking based on non-domination concepts instead of fitness values. Premature convergence is avoided adopting a selection algorithm based on crowding

fitness, meaning that isolated solutions are preferred to solutions surrounded by many individuals. This approach represents the state-of-art in the field of multi-objective optimisation and is implemented in the software TOSCA [19], used in this case.



a)



b)

**Fig. 5.6** – EEP-DB-CYC03 joint: a) Hysteretic curve; b) energy dissipation

In Figs.5.6-5.8, the good accuracy of the calibrated models is testified as evidenced by the overlap between the experimental and predicted curves. In particular, in Fig. 5.6a the moment-rotation curves for EEP-DB-CYC03

have been illustrated while in Fig. 5.6b the energy dissipation-time curves have been reported; it is possible to notice that the maximum difference between the experimental and calibrated values of the dissipated energy is equal to 0.2%.

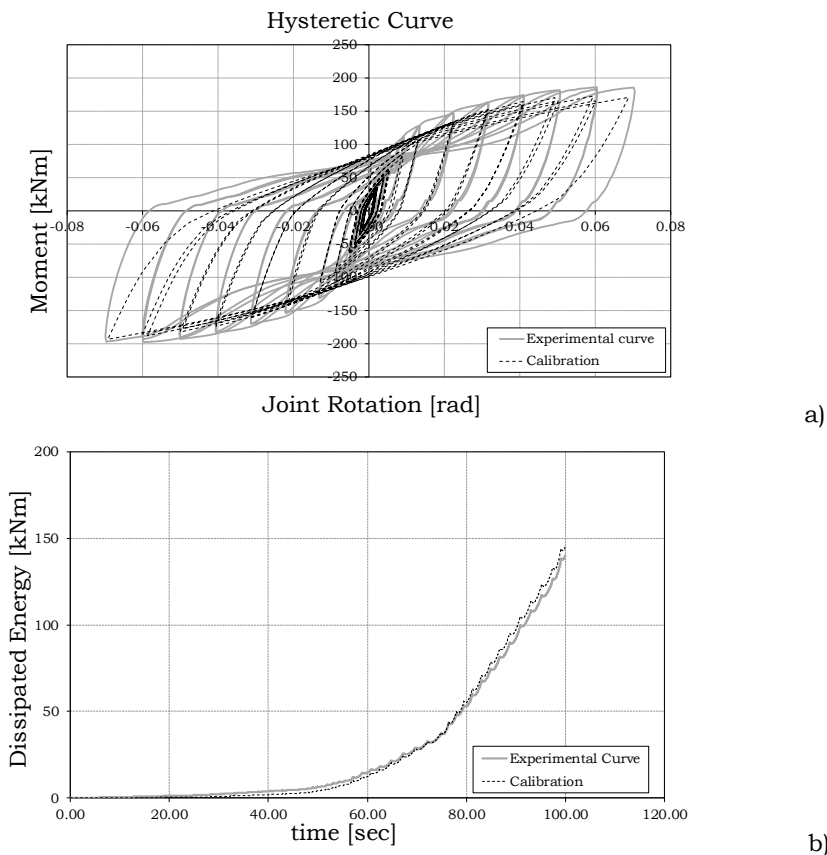
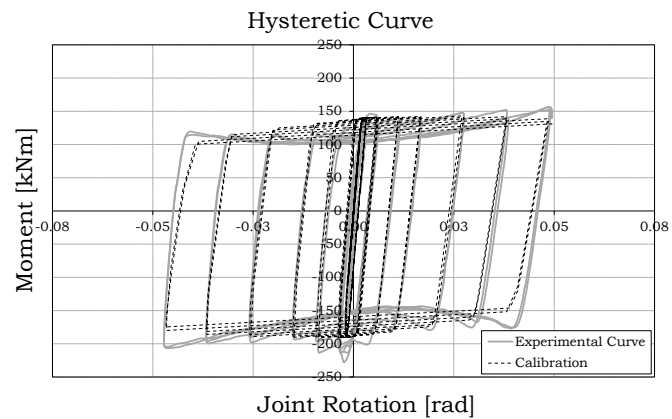


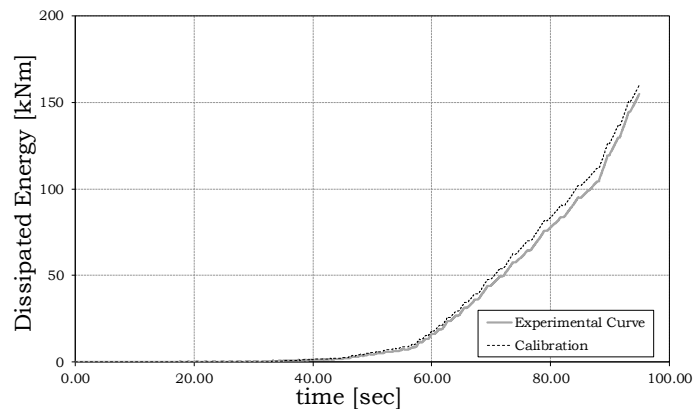
**Fig. 5.7** – TS-CYC04 joint: a) hysteretic curve; b) energy dissipation

For the TS-CYC 04 connection, the moment-rotation (Fig. 5.7a) curves and the energy dissipation-time curves (Fig. 5.7b) have been reported. In

this case, the maximum difference between the experimental and calibrated values of the dissipated energy is equal to 5%.



a)



b)

**Fig. 5.8** – FREEDAM-CYC01 joint: a) hysteretic curve; b) energy dissipation

Finally, with reference to the friction connection FREEDAM-CYC 01, the moment-rotation curves and the energy dissipation-time curves have been reported in Fig.5.8. The maximum difference between the experimental and calibrated values of the dissipated energy is equal to

3%. The calibrated parameters have been summarized, for each joint typologies, in Table 5.3:

**Table 5.3** – Parameters of the smooth model

		<b>EEP-DB-CYC 03</b>	<b>TS-CYC 04</b>	<b>FREEDAM-CYC 01</b>
Initial rotational stiffness	EI	41687.772	14662.215	73063.723
First yielding moment	PCP	+108.518	+114.050	+70.163
		-108.518	-114.050	-95.335
Plastic moment	PYP	+217.035	+228.081	+140.326
		-217.035	-228.081	-190.671
Yield rotation	UYP	+0.096	+0.106	+0.074
		-0.096	-0.106	-0.074
Ultimate rotation	UUP	+0.193	+0.211	+0.148
		-0.193	-0.211	-0.148
Post Yield stiffness ratio as % of elastic		0.008	0.059	0.005
Stiffness degradation parameter	HC	9.700	10.700	20.000
Strength degradation parameter based on ductility	HBD	0.226	0.416	0.191
Strength degradation parameter based on energy dissipation	HBE	0.274	0.388	0.103
Parameter controlling smoothness of elastic-plastic transition	NTRANS	0.873	0.173	13.646
Parameter controlling the shape of unloading curve	ETA	0.567	0.977	0.809
Parameter controlling the slip length	HSR	0.070	2.000	0.190
Parameter controlling the slip curve	HSS	0.090	0.310	-0.080
Parameter controlling the slip at mean moment	HSM	1.360	1.360	1.920
Gap closing spring exponent	NGAP	1.000	2.089	1.000
Parameter controlling the gap closing curve	PHIGAP	1.000	0.100	1000.000
Parameter controlling the gap closing stiffness	STIFFGAP	1.000	1.731	1.000

## 5.4. Individuation of the earthquake record

In order to evaluate the seismic performance of the structure equipped with traditional and innovative beam-to-column joints, dynamic analyses have been performed by means of the computer program SeismoStruct v.2016 (Fig. 5.9).

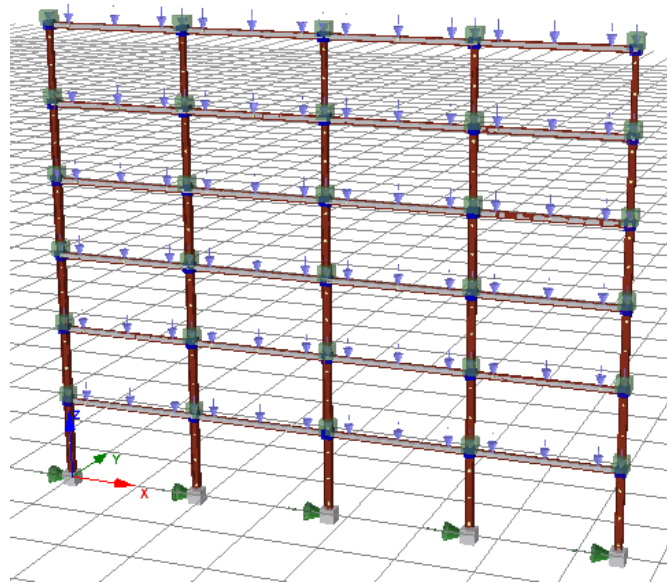


**Fig. 5.9** – Analysed structure modelled in SeismoStruct v.2016 computer program

A set constituted by 8 ground motion records have been considered and the IDA have been performed increasing progressively the spectral acceleration up to achievement of the experimental value of the plastic rotation supply. The choice of the set of accelerograms is not accidental: only the seismic events whose average spectrum have a spectrum compatible with the design spectrum given by Eurocode 8 for the soil type C have been considered [6]. In Fig. 5.10 the elastic spectrum of the

analysed earthquakes, the design spectrum given by Eurocode 8 and the average spectrum have been reported.

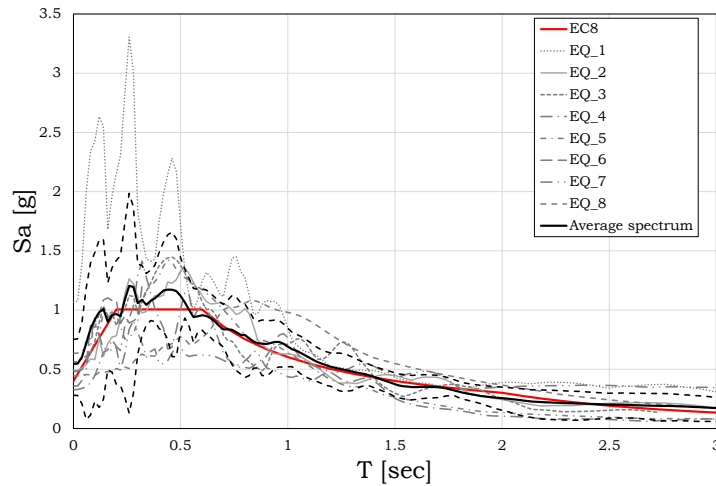


**Fig. 5.10** – Spectrum

If the structural response is governed by the first mode of vibration, its variability will be equal to zero because the structure, for each accelerogram, will be subjected exactly to the spectral acceleration corresponding to the first period of vibration. Conversely, since the response of the structure is influenced by the higher modes and for higher values of the spectral acceleration the structure is more deformed and less stiffened, the vibration period is great and the correspondent acceleration is different for each selected accelerogram. In terms of *record-to-record variability*, these are the main factors that influence the response of the structures.

In Table 5.4 the earthquakes data have been summarized:



**Table 5.4** – Basic data of the selected ground motions

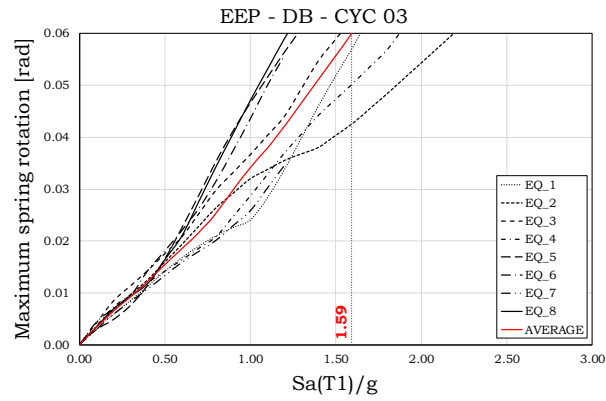
<i>ID</i>	<i>Earthquake name</i>	<i>Date</i>	<i>Station name</i>	<i>Sation Country</i>	<i>Magnitude</i>	<i>Fault mechanism</i>	<i>PGA [g]</i>
EQ_1	Alkion	24.02.1981	Xylokaastro-O.T.E.	Greece	6.6	Normal	1.066
EQ_2	Montenegro	24.05.1979	Skupstina Opstine	Montenegro	6.2	Reverse	0.492
EQ_3	Izmit	13.09.1999	Usgs Golden Station Kor	Turkey	5.8	Strike-Slip	0.375
EQ_4	Aigion	15.06.1995	Aigio-OTE	Greece	6.5	Normal	0.313
EQ_5	Umbria-Marche	26.09.1997	Castelnuovo-Assisi	Italy	6.0	Normal	0.369
EQ_6	Izmit	17.08.1999	Istanbul-Zeytinburnu	Turkey	7.4	Strike-Slip	0.480
EQ_7	Olfus	29.05.2008	Ljosafoss-Hydroelectric Power	Iceland	6.3	Strike-Slip	0.315
EQ_8	Olfus	29.05.2008	Selfoss-City Hall	Iceland	6.3	Strike-Slip	0.309

All accelerograms have been preliminarily scaled to the value of the spectral acceleration corresponding to the fundamental period of vibration of the structure, equal to  $T_1=1.58$  sec for frames with EEP-DB-CYC03 connections, equal to  $T_1=1.79$  sec for frame with TS-CYC04 connections and equal to  $T_1=1.53$  sec for frames with FREEDAM-CYC01 connections.

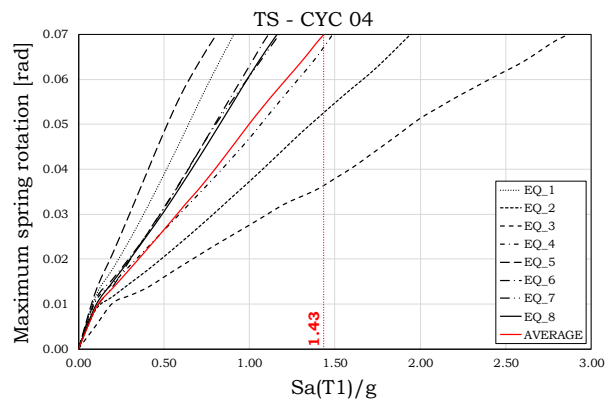
## 5.5. Seismic response of steel MRFs

The IDA have been performed increasing progressively the spectral acceleration up to achievement of the ultimate condition corresponding to the attainment of the experimental ultimate value of the plastic rotation supply equal to 0.06 rad for EEP-DB-CYC03 and equal to 0.07 rad for TS-CYC04, and by the target maximum interstorey drift, equal to 0.10 according to FEMA [19], for frame with FREEDAM-CYC01

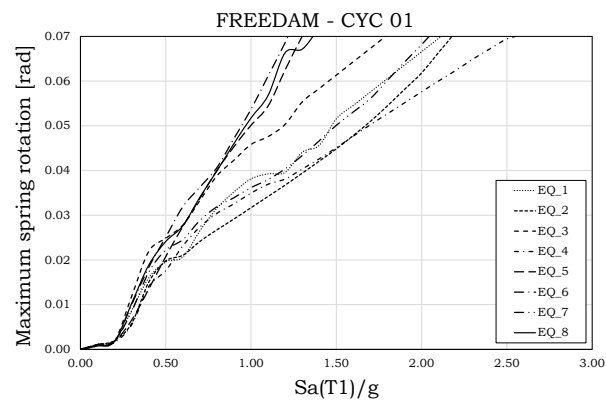
connections which practically don't have any limitation in terms of rotational capacity if the length of the holes for the sliding of bolts is sufficiently great. In the following the IDA curves have been reported in terms of *Maximum spring rotation* and *Maximum intersorey drift* versus the *spectral acceleration* for the eight earthquakes. In addition, the average IDA curves have been reported. The results of the IDA, in terms of maximum spring rotation, are illustrated in Fig. 5.11, while the results of IDA in terms of maximum interstorey drift are illustrated in Fig. 5.12.



a)

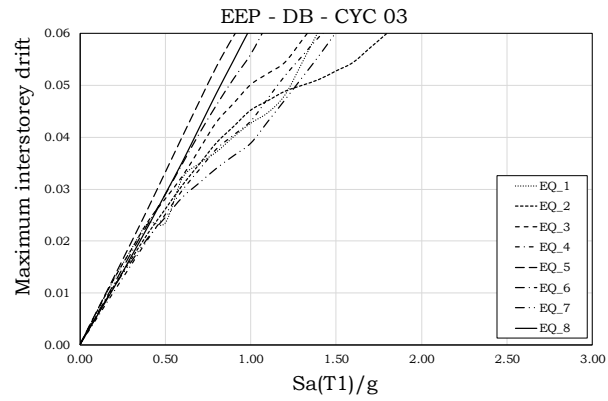


b)

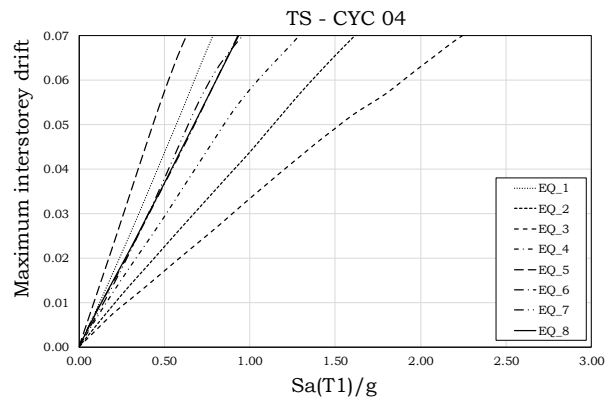


c)

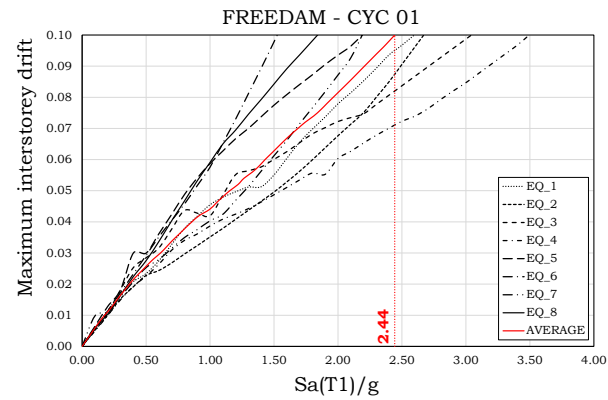
**Fig. 5.11** – Results of IDA in terms of maximum spring rotation versus spectral acceleration: a) EEP-DB-CYC03; b) TS-CYC04; c) FREEDAM-CYC01



a)



b)



c)

**Fig. 5.12** – Results of IDA in terms of maximum interstorey drift versus spectral acceleration: a) EEP-DB-CYC03; b) TS-CYC04; c) FREEDAM-CYC01

The value of the spectral acceleration up to achievement of the ultimate conditions, i.e. the attainment of the experimental ultimate value of the plastic rotation supply for EEP-DB-CYC03 and TS-CYC04 joints, and of the target maximum interstorey drift for frame with FREEDAM-CYC01 connections, are summarized in Table 5.5. It can be observed that the frame with TS-CYC-04 (double split Tee connections) and the EEP-DB-CYC-03 (RBS connections) show the similar seismic performance. In particular, the frame with TS-CYC-04 joints, since the joints are characterized by cyclic behaviour with significant pinching, exhibits a maximum value of the PGA at collapse - equal to 1.43 - less than the frame with EEP-DB-CYC03 joints - equal to 1.59. The frame equipped with friction dampers shows the best performance testifying the good potentialities of the dissipative joints which could represents a more suitable solution for steel frames under destructive earthquake.

**Table 5.5** – Spectral acceleration up to achievement of the ultimate conditions

Earthquakes		EEP-DB-CYC 03 [g]	TS-CYC 04 [g]	FREEDAM-CYC 01 [g]
EQ_1	Alkion	1.64	0.91	2.60
EQ_2	Montenegro	2.19	1.94	2.67
EQ_3	Izmit	1.53	2.87	3.04
EQ_4	Aigion	1.87	1.49	3.49
EQ_5	Umbria-Marche	1.28	0.81	2.19
EQ_6	Izmit	1.27	1.11	1.53
EQ_7	Olfus	1.73	1.18	2.19
EQ_8	Olfus	1.22	1.16	1.84
$E[S_a(T_1)/g]_{collapse}$		<b>1.59</b>	<b>1.43</b>	<b>2.44</b>

*Robustness and seismic behaviour of structures equipped with traditional and innovative beam-to-column connections*

The Incremental Dynamic Analysis performed on a four bays-six storeys steel frames equipped with Full and Partial Strength Joints, evidenced that semirigid partial-strength connections, if well designed, can be considered to have adequate ductility and dissipation capacity in order to satisfy the seismic demand. In particular, the Double Tee Joints, even though are characterized by cyclic behaviour with significant pinching, due to their greater plastic rotational capacity, provide a similar maximum value of the PGA at collapse with respect to Full Strength Joint. However, the Incremental Dynamic Analysis performed on a frame equipped with FREEDAM joints shows a very significant improvement of the PGA at collapse for both solutions, which are promising for the full development of innovative beam-to-column joints.

## 5.6. References

- [1] F. Iannone, M. Latour, V. Piluso, G. Rizzano: “*Experimental Analysis of Bolted Steel Beam-to-Column Connections: Component Identification*”, Journal of Earthquake Engineering, Vol. 15, (2), 214-244, 2011.
- [2] M. Latour, V. Piluso, G. Rizzano, “*Cyclic Modelling of Bolted Beam-to-Column Connections: Component Approach*”, Journal of Earthquake Engineering, Vol. 15, (4), pp. 537- 563, 2011.
- [3] M. Latour, V. Piluso, G. Rizzano, “*Experimental Analysis of innovative dissipative bolted double split tee beam-to-column connections*”, Steel Constructions, Vol. 4, (2), 53-64, 2011.
- [4] F. M. Mazzolani and V. Piluso: “*Plastic design of seismic resistant steel frames*”, Earthquake Engineering and Structural Dynamics 26, 167-191, 1997.
- [5] R. Montuori, E. Nistri and V. Piluso: “*Advances in the Theory of plastic mechanism control: Closed form solution for MRFs*”. Earthquake Engineering and Structural Dynamics 44, Issue 7, 1035-1054, 2015.
- [6] CEN, EN 1998-1-1: “*Eurocode 8: Design of structures for earthquake resistance - Part 1: General rules, seismic actions and rules for buildings*”, European committee for standardization, 2005.
- [7] R.W. Clough and J. Penzien: “*Dynamics of Structures*”, 2nd Edition, McGraw Hill, 1994;
- [8] A.K. Chopra: “*Dynamics of Structures: Theory and Applications to Earthquake Engineering*”, Prentice-Hall, 1995;
- [9] M. Wakabayashi: “*Design of earthquake-resistant buildings*”, McGraw-Hill, USA, 1986;
- [10] R. H. Byrd, R. B. Schnabel and G. A. Shultz: “*A trust region algorithm for nonlinearly constrained optimization*” SIAM Journal on Numerical Analysis, vol. 24, no. 5, pp. 1152--1170, 1987;
- [11] P. T. Boggs and J. W. Tolle: “*Sequential quadratic programming*”, Acta numerica, vol. 4, pp. 1-51, 1995.
- [12] J. Nelder and R. Mead: “*A simplex method for function minimization*” , Comput. J., vol. 7, no. 4, pp. 308-313, 1965;

- [13] D. E. Goldberg: *“Genetic Algorithms in Search, Optimization and Machine Learning”*, Addison-Wesley, 1989;
- [14] The American Society For Mechanical Engineers: *“Guide for Verification and Validation in Computational Solid Mechanics”*, ASME, 2006;
- [15] T. Trucano, L. Swiler, T. Igusa, W. Oberkampf and M. Pilch: *“Calibration, validation, and sensitivity analysis: What’s what”*, Reliability Engineering and System Safety, vol. 91, pp. 1331-1357, 2006;
- [16] K. Miettinen: *“Nonlinear multiobjective optimization”*, Springer, 1999;
- [17] W. Stadler, *“A Survey of Multicriteria Optimization, or the Vector Maximum Problem”*, Journal of Optimization Theory and Applications, vol. 29, pp. 1-52, 1979;
- [18] K. Deb, A. Pratap, S. Agarwal and T. Meyarivan: *“A Fast and Elitist Multiobjective Genetic Algorithm: NSGA-II”* IEEE Transactions on Evolutionary Computation, vol. 6, no. 2, pp. 182-197, 2002;
- [19] C. Chisari, Inverse techniques for model identification of masonry structures, University of Trieste: PhD Thesis, 2015;
- [20] FEMA-350: *“Recommended Seismic Design Criteria for New Steel Moment-Frame Buildings”*, prepared by the SAC Joint Venture for the Federal Emergency Management Agency, Washington, DC, 2000.



# **Chapter 6**

**Influence of the beam-to-column joints on  
the structural robustness**



## 6.1. Introduction

Robustness of Moment Resistant Frames (MRFs) designed according to current seismic codes and subjected to a loss-of-column scenario is strictly linked to the deformation capacity of beam-to-column connections, which are usually subjected to combined axial and bending loads. In the seismic design of steel frames, once avoided the yielding of columns, a global dissipative collapse mechanism has to be ensured by imposing the formation of plastic hinges at the ends of the beams or in the connections and guarantying, provided that the elements involved in plastic range have an adequate energy dissipation capacity. To this scope, beam-to-column joints play a role of paramount importance. Therefore, in the field of the seismic applications in order to predict accurately the structural response up to failure, an accurate modelling of the ultimate behaviour of beam-to-column joints subjected to bending loads has been developed. Within this framework, in this chapter the influence of the response of the connections designed for seismic application on the global behaviour of MRFs under a loss-of-column scenario providing an accurate modelling of connections subjected to combined axial and bending loads, has been analysed. To this scope the beam-to-column joints described in the previous chapters, have been modelled and introduced in the case-study structure - analysed in chapter 5 under seismic conditions - whose response has been assessed by means of push-down analyses. The pushdown analyses of the structures by varying the beam-to-column connections have been performed in SAP 2000 computer program [1]. To this scope, preliminarily the component method for predicting the

whole moment-rotation curve of the joint has been modified in order to account for the development of axial forces and to introduce the ultimate deformation of the single joint components. In particular, a refined model for the prediction of the ultimate behaviour, i.e. in terms of stiffness, resistance and ductility, of the T-stub has been considered [2]. In addition, this approach has been extended to the other joint components that could be modelled by means of an equivalent T-stub. The performances of the analysed frames have been analysed and are compared using the Residual Reserve Strength Ratio (RRSR) index combined with the energy balance method.

## **6.2. Robustness of the structures: general aspects**

After the recent events, as terrorist attacks, explosions, etc., the progressive collapse and the robustness of the structures designed according to the seismic codes [3] are considered as important aspects to investigate. It is well known that the resisting capacity to the progressive collapse of the structures is strictly linked to their ductility supply and, consequently, to their dissipation capacity. Generally, steel Moment Resisting Frames (MRFs) are considered to be highly ductile and thus more suitable to resist to the collapse caused by the local failure of the major loading resisting elements. However, during severe earthquakes like Northridge and Kobe earthquakes, several brittle failure occurred in the beam-to-column joints. This testify the rule of paramount importance assumed by the joints in the seismic design both in case in which they are designed as Full Strength (FS) so that the seismic input energy is absorbed by means of cyclic excursions of the

beam ends in plastic range and in the case in which they are designed as Partial Strength (PS) so that the plastic engagement of ductile joint components supplies the required dissipation capacity. Therefore, in order to predict accurately the structural response up to failure, a modelling of the ultimate behaviour of beam-to-column joints is necessary. The current methodology for the prediction of behaviour of joints suggested by Eurocode 3 [4] is based on the so-called component method [5-7], which provides to break-up joints in single components that are first characterized in terms of stiffness and resistance and then assembled in a mechanical model able to provide the response of the whole connection. Nevertheless, even though the component method is already very advanced, there are still some limitations related to the prediction of the ductility of each joint component and to the possibility to account for axial forces due to the development of catenary effects. These two aspects will be analysed and modelled in the following. Regarding the evaluation of the structural robustness, several approach can be followed:

- Risk based robustness index [8];
- Energy based partial pushdown analysis [9];
- Deterministic robustness indexes [10].

In this thesis, the performance of the analysed frames is evaluated and compared using the Residual Reserve Strength Ratio (RRSR) index [10-12], i.e. a quantitative index to assess the robustness of damaged structures, and to quantify the progressive collapse resistance of real complex structures. This approach has been combined with the energy balance method [13] that adopts a simplify approach evaluating the maximum dynamic response from nonlinear static response.

### 6.3. Modelling of the connections in order to evaluate the structural robustness

Starting from the analysed joint typologies, the attention is focused on their performances when adopted in Steel Moment Resisting frames subjected to a loss of a column scenario. The joint typologies considered even in the development of the Robustness analyses are: the dog-bone connection (EEP-DB-CYC03), the partial strength Double Split Tee (DST) joint (TS-CYC04) and the partial strength FREE from DAMage connection with friction dampers (FREEDAM-CYC01).

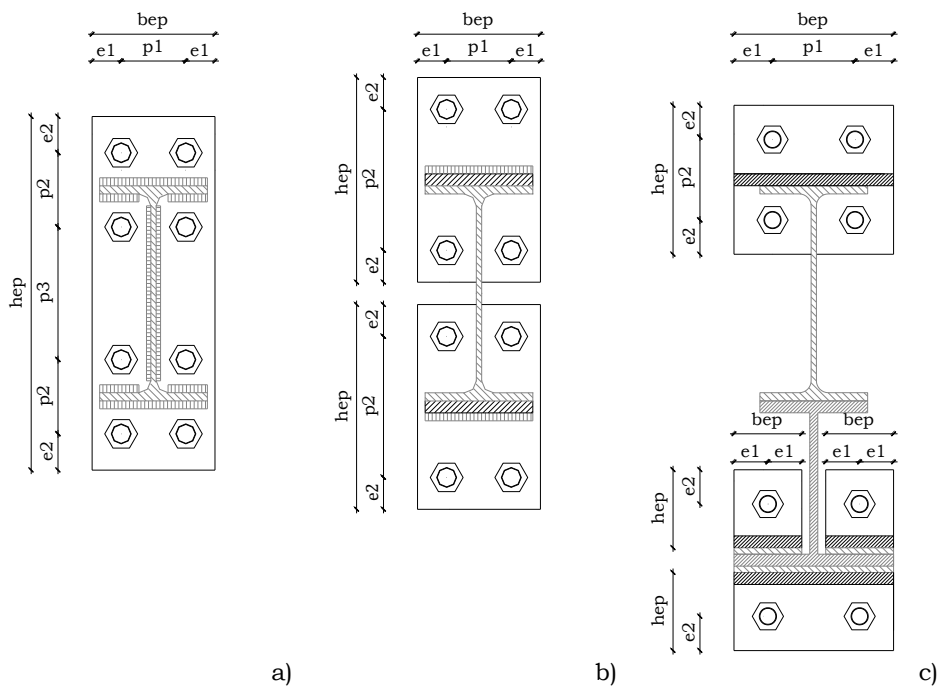


**Fig. 6.1** – Notation for the geometrical properties: a) EEP-DB-CYC03;  
b) TS-CYC014; c) FREEDAM-CYC01

The main geometrical parameters of the connecting elements of the beam-to-column joints are reported in Table 6.1 with reference to the notation of Fig. 6.1.

**Table 6.1** – Measured geometrical properties of the joints

<b>Joint</b>	<b>EEP-DB-CYC 03</b>	<b>TS-CYC 04</b>	<b>FREEDAM-CYC 01</b>
<b>Bolts</b>	8 M24 (10.9)	8 M20 (10.9)	8 M20 (10.9)
<b>Pre-loading</b>	550 Nm	550 Nm	445 Nm
<b><math>b_{ep}</math></b>	427.0	154.0	200.0
<b><math>h_{ep}</math></b>	161.0	2x257	187 – (T-stub) 2x98 – (L-stub)
<b><math>t_{ep}</math></b>	25.3	25.2	20
<b><math>e_1</math></b>	36.0	30.2	48.3 – (T-stub) 42.5 – (L-stub)
<b><math>e_2</math></b>	33.0	39.0	43
<b><math>p_1</math></b>	89.0	94.3	103.4 – (T-stub) 115.0 – (L-stub)
<b><math>p_2</math></b>	99.0	177	101
<b><math>p_3</math></b>	163.0	-	-

In addition, the mechanical properties of the dissipative elements of the joints represented by the endplate for EEP-DB-CYC 03 and by the flange of the tee elements for the TS-CYC 04, are given in Table 6.2. For the FREEDAM-CYC 01 joint typology, the nominal values of the mechanical properties of all the joint components have been considered.

**Table 6.2** – Endplate mechanical properties

<b>Joint</b>	<b>EEP-DB-CYC 03</b>	<b>TS-CYC 04</b>
$f_y$ [N/mm <sup>2</sup> ]	290	295
$f_u$ [N/mm <sup>2</sup> ]	493.7	520
<b>E</b> [N/mm <sup>2</sup> ]	207288	210000
$\epsilon_h / \epsilon_y$	11.3	12.2
$\epsilon_u / \epsilon_y$	589	486
<b>E/E<sub>h</sub></b>	86.5	103.4
<b>E/E<sub>u</sub></b>	632.8	486.0

Finally, in Table 6.3, the mechanical properties of the column and beam are summarized. In EEP-DB-CYC 03 and TS-CYC 04 joints configuration, the column size is HE 200 B while the beam size is IPE 270 while in FREEDAM-CYC 01 the column size is HE 220M and the beam size is still IPE 270.

**Table 6.3** – Column and beam mechanical properties

<b>Joint</b>	<b>EEP-DB-CYC 03</b>		<b>TS-CYC 04</b>		<b>FREEDAM-CYC 01</b>	
	beam	column	beam	column	beam	column
$f_{y,f}$ [N/mm <sup>2</sup> ]	405	430	405	430	355	
$f_{u,f}$ [N/mm <sup>2</sup> ]	546	523	546	523	510	
$f_{y,w}$ [N/mm <sup>2</sup> ]	387	382.5	387	382.5	355	
$f_{u,w}$ [N/mm <sup>2</sup> ]	534	522	534	522	510	



### 6.3.1. Extension of the component approach to joint subjected to axial and bending loads

In the component approach, the flexural capacity of the whole joint is related to those of the single components. As aforementioned in the chapter 2, starting from the definition of the joint as the assembling of connection and panel zone of the column web, the concept of beam-joint system has been taken up so that the joint and the beam are considered as two macro-elements in series whose contribution to the plastic deformation capacity is given by means of an accurate balance of the thresholds of the first plasticization and ultimate strength [5,17]. These two macro-elements has been properly modelled. Specifically, the dissipative capacity of the beam could be taken into account by means of a plastic hinge characterized by a constitutive law obtained by means of FEM analyses performed using ABAQUS 6.13 software.

In detail, the moment-rotation curves characterizing the behaviour of the members when subjected to combined tensile force and bending moment, have been obtained for five fixed values of the axial force and by increasing progressively the value of the bending moment (Fig.6.1). Defined  $\rho$  as the ratio between the applied axial force  $N$  and the plastic resistance of the cross section  $N_{pl}$ , the analyses have been performed considering:

- $\rho = 0 \quad \rightarrow \quad N = 0kN$
- $\rho = 0.2 \quad \rightarrow \quad N \cong 372kN$
- $\rho = 0.4 \quad \rightarrow \quad N \cong 744kN$
- $\rho = 0.6 \quad \rightarrow \quad N \cong 1117kN$
- $\rho = 0.8 \quad \rightarrow \quad N \cong 1489kN$

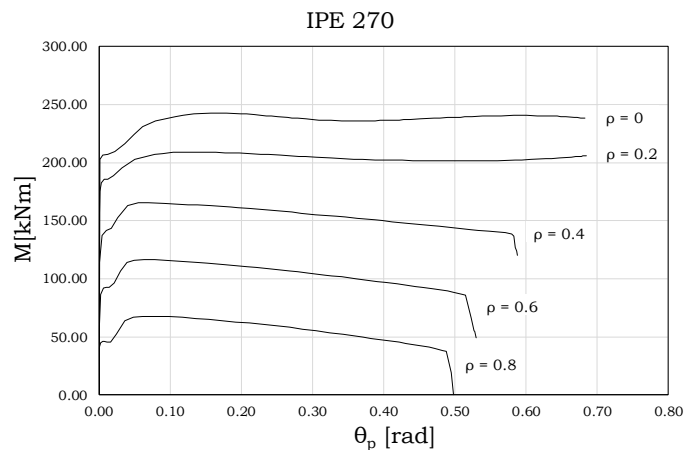


**Fig. 6.2** – Moment - rotation curves for the IPE 270 profile

The results illustrated in Fig.6.2 evidence that for low values of the axial force, i.e. when  $\rho = 0$  and  $\rho = 0.2$ , the ultimate condition is represented by the achievement of the ultimate material deformation while for greater values of  $N$  the tensile resistance of the member is reached.

Similarly, the analyses have been performed with reference to the reduced section of the beam of the EEP-DB-CYC 03 connection (Fig. 6.3). The plastic resistance of the reduced cross section  $N_{pLRBS}$  is equal to 1497 kN so that the value of the applied axial force considered in the analyses are:

- $\rho = 0 \quad \rightarrow \quad N = 0kN$
- $\rho = 0.2 \quad \rightarrow \quad N \cong 299kN$
- $\rho = 0.4 \quad \rightarrow \quad N \cong 599N$
- $\rho = 0.6 \quad \rightarrow \quad N \cong 898kN$
- $\rho = 0.8 \quad \rightarrow \quad N \cong 1198kN$

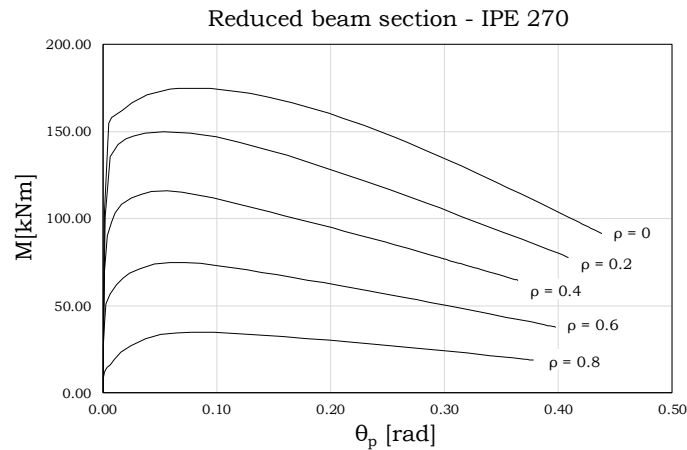


**Fig. 6.3** – Moment - rotation curves for the reduced beam section

Generally, in case of column loss, the joints are subjected to combined bending moments and axial forces; nevertheless, also in these cases, as the components behaviour is independent from the load typologies applied on the joints, the component method is still valid. In particular, in order to take into account for both bending and axial actions, each component has been characterized by an extensional spring represented by a  $F$ - $\delta$  curve, where  $F$  is the force action in the component and  $\delta$  is the related displacement. With reference to the all considered joints typologies, the following components have been modelled in terms of stiffness, resistance and ductility: column web in shear (*cws*), column web in compression (*cwc*), column web in tension (*cwt*), beam flange and web in compression (*bfc*), beam web in tension (*bwt*), column flange in bending (*cfb*), bolt in tension (*bt*), endplate in bending (*epb*), beam flange in tension (*bft*). In addition, for the bolted tee-stub connections other components have been considered: T-stub web in compression (*Twc*), t-stub web in bearing (*Twb*), beam flange in bearing (*bfb*), bolts in shear

(bs); T-stub web in tension (*Twt*). In particular, three of the previous components are considered as rigid-plastic, i.e. the beam flange and web in compression, beam web in tension, plate in tension. In Table 6.4, the adopted formulations provided by Eurocode 3 for the rigid-plastic component, are summarized.

**Table 6.4** – Resistance of the rigid-plastic components

<b>Component</b>	<b>Stiffness</b>	<b>Resistance</b>
Beam flange and web in compression	$\infty$	$F_{bfb} = \frac{M_{b,Rd}}{(h_t - t_{bf})}$
Beam web in tension	$\infty$	$F_{bwt} = \frac{b_{eff,wb} \cdot t_{bf} \cdot f_{y,wb}}{\gamma_{M0}}$
Plate in tension	$\infty$	$F_{pt;Rd} = \min \left\{ \frac{A f_{yd}}{\gamma_{M0}}; \frac{A_{net} f_{ud}}{\gamma_{M2}} \right\}$

$M_{b,Rd}$  is the design moment resistance of the beam cross-section,  $h_t$  is the depth of the connected beam,  $t_{bf}$  is the flange thickness of the connected beam,  $b_{eff,wb}$  is the effective width of the beam web,  $f_{y,wb}$  is the yielding resistance of the beam web,  $\mu$  is the slip factor,  $n$  is the number of bolts,  $n_s$  is the number of the friction surfaces,  $A_s$  is the resistant area of the bolt,  $f_{ub}$  is the ultimate resistance of the bolt,  $A$  is the gross area of the plate,  $f_{yd}$  is the yielding resistance of the plate,  $A_{net}$  is the net section of the plate,  $f_{ud}$  is the ultimate resistance of the plate and  $\gamma_{M0}$ ,  $\gamma_{M2}$  and  $\gamma_{M3}$  are partial safety factors given by EC3 Part 1-1.

**Table 6.5** – Resistance of the elasto-plastic components

Component	Stiffness	Resistance
		$F_{cwc,Rd} = 0.9 \frac{f_{y,cw} \cdot A_{vc}}{\sqrt{3} \cdot \gamma_{M0}} + F_{cwc,Rd,add}$
		with
Column web in shear	$k_{cws} = \frac{0.38 \cdot A_{vc}}{\beta \cdot z}$	$F_{cwc,Rd,add} = \frac{4M_{pl,fc,Rd}}{d_s}$
		but
		$F_{cwc,Rd,add} \leq \frac{2M_{pl,fc,Rd} + 2M_{pl,st,Rd}}{d_s}$
Column web in compression	$k_{cwc} = \frac{0.7 \cdot b_{eff,cwc} \cdot t_{wc}}{d_c}$	$F_{cwc,Rd} = \omega \cdot \left[ b_{eff,cwc} (t_{cw} + 2 \cdot t_{cw}) \cdot \frac{f_{y,cw}}{\gamma_{M0}} \right]$
Column web in tension	$k_{cwt} = \frac{0.7 \cdot b_{eff,cwt} \cdot t_{wc}}{d_c}$	$F_{cwt,Rd} = \frac{\omega \cdot b_{eff,cwt} \cdot t_{wc} \cdot f_{y,cw}}{\gamma_{M0}}$
Bolt in shear	$k_{bs} = \frac{16 \cdot n_b \cdot d^2 \cdot f_{ub}}{E \cdot d_{M16}}$	$F_{v,Rd} = \frac{\alpha_v \cdot A_s \cdot f_{ub}}{\gamma_{M2}}$
Plate and beam in bearing	$k_{be} = \frac{24 \cdot n_b \cdot k_b \cdot k_t \cdot d \cdot f_u}{E}$	$F_{p,Rd} = \frac{k_1 \cdot \alpha_b \cdot d \cdot f_u \cdot t_p}{\gamma_{M2}}$

According to Eurocode 3 [2], in Table 6.5 the resistance values and the stiffness coefficient of the elastic perfectly plastic components, are summarized, where  $A_{vc}$  is the shear area,  $f_{y,cw}$  is the yielding resistance of the column web,  $M_{pl,fc,Rd}$  is the design plastic moment resistance of a column flange,  $M_{pl,st,Rd}$  is the design plastic moment resistance of a stiffener,  $d_s$  is the distance between the centrelines of the stiffeners,  $\beta$  is a transformation parameter,  $z$  is the lever arm;  $\omega$  is a reduction factor to

allow for the possible effects of interaction with shear in the column web panel,  $b_{\text{eff.cwc}}$  is the effective width of the column web in compression,  $t_{\text{cw}}$  is the thickness of the column web,  $b_{\text{cp}}$  is the width of the continuity plate,  $t_{\text{cp}}$  is the thickness of the continuity plate,  $d_c$  is the clear depth of the column web,  $b_{\text{eff.cwt}}$  is the effective width of the column web in tension,  $\alpha_v$  is a coefficient depending on the bolt class,  $d$  is the bolt diameter,  $n_b$  is the number of the bolt-rows in shear,  $d_{\text{M16}}$  is the nominal diameter of an M16 bolt,  $E$  is the young modulus,  $k_1, \alpha_b, k_b, k_t$  are parameters depending on the position of the bolts,  $t_p$  is the thickness of the element (plate or beam) and  $f_u$  is the corresponding ultimate resistance.

Regarding the joint components modelled by means of an equivalent T-stub, i.e. the column flange in bending, endplate in bending and tee elements in bending, a theoretical model has been developed [2] and detailed in the ANNEX B. This model allows to the definition of the T-stub response up to failure, starting from the definition of the geometry of the elements, the boundary conditions and the non-linear behaviour of its subcomponents, i.e., the plate and the bolts. The behaviour of the plate is defined adopting a lumped plasticity approach by means of nonlinear plastic hinges located in the T-stub flange, according to EC3, in correspondence of the bolt axis and in the section close to the T-stub web [3]. The characteristics of the plastic hinges are derived starting from the moment-curvature diagram of the cross-section representing the plate, according to the approach already proposed by Piluso et al. [21]. In a similar way, also the non-linear spring modelling the bolt shank behaviour is characterized starting from the knowledge of the stress-strain law of the basic material according to the approach

detailed in the next section. The failures of the sub-components of the T-stub, i.e. the bolts and the plate, are modelled by checking the ultimate condition on the stress-strain laws of the materials. In particular, the failure of the plastic hinges of the plate is individuated as corresponding to the plastic rotation leading to the attainment the ultimate strain at the most external fibre, while the failure of the bolt is identified in correspondence to the uplift value leading to the fracture elongation of the material composing the bolt. The displacements of the T-stub are evaluated step-by-step as the sum of the elastic and plastic parts. Finally, starting from the force-displacement curve of the each joint component, the mechanical models of the whole joints have been obtained for the robustness analyses of steel frames.

In the following an explanation of the behaviour of connections analysed will take place.

#### ***EEP-DB-CYC 03 connection***

With reference to the prediction of the response of the connections, it should be highlighted that, in case of bolted extended endplate connections having two or more bolt rows in tension, a refined model (Fig.6.2a) has to be adopted in order to take into account the interaction between the different bolt rows. Nevertheless, in the case of two bolt rows in tension, with the aim of simplifying the modelling of the connection, the prediction of the response of the connections can be carried out by means of the simplified mechanical model proposed by the Eurocode 3 [2] and depicted in Fig. 6.2b.

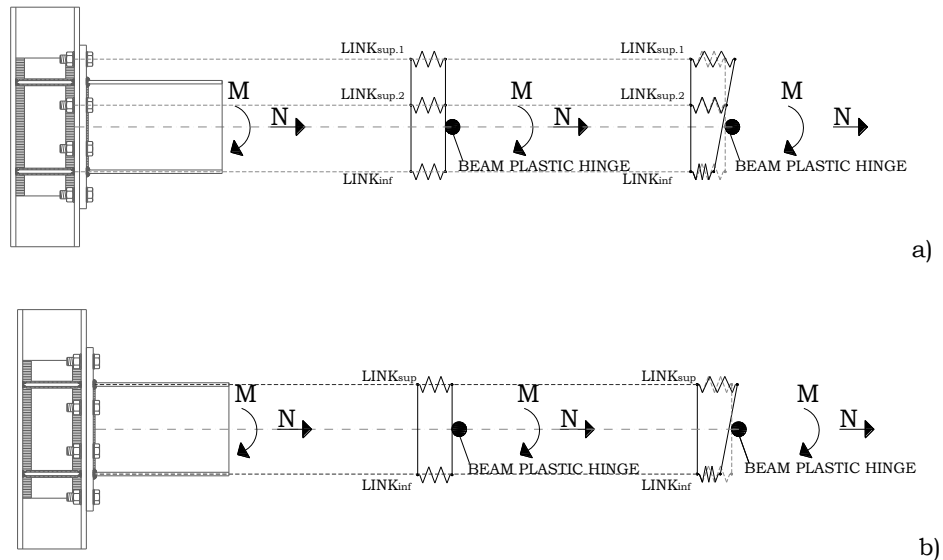


**Fig. 6.4** – Mechanical model for the bolted connections: a) refined model;  
b) simplified model

In particular, when subjected to both sagging and hogging moment, the following components have to be taken into account in order to evaluate the stiffness and the resistance of the whole joint (Fig 6.3):

- column web in shear (cws);
- column web in compression (cwc);
- beam flange and web in compression (bfc);
- column web in tension (cwt);
- column flange in bending (cfb);
- endplate in bending (epb);
- bolt in tension (bt);
- beam web in tension (bwt).



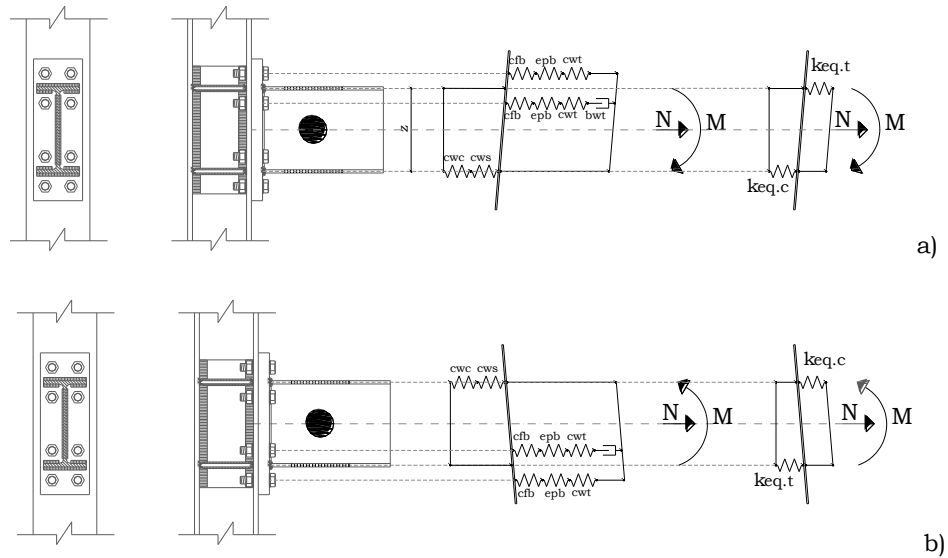


**Fig. 6.5** – EEP-DB-CYC 03: Mechanical model

Aiming to obtain the force – displacement curves characterising the equivalent springs both in tensile and compression zone, the individual stiffness of each component and their resistance has been evaluated according to the formulas provided in Tables 6.4 and 6.5. Subsequently, the total stiffness  $S = E \cdot k_{eq}$  of the connection has been derived by assembling the stiffness of the single components while the resistance of the connection  $F_{Rd}$  has been determined considering the minimum resistance of the involved components. Finally, the relationship between the determined parameters and the corresponding displacements is:

$$F_{Rd} = S \cdot \delta \quad \rightarrow \quad \delta = \frac{F_{Rd}}{S} \quad (6.1)$$

Since the analysed frame, designed according to the procedure illustrated in the previous chapter, is characterized by having the columns whose size decreases in height, the springs modelling the beam-to-column behaviour have to be properly detailed for each subassembly. In addition, both external and internal joints have been detailed.

- **HE 300 B – IPE 270 joint:**

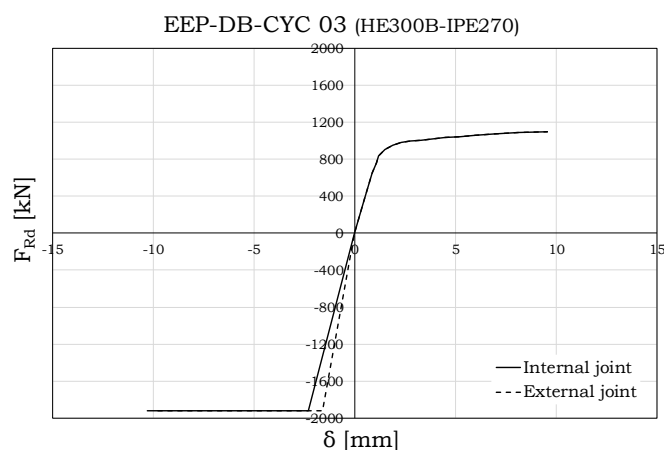
**Table 6.6** – EEP-DB-CYC 03: Stiffness coefficients (HE300B – IPE 270)

<b>TENSILE PART</b>					
	$k_{cfb}$ [mm]	$k_{epb}$ [mm]	$k_{cwt}$ [mm]	$k_{eq,t}$ [mm]	$S_t$ [kN/mm]
<b>INTERNAL AND EXTERNAL JOINTS</b>	35.63	20.18		3.68	<b>772</b>
	35.63	15.88		3.50	<b>736</b>
	35.63	12.98		3.34	<b>701</b>
	22.39	12.98		3.34	<b>701</b>
	22.39	7.82		2.85	<b>599</b>
	22.39	5.22		2.42	<b>507</b>
	22.39	3.72		2.04	<b>427</b>
	22.39	2.77		1.71	<b>360</b>
	22.39	2.17	5.14	1.46	<b>307</b>
	22.39	1.73		1.25	<b>263</b>
	22.39	1.44		1.09	<b>229</b>
	22.39	1.21		0.96	<b>201</b>
	22.39	1.04		0.84	<b>177</b>
	22.39	0.88		0.74	<b>154</b>
	22.39	0.74		0.63	<b>133</b>
22.39	0.62		0.55	<b>115</b>	
<b>COMPRESSIVE PART</b>					
	$k_{cws}$ [mm]	$k_{cwc}$ [mm]		$k_{eq,c}$ [mm]	$S_c$ [kN/mm]
<b>EXTERNAL JOINTS</b>	12.77	10.59		5.79	<b>1215</b>
<b>INTERNAL JOINTS</b>	6.38	10.59		3.98	<b>836</b>

**Table 6.7** – EEP-DB-CYC 03: Resistance parameters (HE300B – IPE 270)

<b>TENSILE PART</b>				
	$F_{cfb}$ [kN]	$F_{epb}$ [kN]	$F_{cwt}$ [kN]	$F_{Rd,t}$ [kN]
<b>EXTERNAL JOINTS</b>	1484	1100	1451	<b>1100</b>
<b>INTERNAL JOINTS</b>	1504	1100	1389	<b>1100</b>
<b>COMPRESSIVE PART</b>				
	$F_{cws}$ [kN]	$F_{cwc}$ [kN]		$F_{Rd,c}$ [kN]
<b>EXTERNAL JOINTS</b>	1921	2358		<b>1921</b>
<b>INTERNAL JOINTS</b>	1921	2043		<b>1921</b>

The force - displacement curves obtained for the connection HE300B and IPE270, for both internal and external joints, are reported in Fig.6.4.

**Fig. 6.6** – EEP-DB-CYC 03: Force – displacement curve (HE300B – IPE 270)

- **HE 280 B – IPE 270 joint:****Table 6.8** – EEP-DB-CYC 03: Stiffness coefficients (HE280B – IPE 270)

<b>TENSILE PART</b>					
	$k_{cfb}$ [mm]	$k_{epb}$ [mm]	$k_{cwt}$ [mm]	$k_{eq,t}$ [mm]	$S_t$ [kN/mm]
<b>INTERNAL AND EXTERNAL JOINTS</b>	31.74	20.18		4.03	<b>845</b>
	31.74	15.88		3.82	<b>802</b>
	31.74	12.98		3.62	<b>761</b>
	21.31	12.98		3.62	<b>761</b>
	21.31	7.82		3.06	<b>643</b>
	21.31	5.22		2.56	<b>538</b>
	21.31	3.72		2.14	<b>449</b>
	21.31	2.77		1.79	<b>375</b>
	21.31	2.17	5.98	1.51	<b>318</b>
	21.31	1.73		1.29	<b>271</b>
	21.31	1.44		1.12	<b>235</b>
	21.31	1.21		0.98	<b>205</b>
	21.31	1.04		0.86	<b>181</b>
	21.31	0.88		0.75	<b>157</b>
	21.31	0.74		0.64	<b>135</b>
	21.31	0.62		0.56	<b>117</b>
<b>COMPRESSIVE PART</b>					
	$k_{cws}$ [mm]	$k_{cwc}$ [mm]		$k_{eq,c}$ [mm]	$S_c$ [kN/mm]
<b>EXTERNAL JOINTS</b>	11.52	10.25		5.42	<b>1139</b>
<b>INTERNAL JOINTS</b>	5.76	10.25		3.39	<b>774</b>

**Table 6.9** – EEP-DB-CYC 03: Resistance parameters (HE280B – IPE 270)

<b>TENSILE PART</b>				
	$F_{cfb}$ [kN]	$F_{epb}$ [kN]	$F_{cwt}$ [kN]	$F_{Rd,t}$ [kN]
<b>EXTERNAL JOINTS</b>	1358	1100	1559	<b>1100</b>
<b>INTERNAL JOINTS</b>	1358	1100	1468	<b>1100</b>
<b>COMPRESSIVE PART</b>				
	$F_{cws}$ [kN]	$F_{cwc}$ [kN]		$F_{Rd,c}$ [kN]
<b>EXTERNAL JOINTS</b>	1723	2143		<b>1723</b>
<b>INTERNAL JOINTS</b>	1723	1863		<b>1723</b>

*Robustness and seismic behaviour of structures equipped with traditional and innovative beam-to-column connections*

The curves obtained for the connection HE280B and IPE270, for both internal and external joints, are illustrated in Fig.6.5.

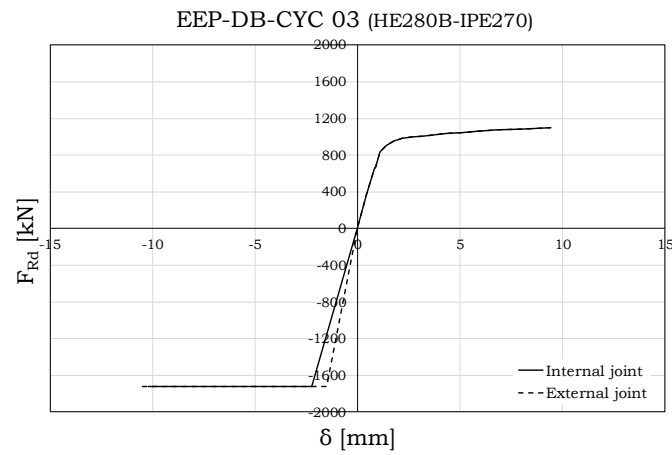


**Fig. 6.7** - EEP-DB-CYC 03: Force - displacement curve (HE280B - IPE 270)

- **HE 260 B – IPE 270 joint:****Table 6.10** – EEP-DB-CYC 03: Stiffness coefficients (HE260B – IPE 270)

<b>TENSILE PART</b>					
	$k_{cfb}$ [mm]	$k_{epb}$ [mm]	$k_{cwt}$ [mm]	$k_{eq,t}$ [mm]	$S_t$ [kN/mm]
<b>INTERNAL AND EXTERNAL JOINTS</b>	31.74	20.18		4.14	<b>870</b>
	31.74	15.88		3.93	<b>824</b>
	31.74	12.98		3.72	<b>781</b>
	21.31	12.98		3.72	<b>781</b>
	21.31	7.82		3.13	<b>657</b>
	21.31	5.22		2.61	<b>548</b>
	21.31	3.72		2.17	<b>456</b>
	21.31	2.77		1.81	<b>380</b>
	21.31	2.17	6.24	1.53	<b>322</b>
	21.31	1.73		1.30	<b>273</b>
	21.31	1.44		1.13	<b>237</b>
	21.31	1.21		0.98	<b>207</b>
	21.31	1.04		0.87	<b>182</b>
	21.31	0.88		0.75	<b>158</b>
	21.31	0.74		0.65	<b>136</b>
	21.31	0.62		0.56	<b>117</b>
<b>COMPRESSIVE PART</b>					
	$k_{cws}$ [mm]	$k_{cwc}$ [mm]		$k_{eq,c}$ [mm]	$S_c$ [kN/mm]
<b>EXTERNAL JOINTS</b>	10.46	10.51		5.24	<b>1101</b>
<b>INTERNAL JOINTS</b>	5.23	10.51		3.49	<b>733</b>

**Table 6.11** – EEP-DB-CYC 03: Resistance parameters (HE260B – IPE 270)

<b>TENSILE PART</b>				
	$F_{cfb}$ [kN]	$F_{epb}$ [kN]	$F_{cwt}$ [kN]	$F_{Rd,t}$ [kN]
<b>EXTERNAL JOINTS</b>	1358	1100	1559	<b>1100</b>
<b>INTERNAL JOINTS</b>	1358	1100	1468	<b>1100</b>
<b>COMPRESSIVE PART</b>				
	$F_{cws}$ [kN]	$F_{cwc}$ [kN]		$F_{Rd,c}$ [kN]
<b>EXTERNAL JOINTS</b>	1561	1994		<b>1561</b>
<b>INTERNAL JOINTS</b>	1561	1719		<b>1561</b>

*Robustness and seismic behaviour of structures equipped with traditional and innovative beam-to-column connections*

The curves obtained for the connection HE260B and IPE270 are reported in Fig.6.6.

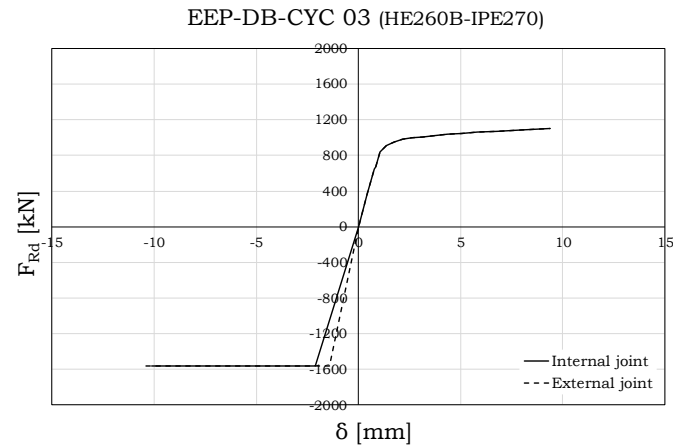


**Fig. 6.8** – EEP-DB-CYC 03: Force – displacement curve (HE260B – IPE 270)

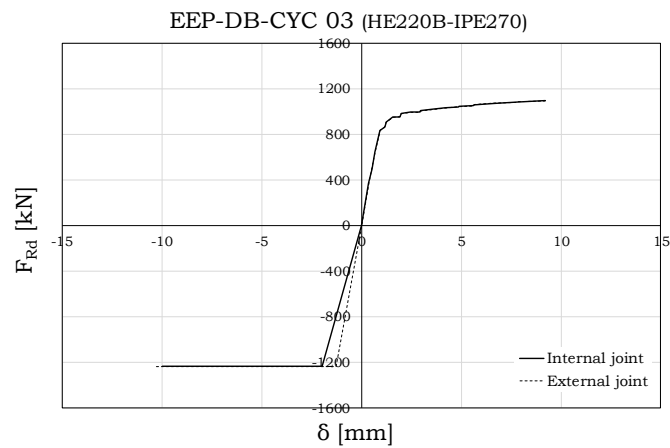
- **HE 220 B – IPE 270 joint:****Table 6.12** – EEP-DB-CYC 03: Stiffness coefficients (HE220B – IPE 270)

<b>TENSILE PART</b>					
	$k_{cfb}$ [mm]	$k_{epb}$ [mm]	$k_{cwt}$ [mm]	$k_{eq,t}$ [mm]	$S_t$ [kN/mm]
<b>INTERNAL AND EXTERNAL JOINTS</b>	23.80	20.18		4.83	<b>1015</b>
	23.80	15.88		4.54	<b>953</b>
	18.86	15.88		4.54	<b>953</b>
	18.86	12.98		4.27	<b>896</b>
	18.86	7.82		3.50	<b>736</b>
	11.22	7.82		3.50	<b>736</b>
	11.22	5.22		2.87	<b>602</b>
	11.22	3.72		2.35	<b>493</b>
	6.76	3.72		2.35	<b>493</b>
	6.76	2.77		1.93	<b>405</b>
	6.76	2.17		1.62	<b>339</b>
	4.77	2.17	8.67	1.62	<b>339</b>
	4.77	1.73		1.36	<b>286</b>
	4.77	1.44		1.17	<b>247</b>
	4.77	1.21		1.02	<b>214</b>
	3.67	1.21		1.02	<b>214</b>
	3.67	1.04		0.89	<b>188</b>
	2.93	1.04		0.89	<b>188</b>
	2.93	0.88		0.77	<b>162</b>
	2.93	0.74		0.66	<b>139</b>
2.22	0.74		0.66	<b>139</b>	
2.22	0.62		0.57	<b>119</b>	
1.66	0.62		0.57	<b>119</b>	
<b>COMPRESSIVE PART</b>					
	$k_{cws}$ [mm]	$k_{cwc}$ [mm]		$k_{eq,c}$ [mm]	$S_c$ [kN/mm]
<b>EXTERNAL JOINTS</b>	8.36	10.62		5.42	<b>1139</b>
<b>INTERNAL JOINTS</b>	4.18	10.62		3.39	<b>774</b>



**Table 6.13** – EEP-DB-CYC 03: Resistance parameters (HE220B – IPE 270)

<b>TENSILE PART</b>				
	$F_{cfb}$ [kN]	$F_{epb}$ [kN]	$F_{cwt}$ [kN]	$F_{Rd,t}$ [kN]
<b>EXTERNAL JOINTS</b>	1160	1100	1693	<b>1100</b>
<b>INTERNAL JOINTS</b>	1160	1100	1493	<b>1100</b>
<b>COMPRESSIVE PART</b>				
	$F_{cws}$ [kN]	$F_{cwc}$ [kN]		$F_{Rd,c}$ [kN]
<b>EXTERNAL JOINTS</b>	1237	1665		<b>1237</b>
<b>INTERNAL JOINTS</b>	1237	1428		<b>1237</b>

**Fig. 6.9** – EEP-DB-CYC 03: Force – displacement curve (HE220B – IPE 270)

### TS-CYC 04 connection

In case of the double split tee connections, when subjected to both sagging and hogging moment, the following components have to be taken into account in order to evaluate the stiffness and the resistance of the whole joint (Fig 6.8):

- column web in shear (*cws*);
- column web in compression (*cwc*);
- beam flange and web in compression (*bfc*);
- column web in tension (*cwt*);
- column flange in bending (*cfb*);
- T-stub in bending (*Tsb*);

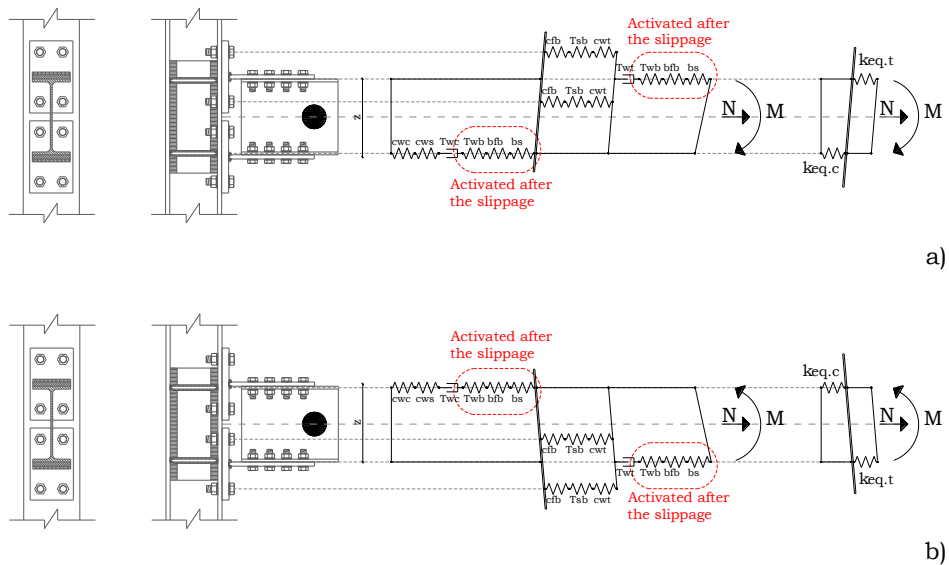


**Fig. 6.10** – TS-CYC 04: Mechanical model

Since the bolts connecting the T-stub webs and the beam flanges have been pre-loaded, at the beginning no sliding of the metallic interface occurs. However, after reaching the sliding resistance, three components must be added to the resistance of the connection (Fig. 6.8):

- the bolts in shear (*bs*);
- the T-stub web in bearing (*Tswbe*);
- the beam flange in bearing (*bfbe*).

Those components will provoke a decrease of the initial stiffness. In the following procedure, the initial stiffness is calculated and after reaching the sliding resistance of the steel on steel interface, a modified value is obtained. In terms of resistance, it is important to underline that, on the basis of additional tests performed in FREEDAM Project, the contribution of these components has been added to the sliding resistance of the connection.

Finally, before reaching the sliding resistance, the displacements have been determined according to Eq. (6.1) and according to Eq. (6.2) when the sliding occurs:

$$\delta|_{F>F_{slid}} = \frac{F}{S_1} + \frac{F - F_{slid}}{S_2} \quad (6.2)$$

Obviously, the springs modelling the beam-to-column behaviour for each subassembly - and both for external and internal joints - have been detailed. The resistance parameters and the stiffness coefficients have been reported in Tables 6.14-6.21 while the force - displacement curves are illustrated in Figs. 6.9-6.12.

## - HE 300 B – IPE 270 joint:

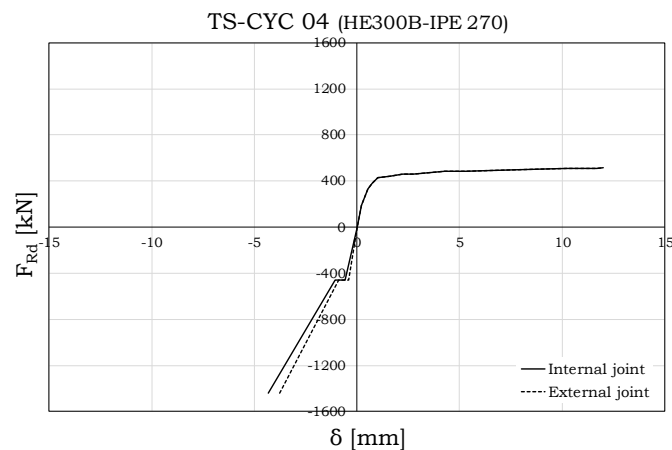
Table 6.14 – TS -CYC 04: Stiffness coefficients (HE300B – IPE 270)

<b>TENSILE PART</b>										
<i>BEFORE THE SLIPPAGE</i>										
<b>INTERNAL AND EXTERNAL JOINTS</b>	$k_{cfb}$	$k_{tsb}$	$k_{eq,t}$	$S_t$						
	[mm]	[mm]	[mm]	[kN/mm]						
			4.41	3.68	<b>772</b>					
			3.29	3.50	<b>736</b>					
		35.63	2.62	3.34	<b>701</b>					
			2.10	3.34	<b>701</b>					
			1.36	2.85	<b>599</b>					
		1.00	2.42	<b>507</b>						
<i>AFTER THE SLIPPAGE</i>										
	$k_{cfb}$	$k_{tsb}$	$k_{eq,t}$	$S_{t.1}$	$k_{Tsube}$	$k_{b/be}$	$k_{bs}$	$k_{eq,t}$	$S_{t.2}$	
	[mm]	[mm]	[mm]	[kN/mm]	[mm]	[mm]	[mm]	[mm]	[kN/mm]	
		0.78	0.76	<b>160</b>						
		0.63	0.62	<b>130</b>						
		0.50	0.49	<b>103</b>						
		0.41	0.40	<b>84</b>						
	35.65	0.34	0.34	<b>71</b>	11.14	4.67	7.62	2.30	<b>483</b>	
		0.29	0.29	<b>60</b>						
		0.25	0.25	<b>53</b>						
		0.22	0.22	<b>46</b>						
		0.20	0.20	<b>41</b>						
<b>COMPRESSIVE PART</b>										
<i>BEFORE THE SLIPPAGE</i>										
<b>EXTERNAL JOINTS</b>	$k_{cws}$	$k_{cwc}$	$k_{eq,c}$	$S_c$						
	[mm]	[mm]	[mm]	[kN/mm]						
	11.28		5.53	<b>1162</b>						
<b>INTERNAL JOINTS</b>	6.38	9.76	3.86	<b>811</b>						
<i>AFTER THE SLIPPAGE</i>										
	$k_{cws}$	$k_{cwc}$	$k_{eq,c}$	$S_{c.1}$	$k_{Tsube}$	$k_{b/be}$	$k_{bs}$	$k_{eq,c}$	$S_{c.2}$	
	[mm]	[mm]	[mm]	[kN/mm]	[mm]	[mm]	[mm]	[mm]	[kN/mm]	
<b>EXTERNAL JOINTS</b>	11.28		5.53	<b>1162</b>						
<b>INTERNAL JOINTS</b>	6.38	9.76	3.86	<b>811</b>	11.14	4.67	7.62	2.30	<b>483</b>	

Robustness and seismic behaviour of structures equipped with traditional and innovative beam-to-column connections

**Table 6.15** – TS-CYC 04: Resistance parameters (HE300B – IPE 270)

<b>TENSILE PART</b>							
	$F_{cfb}$ [kN]	$F_{Tsb}$ [kN]	$F_{cwt}$ [kN]	$F_{Tswbe}$ [kN]	$F_{bfbe}$ [kN]	$F_{bs}$ [kN]	$F_t$ [kN]
<b>EXTERNAL JOINTS</b>			1451				<b>515</b>
<b>INTERNAL JOINTS</b>	1463	516		3217	2151	1439	<b>515</b>
<b>COMPRESSIVE PART</b>							
	$F_{cws}$ [kN]	$F_{cwc}$ [kN]	$F_{Tswbe}$ [kN]	$F_{bfbe}$ [kN]	$F_{bs}$ [kN]		$F_c$ [kN]
<b>EXTERNAL JOINTS</b>		2251					<b>1921</b>
<b>INTERNAL JOINTS</b>	1921		3217	2151	1439		<b>1921</b>

**Fig. 6.11** – TS-CYC 04: Force – displacement curve (HE300B – IPE 270)

## - HE 280 B – IPE 270 joint:

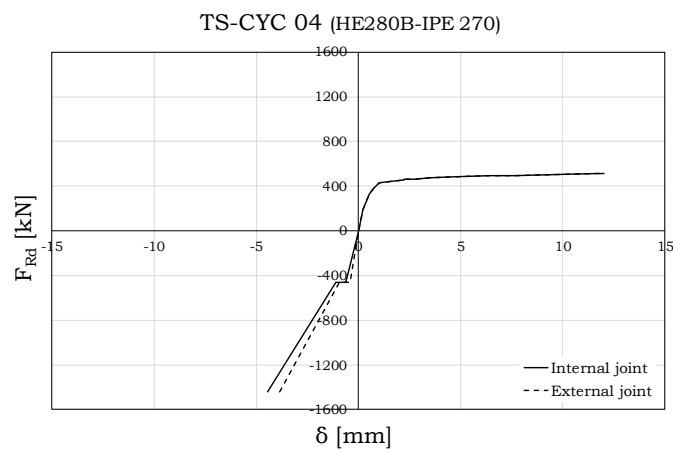
Table 6.16 – TS -CYC 04: Stiffness coefficients (HE280B – IPE 270)

<b>TENSILE PART</b>										
<i>BEFORE THE SLIPPAGE</i>										
	$k_{cfb}$ [mm]	$k_{tsb}$ [mm]	$k_{eq,t}$ [mm]	$S_t$ [kN/mm]						
<b>INTERNAL AND EXTERNAL JOINTS</b>	31.74	4.41	3.87	<b>813</b>						
		3.29	2.98	<b>626</b>						
		2.62	2.42	<b>508</b>						
		2.10	1.97	<b>413</b>						
		1.36	1.31	<b>274</b>						
		1.00	0.97	<b>203</b>						
	<i>AFTER THE SLIPPAGE</i>									
		$k_{cfb}$ [mm]	$k_{tsb}$ [mm]	$k_{eq,t}$ [mm]	$S_{t.1}$ [kN/mm]	$k_{Tsube}$ [mm]	$k_{b/be}$ [mm]	$k_{bs}$ [mm]	$k_{eq,t}$ [mm]	$S_{t.2}$ [kN/mm]
			0.78	0.76	<b>160</b>	11.14	4.67	7.62	2.30	<b>483</b>
			0.63	0.62	<b>129</b>					
		0.50	0.49	<b>103</b>						
		0.41	0.40	<b>84</b>						
31.74		0.34	0.34	<b>70</b>						
		0.29	0.29	<b>60</b>						
		0.25	0.25	<b>52</b>						
		0.22	0.22	<b>46</b>						
	0.20	0.20	<b>41</b>							
<b>COMPRESSIVE PART</b>										
<i>BEFORE THE SLIPPAGE</i>										
	$k_{cws}$ [mm]	$k_{cwc}$ [mm]	$k_{eq,c}$ [mm]	$S_c$ [kN/mm]						
<b>EXTERNAL JOINTS</b>	11.52	9.37	5.17	<b>1085</b>						
<b>INTERNAL JOINTS</b>	5.76		3.57	<b>749</b>						
<i>AFTER THE SLIPPAGE</i>										
	$k_{cws}$ [mm]	$k_{cwc}$ [mm]	$k_{eq,c}$ [mm]	$S_{c.1}$ [kN/mm]	$k_{Tsube}$ [mm]	$k_{b/be}$ [mm]	$k_{bs}$ [mm]	$k_{eq,c}$ [mm]	$S_{c.2}$ [kN/mm]	
<b>EXTERNAL JOINTS</b>	11.52	9.37	5.17	<b>1085</b>	11.14	4.67	7.62	2.30	<b>483</b>	
<b>INTERNAL JOINTS</b>	5.76		3.57	<b>749</b>						

Robustness and seismic behaviour of structures equipped with traditional and innovative beam-to-column connections

**Table 6.17** – TS-CYC 04: Resistance parameters (HE280B – IPE 270)

<b>TENSILE PART</b>							
	$F_{cfb}$ [kN]	$F_{Tsb}$ [kN]	$F_{cwt}$ [kN]	$F_{Tswbe}$ [kN]	$F_{bfbe}$ [kN]	$F_{bs}$ [kN]	$F_t$ [kN]
<b>EXTERNAL JOINTS</b>	1358	515	1559	3217	2151	1439	<b>515</b>
<b>INTERNAL JOINTS</b>			1468				
<b>COMPRESSIVE PART</b>							
	$F_{cws}$ [kN]	$F_{cwc}$ [kN]	$F_{Tswbe}$ [kN]	$F_{bfbe}$ [kN]	$F_{bs}$ [kN]	$F_c$ [kN]	
<b>EXTERNAL JOINTS</b>	1723	2040	3217	2151	1439	<b>1723</b>	
<b>INTERNAL JOINTS</b>		1805					

**Fig. 6.12** – TS-CYC 04: Force – displacement curve (HE280B – IPE 270)

## - HE 260 B – IPE 270 joint:

Table 6.18 – TS -CYC 04: Stiffness coefficients (HE260B – IPE 270)

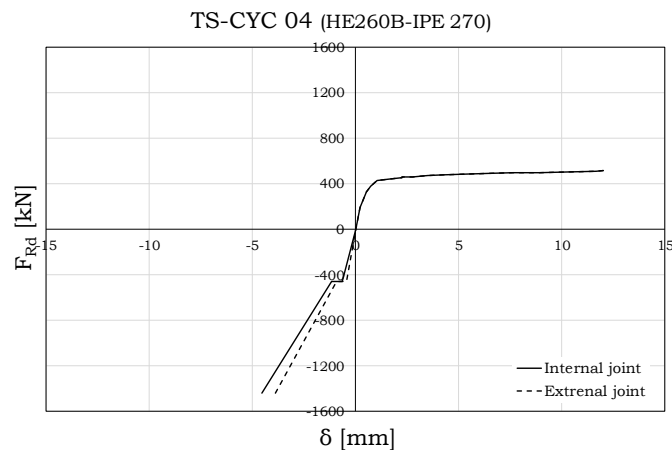
<b>TENSILE PART</b>										
<i>BEFORE THE SLIPPAGE</i>										
	$k_{cfb}$ [mm]	$k_{tsb}$ [mm]	$k_{eq,t}$ [mm]	$S_t$ [kN/mm]						
<b>INTERNAL AND EXTERNAL JOINTS</b>	31.74	4.41	3.87	<b>813</b>						
		3.29	2.98	<b>626</b>						
		2.62	2.42	<b>508</b>						
		2.10	1.97	<b>413</b>						
		1.36	1.31	<b>274</b>						
		1.00	0.97	<b>203</b>						
	<i>AFTER THE SLIPPAGE</i>									
		$k_{cfb}$ [mm]	$k_{tsb}$ [mm]	$k_{eq,t}$ [mm]	$S_{t.1}$ [kN/mm]	$k_{Tsube}$ [mm]	$k_{b/be}$ [mm]	$k_{bs}$ [mm]	$k_{eq,t}$ [mm]	$S_{t.2}$ [kN/mm]
			0.78	0.76	<b>160</b>	11.14	4.67	7.62	2.30	<b>483</b>
			0.63	0.62	<b>129</b>					
		0.50	0.49	<b>103</b>						
		0.41	0.40	<b>84</b>						
31.74		0.34	0.34	<b>70</b>						
		0.29	0.29	<b>60</b>						
		0.25	0.25	<b>52</b>						
		0.22	0.22	<b>46</b>						
	0.20	0.20	<b>41</b>							
<b>COMPRESSIVE PART</b>										
<i>BEFORE THE SLIPPAGE</i>										
	$k_{cws}$ [mm]	$k_{cwc}$ [mm]	$k_{eq,c}$ [mm]	$S_c$ [kN/mm]						
<b>EXTERNAL JOINTS</b>	10.46		5.00	<b>1050</b>						
<b>INTERNAL JOINTS</b>	5.23	9.57	3.38	<b>710</b>						
<i>AFTER THE SLIPPAGE</i>										
	$k_{cws}$ [mm]	$k_{cwc}$ [mm]	$k_{eq,c}$ [mm]	$S_{c.1}$ [kN/mm]	$k_{Tsube}$ [mm]	$k_{b/be}$ [mm]	$k_{bs}$ [mm]	$k_{eq,c}$ [mm]	$S_{c.2}$ [kN/mm]	
<b>EXTERNAL JOINTS</b>	10.46		5.00	<b>1050</b>	11.14	4.67	7.62	2.30	<b>483</b>	
<b>INTERNAL JOINTS</b>	5.23	9.57	3.38	<b>710</b>						

Robustness and seismic behaviour of structures equipped with traditional and innovative beam-to-column connections



**Table 6.19** – TS-CYC 04: Resistance parameters (HE260B – IPE 270)

<b>TENSILE PART</b>							
	$F_{cfb}$ [kN]	$F_{Tsb}$ [kN]	$F_{cwt}$ [kN]	$F_{Tswbe}$ [kN]	$F_{bfbe}$ [kN]	$F_{bs}$ [kN]	$F_t$ [kN]
<b>EXTERNAL JOINTS</b>			1497				<b>516</b>
<b>INTERNAL JOINTS</b>	1358	516		3217	2151	1439	<b>516</b>
<b>COMPRESSIVE PART</b>							
	$F_{cws}$ [kN]	$F_{cwc}$ [kN]	$F_{Tswbe}$ [kN]	$F_{bfbe}$ [kN]	$F_{bs}$ [kN]		$F_c$ [kN]
<b>EXTERNAL JOINTS</b>		1898					<b>1439</b>
<b>INTERNAL JOINTS</b>	1561		3217	2151	1439		<b>1439</b>

**Fig. 6.13** – TS-CYC 04: Force – displacement curve (HE260B – IPE 270)

## - HE 220 B – IPE 270 joint:

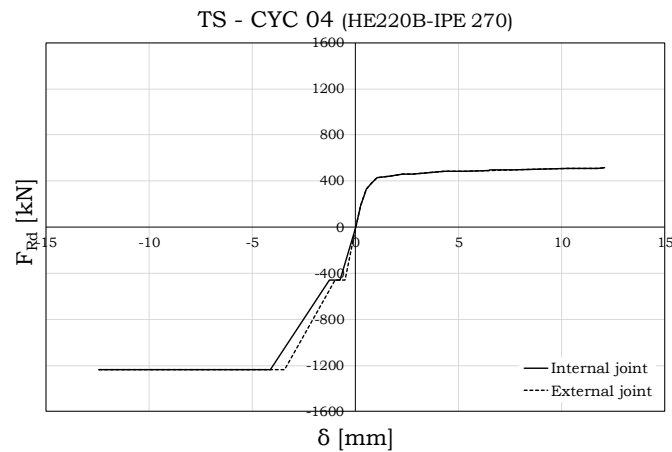
Table 6.20 – TS-CYC 04: Stiffness coefficients (HE220B – IPE 270)

<b>TENSILE PART</b>										
<i>BEFORE THE SLIPPAGE</i>										
<b>INTERNAL AND EXTERNAL JOINTS</b>	$k_{cfb}$	$k_{tsb}$	$k_{eq,t}$	$S_t$						
	[mm]	[mm]	[mm]	[kN/mm]						
			4.41	3.87	<b>813</b>					
			3.29	2.98	<b>626</b>					
	23.80		2.62	2.42	<b>508</b>					
			2.10	1.97	<b>413</b>					
			1.36	1.31	<b>274</b>					
		1.00	0.97	<b>203</b>						
<i>AFTER THE SLIPPAGE</i>										
<b>INTERNAL AND EXTERNAL JOINTS</b>	$k_{cfb}$	$k_{tsb}$	$k_{eq,t}$	$S_{t.1}$	$k_{Tsube}$	$k_{b/be}$	$k_{bs}$	$k_{eq,t}$	$S_{t.2}$	
	[mm]	[mm]	[mm]	[kN/mm]	[mm]	[mm]	[mm]	[mm]	[kN/mm]	
	23.80	0.78	0.75	<b>158</b>						
	23.80	0.63	0.61	<b>129</b>						
	23.80	0.50	0.49	<b>102</b>						
	23.80	0.41	0.40	<b>84</b>						
	23.80	0.34	0.33	<b>70</b>	11.14	4.67	7.62	2.30	<b>483</b>	
	18.86	0.29	0.29	<b>60</b>						
	18.86	0.25	0.25	<b>52</b>						
	18.86	0.22	0.22	<b>46</b>						
18.86	0.20	0.20	<b>41</b>							
<b>COMPRESSIVE PART</b>										
<i>BEFORE THE SLIPPAGE</i>										
<b>EXTERNAL JOINTS</b>	$k_{cws}$	$k_{cwc}$	$k_{eq,c}$	$S_c$						
	[mm]	[mm]	[mm]	[kN/mm]						
	8.36		4.45	<b>935</b>						
<b>INTERNAL JOINTS</b>	4.18	9.52	2.91	<b>610</b>						
	<i>AFTER THE SLIPPAGE</i>									
<b>EXTERNAL JOINTS</b>	$k_{cws}$	$k_{cwc}$	$k_{eq,c}$	$S_{c.1}$	$k_{Tsube}$	$k_{b/be}$	$k_{bs}$	$k_{eq,c}$	$S_{c.2}$	
	[mm]	[mm]	[mm]	[kN/mm]	[mm]	[mm]	[mm]	[mm]	[kN/mm]	
	8.36		4.45	<b>935</b>						
<b>INTERNAL JOINTS</b>	4.18	9.52	2.91	<b>610</b>	11.14	4.67	7.62	2.30	<b>483</b>	

*Robustness and seismic behaviour of structures equipped with traditional and innovative beam-to-column connections*

**Table 6.21** – TS-CYC 04: Resistance parameters (HE220B – IPE 270)

<b>TENSILE PART</b>							
	$F_{cfb}$ [kN]	$F_{Tsb}$ [kN]	$F_{cwt}$ [kN]	$F_{Tswbe}$ [kN]	$F_{bfbe}$ [kN]	$F_{bs}$ [kN]	$F_t$ [kN]
<b>EXTERNAL JOINTS</b>			1693				<b>516</b>
<b>INTERNAL JOINTS</b>	1160	516		3217	2151	1439	<b>516</b>
<b>COMPRESSIVE PART</b>							
	$F_{cws}$ [kN]	$F_{cwc}$ [kN]	$F_{Tswbe}$ [kN]	$F_{bfbe}$ [kN]	$F_{bs}$ [kN]		$F_c$ [kN]
<b>EXTERNAL JOINTS</b>		1576					<b>1237</b>
<b>INTERNAL JOINTS</b>	1237		3217	2151	1439		<b>1237</b>

**Fig. 6.14** – TS-CYC 04: Force – displacement curve (HE220B – IPE 270)

***FREEDAM-CYC 01 connection***

The innovative connections are characterized for having a fixed T-stub at the upper level of the beam and a friction device bolted to the beam lower level. In the following procedure, the hogging and sagging moments are analysed separately due to asymmetries of the joints. So that with reference to the case in which the connection is subjected to hogging moment, the joint components involved are:

- column web in shear (*cws*);
- column web in compression (*cwc*);
- beam flange and web in compression (*bfc*);
- column web in tension (*cwt*);
- column flange in bending (*cfb*);
- T-stub in bending (*Tsb*).

As in case of TS-CYC 04 connection, at the beginning no sliding occurs, neither for the friction damper neither for the metallic interface between the T-stub web and the upper beam flange. However, after reaching the sliding resistance of the upper interface, other three components are involved (Fig 6.13a):

- the bolts in shear (*bs*);
- the T-stub web in bearing (*Twb*);
- the beam flange in bearing (*bfb*).

In addition, when the stroke end of the slotted holes in the L-stub web and haunch flange interface is reached other three components are involved (Fig 6.13a):

- the bolts in shear ( $bs$ );
- the L-stub web in bearing ( $Lwb$ );
- the haunch flange in bearing ( $Hfb$ ).

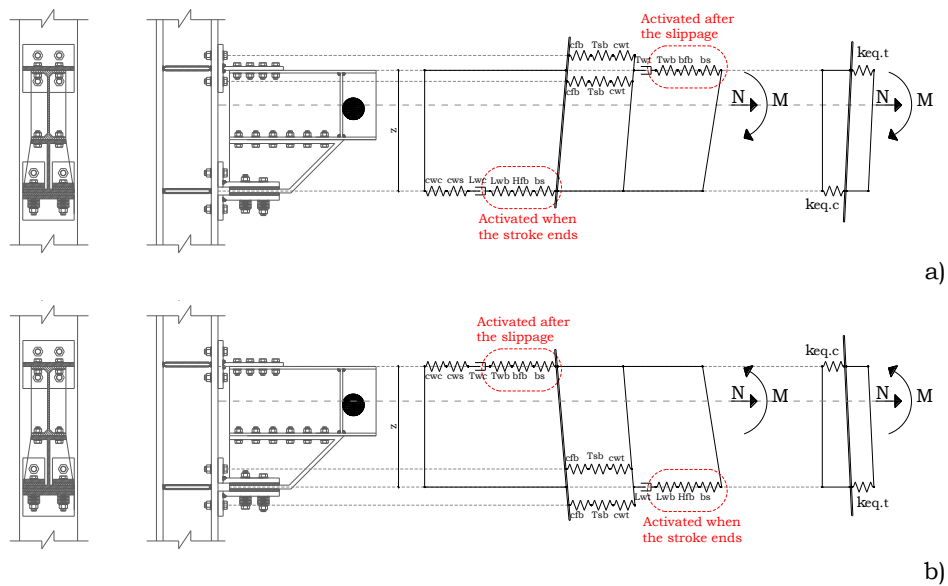


**Fig. 6.15** – Mechanical model of FREEDAM-CYC 01 joint: a) hogging moment; b) sagging moment

In case of sagging moment, the components involved result to be (Fig 6.13b):

- column web in shear (*cws*);
- column web in compression (*cwc*);
- beam flange and web in compression (*bfc*);
- column web in tension (*cwt*);
- column flange in bending (*cfb*);
- L-stub in bending (*Lsb*).

Similarly, after reaching the sliding resistance of the upper interface, additional components are involved (Fig 6.13b):

- the bolts in shear (*bs*);
- the T-stub web in bearing (*Twb*);
- the beam flange in bearing (*bfb*).

and when the stroke end of the slotted holes in the L-stub web and haunch flange interface is reached the other components involved are (Fig 6.13a):

- the bolts in shear (*bs*);
- the L-stub web in bearing (*Lwb*);
- the haunch flange in bearing (*Hfb*).

Even in this case, the springs modelling the beam-to-column behaviour for each subassembly and both for external and internal joints have been detailed. The resistance parameters and the stiffness coefficients have been reported in Tables 6.22-6.28 while the force – displacement curves are illustrated in Figs. 6.14-6.17.

- **HE 300 B – IPE 270 joint:**

**Table 6.22 – FREEDAM-CYC 01: Stiffness coefficients (HE300B – IPE 270) – UPPER SPRING**

<b>TENSILE PART</b>									
<i>BEFORE THE SLIPPAGE</i>									
	$k_{cfb}$ [mm]	$k_{tsb}$ [mm]	$k_{eq,t}$ [mm]	$S_t$ [kN/mm]					
		10.87	7.52	<b>1579</b>					
	24.39	8.41	6.25	<b>1313</b>					
		6.82	5.33	<b>1119</b>					
<i>AFTER THE SLIPPAGE</i>									
	$k_{cfb}$ [mm]	$k_{tsb}$ [mm]	$k_{eq,t}$ [mm]	$S_{t.1}$ [kN/mm]	$k_{Tswbe}$ [mm]	$k_{bfbe}$ [mm]	$k_{bs}$ [mm]	$k_{eq,t}$ [mm]	$S_{t.2}$ [kN/mm]
<b>INTERNAL AND EXTERNAL JOINTS</b>	24.39	6.82	5.33	<b>1119</b>					
	14.53	6.82	4.64	<b>975</b>					
	14.53	3.58	2.87	<b>603</b>					
	14.53	2.36	2.03	<b>427</b>					
	14.53	1.71	1.53	<b>321</b>					
	14.53	1.27	1.17	<b>245</b>	7.21	4.51	6.17	1.92	<b>402</b>
	14.53	0.99	0.93	<b>194</b>					
	14.53	0.81	0.77	<b>161</b>					
	14.53	0.67	0.64	<b>134</b>					
	14.53	0.55	0.53	<b>111</b>					
	14.53	0.46	0.44	<b>93</b>					
<b>COMPRESSIVE PART</b>									
<i>BEFORE THE SLIPPAGE</i>									
	$k_{cws}$ [mm]	$k_{cwc}$ [mm]	$k_{eq,c}$ [mm]	$S_c$ [kN/mm]					
<b>EXTERNAL JOINTS</b>	6.80		4.17	<b>876</b>					
<b>INTERNAL JOINTS</b>	3.40	10.79	2.59	<b>543</b>					
<i>AFTER THE SLIPPAGE</i>									
	$k_{cws}$ [mm]	$k_{cwc}$ [mm]	$k_{eq,c}$ [mm]	$S_{c.1}$ [kN/mm]	$k_{Tswbe}$ [mm]	$k_{bfbe}$ [mm]	$k_{bs}$ [mm]	$k_{eq,c}$ [mm]	$S_{c.2}$ [kN/mm]
<b>EXTERNAL JOINTS</b>	6.80		4.17	<b>876</b>					
<b>INTERNAL JOINTS</b>	3.40	10.79	2.59	<b>543</b>	7.21	4.51	6.17	1.92	<b>402</b>

*Robustness and seismic behaviour of structures equipped with traditional and innovative beam-to-column connections*

**Table 6.23** – FREEDAM-CYC 01: Resistance parameters (HE300B – IPE 270) – UPPER SPRING

<b>TENSILE PART</b>							
	$F_{cfb}$ [kN]	$F_{Tsb}$ [kN]	$F_{cwt}$ [kN]	$F_{Tswbe}$ [kN]	$F_{bfbe}$ [kN]	$F_{bs}$ [kN]	$F_t$ [kN]
<b>EXTERNAL JOINTS</b>			1565				<b>721</b>
<b>INTERNAL JOINTS</b>	1163	721		2130	1626	1350	<b>721</b>
<b>COMPRESSIVE PART</b>							
	$F_{cws}$ [kN]	$F_{cwc}$ [kN]	$F_{Tswbe}$ [kN]	$F_{bfbe}$ [kN]	$F_{bs}$ [kN]		$F_c$ [kN]
<b>EXTERNAL JOINTS</b>		2079					<b>1016</b>
<b>INTERNAL JOINTS</b>	1016	1696	2130	1626	1350		<b>1016</b>



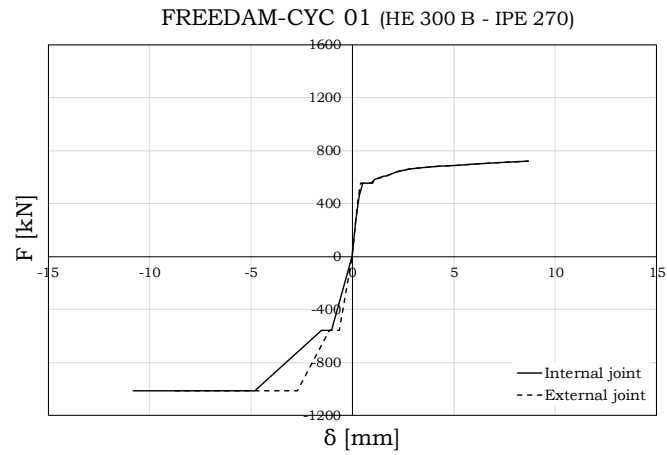
**Table 6.24** – FREEDAM-CYC 01: Stiffness coefficients (HE300B – IPE 270) – LOWER SPRING

<b>TENSILE PART</b>										
<i>BEFORE THE SLIPPAGE</i>										
	$k_{cfb}$ [mm]	$k_{Lsb}$ [mm]	$k_{eq,c}$ [mm]	$S_c$ [kN/mm]						
<b>INTERNAL AND EXTERNAL JOINTS</b>	24.39	13.73	8.78	<b>1845</b>						
		10.83	7.50	<b>1575</b>						
	<i>AFTER THE SLIPPAGE</i>									
		$k_{cfb}$ [mm]	$k_{Lsb}$ [mm]	$k_{eq,c}$ [mm]	$S_{c.1}$ [kN/mm]	$k_{Lswbe}$ [mm]	$k_{bfbe}$ [mm]	$k_{bs}$ [mm]	$k_{eq,t}$ [mm]	$S_{c.2}$ [kN/mm]
		24.39	10.83	7.50	<b>1575</b>					
		24.39	8.88	6.51	<b>1367</b>					
		14.53	8.88	5.51	<b>1157</b>					
		14.53	5.14	3.80	<b>797</b>					
		14.53	3.32	2.70	<b>568</b>					
		14.53	2.41	2.07	<b>435</b>	4.06	1.33	1.90	0.66	<b>138</b>
		14.53	1.79	1.59	<b>334</b>					
		14.53	1.40	1.28	<b>268</b>					
		14.53	1.13	1.05	<b>220</b>					
		14.53	0.92	0.87	<b>182</b>					
	14.53	0.77	0.73	<b>153</b>						
<b>COMPRESSIVE PART</b>										
<i>BEFORE THE SLIPPAGE</i>										
	$k_{cws}$ [mm]	$k_{cwc}$ [mm]	$k_{eq,c}$ [mm]	$S_c$ [kN/mm]						
<b>EXTERNAL JOINTS</b>	6.80	10.79	4.17	<b>876</b>						
<b>INTERNAL JOINTS</b>	3.40		2.59	<b>543</b>						
<i>AFTER THE SLIPPAGE</i>										
	$k_{cws}$ [mm]	$k_{cwc}$ [mm]	$k_{eq,c}$ [mm]	$S_{c.1}$ [kN/mm]	$k_{Lswbe}$ [mm]	$k_{bfbe}$ [mm]	$k_{bs}$ [mm]	$k_{eq,c}$ [mm]	$S_{c.2}$ [kN/mm]	
<b>EXTERNAL JOINTS</b>	6.80	10.79	4.17	<b>876</b>	4.06	1.33	1.90	0.66	<b>138</b>	
<b>INTERNAL JOINTS</b>	3.40		2.59	<b>543</b>						

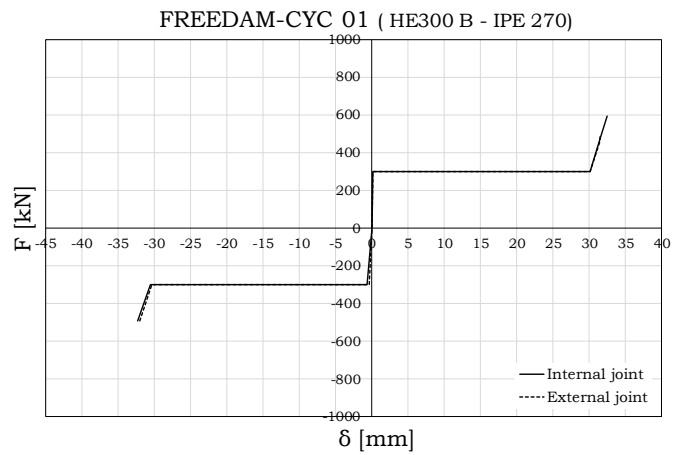
*Robustness and seismic behaviour of structures equipped with traditional and innovative beam-to-column connections*

**Table 6.25** – FREEDAM-CYC 01: Resistance parameters (HE300B – IPE 270) – LOWER SPRING

<b>TENSILE PART</b>							
	$F_{cfb}$ [kN]	$F_{tsb}$ [kN]	$F_{cwt}$ [kN]	$F_{tswbe}$ [kN]	$F_{bfbe}$ [kN]	$F_{bs}$ [kN]	$F_t$ [kN]
<b>EXTERNAL JOINTS</b>			1565				<b>765</b>
<b>INTERNAL JOINTS</b>	1163	765		816	564	492	<b>765</b>
<b>COMPRESSIVE PART</b>							
	$F_{cws}$ [kN]	$F_{cwc}$ [kN]	$F_{Tswbe}$ [kN]	$F_{bfbe}$ [kN]	$F_{bs}$ [kN]		$F_c$ [kN]
<b>EXTERNAL JOINTS</b>		2079					<b>1016</b>
<b>INTERNAL JOINTS</b>	1016	1696	816	564	492		<b>1016</b>



a)



b)

**Fig. 6.16** – FREEDAM-CYC 01: Force – displacement curve (HE300B – IPE 270); a) spring modelling the upper part; b) spring modelling the lower part

## - HE 280 B – IPE 270 joint:

**Table 6.26** – FREEDAM-CYC 01: Stiffness coefficients (HE280B – IPE 270) – UPPER SPRING

<b>TENSILE PART</b>									
<i>BEFORE THE SLIPPAGE</i>									
	$k_{cfb}$ [mm]	$k_{tsb}$ [mm]	$k_{eq,t}$ [mm]	$S_t$ [kN/mm]					
		10.87	7.30	<b>1533</b>					
	22.23	8.41	6.10	<b>1281</b>					
		6.82	5.22	<b>1096</b>					
<i>AFTER THE SLIPPAGE</i>									
	$k_{cfb}$ [mm]	$k_{tsb}$ [mm]	$k_{eq,t}$ [mm]	$S_{t.1}$ [kN/mm]	$k_{Tswbe}$ [mm]	$k_{bfbe}$ [mm]	$k_{bs}$ [mm]	$k_{eq,t}$ [mm]	$S_{t.2}$ [kN/mm]
<b>INTERNAL AND EXTERNAL JOINTS</b>	22.23	6.82	5.22	<b>1096</b>					
	11.97	6.82	4.34	<b>912</b>					
	11.97	3.58	2.75	<b>578</b>					
	11.97	2.36	1.97	<b>415</b>					
	11.97	1.71	1.49	<b>314</b>					
	11.97	1.27	1.15	<b>241</b>	7.21	4.51	6.17	1.92	<b>402</b>
	11.97	0.99	0.91	<b>192</b>					
	11.97	0.81	0.76	<b>159</b>					
	11.97	0.67	0.63	<b>132</b>					
	11.97	0.55	0.52	<b>110</b>					
	11.97	0.46	0.44	<b>92</b>					
<b>COMPRESSIVE PART</b>									
<i>BEFORE THE SLIPPAGE</i>									
	$k_{cws}$ [mm]	$k_{cwc}$ [mm]	$k_{eq,c}$ [mm]	$S_c$ [kN/mm]					
<b>EXTERNAL JOINTS</b>	5.90	10.60	3.79	<b>796</b>					
<b>INTERNAL JOINTS</b>	2.95		2.31	<b>485</b>					
<i>AFTER THE SLIPPAGE</i>									
	$k_{cws}$ [mm]	$k_{cwc}$ [mm]	$k_{eq,c}$ [mm]	$S_{c.1}$ [kN/mm]	$k_{Tswbe}$ [mm]	$k_{bfbe}$ [mm]	$k_{bs}$ [mm]	$k_{eq,c}$ [mm]	$S_{c.2}$ [kN/mm]
<b>EXTERNAL JOINTS</b>	5.90	10.60	3.79	<b>796</b>	7.21	4.51	6.17	1.92	<b>402</b>
<b>INTERNAL JOINTS</b>	2.95		2.31	<b>485</b>					

*Robustness and seismic behaviour of structures equipped with traditional and innovative beam-to-column connections*

**Table 6.27** – FREEDAM-CYC 01: Resistance parameters (HE280B – IPE 270) – UPPER SPRING

<b>TENSILE PART</b>							
	$F_{cfb}$ [kN]	$F_{Tsb}$ [kN]	$F_{cwt}$ [kN]	$F_{Tswbe}$ [kN]	$F_{bfbe}$ [kN]	$F_{bs}$ [kN]	$F_t$ [kN]
<b>EXTERNAL JOINTS</b>			1599				<b>721</b>
<b>INTERNAL JOINTS</b>	1064	721		2130	1626	1350	<b>721</b>
			1266				
<b>COMPRESSIVE PART</b>							
	$F_{cws}$ [kN]	$F_{cwc}$ [kN]	$F_{Tswbe}$ [kN]	$F_{bfbe}$ [kN]	$F_{bs}$ [kN]		$F_c$ [kN]
<b>EXTERNAL JOINTS</b>		1881					<b>876</b>
<b>INTERNAL JOINTS</b>	876		2130	1626	1350		<b>876</b>
		1539					

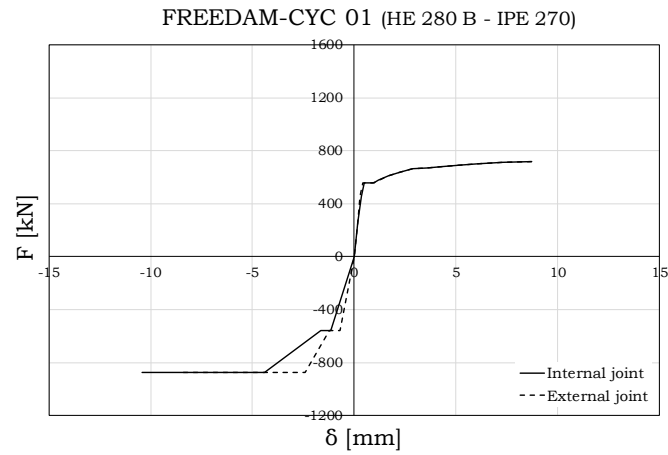
**Table 6.28** – FREEDAM-CYC 01: Stiffness coefficients (HE280B – IPE 270) – LOWER SPRING

<b>TENSILE PART</b>									
<i>BEFORE THE SLIPPAGE</i>									
	$k_{cfb}$ [mm]	$k_{Lsb}$ [mm]	$k_{eq,c}$ [mm]	$S_c$ [kN/mm]					
	22.23	13.73	8.49	<b>1782</b>					
		10.83	7.28	<b>1529</b>					
<i>AFTER THE SLIPPAGE</i>									
	$k_{cfb}$ [mm]	$k_{Lsb}$ [mm]	$k_{eq,c}$ [mm]	$S_{c.1}$ [kN/mm]	$k_{Lsube}$ [mm]	$k_{bfbe}$ [mm]	$k_{bs}$ [mm]	$k_{eq,t}$ [mm]	$S_{c.2}$ [kN/mm]
<b>INTERNAL AND EXTERNAL JOINTS</b>	22.23	10.83	7.28	<b>1529</b>					
	22.23	8.88	6.34	<b>1332</b>					
	11.97	5.14	5.10	<b>1071</b>					
	11.97	5.14	3.60	<b>755</b>					
	11.97	3.32	2.60	<b>546</b>					
	11.97	2.41	2.01	<b>422</b>					
	11.97	1.79	1.55	<b>326</b>	4.06	1.33	1.90	0.66	<b>138</b>
	11.97	1.40	1.25	<b>263</b>					
	11.97	1.13	1.03	<b>217</b>					
	11.97	0.92	0.86	<b>180</b>					
	11.97	0.77	0.72	<b>151</b>					
	11.97	0.63	0.60	<b>126</b>					
	11.97	0.52	0.50	<b>105</b>					
<b>COMPRESSIVE PART</b>									
<i>BEFORE THE SLIPPAGE</i>									
	$k_{cws}$ [mm]	$k_{cwc}$ [mm]	$k_{eq,c}$ [mm]	$S_c$ [kN/mm]					
<b>EXTERNAL JOINTS</b>	5.90	7.98	3.39	<b>712</b>					
<b>INTERNAL JOINTS</b>	2.95		2.15	<b>452</b>					
<i>AFTER THE SLIPPAGE</i>									
	$k_{cws}$ [mm]	$k_{cwc}$ [mm]	$k_{eq,c}$ [mm]	$S_{c.1}$ [kN/mm]	$k_{Lsube}$ [mm]	$k_{bfbe}$ [mm]	$k_{bs}$ [mm]	$k_{eq,c}$ [mm]	$S_{c.2}$ [kN/mm]
<b>EXTERNAL JOINTS</b>	5.90	7.98	3.39	<b>712</b>	4.06	1.33	1.90	0.66	<b>138</b>
<b>INTERNAL JOINTS</b>	2.95		2.15	<b>452</b>					

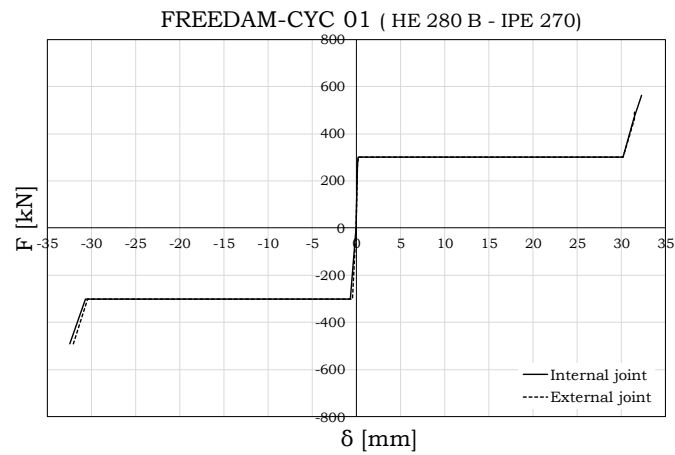
*Robustness and seismic behaviour of structures equipped with traditional and innovative beam-to-column connections*

**Table 6.29** – FREEDAM-CYC 01: Resistance parameters (HE280B – IPE 270) – LOWER SPRING

<b>TENSILE PART</b>							
	$F_{cfb}$ [kN]	$F_{tsb}$ [kN]	$F_{cwt}$ [kN]	$F_{tswbe}$ [kN]	$F_{bfbe}$ [kN]	$F_{bs}$ [kN]	$F_t$ [kN]
<b>EXTERNAL JOINTS</b>			1599				<b>492</b>
<b>INTERNAL JOINTS</b>	1147	876		816	564	492	<b>492</b>
			1266				
<b>COMPRESSIVE PART</b>							
	$F_{cws}$ [kN]	$F_{cwc}$ [kN]	$F_{Tswbe}$ [kN]	$F_{bfbe}$ [kN]	$F_{bs}$ [kN]		$F_c$ [kN]
<b>EXTERNAL JOINTS</b>		2069					<b>492</b>
<b>INTERNAL JOINTS</b>	876		816	564	492		<b>492</b>
		1592					



a)



b)

**Fig. 6.17** – FREEDAM-CYC 01: Force – displacement curve (HE280B – IPE 270); a) spring modelling the upper part; b) spring modelling the lower part



- **HE 260 B – IPE 270 joint:**

**Table 6.30** FREEDAM-CYC 01: Stiffness coefficients (HE260B – IPE 270) – UPPER SPRING

<b>TENSILE PART</b>									
<i>BEFORE THE SLIPPAGE</i>									
	$k_{cfb}$ [mm]	$k_{tsb}$ [mm]	$k_{eq,t}$ [mm]	$S_t$ [kN/mm]					
		10.87	7.25	<b>1523</b>					
	21.82	8.41	6.07	<b>1275</b>					
		6.82	5.20	<b>1091</b>					
<i>AFTER THE SLIPPAGE</i>									
	$k_{cfb}$ [mm]	$k_{tsb}$ [mm]	$k_{eq,t}$ [mm]	$S_{t.1}$ [kN/mm]	$k_{Tsube}$ [mm]	$k_{bfe}$ [mm]	$k_{bs}$ [mm]	$k_{eq,t}$ [mm]	$S_{t.2}$ [kN/mm]
<b>INTERNAL AND EXTERNAL JOINTS</b>		6.82	4.31	<b>904</b>					
			3.58	<b>575</b>					
			2.36	<b>413</b>					
			1.71	<b>313</b>					
		11.68	1.27	<b>241</b>	7.21	4.51	6.17	1.92	<b>402</b>
			0.99	<b>192</b>					
			0.81	<b>159</b>					
			0.67	<b>132</b>					
			0.55	<b>110</b>					
			0.46	<b>92</b>					
<b>COMPRESSIVE PART</b>									
<i>BEFORE THE SLIPPAGE</i>									
	$k_{cws}$ [mm]	$k_{cwc}$ [mm]	$k_{eq,c}$ [mm]	$S_c$ [kN/mm]					
<b>EXTERNAL JOINTS</b>	5.38		3.61	<b>758</b>					
<b>INTERNAL JOINTS</b>	2.69	10.95	2.16	<b>454</b>					
<i>AFTER THE SLIPPAGE</i>									
	$k_{cws}$ [mm]	$k_{cwc}$ [mm]	$k_{eq,c}$ [mm]	$S_{c.1}$ [kN/mm]	$k_{Tsube}$ [mm]	$k_{bfe}$ [mm]	$k_{bs}$ [mm]	$k_{eq,c}$ [mm]	$S_{c.2}$ [kN/mm]
<b>EXTERNAL JOINTS</b>	5.38		3.61	<b>758</b>	7.21	4.51	6.17	1.92	<b>402</b>
<b>INTERNAL JOINTS</b>	2.69	10.95	2.16	<b>454</b>					

*Robustness and seismic behaviour of structures equipped with traditional and innovative beam-to-column connections*

**Table 6.31** – FREEDAM-CYC 01: Resistance parameters (HE260B – IPE 270) – UPPER SPRING

<b>TENSILE PART</b>							
	$F_{cfb}$ [kN]	$F_{Tsb}$ [kN]	$F_{cwt}$ [kN]	$F_{Tswbe}$ [kN]	$F_{bfbe}$ [kN]	$F_{bs}$ [kN]	$F_t$ [kN]
<b>EXTERNAL JOINTS</b>			1521				<b>721</b>
<b>INTERNAL JOINTS</b>	1036	721		2130	1626	1350	<b>721</b>
			1185				
<b>COMPRESSIVE PART</b>							
	$F_{cws}$ [kN]	$F_{cwc}$ [kN]	$F_{Tswbe}$ [kN]	$F_{bfbe}$ [kN]	$F_{bs}$ [kN]		$F_c$ [kN]
<b>EXTERNAL JOINTS</b>		1737					<b>795</b>
<b>INTERNAL JOINTS</b>	795		2130	1626	1350		<b>795</b>
		1410					

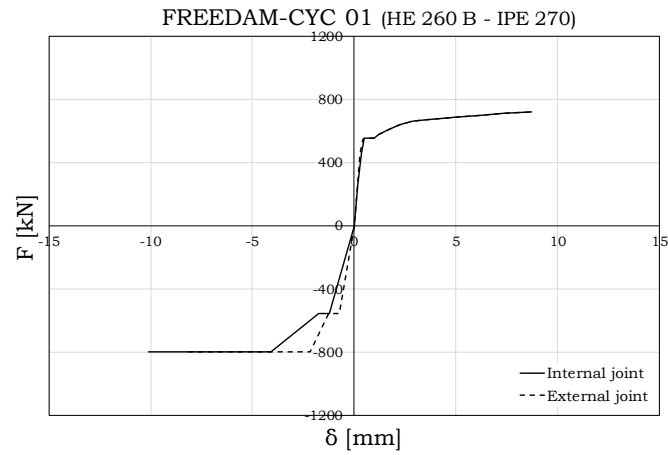
**Table 6.32** – FREEDAM-CYC 01: Stiffness coefficients (HE260B – IPE 270) – LOWER SPRING

<b>TENSILE PART</b>									
<i>BEFORE THE SLIPPAGE</i>									
	$k_{cfb}$ [mm]	$k_{Lsb}$ [mm]	$k_{eq,t}$ [mm]	$S_t$ [kN/mm]					
	21.82	13.73	8.43	<b>1770</b>					
		10.83	7.24	<b>1520</b>					
<i>AFTER THE SLIPPAGE</i>									
	$k_{cfb}$ [mm]	$k_{Lsb}$ [mm]	$k_{eq,t}$ [mm]	$S_{t.1}$ [kN/mm]	$k_{Lsube}$ [mm]	$k_{bfbe}$ [mm]	$k_{bs}$ [mm]	$k_{eq,t}$ [mm]	$S_{t.2}$ [kN/mm]
<b>INTERNAL AND EXTERNAL JOINTS</b>	21.82	10.83	7.24	<b>1520</b>					
	21.82	8.88	6.31	<b>1325</b>					
	11.68	5.14	5.04	<b>1059</b>					
	11.68	5.14	3.57	<b>750</b>					
	11.68	3.32	2.59	<b>543</b>					
	11.68	2.41	2.00	<b>420</b>					
	11.68	1.79	1.55	<b>325</b>	4.06	1.33	1.90	0.66	<b>138</b>
	11.68	1.40	1.25	<b>262</b>					
	11.68	1.13	1.03	<b>216</b>					
	11.68	0.92	0.86	<b>180</b>					
	11.68	0.77	0.72	<b>151</b>					
	11.68	0.63	0.60	<b>126</b>					
11.68	0.52	0.50	<b>104</b>						
<b>COMPRESSIVE PART</b>									
<i>BEFORE THE SLIPPAGE</i>									
	$k_{cws}$ [mm]	$k_{cwc}$ [mm]	$k_{eq,c}$ [mm]	$S_c$ [kN/mm]					
<b>EXTERNAL JOINTS</b>	5.38	8.17	3.25	<b>681</b>					
<b>INTERNAL JOINTS</b>	2.69		2.02	<b>425</b>					
<i>AFTER THE SLIPPAGE</i>									
	$k_{cws}$ [mm]	$k_{cwc}$ [mm]	$k_{eq,c}$ [mm]	$S_{c.1}$ [kN/mm]	$k_{Lsube}$ [mm]	$k_{bfbe}$ [mm]	$k_{bs}$ [mm]	$k_{eq,c}$ [mm]	$S_{c.2}$ [kN/mm]
<b>EXTERNAL JOINTS</b>	5.38	8.17	3.25	<b>681</b>	4.06	1.33	1.90	0.66	<b>138</b>
<b>INTERNAL JOINTS</b>	2.69		2.02	<b>425</b>					

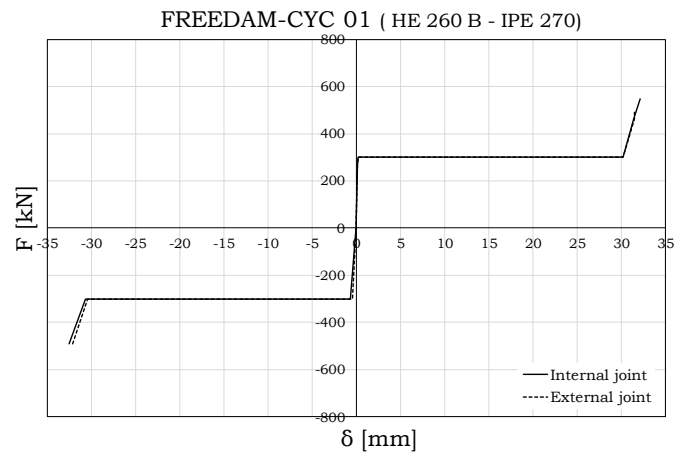
*Robustness and seismic behaviour of structures equipped with traditional and innovative beam-to-column connections*

**Table 6.33** – FREEDAM-CYC 01: Resistance parameters (HE260B – IPE 270) – LOWER SPRING

<b>TENSILE PART</b>							
	$F_{cfb}$ [kN]	$F_{tsb}$ [kN]	$F_{cwt}$ [kN]	$F_{tswbe}$ [kN]	$F_{bfbe}$ [kN]	$F_{bs}$ [kN]	$F_t$ [kN]
<b>EXTERNAL JOINTS</b>			1521				<b>492</b>
<b>INTERNAL JOINTS</b>	1036	765		816	564	492	<b>492</b>
			1185				
<b>COMPRESSIVE PART</b>							
	$F_{cws}$ [kN]	$F_{cwc}$ [kN]	$F_{Tswbe}$ [kN]	$F_{bfbe}$ [kN]	$F_{bs}$ [kN]		$F_c$ [kN]
<b>EXTERNAL JOINTS</b>		1912					<b>492</b>
<b>INTERNAL JOINTS</b>	795		816	564	492		<b>492</b>
		1458					



a)



b)

**Fig. 6.18** – FREEDAM-CYC 01: Force – displacement curve (HE260B – IPE 270); a) spring modelling the upper part; b) spring modelling the lower part

- **HE 220 B – IPE 270 joint:****Table 6.34** FREEDAM-CYC 01: Stiffness coefficients (HE220B – IPE 270) – UPPER SPRING

<b>TENSILE PART</b>										
<i>BEFORE THE SLIPPAGE</i>										
	$k_{cfb}$ [mm]	$k_{tsb}$ [mm]	$k_{eq,t}$ [mm]	$S_t$ [kN/mm]						
		10.87	6.85	<b>1438</b>						
	18.51	8.41	5.78	<b>1214</b>						
		6.82	4.98	<b>1047</b>						
<i>AFTER THE SLIPPAGE</i>										
	$k_{cfb}$ [mm]	$k_{tsb}$ [mm]	$k_{eq,t}$ [mm]	$S_{t.1}$ [kN/mm]	$k_{Tsube}$ [mm]	$k_{bfe}$ [mm]	$k_{bs}$ [mm]	$k_{eq,t}$ [mm]	$S_{t.2}$ [kN/mm]	
<b>INTERNAL AND EXTERNAL JOINTS</b>		6.82	3.86	<b>810</b>						
			3.58	<b>535</b>						
			2.36	<b>392</b>						
			1.71	<b>301</b>						
		8.88	1.27	1.11	<b>233</b>	7.21	4.51	6.17	1.92	<b>402</b>
			0.99	0.89	<b>187</b>					
			0.81	0.74	<b>156</b>					
			0.67	0.62	<b>130</b>					
			0.55	0.52	<b>109</b>					
			0.46	0.43	<b>91</b>					
<b>COMPRESSIVE PART</b>										
<i>BEFORE THE SLIPPAGE</i>										
	$k_{cws}$ [mm]	$k_{cwc}$ [mm]	$k_{eq,c}$ [mm]	$S_c$ [kN/mm]						
<b>EXTERNAL JOINTS</b>	4.00		2.96	<b>622</b>						
<b>INTERNAL JOINTS</b>	2.00	11.39	1.70	<b>358</b>						
<i>AFTER THE SLIPPAGE</i>										
	$k_{cws}$ [mm]	$k_{cwc}$ [mm]	$k_{eq,c}$ [mm]	$S_{c.1}$ [kN/mm]	$k_{Tsube}$ [mm]	$k_{bfe}$ [mm]	$k_{bs}$ [mm]	$k_{eq,c}$ [mm]	$S_{c.2}$ [kN/mm]	
<b>EXTERNAL JOINTS</b>	4.00		2.96	<b>622</b>	7.21	4.51	6.17	1.92	<b>402</b>	
<b>INTERNAL JOINTS</b>	2.00	11.39	1.70	<b>358</b>						

*Robustness and seismic behaviour of structures equipped with traditional and innovative beam-to-column connections*

**Table 6.35** – FREEDAM-CYC 01: Resistance parameters (HE220B – IPE 270) – UPPER SPRING

<b>TENSILE PART</b>							
	$F_{cfb}$ [kN]	$F_{Tsb}$ [kN]	$F_{cwt}$ [kN]	$F_{Tswbe}$ [kN]	$F_{bfbe}$ [kN]	$F_{bs}$ [kN]	$F_t$ [kN]
<b>EXTERNAL JOINTS</b>			1513				<b>721</b>
<b>INTERNAL JOINTS</b>	934	721		2130	1626	1350	<b>721</b>
			1030				
<b>COMPRESSIVE PART</b>							
	$F_{cws}$ [kN]	$F_{cwc}$ [kN]	$F_{Tswbe}$ [kN]	$F_{bfbe}$ [kN]	$F_{bs}$ [kN]		$F_c$ [kN]
<b>EXTERNAL JOINTS</b>		1420					<b>795</b>
<b>INTERNAL JOINTS</b>	556		2130	1626	1350		<b>795</b>
		1147					

**Table 6.36** – FREEDAM-CYC 01: Stiffness coefficients (HE220B – IPE 270) – LOWER SPRING

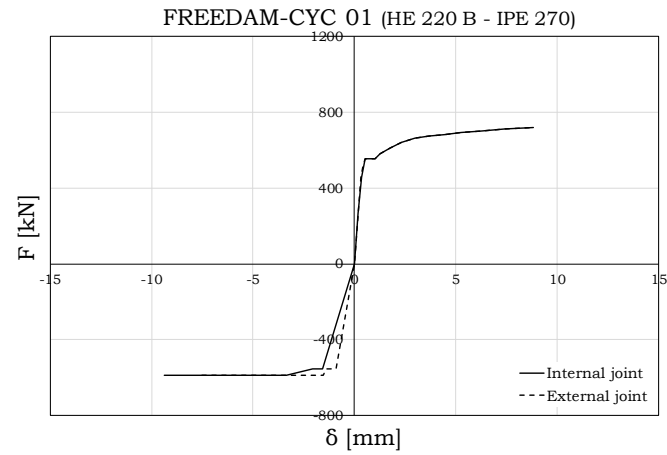
<b>TENSILE PART</b>									
<i>BEFORE THE SLIPPAGE</i>									
	$k_{cfb}$ [mm]	$k_{Lsb}$ [mm]	$k_{eq,t}$ [mm]	$S_t$ [kN/mm]					
	18.51	13.73	7.88	<b>1655</b>					
		10.83	6.83	<b>1435</b>					
<i>AFTER THE SLIPPAGE</i>									
	$k_{cfb}$ [mm]	$k_{Lsb}$ [mm]	$k_{eq,t}$ [mm]	$S_{t.1}$ [kN/mm]	$k_{Lsube}$ [mm]	$k_{bfbe}$ [mm]	$k_{bs}$ [mm]	$k_{eq,t}$ [mm]	$S_{t.2}$ [kN/mm]
<b>INTERNAL AND EXTERNAL JOINTS</b>	18.51	10.83	6.83	<b>1435</b>					
	18.51	8.88	6.00	<b>1260</b>					
	8.95	5.14	4.46	<b>936</b>					
	8.95	5.14	3.26	<b>686</b>					
	8.95	3.32	2.42	<b>509</b>					
	8.95	2.41	1.90	<b>399</b>					
	8.95	1.79	1.49	<b>313</b>	4.06	1.33	1.90	0.66	<b>138</b>
	8.95	1.40	1.21	<b>254</b>					
	8.95	1.13	1.00	<b>210</b>					
	8.95	0.92	0.84	<b>176</b>					
	8.95	0.77	0.71	<b>148</b>					
	8.95	0.63	0.59	<b>124</b>					
	8.95	0.52	0.49	<b>103</b>					
<b>COMPRESSIVE PART</b>									
<i>BEFORE THE SLIPPAGE</i>									
	$k_{cws}$ [mm]	$k_{cwc}$ [mm]	$k_{eq,c}$ [mm]	$S_c$ [kN/mm]					
<b>EXTERNAL JOINTS</b>	4.00	7.96	2.66	<b>559</b>					
<b>INTERNAL JOINTS</b>	2.00		1.60	<b>336</b>					
<i>AFTER THE SLIPPAGE</i>									
	$k_{cws}$ [mm]	$k_{cwc}$ [mm]	$k_{eq,c}$ [mm]	$S_{c.1}$ [kN/mm]	$k_{Lsube}$ [mm]	$k_{bfbe}$ [mm]	$k_{bs}$ [mm]	$k_{eq,c}$ [mm]	$S_{c.2}$ [kN/mm]
<b>EXTERNAL JOINTS</b>	4.00	7.96	2.66	<b>559</b>	4.06	1.33	1.90	0.66	<b>138</b>
<b>INTERNAL JOINTS</b>	2.00		1.60	<b>336</b>					

*Robustness and seismic behaviour of structures equipped with traditional and innovative beam-to-column connections*

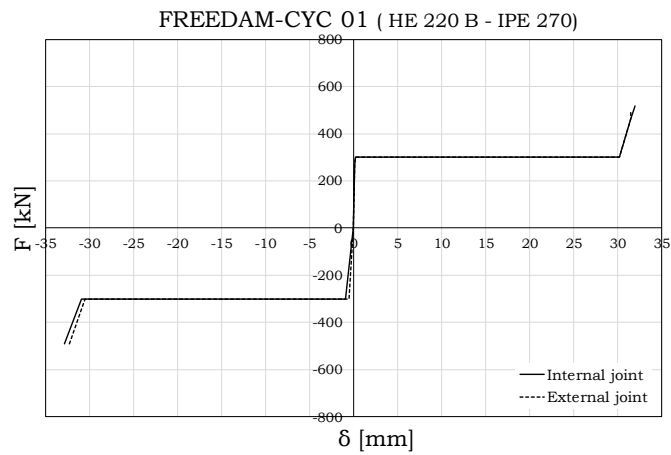


**Table 6.37** – FREEDAM-CYC 01: Resistance parameters (HE220B – IPE 270) – LOWER SPRING

<b>TENSILE PART</b>							
	$F_{cfb}$ [kN]	$F_{tsb}$ [kN]	$F_{cwt}$ [kN]	$F_{tswbe}$ [kN]	$F_{bfbe}$ [kN]	$F_{bs}$ [kN]	$F_t$ [kN]
<b>EXTERNAL JOINTS</b>			1521				<b>492</b>
<b>INTERNAL JOINTS</b>	943	765		816	564	492	<b>492</b>
			1030				
<b>COMPRESSIVE PART</b>							
	$F_{cws}$ [kN]	$F_{cwc}$ [kN]	$F_{Tswbe}$ [kN]	$F_{bfbe}$ [kN]	$F_{bs}$ [kN]		$F_c$ [kN]
<b>EXTERNAL JOINTS</b>		1570					<b>492</b>
<b>INTERNAL JOINTS</b>	795		816	564	492		<b>492</b>
		1184					



a)



b)

**Fig. 6.19** – FREEDAM-CYC 01: Force – displacement curve (HE220B – IPE 270); a) spring modelling the upper part; b) spring modelling the lower part

## 6.4. Analyses of frames under exceptional loads

Generally, the robustness analyses of structures subjected to a loss-of-column scenario are performed removing one or several primary elements and then analysing the capability of the structure to absorb the damage [22]. Different methods for analysing the progressive collapse are available [23]: linear-elastic static, nonlinear static, linear-elastic dynamic and nonlinear dynamic procedures. In the former method, the structure is analysed in elastic range under amplified combination of loads and the structural response is evaluated in terms of ratios between demands capacities; however, this kind of analysis is limited to the structures whose dynamic and nonlinear behaviour is easily predictable. Although the linear-elastic dynamic analyses and even more the nonlinear ones are very accurate, they are usually avoided due to their complexity and because the evaluation and the comparison of the results are very time-consuming. Therefore, the nonlinear static analyses represent the most approach for robustness analyses which are able to take into account the nonlinear effects and allow to the determination of the elastic and failure limits of the structure. The capacity of the damaged structure is evaluated in terms of overload factor  $\lambda$  corresponding to the occurrence of the first failure in the structure. This approach, often called pushdown analyses, has been followed in this paper in order to assess the robustness of study case frames.

According to the seismic design, in MRFs the energy dissipation is concentrated in some zones of members that are engaged in plastic range so that they have been properly detailed.

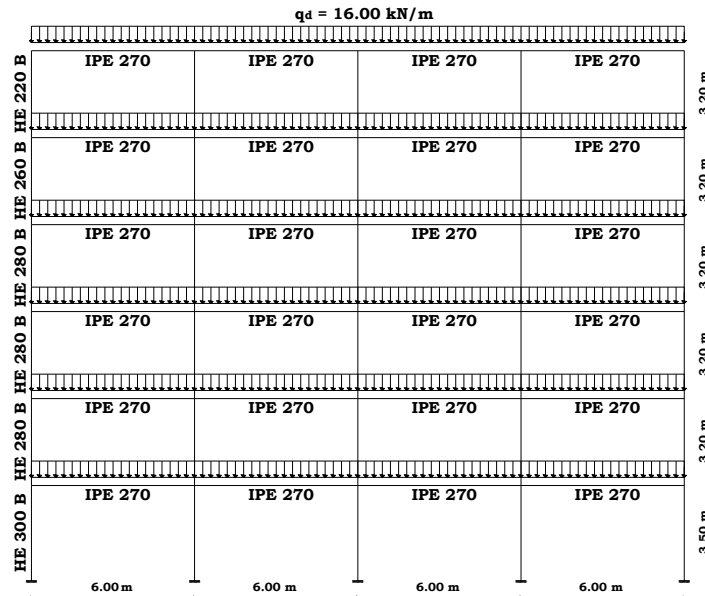


**Fig. 6.20** – Analysed structural scheme: initial conditions

The structural typologies herein investigated is a MRF designed according to the theory of plastic mechanism control detailed in the previous chapter. This design procedure is based on rigid-plastic analysis and on the kinematic theorem of plastic collapse extended to the concept of mechanism equilibrium curve [24-27].

Regarding the design loads, as described in the previous chapter, a uniform dead load  $G_k = 12.00 \text{ kN/m}$  and a uniform live load  $Q_k = 6 \text{ kN/m}$  have been considered. In order to perform pushdown analyses, the design vertical load distribution has been determined in accordance with the accidental load combination, i.e.  $q = G_k + Q_k = 18.00 \text{ kN/m}$  (Fig.6.18).

The structure has been modelled and analysed in SAP 2000 analysis software [1] (Fig.6.19).

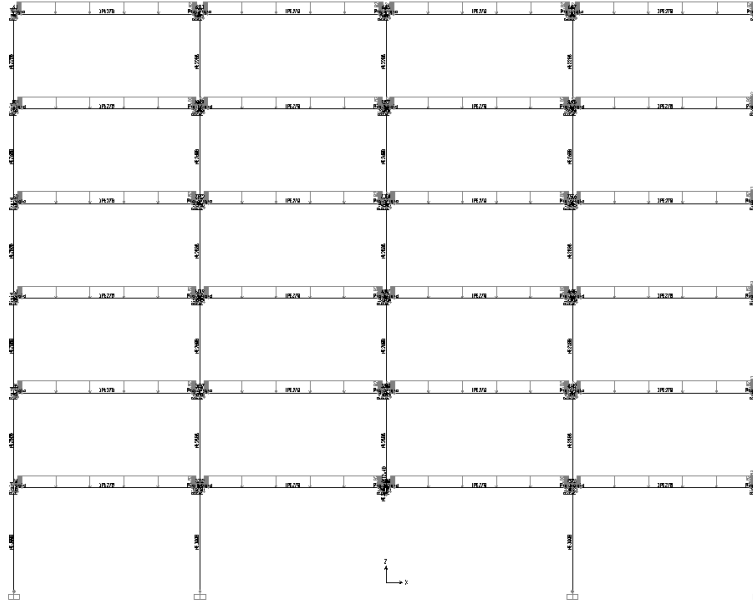


**Fig. 6.21** – Analysed MRF: SAP2000 model

The model is conceived to account for both material and geometrical nonlinearities. With reference to the members, they have been modelled by means of *frame* adopting a lumped plasticity approach: both for beams and columns a plastic hinges accounting for the M-N interaction [28], defined according to European code [3], have been considered.

It should be underlined that an accurate model, such as a *fibre plastic hinge*, of the plastic hinges modelling the beam behaviour when subjected to combined large axial load and bending moment should be considered. However, aiming to the comparison among the robustness performances of MRFs, this limitation could be acceptable.

Beam-to-column connections have been modelled by means of *link elements* connected by *rigid frame* accounting for the stiffening effect of the beam web and the distance between the axis of the beam flange in

tension and the centre of compression, i.e. the lever arm  $z$  (Fig.6.20) according to the simplified method proposed by the Eurocode 3 [4].

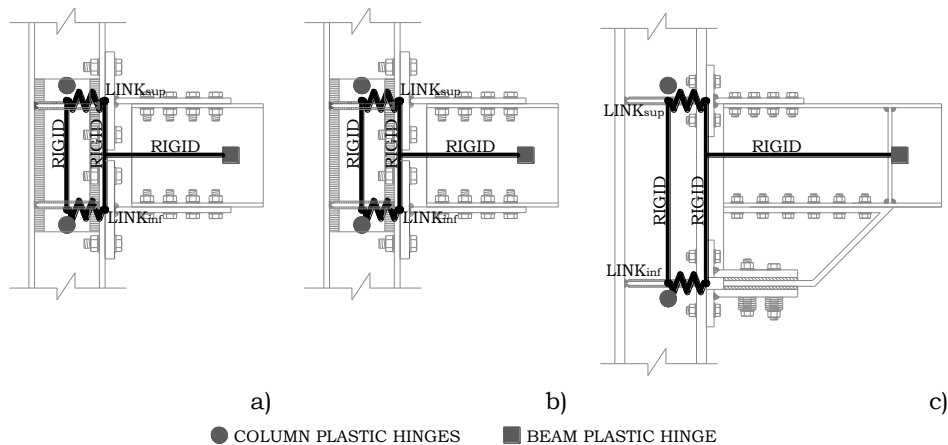


**Fig. 6.22** – Bolted joint' structural scheme: a) dogbone connection; b) tee-stub connections; c) FREEDAM connections

In particular, in the analysed connections, this assumption is acceptable because the bolt-rows in tension are close enough and symmetric with respect to the beam flange or the T-stub web.

## 6.5. Results of the Pushdown analyses

For the pushdown analyses, the internal force distribution in the element to be removed, i.e. the central column at the first storey, has been initially determined and the column element has been replaced by the equivalent axial reaction  $F_{stat}$  (Fig. 6.21). Subsequently, the pushdown curve has been obtained by increasing vertical displacements of the node to which equivalent column reaction force has been applied.

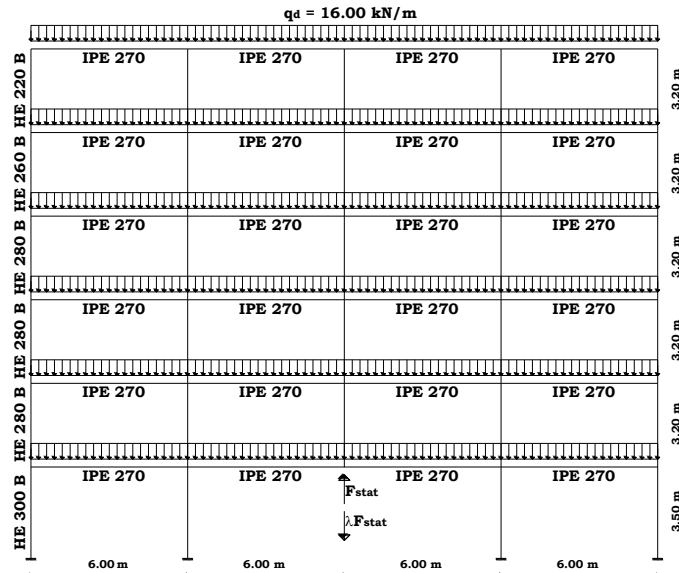


**Fig. 6.23** – Analysed structural scheme: pushdown configuration

In detail, a force  $\lambda F$ , acting in the opposite direction, has been applied in this node (Fig.6.21) to simulate the gradual loss of the column. A value of  $\lambda$  equal to 0 corresponds to the presence of the column while a value of  $\lambda$  equal or greater than 1 points the total loss of the column.

The typical curve representing the evolution of the vertical displacements according to the progressively remove of the column, is reported in Fig.6.22.

In particular, 3 phases can be recognized [29,30]: the first phase corresponds the elastic behaviour; the second phase begins when the first plastic hinge axis; the third phase starts when actions in the collapsed column reach the zero value. In the last phase high deformations and second order effect became very important factors to

be taken into account and catenary effects develop in the beams of the directly affected part.

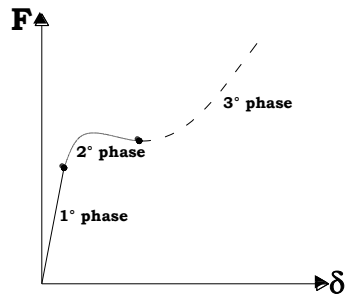


**Fig. 6.24** – Push-down curve

With the aim to compare the structural performance of the MRFs analysed by varying the beam-to-column detail, the Residual Resistance Strength Ratio has been determined. This parameter has been evaluated starting from the energy balance method proposed by Izzudin et al. [13]. Following this approach, the energy conservation has been used in order to estimate the maximum dynamic response starting from the static response obtained by means of nonlinear analyses as the pushdown ones. In particular, in order to take into account the inertial and nonlinear effects, a **Dynamic Load Factor** (DLF) can be expressed as:

$$DLF = \frac{F_{dyn,dam}}{F_{stat}} \quad (6.3)$$

where  $F_{dyn,dam}$  is the equivalent amplified force for which the system reaches equilibrium in the damage state and  $F_{stat}$  is the value of the static gravity loads on the resisting element before to notional removal (Fig. 6.23).



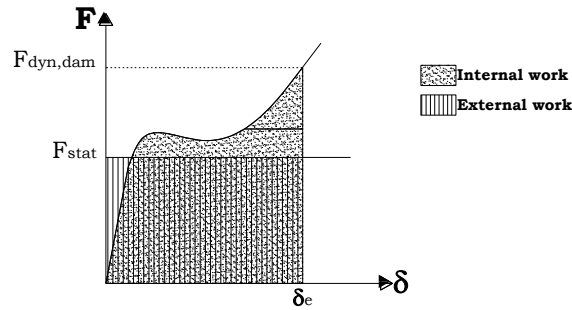


**Fig. 6.25** – Nonlinear structural response

It is necessary to evaluate the internal and the external work in order to determine the right value of the DLF for each structural configuration analysed. The internal work is given by:

$$\text{Internal Work} = F_{stat} \cdot \delta_i \quad (6.4)$$

while the external work is computed as:

$$\text{External Work} = \int_0^{\delta_i} F(\delta) \cdot d\delta \quad (6.5)$$

When the internal work is equal to the external one, the equilibrium in the damage state is achieved. Determined the dynamic load factor, the **Residual Reserve Strength Ratio** (RRSR) of the structure has been calculated as:

$$\text{RRSR} = \frac{F_{u,dam}}{F_{dyn,dam}} \quad (6.6)$$

Where  $F_{u,dam}$  is the ultimate capacity of the structural system in the damaged configuration that has been evaluated in correspondence of achievement of the ultimate resistance of the weakest component, whether it is a nodal component or the end of the beam.

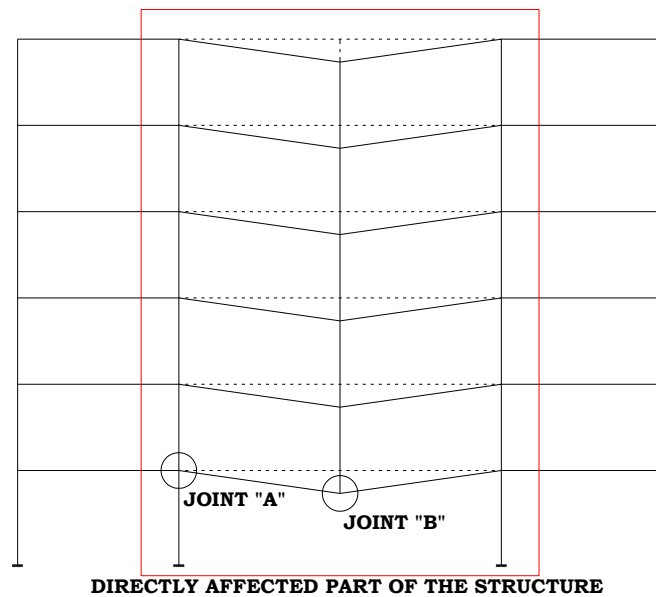
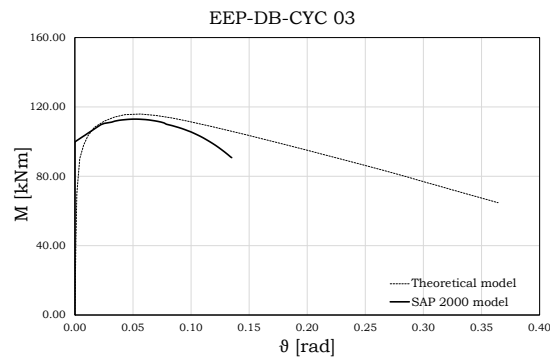


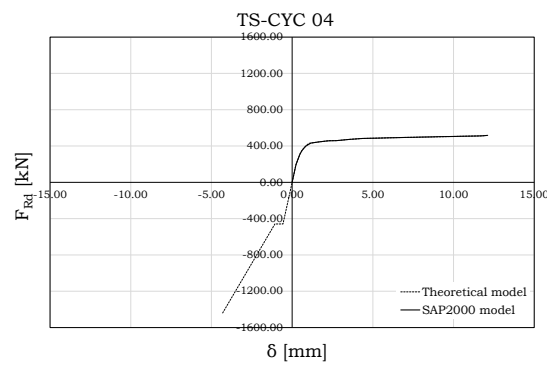
**Fig. 6.26** – Analysed beam-to-column connections of the directly affected structure

With reference to the directly affected part of the structures (Fig. 6.24), the force-displacement curves of the most stressed beam-to-column joints have reported for each performed analysis. In particular, the monitored joint “A” is subjected to the hogging moment whose value increases when the column fails while the joint “B” is subjected to hogging moment when the vertical distributed load are applied and to sagging moment in the loss-of-column scenario. In order to evaluate the ultimate capacity of the structural system in the damaged

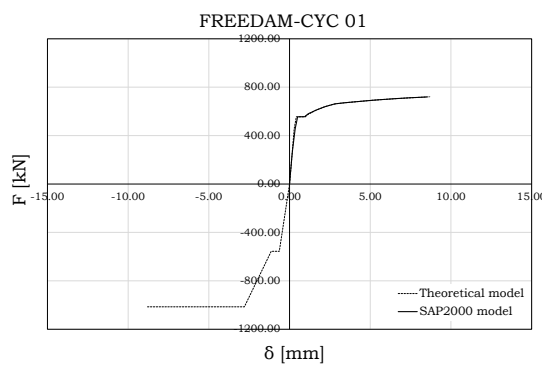
configuration, the ultimate behaviour of the weakest component for each joint typology has been achieved.



a)



b)



c)

**Fig. 6.27** – Achievement of the ultimate conditions: a) EEP-DB-CYC 03; b) TS-CYC 04; c) FREEDAM-CYC 01

Actually, in case of EEP-DB-CYC 03 connection the ultimate rotation provided by the beam is not reached (Fig. 6.25a) because the analyses has been stopped when the non directly affected part of the structure has been interested by the development of plastic hinges in the beam ends but also in the first storey columns (Fig.26). In case of TS-CYC 04 (Fig. 6.25b) and FREEDAM-CYC 01 (Fig. 6.25c) connections the ultimate conditions are represented by the achievement of the ultimate displacement of the upper T-stub.

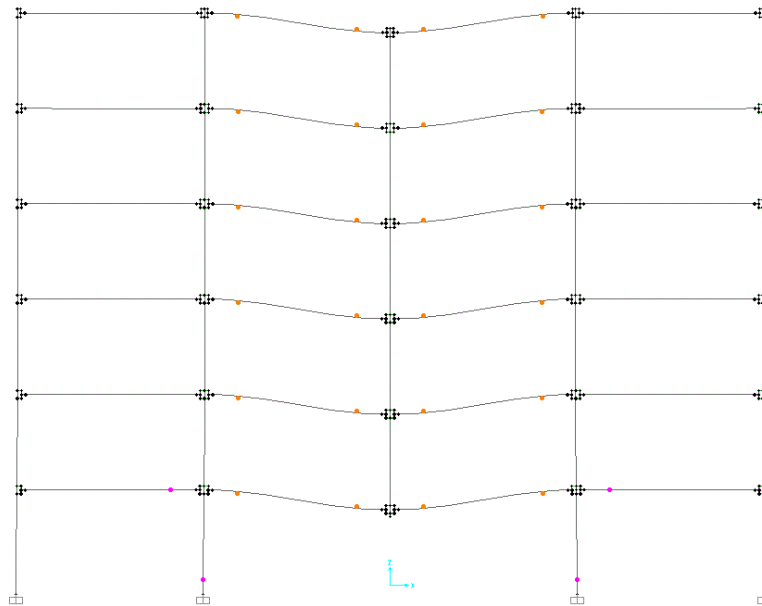


**Fig. 6.28** – Analysed structural scheme equipped with EEP-DB-CYC 03 in the damaged configuration

The obtained results in terms of  $F-\delta$  curve are depicted in Fig. 6.27. The circular markers on the curves represent the static force while the square markets represent the equivalent dynamically amplified force.

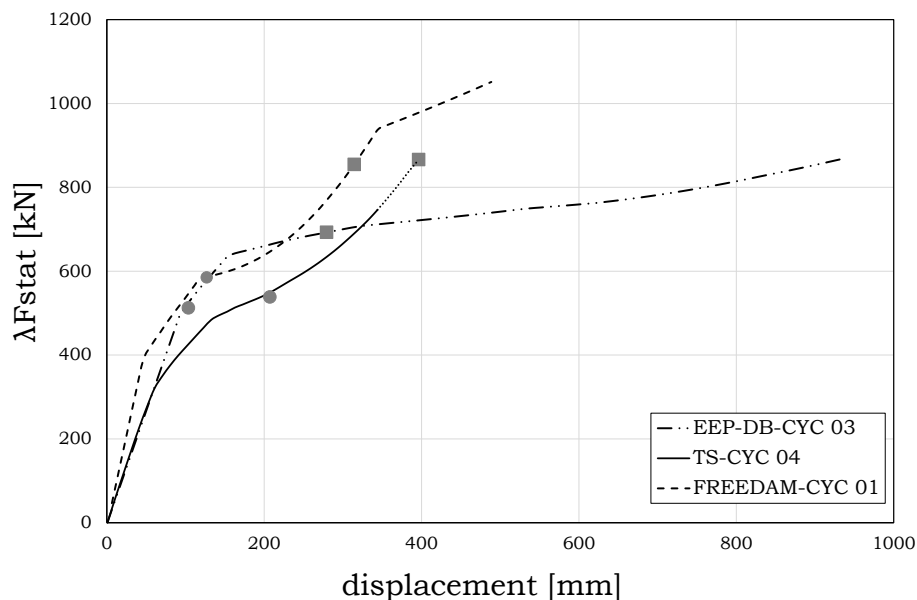


**Fig. 6.29** – Pushdown curves

It can be observed that in case of TS-CYC 04 connection typology, the energy balance is not obtained, therefore the zero kinetic energy condition is not reached and global structural collapse occurs. It means that is not possible, in those cases, to determine the value of the dynamically amplified force and, as a consequence, the residual reserve strength ratio. Conversely, in case of EEP-DB-CYC 03 and FREEDAM-CYC 01 the energy balance is obtained and the structures exhibit a residual strength reserve. In Table 6.38, the main results of the pushdown analyses have been reported. The values of the dynamic load factor are in between 1.35 and 1.61 while the residual reserve strength ratio value is equal to 1.18 in case of EEP-DB-CYC 03 connection and equal to 1.23 in case of FREEDAM-CYC 01 connection.

**Table 6.38** – Main results of pushdown analysis

<b>Joint</b>	<b><math>F_{stat}</math> [kN]</b>	<b>DLF</b>	<b>RRSR</b>	<b>Failure modes</b>
EEP-DB-CYC 03	512.40	1.35	1.18	Connecting beam
TS-CYC 04	538.56	1.61	0.86	Upper T-stub
FREEDAM-CYC 01	585.11	1.46	1.23	Upper T-stub

In table 6.38, an additional information is related to the failure modes of the connection that determine the global collapse. In all the cases, in line to what is expected, the structural collapse is related to behaviour of the joint component designed as the weakest.

Finally, even though MRFs equipped with both traditional and innovative connections result to exhibit a residual strength reserve, the employment of the FREEDAM connections guarantees significant benefits. In fact, the required plastic deformation capacity at the level of the joints is much smaller when using the FREEDAM joints. It is mainly due to the fact that the slip of some joint components during the column loss provides flexibility to the system and so allows activating an alternative load path for the load redistribution before reaching the plastic resistances in the system.

## 6.6. References

- [1] CSI 2007. “SAP 2000: Integrated Finite Element Analysis and Design of Structures. Analysis Reference”. Computer and Structure Inc. University of California, Berkeley.
- [2] A.B. Francavilla, M. Latour, V. Piluso, G. Rizzano (2016), “Bolted T-stubs: a refined model for flange and bolt fracture modes”, Steel and Composites Structures, Vol. 20, (2), 267-293;
- [3] EN 1998-1-1: “Eurocode 8: Design of structures for earthquake resistance - Part 1: General rules, seismic actions and rules for buildings”, European committee for standardization, 2005;
- [4] EN 1998-1: “Eurocode 3: Design of Steel Structures – Part 1-8: Design of Joints”, CEN, 2004;
- [5] Faella C., Piluso V., Rizzano G. (2000): “Structural Semi-Rigid connections” – Theory, Design and Software. CRC Press, Boca Raton, Florida (USA);
- [6] D.B. Moore, F. Wald (ed.) (2003): “Design of Structural connections to Eurocode 3 – Frequently Asked Questions”, Building Research Establishment Ltd, Watford, Project Continuing Education in Structural Connections, No. CZ/00/B/F/PP-134099, Leonardo Da Vinci, Programme;
- [7] J. Jaspart, (1991), “Etude de la Semi-rigidite Des Noeuds Poutre-Colonne et son Influence sur la Resistance et la Stabilité des Ossature en Acier”, Ph.D. Tesis; University of Liege, Liege, Belgium.
- [8] J.W Baker, M. Shubert, M.H. Faber (2008), “On the assessment of robustness”, Structural Safety, 30, 253-267;
- [9] G. Xu and B. Ellingwood (2011), “Probabilistic assessment of pre-Northridge steel moment resisting frames”, Journal of Structural Engineering, 137, 925-934;
- [10] M. Lalani, E.P. Shuttleworth, (1990), “The ultimate state of offshore platforms using reserve and residual strength principles”, the 22<sup>nd</sup> offshore technology conference, Houston, USA;
- [11] D.G. Lu, S.S. Cui, P.J. Song, Z.H. Chen (2010), “Robustness assessment for progressive collapse of framed structures using pushdown analysis

- method*”, 4<sup>th</sup> International Workshop on Reliable Engineering Computing, National University of Singapore;
- [12] D. Cassiano, M. D’Aniello, C. Rebelo, R. Landolfo, L. S. da Silva (2016), “*Influence of seismic design rules on the robustness of steel moment resisting frames*”, *Steel and Composites Structures*, Vol.21, (3), 479-500;
- [13] B. Izzudin, A. Vlassis, A. Elghazouli, D. Nethercot, (2008), “*Progressive collapse of multi-storey buildings due to sudden column loss – Part I: Simplified assessment framework*”, *Eng. Struct*, 30, 1308-1318;
- [14] F. Iannone, M. Latour, V. Piluso, G. Rizzano (2011): “*Experimental Analysis of Bolted Steel Beam-to-Column Connections: Component Identification*”, *Journal of Earthquake Engineering*, Vol. 15, (2), 214-244;
- [15] M. Latour, V. Piluso, G. Rizzano (2011), “*Cyclic Modelling of Bolted Beam-to-Column Connections: Component Approach*”, *Journal of Earthquake Engineering*, Vol. 15, (4), pp. 537- 563;
- [16] M. Latour, V. Piluso, G. Rizzano (2011), “*Experimental Analysis of innovative dissipative bolted double split tee beam-to-column connections*”, *Steel Constructions*, Vol. 4, (2), 53-64.
- [17] V. Piluso, G. Rizzano, M. Latour, A.B. Francavilla (2015), “*Progettazione sismica dei collegamenti flangiati trave-colonna a completo ripristino di resistenza e duttilità*”, XXV CONGRESSO C.T.A., October 1-3, Salerno, Italy;
- [18] F. Mazzolani and V. Piluso: “An attempt of codification of semirigidity for seismic resistant steel structures”, Third international workshop on connections in steel structures, Trent, 28-31 May, 1992.
- [19] U.Kuhlmann (1989), “*Definition of Flange Slenderness Limits on the Basis of Rotation Capacity Values*”, *Journal of Constructional Steel Research*, pp. 21-40;
- [20] B. Kato (1989), “*Rotation Capacity of H-section members as determined by local buckling*”, *Journal of Construction Steel Research*, 13, 95-109;
- [21] Piluso, V., Faella, C. and Rizzano, G. (2001), “*Ultimate behavior of bolted T-stubs. Part I: Theoretical model*”, *J. Struct. Eng. ASCE*, 127(6), 686-693.
- [22] Japanese Society of Steel Construction, Council on Tall Buildings and Urban Habitat (2007), “*Guidelines for collapse control design:*



- constructional of steel buildings with high redundancy*”, Tongji University Press.
- [23] S.M. Marjanishvili, E. Agnew, (2006), “*Comparioson of various procedures for progressive collapse analysis*”, Journal of Performance of Constructed Facilities, Vol. 20, (4), 365-374;
- [24] A. Longo, E. Nistri, V. Piluso, (2014), “*Theory of plastic mechanism control: state of the art*”, The Open Construction and Building Thecnology Journal, Vol. 8, 262-278;
- [25] R. Montuori, E. Nistri, V. Piluso, (2016), “*Theory of plastic mechanism control for MRF-EBF dual system: closed form solution*”, Engineering Structures, Vol 118, 287-306;
- [26] R. Montuori, E. Nistri, V. Piluso, (2015), “*Advances in theory of plastic mechanism control: closed form solution for MR-Frames*”, Earthquake Engineering and Structural Dynamics, Vol. 44, 1035-1054;
- [27] V. Piluso, R. Montuori, M. Troisi, (2014), “*Innovative structural details in MR-frames for free from damage structures*”, Mechanics Research Communications, 58, 146-156.
- [28] F. Cerfontaine, J-P. Jaspart (2005), “*Resistance of joints submitted to combined axial force and bending: analytical procedures and comparison with laboratory tests*”, Eurosteel 2005, June 8-10, Maastricht;
- [29] J-F. Demonceau, L. Comeliau, J-P. Jaspart, (2011), “*Robustness of building structures - recent developments and adopted strategy*”, Steel Construction, Vol. 4 (3), 166-170;
- [30] C. Huvelle, J-P. Jaspart, J-F. Demonceau (2014), “*How to check analytically the robustness of a building submitted to a column loss – a premiere*”, Eurosteel 2014, September 10-12, Naples, Italy.



# **Conclusions**



With reference to Moment Resisting Frames, in this PhD thesis a discussion on the main critical aspects in the design of Full and Partial Strength beam-to-column joint have been performed. In particular, with reference to bolted beam-to-column joints, both the case of Extended End Plate joint and the case of FREEDAM joints have been analysed.

One of the main results of the developed analyses is represented by the set up of design procedures for these kind of connections both for traditional and innovative connections. The two procedures, even though have been separately presented and applied to the case of Full and Partial Strength Joints, are based on the same approach consisting in the application of the principles of the capacity design at level of joint components. In particular, with reference to the full strength full ductility joints, the results obtained, on one hand, have confirmed the accuracy of the design approach and, on the other hand, have pointed out some criticisms of EC8 design criteria. In fact, EC8 provisions do not rationally account for the overstrength due to the beam strain-hardening. In particular, in some cases, the underestimation of the overstrength due to strain hardening is not compensated by the partial safety factor commonly applied in bolt design, thus leading to the brittle failure of the bolts. For the same reason, some joint components are significantly engaged in plastic range when EC8 design criteria are applied so that the resulting behaviour is characterized by a significant sharing of yielding between the connected beam end and such joint components. The effectiveness of the design criteria herein proposed has been demonstrated comparing the damage level of the joints' components. The results obtained shows that, in case of connections

designed according to the criteria proposed, the damage is conspicuously concentrated at the end of the beam which constitutes the main dissipative zone while all the connection's elements practically remain elastic, or only with very limited yielding. Conversely, in case of joints designed according to Eurocode 8, the joint components are significantly engaged in plastic range achieving high strain levels, certainly beyond the yield limit. The developed analyses have demonstrated that following EC8 design procedure, the welds may be engaged in plastic range with deformations up to 38.46 times the yield strain and, in a similar way, the bolts may fail or, in general, undergo severe damages.

Regarding the innovative beam-to-column connections, several experimental tests on the dissipative joint component have been performed in order to evaluate the random friction material variability, the random variation of the bolts' tightening and the influence of the Belleville disc springs.

The tests on the friction materials at low and high velocities have demonstrated that the M4 material performs adequately for FREEDAM joints so that its use has been considered. Additionally, a statistical range of variation of the values of the friction coefficients to be used in design have been effectively evaluated. The experimental tests pointed out that, in order to reduce degradation of stick-slip, it is necessary to limit the preload to a maximum value of the 60% for all the analysed materials. Finally, the typology of bolted assembly does not seem influent on the friction damper behaviour. The use of disc springs helps to stabilize the bolts' force, but this stabilization does not influence significantly the hysteretic loops.

Subsequently, the design procedure for FREEDAM joints have been detailed and applied in order to design the specimens tested under cyclic load conditions at the STRENGTH laboratory (STRuctural ENgineering Testing Hall) of the University of Salerno. In particular, the developed design procedure based on the application of the component method currently codified in EC3 properly integrated with the experimental information on the friction device behaviour seems to be accurate. In addition, the experimental analysis has evidenced that both the configuration with horizontal and vertical dampers are able to avoid, as wanted, damage in all the structural components, meeting therefore the design objectives and thus perform adequately in terms of energy dissipation capacity. Therefore, they can be considered as alternative configurations able to provide a sufficient hysteretic response.

Aiming to evaluate the benefits on the global behaviour of the structures when equipped with innovative beam-to-column connections, incremental dynamic analyses and pushdown analyses have been performed. The obtained results allow to underline the following main aspects:

- a) The Incremental Dynamic Analysis performed on a four bays - six storeys steel frames equipped with full (EEP-DB-CYC 03) and partial (TS-CYC 04) Strength joints, evidenced that semirigid partial-strength connections, if well designed, can be considered to have adequate ductility and dissipation capacity in order to satisfy the seismic demand. In particular, the Double Tee Joints, even though are characterized by cyclic behaviour with significant pinching, due

to their greater plastic rotational capacity, provide the same maximum value of the PGA at collapse with respect to full strength joint.

- b) The Incremental Dynamic Analysis performed on a four bays - six storeys steel frames equipped with FREEDAM connections shows a very significant improvement of the PGA at collapse which are promising for the full development of innovative beam-to-column joints;
- c) The Robustness analyses demonstrate that, even though MRFs equipped with both traditional and innovative connections result to exhibit a residual strength reserve, the employment of the FREEDAM connections guarantees significant benefits. In fact, the slippage of the friction dampers up to the stroke end, before the bolts engage in shear and the stem plate engage in bearing, allows to obtain an increase of the vertical component of the beam axial forces resulting from catenary behaviour after column loss.

As said in the introduction of this PhD thesis, the last version of Eurocode 8, has explicitly opened the door to the use of partial strength joints underlining the possible location of the dissipative zones at the beam ends or in the connections of the beams to the columns. However, the code does not introduce a design procedure of these kind of connections slackening their diffusion in practice. A first answer is given in this work, proving a design procedure for both full and partial connections. Moreover, in order to overcome the drawbacks of the traditional and passive control design strategies, in this work the development of a new design strategy whose goal is the design of



connections able to withstand frequent and occasional seismic events but also destructive earthquakes has been dealt. The innovative beam-to-column connection typology has been accurately analysed and the results obtained allow to the full development of these joints in MRFs. Nevertheless, additional analysis and experimental tests will be performed in the ongoing RFCS project “FREEDAM”, granted by the European Community.



# **Annex A**



## **Full strength beam-to-column connections and design criteria: worked design example**

Seismic design of beam-to-column joints needs the knowledge of the gravity loads acting on the beams in the seismic load combination, the beam and column sections and the material properties. The design is aimed to the evaluation of the required bolt diameter, throat thickness of fillet welds, end-plate thickness, continuity plate thickness and, if needed, thickness of supplementary web plates. Many relationships are needed to develop all the design steps. Therefore, in order to clarify the proposed procedure, a worked design example is herein shown in detail, with reference to the external joint corresponding to study case A, whose input data are given in Table 2.3.

### **Step 1 - Evaluation of the average ultimate moment which the fully yielded and strain hardened beam is able to transmit:**

The distance between the plastic hinge and the column flange is:

$$s_h = \frac{d_b}{2} = \frac{600}{2} = 300 \text{ mm} \quad (\text{A.1})$$

The clear length of the beam is  $L_n = 9000 - 359 = 8641 \text{ mm}$  and the distance between the plastic hinges is  $L_h = L_n - 2s_h = 8641 - 600 = 8041 \text{ mm}$ .

The nominal plastic moment of the beam (steel grade S235) is equal to  $M_{b,p} = 786 \text{ kNm}$ . Considering the beam flange thickness, the overstrength coefficient  $\gamma_{ov.rm}$  accounting for the random variability of the material is given by (see Table 2.2):

$$\gamma_{ov.rm} = \frac{f_{ym.bf}}{f_{y.b}} = \frac{f_0 - \beta t_{bf}}{f_{y.b}} = \frac{313.4 - 2.254 \times 19}{235} = \frac{270.57}{235} = 1.15 \quad (A.2)$$

The average value of the yield stress of the web is equal to:

$$f_{ym.bw} = f_0 - \beta t_{bw} = 313.4 - 2.254 \times 12 = 286.35 \text{ MPa} \quad (A.3)$$

The normalized slenderness parameters of flange and web are equal to:

$$\bar{\lambda}_f = \frac{b_{bf}}{2 t_{bf}} \sqrt{\frac{f_{ym.bf}}{E}} = \frac{220}{2 \cdot 19} \sqrt{\frac{270.57}{210000}} = 0.208 \quad (A.4)$$

$$\bar{\lambda}_w = \frac{d_{bw}}{2 t_{bw}} \sqrt{\frac{f_{ym.w}}{E}} = \frac{562}{2 \cdot 12} \sqrt{\frac{286.35}{210000}} = 0.865 \quad (A.5)$$

The beam shear length is equal to  $L_e = L_h/2 = 8041/2 = 4020.5 \text{ mm}$ .

The overstrength coefficient accounting for the influence of strain hardening is:

$$M_{b.u} = 1.15 \cdot 1.28 \cdot 1.05 \cdot 786 \cong 1214 \text{ kNm} \quad (A.6)$$

With reference to the external joint, the value of the shear action at the plastic hinge axis in the ultimate condition is equal to:

$$V_{bu} = \frac{q L_h}{2} + \frac{n_F F_d}{2} + \frac{2 M_{bu}}{L_h} = \frac{1.25 \cdot 8.041}{2} + \frac{3 \cdot 65.00}{2} + \frac{2 \cdot 1214}{8.041} \quad (A.7)$$

$$\cong 404.6 \text{ kN}$$

**Step 2 - Calculation of bending moment and shear action at the column flange and evaluation of compression force and tensile force to be transmitted at the beam flanges' levels:**

The flexural and shear action, respectively  $M_{cf}$  and  $V_{cf}$ , at the column flange are given by:

$$M_{cf} = M_{bu} + V_{bu} \cdot s_h + \frac{q s_h^2}{2} = 1214 + 404.6 \cdot 0.3 + \frac{1.25 \cdot 0.3^2}{2} \cong 1336 \text{ kNm} \quad (\text{A.8})$$

$$V_{cf} = 404.6 + 1.25 \cdot 0.30 \cong 405 \text{ kN}$$

Consequently, the compression/tensile force to be transmitted at the beam flanges' level is obtained as:

$$T_u = C_u = \frac{M_{cf}}{d_b - t_{bf}} = \frac{1336000}{600 - 19} \cong 2299 \text{ kN} \quad (\text{A.9})$$

**Step 3 - Design of the bolt diameter:**

For the design of the diameter of the bolts in tension side the following actions have to be considered:

$$F_{t,Ed} = \frac{T_u}{n_b} = \frac{2299}{4} = 574.75 \text{ kN} \quad F_{v,Ed} = \frac{V_{cf}}{2 n_b} = \frac{405}{2 \cdot 4} = 50.6 \text{ kN} \quad (\text{A.10})$$

Therefore, according to Eurocode 3, the check under combined shear and tension lead to determine a first minimum value of the resistant area of the bolts. In particular, for 10.9 class:

$$A_{res} \geq \frac{\gamma_{M2}}{f_{tb}} \left( \frac{F_{v,Ed}}{\alpha_v} + \frac{F_{t,Ed}}{1.26} \right) \quad (\text{A.11})$$

$$A_{res} \geq \frac{1.25}{1000} \left( \frac{50600}{0.5} + \frac{574750}{1.26} \right) \cong 696.69 \text{ mm}^2$$

According to Eurocode 3, in any case, the resistant area of the bolts has to be greater than the value determined considering only the tension action:

$$A_{res} \geq \frac{\gamma_{M2} F_{t,Ed}}{0.9 f_{tb}} = \frac{1.25 \cdot 574750}{0.9 \cdot 1000} \cong 798.26 \text{ mm}^2 \quad (\text{A.12})$$

Consequently, bolts M36 have been chosen.

#### **Step 4 – Design of the welds:**

According to Eurocode 3, the design of the welds has been carried out considering the throat thickness of the fillet weld in its actual position. With reference to the welds connecting the flange beam to the end-plate, the length of the both internal and external fillets has been assumed as:

$$l_f = b_{bf} - 2 \cdot r_b - t_{bw} = 220 - 2 \cdot 24 - 12 = 160 \text{ mm} \quad (\text{A.13})$$

Therefore the required throat thickness of the weld is:

$$a_f \geq \frac{T_u}{\sqrt{2} \cdot l_f} \frac{\beta_w \gamma_{M2}}{f_{tk}} = \frac{2299}{160\sqrt{2}} \frac{0.80 \cdot 1.25}{0.360} = 28.23 \text{ mm} \rightarrow a_f = 29 \text{ mm} \quad (\text{A.14})$$



The welds connecting the web beam and the end-plate have to be able to transmit the shear action  $V_{cf}$  and the ultimate flexural action  $M_{w,u}$  that the web flange transmits:

$$\begin{aligned} M_{w,u} &= \gamma_{ov.rm} \cdot \gamma_{ov.sh} \cdot \gamma_{M0} \cdot M_{w,p} = 1.15 \cdot 1.28 \cdot 1.05 \cdot 212.07 \\ &\cong 327.77 \text{ kNm} \end{aligned} \quad (\text{A.15})$$

The length of the fillets is:

$$l_w = d_{bw} - 2 r_b = 562 - 2 \cdot 24 = 514 \text{ mm} \quad (\text{A.16})$$

and the thickness results to be:

$$\begin{aligned} a_w &\geq \frac{\beta_w \gamma_{M2}}{f_{tk}} \frac{1}{l_w} \sqrt{\frac{8 M_{w,u}^2}{l_w^2} + \frac{3}{4} V_{cf}^2} \\ &= \frac{0.8 \cdot 1.25}{360} \frac{1}{514} \sqrt{\frac{8 (327.77 \cdot 10^6)^2}{514^2} + \frac{3}{4} (405 \cdot 10^3)^2} \cong 9.92 \text{ mm} \\ &\rightarrow a_w = 10 \text{ mm} \end{aligned} \quad (\text{A.17})$$

### Step 5 – Design of the end-plate:

Considering the design criteria already adopted for the bolts, failure mechanism type 3 can be excluded. Therefore, only the resistance formulations for mechanism type 1 and mechanism type 2 have to be considered to check the equivalent T-stub modelling the end-plate in bending. It is assumed that the distance  $m$  between the bolt axis and the plastic hinge located close to the beam flange is equal to the minimum technologically compatible,  $m=1.2 d_o$  being  $d_o$  the diameter of the bolt hole. In addition, the width of the plate is defined on the basis

of the code requirements for bolt spacing and of technological conditions.

The horizontal distance between the bolts  $w$  has to satisfy the following limitations:

$$\begin{aligned} w_{\min} &\cong t_{cw} + 2 r_c + 1.8 d_0 = 21 + 2 \cdot 27 + 1.8 \cdot 37.5 = 142.5 \text{ mm} \\ w_{\max} &= b_{cf} - 2.4 d_0 = 309 - 2.4 \cdot 37.5 = 219 \text{ mm} \end{aligned} \quad (\text{A.18})$$

According to the above limitations, the bolt spacing is taken equal to  $w_0 = 170 \text{ mm}$ .

Regarding the width of the end-plate, it should be greater than:

$$b_{ep} = \max\{w + 2.4 d_0; b_{bf}\} = \max\{170 + 2.4 \cdot 37.5; 220\} = 260 \text{ mm} \quad (\text{A.19})$$

and, anyway, smaller than the width of the column that is equal to 309 mm, consequently the width of the end plate is taken equal to 280mm.

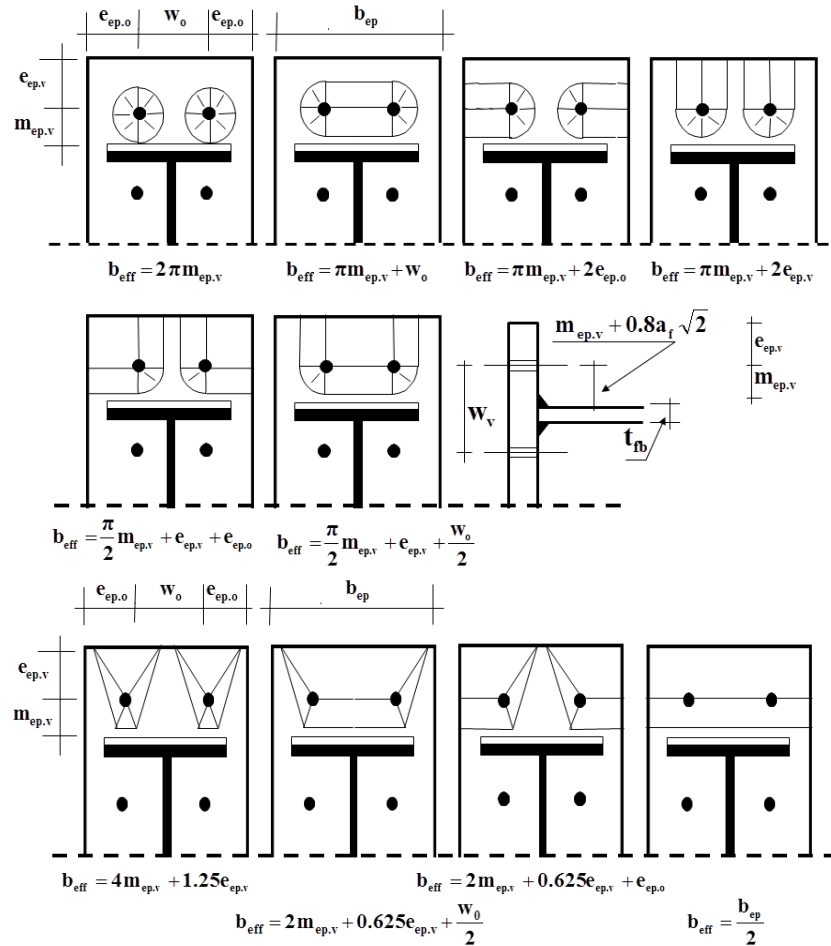


**Fig. A.1** – Determination of the effective length for a single bolt row on the basis of the possible collapse mechanisms

As a consequence, the horizontal distance between the bolt axis and the edge of the plate  $e_{ep,0}$  is:

$$e_{ep,0} = \frac{b_{ep} - w_0}{2} = \frac{280 - 170}{2} = 55 \text{ mm} \quad (\text{A.20})$$

For the evaluation of the effective length of the equivalent T-stub, taken  $m_x = e_x = 1.2d_0 = 45 \text{ mm}$ , it results:

$$\begin{aligned} b_{\text{eff,ep},1} &= \min\{2\pi m_x; \pi m_x + w; \pi m_x + 2e_{\text{ep}}\} \\ &= \min\{282.6; 311.3; 251.3\} = 251.3 \text{ mm} \end{aligned} \quad (\text{A.21})$$

which accounts for the circular patterns and:

$$\begin{aligned} b_{\text{eff,ep},2} &= \min\{4m_x + 1.25e_x; e_{\text{ep}} + 2m_x + 0.625e_x; 0.5w + 2m_x + 0.625e_x\} \\ &= \min\{4 \cdot 45 + 1.25 \cdot 45; 45 + 2 \cdot 45 + 0.625 \cdot 45; 0.5 \cdot 170 + 2 \cdot 45 \\ &\quad + 0.625 \cdot 45\} = \min\{236.25; 173.12; 203.12\} = 203.12 \text{ mm} \end{aligned} \quad (\text{A.22})$$

which accounts for non-circular patterns.

Definitely, the effective length of the equivalent T-stub is:

$$\begin{aligned} b_{\text{eff,ep}} &= \min\{b_{\text{eff,ep},1}; b_{\text{eff,ep},2}; 0.5 b_{\text{ep}}\} = \min\{251.3; 203.12; 0.5 \cdot 280\} \\ &= 140 \text{ mm} \end{aligned} \quad (\text{A.23})$$

The thickness of the end-plate required to avoid the collapse of the equivalent T-stub according to type-1 mechanism is:

$$\begin{aligned} F_{1,Rd} &= 2 \frac{b_{\text{eff}} t_{\text{ep}}^2 f_{y,\text{ep}}}{m \gamma_{M0}} = T_u \rightarrow \\ t_{\text{ep},1} &= \sqrt{\frac{m_x T_u \gamma_{M0}}{2 \cdot b_{\text{eff,ep}} \cdot f_{y,\text{ep}}}} = \sqrt{\frac{45 \cdot 2299000 \cdot 1.05}{2 \cdot 140 \cdot 275}} \cong 37.56 \text{ mm} \end{aligned} \quad (\text{A.24})$$

Similarly, to avoid the collapse of the equivalent T-stub according to type-2 mechanism the required end-plate thickness is:

$$\begin{aligned}
 F_{2,Rd} &= 2 \frac{\frac{f_{y,ep} b_{eff} t_{ep}^2}{2} + 2 F_{t,Rd} n}{m + n} = T_u \quad \rightarrow \\
 t_{ep,2} &= \sqrt{\frac{2 \gamma_{M0}}{b_{eff,ep} f_{y,ep}} \left[ \frac{T_u (m_x + e_x)}{2} - 2 F_{t,Rd} e_x \right]} = \\
 &= \sqrt{\frac{2 \cdot 1.05}{140 \cdot 275} \left[ \frac{2299000 (45 + 45)}{2} - 2 \cdot 588240 \cdot 45 \right]} \cong 52.50 \text{ mm}
 \end{aligned} \tag{A.25}$$

Therefore, the thickness of the end-plate has been assumed equal to 55mm.

**Step 6 - Check of the resistance of the column web in shear and design of supplementary web plates if needed:**

The shear resistant area of the column section is given by:

$$\begin{aligned}
 A_{vc} &= A - 2 b_{cf} t_{cf} + (t_{cw} + 2r_c) t_{cf} \\
 &= 31200 - 2 \cdot 309 \cdot 40 + (21 + 2 \cdot 27) \cdot 40 = 9480 \text{ mm}^2
 \end{aligned} \tag{A.26}$$

The resistance of the column web panel, without continuity and/or supplementary plates, is:

$$V_{wp,Rd} = \frac{0.9 \cdot A_{vc} \cdot f_{y,cw}}{\sqrt{3} \cdot \gamma_{M0}} = \frac{0.9 \cdot 9480 \cdot 355}{\sqrt{3} \cdot 1.05} \cong 1665 \text{ kN} \tag{A.27}$$

Since continuity plates in the both compression and tension zones have been considered, the plastic shear resistance of the column web panel is

incremented by the contribution due to the resistant mechanism activated by the continuity plates.

The plastic moment of the column flange is given by:

$$M_{pl.cf.Rd} = \frac{b_{cf} t_{cf}^2 f_{y,c}}{4} \frac{1}{\gamma_{M0}} = \frac{309 \cdot 40^2 \cdot 355}{4} \frac{1}{1.05} \cong 41.79 \text{ kNm} \quad (\text{A.28})$$

Therefore the contribution due to the additional resistant mechanism activated by the continuity plates results:

$$V_{wp.add.Rd} = \frac{4 \cdot M_{pl.cf.Rd}}{d_s} = \frac{4 \cdot 41.79}{0.581} = 287.7 \text{ kN} \quad (\text{A.29})$$

where  $d_s$  is the distance between the centrelines of the stiffeners.

The total resistance of the column web panel is:

$$V_{wp.Rd.tot} = V_{wp.Rd} + V_{wp.add.Rd} = 1665 + 287.7 \cong 1953 \text{ kN} \quad (\text{A.30})$$

Whereas the shear resistance of the column web panel is lower than the action transmitted by the beam in its ultimate conditions, supplementary web plates are needed whose width is taken equal to:

$$b_{s,max} = d_{cw} - 2r_c = 279 - 2 \cdot 27 = 225 \text{ mm} \quad (\text{A.31})$$

According to Eurocode 3, the resistance of the material constituting the supplementary plates has to be the same of the column; the thickness of the stiffeners results to be:

$$\begin{aligned}
 t_s &\geq \frac{\sqrt{3} \cdot \gamma_{M0} (T_u - V_{wp,add,Rd})}{0.9 \cdot b_s \cdot f_{y,wc}} - \frac{A_{vc}}{b_s} \\
 &= \frac{\sqrt{3} \cdot 1.05 \cdot (2299000 - 287700)}{0.9 \cdot 225 \cdot 355} - \frac{9480}{225} \cong 9.76 \text{ mm}
 \end{aligned}
 \tag{A.32}$$

Consequently, it is possible to use a couple of supplementary plates whose thickness is 5 mm or a single supplementary web plate whose thickness is equal to 10 mm.

**Step 7 - Check of the resistance of the column web in tension and in compression.**

Since continuity plates have been considered in the evaluation of the shear resistance of the column web panel, their design is required. The transverse stiffeners can be designed according to two possible approaches. The first approach requires that the action transmitted from the beam flanges in their ultimate conditions, equal to  $T_u$ , is absorbed relying exclusively on the tensile/compression resistance of continuity plates, neglecting the resistance of the column web. The second approach allows the reduction of the thickness of the continuity plates, taking advantage of the contribution due to the resistance of the column web.

In accordance to the latter, the resistance of the column web in compression and the resistance of the continuity plates have to be determined; the former is given by:

$$\begin{aligned}
 F_{cwc,Rd} &= b_{eff,cwc} (t_{cw} + t_{s,tot}) \cdot \frac{f_{y,cw}}{\gamma_{M0}} = \frac{546.02 (21 + 10) 355}{1.05} \\
 &\cong 5723 \text{ kN}
 \end{aligned}
 \tag{A.33}$$

where  $b_{eff.cwc}$  is the effective length of the column web given by:

$$\begin{aligned} b_{eff.cwc} &= t_{fb} + 2\sqrt{2} a_f + 5(t_{fc} + r_c) + 2 t_{ep} \\ &= 19 + 2\sqrt{2} \cdot 29 + 5(40 + 27) + 2 \cdot 40 \cong 546.02 \text{ mm} \end{aligned} \quad (\text{A.34})$$

and  $t_{s,tot} = 10 \text{ mm}$  is the thickness of the supplementary web plates.

Obviously, if  $F_{cwc.Rd} \geq T_u$  it is possible to evaluate the possibility of omitting the continuity plates. In such a case, it is necessary to check again the resistance of column web in shear according to Step 6.

Subsequently, the welds have been designed:

$$a_{cp} \geq \frac{\beta_w t_{cp} f_{y,cp}}{\sqrt{2} f_{tk}} = \frac{0.85 \cdot 20 \cdot 275}{\sqrt{2} \cdot 430} \cong 7.68 \text{ mm} \quad \rightarrow \quad a_{cp} = 8 \text{ mm} \quad (\text{A.35})$$

### **Step 8 - Check of the resistance of the column flange in bending:**

In bolted connections, an equivalent T-stub in tension may be used to model the design resistance of the column flange in bending. As highlighted for the end-plate in bending, failure mode according to mechanism type-3 can be excluded because of the design criterion adopted for the bolts. Therefore, the design resistances for mechanism type-1 and type-2 have to be evaluated. In particular, the following equation has to be considered:

$$F_{1,Rd} \geq T_u \quad F_{2,Rd} \geq T_u \quad (\text{A.36})$$

where:



$$F_{1,Rd} = 2 \frac{b_{eff} t_{cf}^2 f_{y,cf}}{m \gamma_{M0}} \quad \text{and} \quad F_{2,Rd} = 2 \frac{\frac{f_{y,cf} b_{eff} t_{cf}^2}{\gamma_{M0}} + 2 F_{t,Rd} n}{m + n} \quad (\text{A.37})$$

in which  $b_{eff}$  is the effective length of the equivalent T-stub corresponding to a single bolt row,  $t_{cf}$  is the thickness of the column flange,  $m$  is the distance between the bolt line and the plastic hinge arising at the T-stub stem,  $n$  is the distance between the bolt line and the end of the plate where the contact forces are concentrated and  $f_{y,cf}$  is the yield resistance of the column flange.

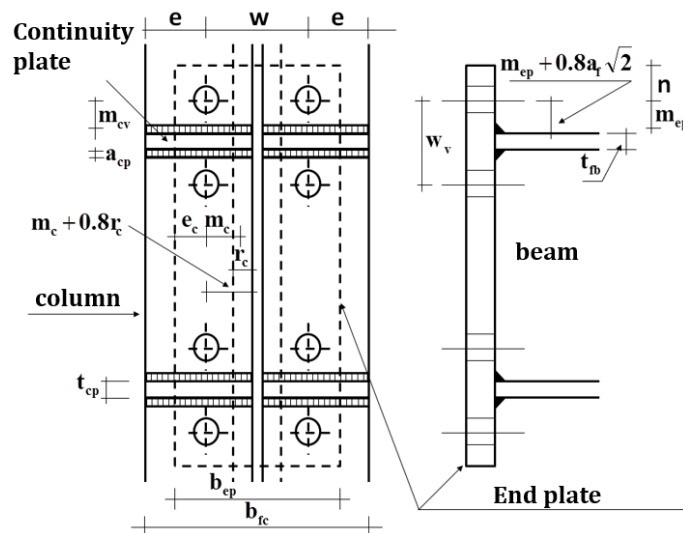


**Fig. A.2** – Geometrical properties of column flange

With reference to Fig. A.2 it is possible to define:

$$m_c = \frac{w - t_{wc} - 1.6 r_c}{2} = \frac{170 - 21 - 1.6 \cdot 27}{2} = 52.9 \text{ mm} \quad (\text{A.38})$$

while the horizontal distance between the bolt axis and the edge of the column flange is:

$$e = \frac{b_c - w}{2} = \frac{309 - 170}{2} = 69.5 \text{ mm} \quad (\text{A.39})$$

The vertical distance between the first and second bolt rows is:

$$\begin{aligned} w_v &= 2 (m + 0.8 a_f \sqrt{2} + t_{fb}/2) = 2 (45 + 0.8 \cdot 29 \sqrt{2} + 19/2) \\ &= 174.62 \text{ mm} \end{aligned} \quad (\text{A.40})$$

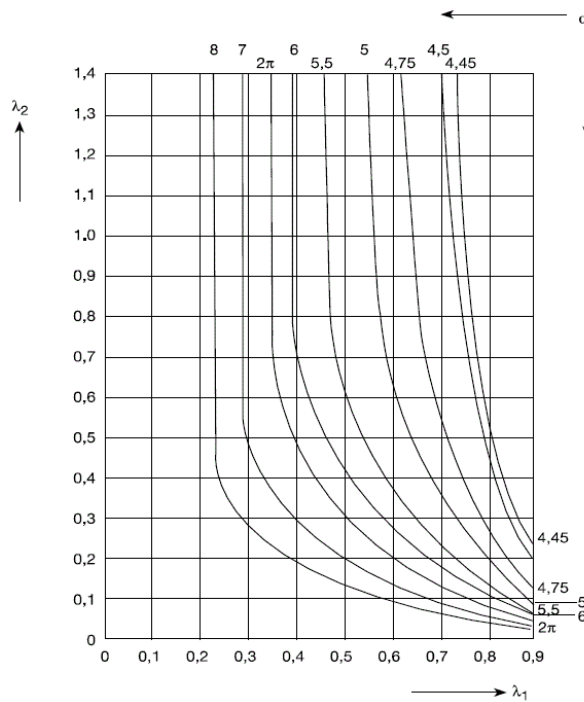


**Fig. A.3** – Abacus

According to Eurocode 3 the effective length, in presence of transverse stiffeners, is given by:

$$b_{eff} = \min\{2\pi m_c; \alpha \cdot m_c\} = \min\{2\pi \cdot 52.9; 5.93 \cdot 52.9\} \cong 313.7 \text{ mm} \quad (\text{A.41})$$

where the parameter  $\alpha$  has been determined considering the geometrical parameters  $\lambda_1$  and  $\lambda_2$ :

$$\lambda_1 = \frac{m_c}{m_c + e} = \frac{52.9}{52.9 + 69.5} = 0.43 \quad \lambda_2 = \frac{m_2}{m_c + e} = \frac{68.26}{52.9 + 69.5} = 0.57 \quad (\text{A.42})$$

by means the abacus in Fig. A.3.

Thereafter, the design resistances for mechanisms type-1 and type-2 are given by:

$$\begin{aligned} F_{1,Rd} &= 2 \frac{f_{y,cf} b_{eff,cf} t_{cf}^2}{m_c} \frac{1}{\gamma_{M0}} = 2 \frac{355 \cdot 313.7 \cdot 40^2}{52.9} \frac{1}{1.05} \cong 6416 \text{ kN} \geq T_u \\ F_{2,Rd} &= 2 \frac{f_{y,cf} \frac{b_{eff,cf} t_{cf}^2}{2} + 2 F_{t,Rd} n}{m_c + n} \frac{1}{\gamma_{M0}} \\ &= 2 \frac{355 \frac{313.7 \cdot 40^2}{2} + 2 \cdot 588240 \cdot 55}{52.9 + 55} \frac{1}{1.05} \cong 2715 \text{ kN} \geq T_u \end{aligned} \quad (\text{A.43})$$

where  $n = \min\{e; e_{ep}; 1.25m_c\} = \min\{69.5; 55; 1.25 \cdot 52.9\} = 55 \text{ mm}$ .

Since the both design resistances are greater than the action  $T_u$ , derived by means of capacity design principles, the check of the column flange in bending is satisfied.



# **Annex B**



## Bolted T-stubs: a refined model for flange and bolt fracture modes

The mechanical modelling of a T-stub can be provided starting from the definition of the geometry of the elements, the boundary conditions and the non-linear behaviour of its sub-components, i.e. the plate and the bolts.

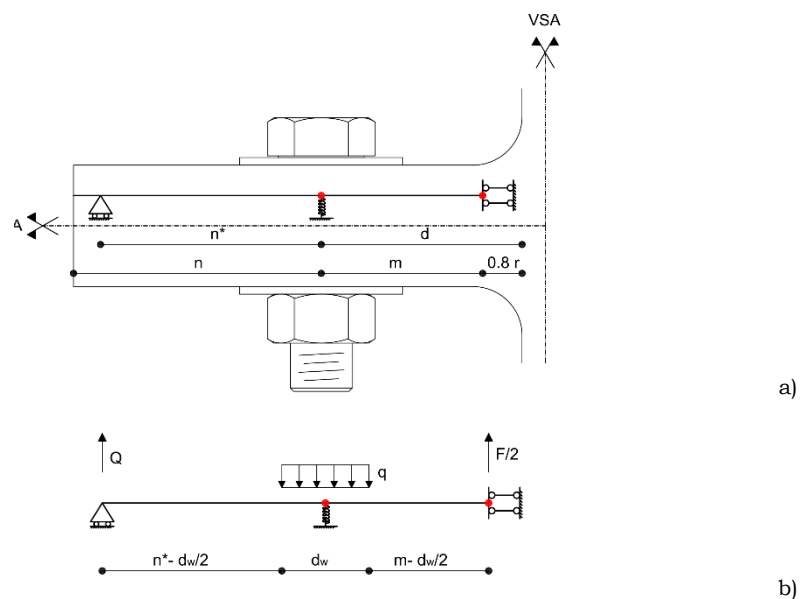


**Fig. B.1** – T-stub model: a) Geometrical discretization of the T-stub; b) Non-linear mechanical model

The approach proposed in this paper aims to provide a modelling of the T-stub in line with the methodology already individuated by Eurocode 3. To this scope, the flange plate is modelled with a simplified beam, whose length is defined according to EC3 criteria, i.e. the distance between the bolt line and the plastic hinge arising at the T-stub stem is

equal to  $m=d-0.8r$ , while  $n$  is defined as the distance between the bolt line and the end of the plate (Fig. B.1a). In order to model the influence of the bolt head on the resistance of the T-stub, which can provide a significant contribution to the resistance, the bolt action is assumed uniformly spread under the bolt head, over a length equal to the washer diameter ( $d_w$ ) (Fig. B.1b). At the same time, the bolt shank is modelled with a translational spring. Such a spring is defined in order to check the resistance of the bolt and to evaluate the respect of the compatibility condition between the elongation of the bolt and the deformation of the plate. Always in line with the EC3 approach, it is assumed that the beam composing the T-stub flange is constrained in correspondence of the stem, due to symmetry condition, with a bi-pendulum. To model the contact zone, as an advance on with respect to the existing models, the prying forces, which are usually assumed concentrated at the end of the plate, are considered applied in a point in between the tip of the plate and the edge of the bolt head. The position of such a point is determined by evaluating the compatibility of the vertical displacements of the plate in order to respect the horizontal symmetry condition.

The behaviour of the plate is defined adopting a lumped plasticity approach by means of non-linear plastic hinges located at the T-stub web and bolt line (Fig. B.1). The characteristics of the plastic hinges are derived starting from the moment-curvature diagram of the cross-section representing the plate, according to the approach already presented by Piluso et al. (2001). In a similar way, also the non-linear spring modelling the bolt shank behaviour is characterized starting from the knowledge of the stress-strain law of the basic material according to the approach reported in the next section. The failure of the sub-components of the T-stub, i.e. the bolts and the plate, is



modelled by checking the ultimate condition on the stress-strain laws of the materials. In particular, the failure of the plastic hinges of the plate is individuated as corresponding to the plastic rotation leading to the attainment ultimate strain at the most external fibre, while the failure of the bolt is identified in correspondence to the uplift value leading to the fracture elongation of the material composing the bolt.

In conclusion, still providing a simplified approach, the model proposed in this paper aims to define the response of the T-stub up to failure including the following advances:

- The bolt forces are considered uniformly distributed under the bolt head;
- The position of the contact forces is determined by evaluating the deformed configuration of the plate in the zone contained in between the bolt line and the tip of the plate;
- Mechanical non-linearities of plate and bolt are accounted for by means of integration of the stress-strain laws of the materials by extending the approach proposed by Piluso et al. for determining the moment-rotation response of the plastic hinges arising on the plate to the bolt force-elongation response;
- The failure of the T-stubs is modelled by checking the ultimate strain of the basic materials composing the plate and the bolts;
- The compatibility condition between the displacements of the plate and the uplift of the bolt is taken into account;
- The displacements of the T-stub are evaluated step-by-step as the sum of the elastic and plastic parts.

Despite these improvements, the following assumptions are still made:

- 3-D effects are neglected;

- Secondary bending effects on bolts are neglected;
- The effect of moment-shear interaction on resistance of the materials is neglected;
- The effect of shear forces in the bolts are neglected;
- Second order effects are neglected;
- The compatibility of the deformed shape of the plate in the zone contained between the prying force and the tip of the plate is not considered.

It is useful to note that, as far as 3-D effects are not considered, the model presented in this paper is mainly devoted to reproduce cases where the yield line pattern is the so-called beam pattern, which is, in practical cases, the pattern usually arising in T-stubs modelling the end-plates. In order to overcome this limitation, the model could be generalized also to other cases, at least for defining the resistance, by adopting the effective lengths already defined in (Zoetemeijer 1974). In addition, second order effects and shear forces in bolts are usually arising only at large displacements and therefore the model remains enough accurate in the range of sufficiently low displacements. In addition the effect of shear forces on the resistance of the materials are neglected and, therefore, in cases of T-stubs characterized by small values of the  $m/t_f$  ratio a slight overestimation of the resistance is expected.

### **B.1. Materials' constitutive laws**

The plastic deformation capacity of steel plates strongly depends on the inelastic properties of the material and, above all, on the value of the ultimate strain. For this reason, in order to predict the ductility supply

of T-stubs, an accurate modelling of the stress-strain relationships up to failure of the basic materials composing bolts and plate is necessary. Preliminarily, it is useful to note that a conventional stress-strain relationship measured in common tensile tests is not representative of the punctual behaviour of the material. In fact, as it is well known, during a tensile test, the engineering stress  $\sigma_n$ , defined as the ratio between the force measured during the test ( $N$ ) and the initial area of the specimen ( $A_0$ ), after necking, starts to decrease due to the reduction of the cross-sectional area of the specimen. Notwithstanding, after the beginning of necking, the true (natural) stress  $\sigma_r$ , referred to the actual cross-sectional area  $A$  increases and the relationship between true stress and true strain of steel always follows an hardening behaviour up to failure.

Therefore, normally, in order to get the true stress-true strain behaviour starting from the results of coupon tensile tests, in the range before the necking phenomenon starts, it is necessary to transform the engineering values of stress and strain in actual values by means of the following relationships (Malvern 1969; Pozzati 1980; Davids, et al. 1982):

$$\varepsilon_r = \ln(1 + \varepsilon_n); \sigma_r = \sigma_n(1 + \varepsilon_n) \quad (\text{B.1})$$

where  $\varepsilon_r$  is the actual (material) strain and  $\varepsilon_n$  is the nominal strain. In addition, in order to define the behaviour of the material in the range after necking up to failure, it is necessary to evaluate the ultimate natural stress  $\sigma_f$  at fracture and the corresponding natural deformation  $\varepsilon_u$  (RILEM 1990) by means of the following expressions:

$$\sigma_f = \frac{F_f}{A_f} \quad \varepsilon_u = \ln \frac{A_0}{A_f} \quad (\text{B.2})$$

where  $F_f$  is the force measured by the testing machine at fracture and  $A_f$  is the area in the necking zone at the end of the test. The relationships here reported can be applied to obtain the actual stress-strain behaviour of steel provided that the results of coupon tensile tests are available. Such tests, are usually carried out only for the plates but not for the bolts some simplifying assumptions concerning the bolt material modelling have to be made.

The material composing the flange plate, as far as the results on coupon tensile tests are available, can be modelled in terms of actual strain vs. actual stress by means of a quadri-linear approximation, which can be derived starting from the experimental results by simply equating the area under the experimental curve with the area under the simplified quadri-linear curve (Fig. B.2a).

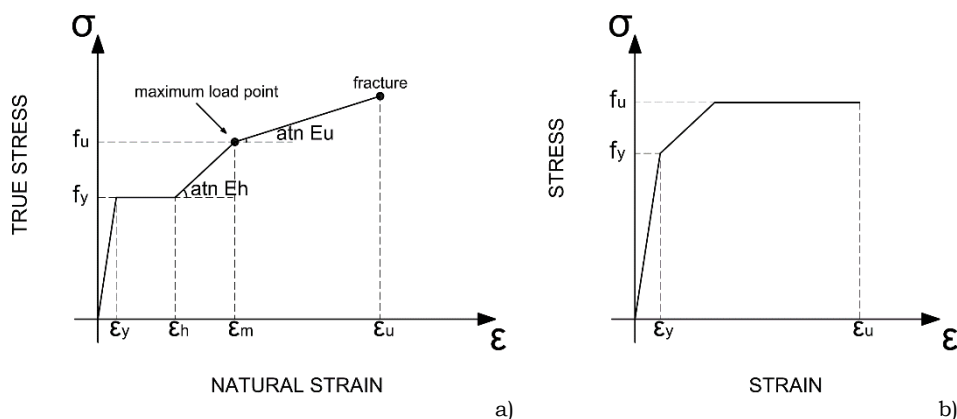


**Fig. B.2** – Stress-strain laws of the materials composing the T-stub:  
a) Flange plate; b) Bolts

Conversely, the material composing the bolts is not easy to accurately characterize as far as no experimental results are usually available. Nevertheless, bolt elongation is very important for the prediction of the ductility of joints. In fact, it may increase significantly the ultimate plastic deformation, allowing the uplift of the plate, in case of mechanisms type-2 or type-3. Also in EC3 no information is given with reference to the ultimate displacement of bolts and, since bolts are designed to remain in elastic range, in technical literature there are only few studies dealing with the characterization of the ultimate deformation of bolts. Within a wide experimental program dealing with the assessment of the behaviour of isolated T-stubs subjected to tension, four series of tests on high strength bolts axially loaded have been carried out (Girao Coelho, et al. 2004). The average ultimate deformation resulting from experimental tests indicated by the authors for short-threaded bolts of 8.8 and 10.9 class, is contained in the range 0.11-0.13. Other research, in a work devoted to propose a model to predict the ductility supply of joints, the authors indicated a value of the ultimate bolt deformation capacity equal to 0.1 (Beg, et al. 2004).

Considering that, in technical literature, there is a common approach and usually the tests on the material composing the bolts used in the T-stub specimens are not available, in this work a simplified approach based on the application of an approximate tri-linear law is adopted (Fig. 2b). In particular, the proposed simplified tri-linear law is defined starting from the knowledge of the average values of the yield and ultimate stress of the material composing the bolt (i.e. for bolts class 8.8 [CoV = 0.07]:  $f_{y,ave} = 723$  MPa,  $f_{u,ave} = 904$  MPa; bolts class 10.9 [CoV=0.02]:  $f_{y,ave} = 930$  MPa,  $f_{u,ave} = 1034$  MPa), the stiffness of the second branch, which is characterized by a value of the Young modulus

equal to  $0.1E$  (Leon & Swanson 2000) and from the ultimate strain of the bolts. Such a strain value, since there are no specific indications in technical literature, is assumed equal to the elongation at fracture provided by the manufacturer of the bolts. This value, according to the manufacturer may vary in a minimum/maximum range according to prescribed values of the coefficient of variation. In particular, it is assumed that for bolt class 8.8,  $CoV = 0.1$ ,  $A_{min} = 0.12$ ,  $A_{max} = 0.18$ , while for bolt class 10.9,  $CoV = 0.1$ ,  $A_{min} = 0.09$ ,  $A_{max} = 0.14$  (Fontana 2004).

### **B.1.1. Flexural behavior of the flange plate**

Classically, the failure mechanisms of a bolted T-stub is dependent on the resistance of the composing elements, i.e. the bolts and the plate. In particular, in failure mechanism type-1, which is the most ductile as it provides the formation of significant plastic deformations in the flange plate under bending, the collapse is due to the formation of four plastic hinges contemporarily arising in correspondence of the flange-to-web connection and bolt line. Conversely, in failure mechanism type-3, the failure mechanism is characterized only by the bolt collapse. Finally, failure mechanism type-2 is intermediate between mechanisms type-1 and type-3, as it provides the collapse of the T-stub due to the failure of the bolt or of the flange plate due to the attainment of the ultimate rotation of the plastic hinges arising at the flange-to-web connection (Fig. B.3).

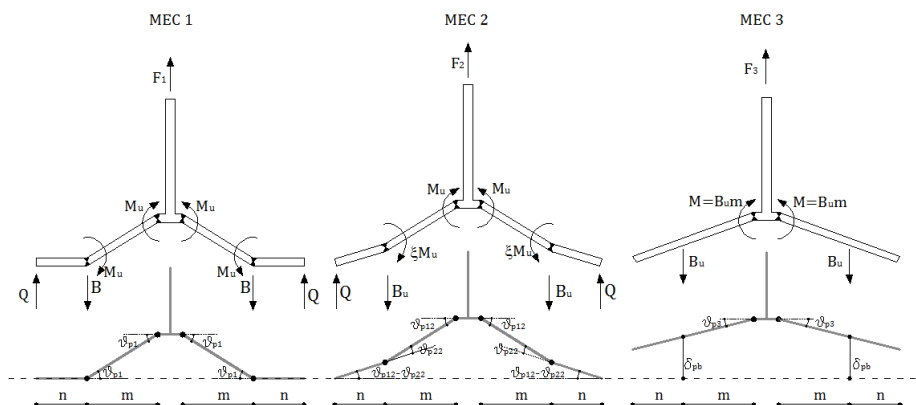


**Fig. B.3** – Classical definition of the failure modes

Considering the classical definition of failure modes and their kinematic mechanisms, it is clear that, in order to accurately predict the complete behaviour of a bolted T-stub, first of all, it is important to accurately define both the rotational capacity of the plastic hinges arising in the flange plate and the force-elongation relationship for the bolt. In fact, in case of mechanism type-1, as the collapse is due to the plate failure, the behaviour and the ductility capacity of the T-stub mainly depends on the ability of the plastic hinges to rotate and, in particular, on their moment-rotation response, while, in case of mechanism type-3, as failure is governed by bolts, it mainly depends on their force-elongation response. Obviously, in case of mechanism type-2, which is intermediate between mechanism type-1 and type-3, both the rotational response of the plastic hinges and the force-elongation response of bolts are of concern, because in this case the failure of the bolt or of the plate mainly depends on the relative resistance and ductility of the two components.

In particular, in the proposed model the plate behaviour is characterized by following an approach similar to that already provided in (Piluso, et al. 2001). Within this approach, the moment-rotation behaviour of the plastic hinges is derived passing from the true stress-true strain response of the basic material composing the plate to the moment-curvature relationship of the plate and, afterwards, it is obtained by means of integration of the curvatures along the plate.

#### Moment–Curvature relationship

Following the same methodology provided by (Piluso, et al. 2001), the behaviour of the plastic hinges arising on the flange plate is defined starting from the moment-curvature  $M - \chi$  relationship of the rectangular cross-section representing the flange plate. Such a relationship assumes four different mathematical laws in correspondence of the boundary strains  $\varepsilon_y, \varepsilon_h, \varepsilon_m, \varepsilon_u$  (Fig. B.2a). Under the hypothesis of pure bending, the significant values of the curvatures can be defined as:

$$\chi_y = \frac{2\varepsilon_y}{t_f}; \chi_h = \frac{2\varepsilon_h}{t_f}; \chi_m = \frac{2\varepsilon_m}{t_f}; \chi_u = \frac{2\varepsilon_u}{t_f} \quad (\text{B.3})$$

where  $t_f$  is the flange plate thickness. For each one of these curvature values, by writing the equilibrium equations the following branches, expressed in terms of non-dimensional bending moment vs non-dimensional curvature  $M/M_y - \chi/\chi_y$ , can be obtained:



- Elastic branch ( $\chi/\chi_y < 1$ ):

$$\frac{M}{M_y} = \frac{\chi}{\chi_y} \quad (\text{B.4})$$

- Yield branch ( $1 < \chi/\chi_y < \chi_h/\chi_y$ ):

$$\frac{M}{M_y} = \frac{1}{2} \left[ 3 - \left( \frac{\chi_y}{\chi} \right)^2 \right] \quad (\text{B.5})$$

- Hardening Branch ( $\chi_h/\chi_y < \chi/\chi_y < \chi_m/\chi_y$ ):

$$\frac{M}{M_y} = \frac{1}{2} \left[ 3 - \left( \frac{\chi_y}{\chi} \right)^2 \right] + \frac{1}{2} \frac{E_h}{E} \left( \frac{\chi - \chi_h}{\chi_y} \right) \left( 1 - \frac{\chi_h}{\chi} \right) \left( 2 + \frac{\chi_h}{\chi} \right) \quad (\text{B.6})$$

- Post-necking ( $\chi_m/\chi_y < \chi/\chi_y < \chi_u/\chi_y$ ):

$$\begin{aligned} \frac{M}{M_y} = & \frac{1}{2} \left[ 3 - \left( \frac{\chi_y}{\chi} \right)^2 \right] + \frac{1}{2} \frac{E_h}{E} \left( \frac{\chi - \chi_h}{\chi_y} \right) \left( 1 - \frac{\chi_h}{\chi} \right) \left( 2 + \frac{\chi_h}{\chi} \right) + \\ & - \frac{1}{2} \frac{E_h - E_u}{E} \frac{\chi - \chi_m}{\chi_y} \left( 1 - \frac{\chi_m}{\chi} \right) \left( 2 + \frac{\chi_m}{\chi} \right) \end{aligned} \quad (\text{B.7})$$

where  $M_y = b_{eff} t_f^2 / 6 f_y$  is the T-stub width and  $f_y$  is the material yield stress. From the previous equations, it is useful to observe from previous equations that the  $M_h/M_y$ ,  $M_m/M_y$ ,  $M_u/M_y$  ratios depend only on the properties of the material composing the flange plate (Fig. B.4).

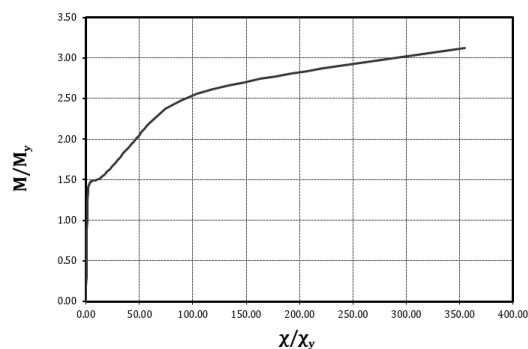


**Fig. B.4** – Example of non-dimensional moment-curvature diagram

#### Moment-rotation behaviour of the plastic hinges

By exploiting the definition of the moment-curvature relationships, the moment-rotation curves of the plastic hinges modelling the non-linear behaviour of the T-stub flange plate can be determined. Following the same approach provided by Piluso et al. (2001) such plastic rotations can be evaluated by means of the following steps:

- Evaluation of the bending moment diagram along the T-stub flange;
- Definition of the curvatures along the flange plate by inverting the moment-curvature relations previously defined;
- Integration of the curvatures on single cantilever beams in order to obtain the rotations of the plastic hinges.

The diagram of the bending moment arising on the T-stub flange plate is not known a priori and it depends on the system of equilibrium and compatibility equations to be solved according to the procedure reported in next section. Nevertheless, it is useful to note that the shape of such a diagram, in any point of the force-displacement T-stub curve, depends only on the applied loads and on the value of the bending moment arising in correspondence of the plastic hinges, whose ratio,

consistently with the kinematic collapse mechanism reported in Fig. B.5 can be defined as  $\psi M_u$ .

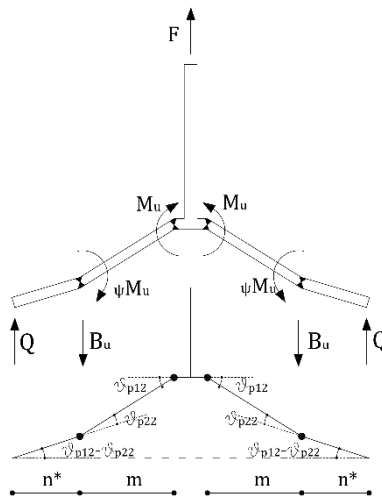


**Fig. B.5** – Assumed kinematic collapse mechanism

Therefore, it is linear in the zone in between the plastic hinge arising at the web and the tip of the bolt head, parabolic in the zone of the bolt head and again linear in the zone contained in between the bolt head and the prying force (Fig. B.6).

Following Piluso et al. (2001) approach [1], starting from the moment distribution arising along the T-stub flange depicted in Fig. B.6, the mathematical laws defining the rotations of the plastic hinges can be obtained by considering, in a simplified way, the three simple cantilever schemes reported in Fig. B.6, which are characterized by a maximum value of the bending moment equal to  $M_1=M$ ,  $M_2=M_3=\psi M$  and lengths  $L_1$ ,  $L_2$  and  $L_3$  equal to:

$$L_1 = \frac{m}{1 + \psi} \quad L_2 = \frac{m\psi}{1 + \psi} \quad L_3 = n \quad (\text{B.8})$$

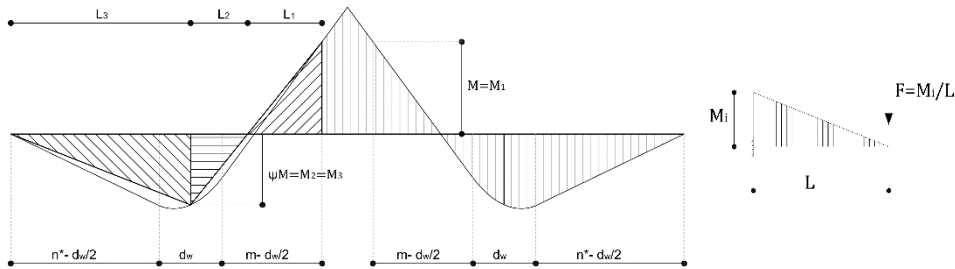


**Fig. B.6** – Cantilever scheme for evaluating the plastic rotations

Within this work, the parabolic part of the bending moment diagram is approximated with a linear segment internal to the actual diagram. This approximation is made in order to simplify the expressions of the mathematical laws providing the values of the rotations of the plastic hinges. It is worth observing that, this approximation leads to a slight overestimation of the rotation of the plastic hinge arising at the T-stub web  $\vartheta_{p1}$  and a slight underestimation of the plastic rotation arising at the bolt line  $\vartheta_{p2}$ .

Therefore, for each simple cantilever scheme, the value of the plastic rotation is obtained from the inversion of the moment-curvature diagram reported in previous paragraph and the integration of the curvatures along the cantilever. Such an integration provides the values of the following functions already defined by Piluso et al. (2001) [1]:

- **Case 1:**  $\xi \leq \xi_1 = \frac{M_y}{M_u}$

$$\vartheta_p = 0 \quad (\text{B.9})$$

- **Case 2:**  $\xi_1 \leq \xi \leq \xi_2 = \frac{M_h}{M_u}$

$$\vartheta_p = \frac{L}{t_f} D(\xi) \quad (\text{B.10})$$

- **Case 3:**  $\xi_2 \leq \xi \leq \xi_3 = \frac{M_m}{M_u}$

$$\vartheta_p = \frac{L}{t_f} F(\xi) \quad (\text{B.11})$$

- **Case 4:**  $\xi_3 \leq \xi \leq 1$

$$\vartheta_p = \frac{L}{t_f} G(\xi) \quad (\text{B.12})$$

where  $\xi$  is equal to the ratio between the bending moment and  $M_u$  and the functions  $D(\xi)$ ,  $F(\xi)$  and  $G(\xi)$  depend only on the mechanical properties of the plate. For the sake of clarity, the complete expressions of the functions are reported in the Annex A of this paper. A typical non-dimensional moment-rotation behaviour of the plastic hinge is delivered in Fig. B.7.

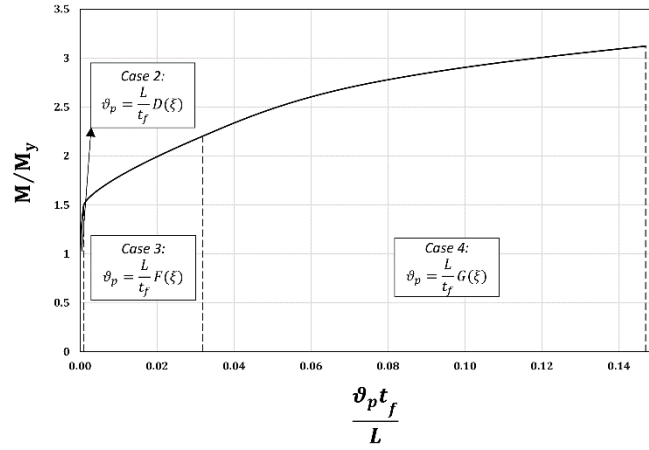


**Fig. B.7** – Typical moment-rotation behaviour of the plastic hinge

With reference to the kinematic collapse mechanism reported in Fig. B.5, it is easy to verify by means of geometrical considerations, that the plastic displacement of the T-stub can be expressed as a function of the plastic hinges rotation by means of the following relationship:

$$\delta_{p,T-stub} = \vartheta_{p1} \cdot m + (\vartheta_{p1} - \vartheta_{p2}) \cdot n^* \quad (\text{B.13})$$

where  $\vartheta_{p1}$  is the plastic rotation of the first cantilever scheme characterized by the length  $L_1$  and the bending moment  $M_1$ ;  $\vartheta_{p2}$  is equal to the sum of the plastic rotations of the other two cantilever schemes defined in Fig. B.6. In addition, due to compatibility requirements with the vertical displacement of the plate in the contact zone,  $\vartheta_{p1}$  has to be greater than  $\vartheta_{p2}$ , otherwise  $\vartheta_{p1} = \vartheta_{p2}$ .

### B.1.2. Axial behavior of the bolt

As aforesaid, analogously to the flange plate, the force-elongation behaviour of the bolt can be characterized starting from the definition of the stress-strain law of the basic material. It is easy to understand that, in this case, the translational spring representing the bolt behaviour can be defined by multiplying the strains and the stresses of the constitutive law by the length ( $L_b$ ) and the net section area ( $A_{res}$ ) of the shank respectively. Consistently with the Eurocode 3 approach, the conventional length of the bolt can be defined as:

$$L_b = 2t_f + \frac{t_n + t_{bh}}{2} + 2t_w \quad (\text{B.14})$$

where  $t_n$  is the nut thickness,  $t_{bh}$  is the thickness of the bolt head and  $t_w$  is the thickness of the washer.

Therefore, the force-elongation behaviour of the bolt can be characterized by means of the following tri-linear behaviour:

- **1<sup>st</sup> Branch:** Elastic ( $\delta \leq \delta_y$ ):

$$B = K_0 \cdot \delta \quad (\text{B.15})$$

- **2<sup>nd</sup> Branch:** Inelastic ( $\delta_y < \delta \leq \delta_h$ ):

$$B = 0.10 \cdot K_0 \cdot \delta \quad (\text{B.16})$$

- **3<sup>rd</sup> Branch:** Plateau ( $\delta > \delta_h$ ):

$$B = B_u \quad (\text{B.17})$$

where the contribution of the initial stiffness of the bolt, with reference to the single tee element, is equal to:

$$K_0 = \frac{2EA_{res}}{L_b} \quad (\text{B.18})$$

while the boundary displacements, dividing the different branches are:

$$\begin{aligned} \delta_y &= \frac{f_y \cdot L_b}{2E} \\ \delta_n &= \delta_y + \frac{(B_u - B_y)}{0.10K_0} \\ \delta_u &= \varepsilon_u L_b \end{aligned} \quad (\text{B.19})$$

Finally, the yielding and ultimate bolt forces are given by:

$$\begin{aligned} B_y &= A_{res} \cdot f_y \\ B_u &= A_{res} \cdot f_u \end{aligned} \quad (\text{B.20})$$

## B.2. Model assembling

As far as the basic assumptions and the mathematical laws defining the non-linear behaviour of flange plate and bolt are defined, it is possible



to define the procedure to assembly the sub-components of the T-stub (i.e. the plate and the bolt) in order to get the whole force-displacement curve up to failure. According to the assumptions made and to the bending moment distribution depicted in Fig. B.6, for a fixed value of the bending moment  $M_f = M_l$  acting in correspondence of the T-stub web, there are five unknown parameters (Fig.B.1b). The force transmitted through the T-stub web ( $F$ ), the prying force ( $Q$ ), the value of the distributed load corresponding to the action provided by the bolt head ( $q$ ), the ratio between the bending moment acting at the bolt line and that arising at the T-stub web ( $\psi$ ) (Fig.B.6) and the location of the prying forces in the contact zone ( $n^*$ ). In order to solve the problem, five equations can be written: the translational equilibrium, the rotational equilibrium around the plastic hinge located in correspondence of the web, the rotational equilibrium of the left portion of the plate beam around the point of application of the bolt force, the compatibility equation between the T-stub flange and the elongation of the bolt at the bolt line and the compatibility equation of the vertical displacements in the contact zone. Therefore, the system of equations to be solved, in its general form, can be written as follows:

$$\left\{ \begin{array}{l} \frac{F_y}{2} + Q - qd_w = 0 \\ Q(m + n^*) - qd_w m + M_y = 0 \\ Qn^* - \frac{qd_w^2}{8} - \psi M_y = 0 \\ \delta_{b.el} + [\vartheta_{p1}(\psi) - \vartheta_{p2}(\psi)]n^* = \frac{qd_w}{K_{sec}} \\ v_1(z_1) + [\vartheta_{p1}(\psi) - \vartheta_{p2}(\psi)]z_1 \Big|_{min} > 0 \end{array} \right. \quad (B.21)$$

where  $\delta_{b,el}$  is the elastic part of the vertical displacement evaluated at the bolt line,  $K_{sec}$  is the value of the bolt secant stiffness determined on the force-elongation curve previously defined,  $\vartheta_{p1}(\psi)$  and  $\vartheta_{p2}(\psi)$  are the plastic rotations of the hinges to be evaluated according to the procedure previously reported, whose values depend on the parameter  $\psi$ ,  $v_1(z_1)$  is the distribution of the plate elastic displacements in the contact zone and  $z_1$  is the value of the abscissa starting from the tip of the plate.

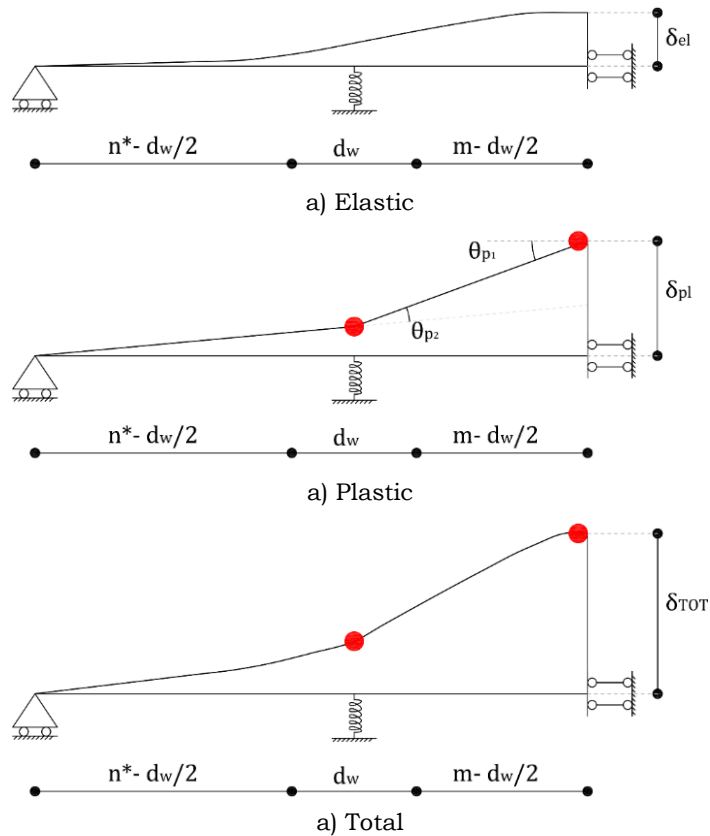


**Fig. B.8** – Deformed shape of the flange

It is worth noting that fourth and fifth equation of system (B.21) depend on the elastic part of the plate displacement (Fig. B.8a) and, due to this reason, it is necessary to define the mathematical laws of the vertical deflections of the plate in a closed form. To this scope, the static beam equations for the three portions  $0 \leq z_1 \leq n^* - d_w/2$ ,  $0 \leq z_2 \leq d_w$  and  $0 \leq z_3 \leq m - d_w/2$  have been written imposing appropriate boundary conditions. For the sake of clarity, the solutions providing the deflections of the plate, are reported in [2].

Observing Eqs.(B.21), it is easy to understand that the solution of the system is untrivial in a closed form. In fact, the equations providing the expressions of the flange plate plastic rotation are quite complicated and, in addition, the point where the prying force is applied is not directly evaluable because it depends on the expression of the vertical deflection of the plate in the contact zone [2].

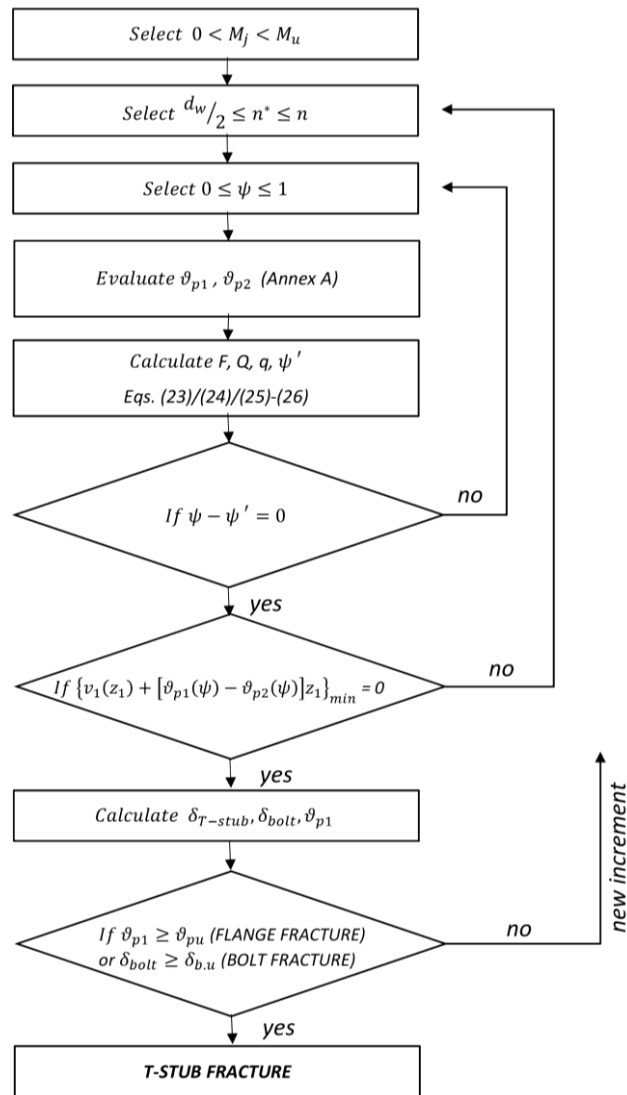


**Fig. B.9** – Flow-chart for solving the system of equation (B.21)

Nevertheless, the system can be solved incrementally by means of the algorithm reported in Fig. B.9. In particular, following this algorithm,

for every assigned value of the bending moment  $M_j$ , the system of equations can be iteratively solved by preliminarily fixing  $n^*$  and an attempt value of  $\psi$  in order to determine  $\vartheta_{p1}$  and  $\vartheta_{p2}$  and, from the first four equations of the system, the values of  $q$ ,  $F$ ,  $Q$ , and a new value  $\psi = \psi'$  of the parameter, providing the bending moment of the bolt axis. In particular,  $q$  can be calculated from the following equations, whose application range depends on the deformation state of the bolt:

Case 1 – Bolt in the elastic range

$$q_1 = \frac{64K_0n^*[3m^2M_j + 6M_jmn^* + 2M_jn^{*2} + 6EI(\vartheta_{p1} - \vartheta_{p2})(m + n^*)]}{d_w\{192EI(m + n^*) + K_0[d_w^2(m + n^*) - 16d_w^2n^*(m + n^*) + 64mn^{*2}(3m + 2n^*)]\}} \quad (\text{B.22})$$

Case 2 – Bolt in the plastic range

$$q_2 = 0.1q_1 + 0.9 \frac{B_y}{d_w} \quad (\text{B.23})$$

Case 3 – Bolt in the plateau range

$$q_3 = 0.1q_1 + 0.9 \frac{B_y}{d_w} \quad (\text{B.24})$$

while  $F, Q$  and  $\psi'$  can be calculated by exploiting the following relationships:

$$F = 2 \frac{(qd_wn^* + M_j)}{m + n^*} \quad (\text{B.25})$$

$$Q = \frac{(qd_w m - M_j)}{m + n^*}$$

$$\psi' = \frac{qd_w [d_w (m + n^*) - 8mn^*] + 8M_j n^*}{8M_j (m + n^*)}$$

Afterwards the accuracy of the solution can be evaluated by checking the respect of last equation of the system and the difference between  $\psi$  and  $\psi'$ . As far as the force-displacement curve of the T-stub is obtained by progressively increasing the bending moment acting on the flange, at the end of each loading step it is possible to check also for the deformation state of plastic hinges and bolt. In this way it is possible to control if the rotations and the elongations are compatible with the plastic deformation capacity provided by the basic materials.

In order to verify the accuracy of the model, a specific program based on the reported algorithm in Visual Basic for Application has been developed. Finally, the accuracy of the proposed model has been investigated by means of a comparison with twelve experimental tests, both in terms of resistance and of plastic deformation capacity, reported in [2].

### **B.3. References**

- [1] A.B. Francavilla, M. Latour, V. Piluso, G. Rizzano (2016), “*Bolted T-stubs: a refined model for flange and bolt fracture modes*”, *Steel and Composites Structures*, Vol. 20, (2), 267-293;
- [2] Piluso, V., Faella, C. and Rizzano, G. (2001), “*Ultimate behavior of bolted T-stubs. Part I: Theoretical model*”, *J. Struct. Eng. ASCE*, 127(6), 686-693.